An Exploratory Study of the Distortion Characteristics of Valve Signal Processors

by

Andrew Kuhn

Thesis presented in partial fulfilment of the requirements for the degree of Master of Music (Music Technology) in the Faculty of Arts and Social Sciences at Stellenbosch University

Supervisor: Dr G. W. Roux

December 2021

Declaration

By submitting this thesis electronically, I declare that the entirety of the work contained therein is my own, original work, that I am the sole author thereof (save to the extent explicitly otherwise stated), that reproduction and publication thereof by Stellenbosch University will not infringe any third party rights and that I have not previously in its entirety or in part submitted it for obtaining any qualification.

Date: December 2021

Abstract

An Exploratory Study of the Distortion Characteristics of Valve Signal Processors

A. Kuhn

Department of Music,
University of Stellenbosch,
Private Bag X1, Matieland 7602, South Africa.

Thesis: MMus (Music Technology)

December 2021

Valve signal processors, a technology ostensibly out of place in the modern world, are still widely used in professional audio practice. It is believed that valves can impart a *euphonic timbre* on audio signals, in a phenomenon known colloquially as *signal colouration*. The inherent electronic limitations of valve signal processing result in a variety of *distortions* to be generated. Subsequently, the generation of distortion corresponds to the emergence of signal colouration. The standard distortion testing methodologies ordinarily employed by engineers have been limited as an analysis tool. These tests were originally designed to analyse the total amount of distortion present in a signal, not the intrinsic distortion character of a signal processor. Therefore, the objective of this thesis was to explore the key *characteristics* of valve signal processing distortion.

The approach to empirical research adopted for this thesis involved the design and implementation of a series of exploratory experiments intended to analyse distortion character. Experiments were conducted on a selection of devices. Data was acquired from three software emulators, and a hardware valve microphone pre-amplifier. The microphone pre-amplifier was able to use two different types of valve for its gain stages, a 12AY7 and 12AX7; data was gathered from both. To make inferences into the processes that lead to the emergence of distortion, MATLAB was used to plot the electronic characteristics of a valve gain stage for analysis, thus permitting the juxtaposition of electronic phenomena to distortion measurements.

The research was definitive in finding that different signal processors generate idiosyncratic profiles of distortion; the extent to which this occurred surpassed prior assumptions. Each device produced distortion profiles that were not static, but dynamic, and evolved with varying input levels. These results suggest that different signal processors can cause distinct timbral changes to audio material under certain conditions.

Uittreksel

'n Verkennende Studie van die Vervormingseienskappe van Vakuumbuis-seinverkers

("An Exploratory Study of the Distortion Characteristics of Valve Signal Processors")

A. Kuhn

Departement Musiek,
Universiteit van Stellenbosch,
Privaatsak X1, Matieland 7602, Suid Afrika.

Tesis: MMus (Musiektegnologie)

Desember 2021

Alhoewel vakuumbuise nie meer algemeen gebruik word in in moderne elektronika nie, word dit steeds wyd aangewend in klankverwerking waar die seinverkleuring wat deur die vakuumbuis se nie-liniere gedrag, gewensd is. Die verskeie tipes klankvervorming wat vakuumbuise skep veroorsaak kombineer tot 'n ontluikende effek in die vorm van klankverkleuring. Standaardtoesprosedures wat gebruik word om seinvervorming te meet is gerig daarop om die totale vervorming te meet en nie die spesifieke eienskappe van vervorming wat hoog aangeprys word vanuit 'n toonkleurperspektief nie. Die doelstelling van hierdie tesis was om die *kern-eienskappe* van vakuumbuisvervorming op klankseine te verken.

Die empiriese navorsing in hierdie tesis is die ontwerp en implementering van 'n reeks verkennende eksperimente om vakuumbuisvervorming te analiseer. Eksperimente is uitgevoer op 'n verskeidenheid van toestelle. Data is gemyn van drie sagteware-emulators en 'n vakuumbuis mikrofoonvoorversterker. Die mikrofoonvoorversterker was in staat om twee verskillende tipes vakuumbuise in die aanwinsvlak te gebruik, 'n 12AY7 en 12AX7 buis. Om afleidings te maak omtrent die prosesse wat lei tot die ontluiking van ververvorming, is MATLAB gebruik om die elektroniese eienskappe van 'n vakuumbuisbuisaanwinsvlak te stip vir ontledingsdoeleindes. Dit stel 'n vergelyking van elektroniese eienskappe met vervormingsmeting in staat.

Die navorsing het bevind dat verskillende seinverwerkers unieke vervormingsprofiele genereer en die mate waartoe dit plaasvind het voormalige aannames oortref. Elke toestel het vervormseienskappe vertoon wat dinamies is en wat verander op grond van die intreeseinvlakke. Die resultate vertoon die invloed van verskillende seinverwerkers op toonkleureienskappe onder sekere toestande.

Acknowledgements

I would like to express my sincere gratitude to the following people and organisations:

- The Stellenbosch University Department of Music, thank you for so graciously accepting me into your masters programme.
- The Myra Chapman Educational Trust, thank you for the scholarship, I would not have made it otherwise.
- Dr Gerhard Roux, my supervisor, thank you for all of your kind advice and guidance, as well as for the translating of the abstract.
- To my family, thank you for getting me through this.
- Neville Scott, thank you for the laptop and for the maths and electronics help.

Contents

List of Figures

Listings

Nomenclature

Acronyms and Abbreviations

AC	Alternating Current
ADSR	Attack Decay Sustain Release
ANSI	American National Standards Institute
CCS	Constant Current Source
DAC	Digital to Analogue Converter
DC	Direct Current
DFD	Difference Frequency Distortion
DIN	Deutsches Institut für Normung
DSP	Digital Signal Processing
DUT	Device Under Test
FFT	Fast Fourier Transform
HT	High Tension
ISO	International Organization for Standardization
IEEE	Institute of Electrical and Electronics Engineers
IMD	Intermodulation Distortion
RMS	Root Mean Square
SMPTE	Society of Motion Picture and Television Engineers
SIL	Sound Intensity Level
SPL	Sound Pressure Level
THD	Total Harmonic Distortion
TID	Transient Intermodulation Distortion
WCF	White Cathode Follower

Constants

$\pi =$	3.141 592 654
$j =$	$\sqrt{-1}$

Variables with Units

f	Frequency	[Hz]

τ	Period	[s]
φ	Phase Angle	[rad]
ω	Angular Frequency	[rad/s]
V	Voltage	[V]
I	Current	[A]
R	Resistance	[Ω]
X	Reactance	[Ω]
C	Capacitance	[F]
L	Inductance	[H]
Z	Impedance	[Ω]
dB	Decibel	[dB]

Variables without Units

H	Transfer Function
k	Cathode
a	Anode
g	Control Grid
μ	Amplification Factor
g_m	Transconductance
r_a	Anode Resistance

Chapter 1

Introduction

AUDIO technology has progressed at an unprecedented rate during the late 20th and early 21st century. Audio signal processing devices have become increasingly compact, convenient, and cost effective. Modern signal processors exhibit near perfect fidelity, as their distortion levels have dropped below the threshold of human perception. However, many precursor or *vintage* audio signal processing technologies have evaded obsolescence, and remain conspicuously popular amongst a significant number of *audio professionals*[1], ostensibly at odds with the notion of technological progress (Newell, 2012:xxxi; Pinch & Reinecke, 2009:152–153; Robjohns, 2010).

The inherent electronic limitations of valve signal processing result in a variety of *distortions* to be generated. Subsequently, the generation of distortion corresponds to the emergence of *signal colouration*. Audio professionals often use the signal colouration produced by vintage audio signal processing devices to achieve a desired sonic effect, whereby the timbre of an audio signal is manipulated for aesthetic ends. Many audio professionals describe this effect as adding *cohesion* and *clarity* to audio material (Case, 2011:74–75; Winer, 2017:57), while others describe signal colouration as having a *warm*, *natural*, *fat*, or *coloured* timbre[2] (Corey & Benson, 2017:101); these properties are sometimes found to be lacking in modern audio technologies (Pinch & Reinecke, 2009:163–164).

The aforementioned descriptors are vernacular terms that are inadequately defined, purely subjective, and have no scientific measurements associated with them; consequently, it is difficult to evaluate them quantitatively (Everest & Pohlmann, 2014:65). The signal colouration induced by vintage signal processors is an emergent[3] timbral *qualia*[4] that *supervene* out of residual distortion caused by the *complex system* of interactions within audio signal processing systems. Signal colouration can become so distinct that certain audio technologies have be-

[1] The term *audio professional* in this thesis encompasses recording, mixing, and mastering engineers, as well as music producers, and composers.

[2] "That attribute of auditory sensation which enables the listener to judge that two non-identical sounds, similarly presented and having the same loudness and pitch, are dissimilar" (ANSI S1.1-1994, 2005:12.09). Although there appears to be a lack of consensus as to the exact definition of timbre, see Chapter 2.4.3.

[3] "[...] emergent entities (properties or substances) 'arise' out of more fundamental entities and yet are 'novel' or 'irreducible' with respect to them [...]. Emergent properties are systemic features of complex systems which could not be predicted [...] from the standpoint of a pre-emergent stage, despite a thorough knowledge of the features of, and laws governing, their parts." (O'Connor & Wong, 2015:emergent properties)

[4] "[...] qualia are intrinsic properties of experiences that are also ineffable, nonphysical, and 'given' to their subjects incorrigibly (without the possibility of error.)." (Tye, 2018)

come renowned for the unique perceptual features that they impart on musical material (Moore *et al.*, 2016:1; Gottinger, 2007:18,413). Despite being considered objectionable by some audio professionals (Bohn, 2016:distortion), signal colourations are in vogue and widespread within many genres of music. Plausibly, this is due to the many popular (and therefore widely disseminated) recordings that were subjected to these precursor technologies. The sonic imperfections introduced by vintage technologies have become culturally and historically significant and are associated with the *sound* or timbre of particular genres or musical eras. (Gottinger, 2007:384; Barlindhaug, 2007:77–78)

This thesis will focus on technologies that employ the *valve* (known as the *vacuum tube* in the USA)[5], an active component used to amplify audio signals; this technology is particularly venerated[6] by many audio professionals. Recent technological advancements have allowed for the software emulation of this colouration effect via digital signal processing (DSP). While software emulators offer affordability, convenience, and no maintenance costs; many audio professionals believe that hardware devices offer superior performance (Barbour, 1998:24–27; Temme, 1992:5; Robjohns, 2010).

The relationship between technology and audio professionals is an incontrovertibly complex phenomenon that comprises a number of integrative levels. The *audio studio*[7] and music production processes garner interest from a broad range of academic disciplines. Audio studios are a complex environment, and audio professionals are required to have acute technical and aesthetic acumen. However, the technology of professional audio practice tends to be neglected by conventional musicological studies (Zagorski-Thomas & Frith, 2012:2–3). There appears to be an aversion amongst academics towards conflating the aesthetic perceptual properties associated with audio technology, with engineering practice (Gottinger, 2007:7). The predominant philosophy of many organisations dedicated to audio technology research and design has been that of *technological utopianism*. This philosophy emphasises fidelity and the elimination of distortion within audio technology. While fidelity is certainly an important objective, the phenomenon of signal colouration should not be overlooked (Bennett, 2012:1; Gottinger, 2007:1).

A preliminary survey of the extant academic literature reveals a deficiency of research on this phenomenon. Standard testing methodologies ordinarily employed by researchers have been limited as an analysis tool. Typically, audio signal distortion tests employ the THD and IMD protocols. These tests are well suited for determining the general fidelity of an audio system. However, they provide only a superficial insight into distortion characteristics. Herein lies the problem; the *characteristic features* of valve distortion have no adequate means of measurement, analysis, and interpretation.

---

[5] "An electron tube where virtually all the air has been removed (creating a vacuum), thus permitting electrons to move freely, with low interaction with any remaining air molecules." (Bohn, 2016:vacuum tube)

[6] An interesting case of this technology in professional practice is the modern classical record label TACET (www.tacet.de). They have released over 350 albums on phonograph disc, each album is recorded solely on valve based technology, from the microphones all the way to the disc mastering; these albums are in effect *transistorless*.

[7] The term *audio studio* in this thesis encompasses recording, mixing, and mastering studios.

In order to critically address the research problem, this thesis had to accomplish specific objectives; the primary aim was to:

- Analyse the characteristics of audio distortion generated by valve signal processing devices.

Three secondary objectives supplement the primary objective:

- Observe for significant differences between the distortion profile of hardware valve signal processors and DSP emulators.
- Expand on the current methodological approaches to measuring and analysing the properties of audio distortion.
- Use software to plot the characteristics of a valve audio amplification circuit for analysis.

This thesis took the form of an exploratory study and thus intended to inquire into the following research questions:

- What is the nature of the signal distortion characteristics imparted by valve signal processors?
- Do different valve signal processors exhibit significant differences in their individual distortion profiles?
- Are there any significant differences in the distortion profile of valve signal processors and software emulations?

Experiments were conducted on a selection of audio devices, a valve microphone pre-amplifier and three software emulators. The microphone pre-amplifier could use two valve types (a 12AY7 and 12AX7) for its gain stages, and both valves were used in the experiments to observe for characteristics unique to each. The experiments involved making measurements of the distortion properties of each device, and the results were analysed and discussed accordingly. Conducting experiments with a high degree of rigour is contingent on powerful data gathering and analysis instrumentation tools. Stellenbosch University provides students with access to computer software known as MATLAB[8], an advanced and powerful proprietary software package and computer programming language[9] used by scientists and engineers for specialised tasks. The key features of MATLAB that apply to this research are its signal processing abilities. These include calculations, analysis, visualisation, and processing of audio data. External *toolboxes* have been developed that perform specialised functions when integrated into the MATLAB software environment. The *Audio Toolbox*[10] provides tools for audio processing and allows the user to import, manipulate, and extract key features from audio data. The *DSP System Toolbox*

[8] MATLAB is a portmanteau of *matrix* and *laboratory*.

[9] A computer programming language is a notated *set of instructions* analogous to the vocabulary of spoken languages, these are interpreted by computers to perform particular tasks; many computer languages may operate on a single computer (Tarr, 2018:3).

[10] Additional information is available at: https://www.mathworks.com/products/audio.html [Visited 2020-4-10].

provides tools for analysing audio signal processing systems. The data generated by the experiments was presented in the form of *oscillogram* (time domain) and *spectrogram* (frequency domain) graphical representations.

Sources from a wide range of relevant academic disciplines were consulted to compile a rigorous theoretical foundation for the data gathering and analysis phases. This thesis is structured as follows:

Chapter 2 - Background: Outlines the elementary concepts of sound and electronics relevant to the research. The concept of distortion and standard distortion testing protocols received considerable deliberation. A substantial portion is dedicated to audio transformers, as these also generate distortion and cause signal colouration. Importantly, there is a comprehensive study of the valve, and the functions of the internal electrodes, biasing, and gain staging, are examined.

Chapter 3 - Research Methodology: The approaches towards research design, data gathering, implementation of analysis instrumentation, are described. The devices under test are introduced, and the experiment processes are elaborated.

Chapter 4 - Results & Analysis: Comprises the results of the experiments and followed by a comprehensive analysis and discussion of those results.

Chapter 5 - Conclusion: Final conclusions and recommendations for further study.

Chapter 2

Background

2.1 Fundamentals of Sound

ACOUSTICS is the branch of physics that is concerned with the phenomenon of sound and vibration. Sound is the propagation of mechanical energy through air (or any elastic medium) in the form of a *longitudinal wave*. A sound wave is as a series of *compressions* (increase in pressure) and *rarefactions* (decrease in pressure) of air particles, where individual particles pass *momentum* to and from one another. The velocity of these air particles is at a maximum at the point of equilibrium, and zero at the maximum point of displacement; analogous to the motion of a pendulum. As longitudinal waves are arduous to represent graphically, it is standard to plot sound waves as *transverse waves*, with the x-axis representing amplitude and the y-axis representing time. Figure 2.1 illustrates this concept, where *atmospheric pressure* is the point of equilibrium. The compression phase is above atmospheric pressure and represented in the positive domain, while the rarefaction phase is below atmospheric pressure and represented in the negative domain. (Everest & Pohlmann, 2014:1–6)

2.1.1 The Sine Wave

Ideal sine waves are the simplest form of periodic wave and are one of the most fundamental concepts in physics. Importantly, sine waves can model the physical behaviour of the oscillations that manifest in physical entities. Sine waves have only three parameters, *amplitude*, *frequency*, and *phase*. *Amplitude* is the apparent *strength* of a sound wave and is generally represented in three possible ways, as seen in Figure 2.1. The *peak amplitude* (A_{pk}) refers to the maximum instantaneous magnitude from the zero point that a waveform takes. The *peak-to-peak amplitude* (A_{pp}) is the instantaneous magnitude between the positive peak excursion, and negative peak excursion of the waveform. The *root mean square* (RMS or A_{RMS} in Figure 2.1) is the average energy content of the waveform; if the waveform is squared, averaged over a designated time period, the square root of this averaged value will be the RMS value. For a sine wave this value is approximately 0.707 times A_{pk}, for other types of waveforms this value will have to be calculated. (Tarr, 2018:72–74; White & Louie, 2005:19, 282, 355)

A *wavelength* is the distance a *periodic* wave travels before it starts to repeat itself. A waveform is considered to be *periodic* if the shape of the waveform is repeated at a constant rate, with the *period* (τ) referring to the time each individual repetition takes. The rate at which a

period repeats itself is its *frequency*, which is equivalent to the reciprocal of the period, or waveform cycles per second; with an associated unit of measurement known as the *Hertz* (Hz). For example, if the wavelength in Figure 2.1 completed a 1000 cycles every second, it would have a frequency value of 1000 Hz. (Howard & Angus, 2006:9–10; White & Louie, 2005:284–285; Laplante, 2005:741)

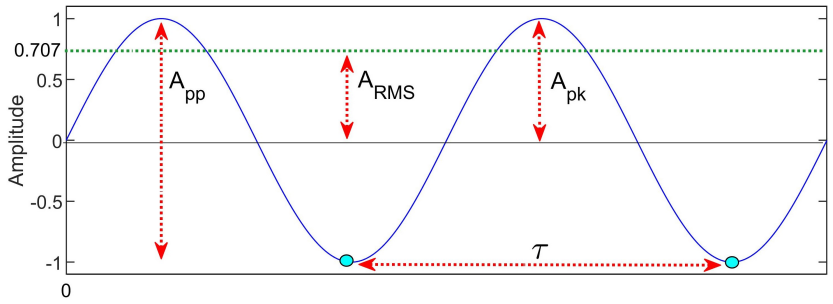

Figure 2.1: Representation of a wavelength as a function of amplitude in time. (Everest & Pohlmann, 2014:7)

Sine waves are described by the following mathematical formulae:

$$f = \frac{1}{\tau} \tag{2.1}$$

$$\omega = \frac{2}{\pi}.f \tag{2.2}$$

$$f(t) = A\sin(\omega t + \phi) \tag{2.3}$$

Equations 2.1 & 2.2 describe how the radian frequency[1] (ω) is derived; f is the frequency in Hz, and τ is the period in seconds. In Equation 2.3, $f(t)$ is the sinusoid, while A denotes the amplitude (the peak deviation of the function $f(t)$ from 0), t is time (in seconds), and φ is the phase angle of the sine wave. This is illustrated in Figure 2.2 , if point R rotates in a uniform manner around the circle, with period (τ), the projection point (P) moves up and down along the y-axis, thereby creating a sinusoid $f(t)$ with simple harmonic motion. The motion is symmetrical around the equilibrium position 0, when point R crosses the y-axis on the circle, the sinusoid $f(t)$ will reach its peak positive or negative amplitude, though when it crosses the x-axis on the circle, $f(t)$ will be at equilibrium. The phase angle (φ) describes the starting point of the wave; if φ was 0, then $f(t)$ would start at the point of equilibrium, if φ was $\pi/2$ radians, $f(t)$ would start at the point of peak positive amplitude. Additionally, if φ was π radians, $f(t)$ would start at the point of equilibrium, but instead of ascending towards the positive peak, it would descend toward the negative peak. Figure 2.3 introduces a new sinusoid

[1] This is radians per second.

with a projection point (Q) that has a different a different phase angle (φ_2), this results in the waveform crossing the point of equilibrium at a different point in time (t_2), while the period of τ remains unchanged. Phase can also be described in *degrees*, for example a phase shift of 90° is the same as $\pi/2$, 180° is the same as π, 270° is the same as $3\pi/2$, and a full rotation of 360° the same as 2π. (Roederer, 2008:26–27; Everest & Pohlmann, 2014:9–10)

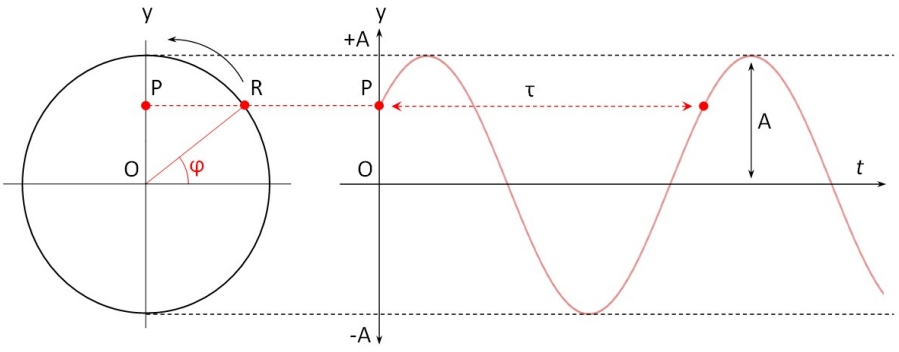

Figure 2.2: Simple sinusoidal motion. (Roederer, 2008:26)

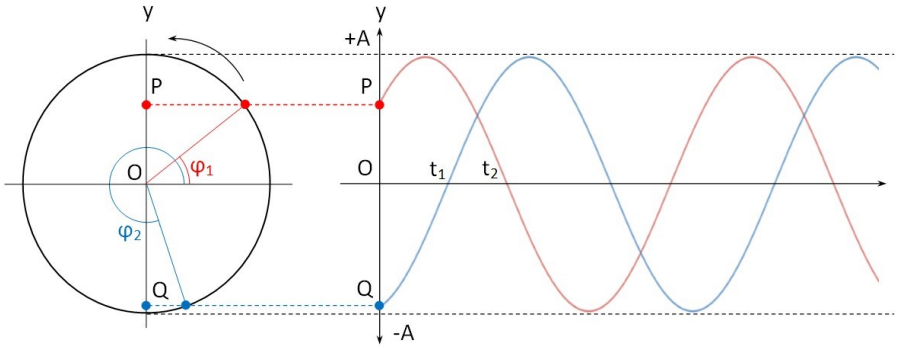

Figure 2.3: Sinusoidal motion of two points with the same amplitude and frequency, but different phases. (Roederer, 2008:27)

2.1.2 Complex Waves

Unlike the simple sine wave, the types of sounds encountered in reality, such as speech and music, are markedly different. *Complex waveforms* are a composite of more than one sine wave; conversely, any complex wave can be *decomposed* into a series of sine waves of various frequencies, amplitudes, and phases. Complex waves are constituted of a *fundamental frequency*, *harmonics*, and *inharmonic partials*. The fundamental frequency is generally the lowest frequency component of a complex wave; its frequency is the repetition rate of the entire complex waveform. It can be thought of as the *foundation* of the other components. Harmonics are sinusoidal frequency components related to the *harmonic series*, and are *integer multiples* of the fundamental frequency. Conversely, inharmonic partials share no explicit mathematical relation to the fundamental frequency, and in certain instances can even be of a lower frequency. Harmonics and partials are believed to give complex waves produced by musical instruments their

intrinsic sonic character, or *timbre*. (White & Louie, 2005:167–168, 178; ANSI S1.1-1994, 2005:13.05)

The addition of harmonics to a fundamental frequency can be observed in Figure 2.4a, f_{1a} is the fundamental. The waveform f_{2a} has a frequency that is twice the fundamental's, with half its amplitude; f_{3a} has a frequency that is three times fundamental's, also with half its amplitude. Relative to f_{1a}, f_{2a} is the second harmonic, and f_{3a} is the third harmonic; further harmonics can be added *ad infinitum*. The result of combining the waveforms (f_{4a}) can be observed in Figure 2.4c. Figure 2.4b demonstrates the effects of a phase shift on each harmonic; f_{2b} is shifted by 90°, or $\pi/2$ radians, and f_{3b}, has a phase shift of 270°, or $3\pi/2$ radians. Once again all three of the waves are combined (f_{4b}) with the result (f_{4b}) depicted in Figure 2.4b. When comparing the combined waveforms in Figure 2.4c, it can be observed that the relative phase shift of each harmonic has a considerable influence on the overall shape of a waveform. (Everest & Pohlmann, 2014:8–12)

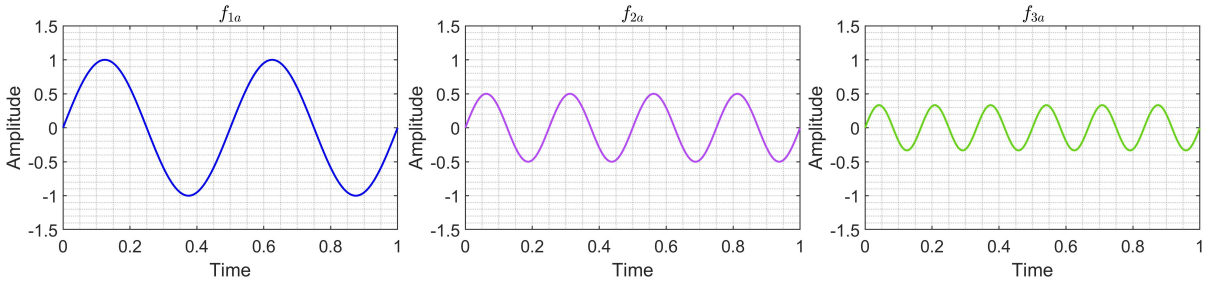

(a) Combination of sine waves that are in phase.

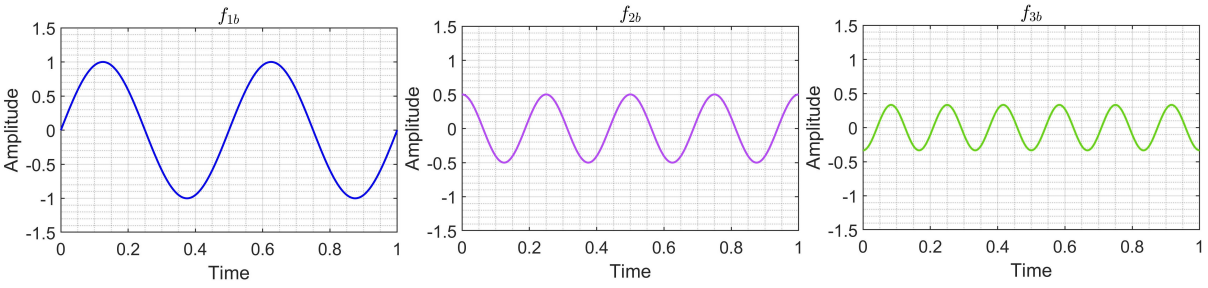

(b) Combination of sine waves with varying phases.

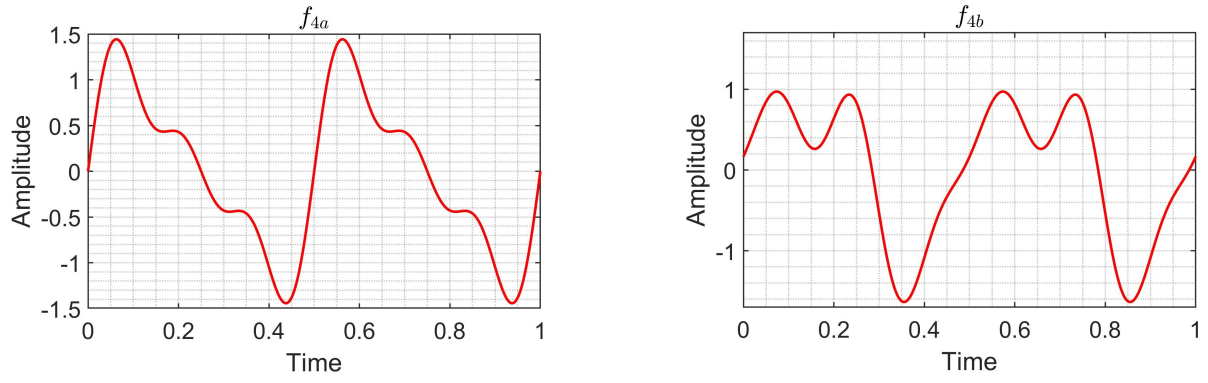

(c) Results of waveform combination.

Figure 2.4: The effect of phase shifts on complex waves. (Everest & Pohlmann, 2014:8–12)

2.1.3 Temporal Envelope

The amplitudes of waveforms encountered in the real world, such as the human voice and musical instruments, evolve over time; this phenomenon is known as the *temporal* (or *amplitude*) *envelope*. There are multitudes of shapes that an envelope can take. For example, sounds can begin abruptly and then fade into silence, or they can gradually increase in amplitude and then end suddenly. The temporal envelope is the profile of sound energy over time, or more succinctly, a time function that indicates the amplitude of a signal over time. (Sueur, 2018:125)

The temporal envelope can be divided into a series of distinct phases. The start of a sound event is known as the *acoustic onset time*, it occurs when the sound event becomes physically measurable (point n_0 in Figure 2.5). Figure 2.5 illustrates what is commonly referred to as an ADSR envelope, which is a highly simplified model of a typical temporal envelope, each stage is described below. (Howard & Angus, 2006:220; Johnston & Johnston, 2009:306; Lerch, 2012:119–120)

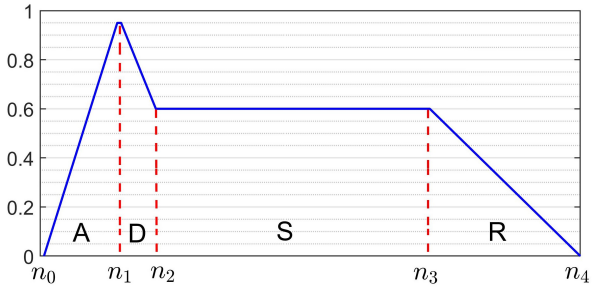

Figure 2.5: An ADSR amplitude envelope. (Tarr, 2018:382)

Attack (n_0–n_1): Also known as the *starting transient*, it is the portion of the envelope that rises from zero amplitude to the highest amplitude value. It is usually only a few tens of milliseconds in duration, and rich in inharmonic partials. (Howard & Angus, 2006:217, 229; Johnston & Johnston, 2009:305–306)

Decay (n_1–n_2): Once the attack has reached its apex, it quickly loses amplitude, this *slope* is known as the decay; the decay subsequently rests on the sustain/steady state. It must be noted that not all sounds have a distinct decay phase, especially sounds with a gradual or slow attack. (Bohn, 2016:decay)

Sustain/Steady State (n_2–n_3): Occurs when the signal amplitude maintains a relatively constant amplitude for an extended period of time. (Howard & Angus, 2006:217, 229; Johnston & Johnston, 2009:306)

Release (n_3–n_4): This is when the signal amplitude descends to zero, or when the sound energy returns to silence after the sustain/steady state phase. (Howard & Angus, 2006:217, 229; Johnston & Johnston, 2009:306)

2.1.4 Periodic Waveforms

Sine Wave: The properties of sine waves have been covered in Chapter 2.1.1.

Square Wave: These waveforms consist of a single positive and a single negative value, continuously alternating between each value. Square waves consist of multiple harmonic component frequencies that share an odd integer relationship with the fundamental frequency; these harmonics are in phase with the fundamental frequency. The harmonics decrease in magnitude as the frequency increases, thus sharing an inversely proportional relationship with the fundamental. For example, the third harmonic will have a magnitude value that is a third of the fundamentals. Qualitatively, the square wave is described as having a *hollow* timbre, similar to that of a clarinet. (Tarr, 2018:87–89; Russ, 2012:109–110; White & Louie, 2005:369)

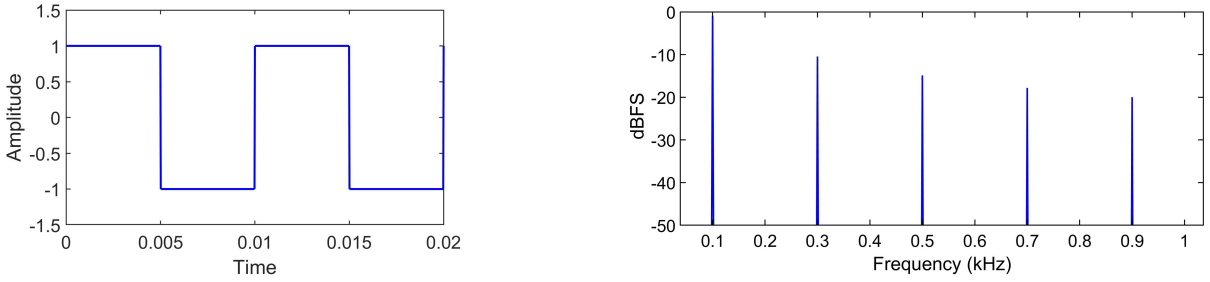

(a) Square wave in the time domain.

(b) Square wave in the frequency domain.

Figure 2.6: Square wave representations. (Tarr, 2018:87–89)

A square wave can be built by adding odd harmonics to a fundamental frequency *ad infinitum*; the inversely proportional relationship between the harmonic number and magnitude is described mathematically by Equations 2.4 & 2.5. Figure 2.6 depicts a line spectrum of a square wave, where the harmonics can be seen to decrease linearly. (Tarr, 2018:89–90)

$$Square(x) = \frac{4}{\pi}\left(\sin(x) + \frac{1}{3}\sin(3x) + \frac{1}{5}\sin(5x) + \ldots\right) \tag{2.4}$$

$$Square(x) = \frac{4}{\pi}\sum_{n=1,3,5\ldots}^{\infty}\frac{1}{n}\sin(nx) \tag{2.5}$$

Sawtooth Wave: This waveform has a linear rate of change between positive and negative values; when the wave's amplitude has reached its maximum value, it immediately returns to its minimum value and repeats the cycle. Sawtooth waves contain harmonics that are related at odd and even multiple integers to the fundamental; like the square wave these harmonics decrease in an inversely proportional manner, as can be seen in Figure 2.7. Equations 2.6 & 2.7 describe how sawtooth waveforms are constructed mathematically. (Tarr, 2018:91–93)

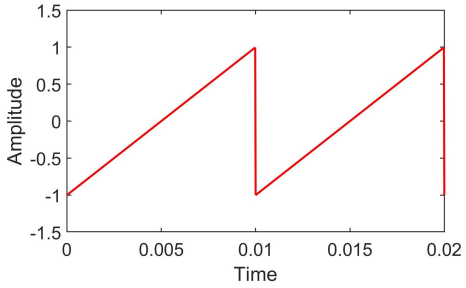

(a) Sawtooth wave in the time domain.

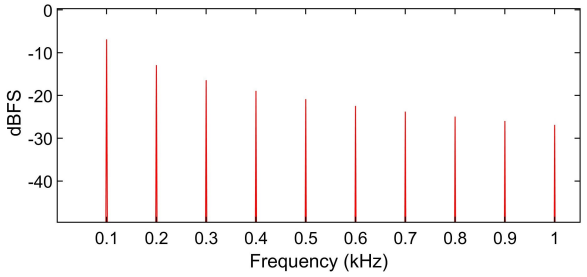

(b) Sawtooth wave in the frequency domain.

Figure 2.7: Square wave representations. (Tarr, 2018:91–93)

$$Sawtooth(x) = \frac{1}{2} - \frac{1}{\pi}\left(\sin(x) + \frac{1}{2}\sin(2x) + \frac{1}{3}\sin(3x) + ...\right) \tag{2.6}$$

$$Sawtooth(x) = \frac{1}{2} - \frac{1}{\pi}\sum_{n=1}^{\infty}\frac{1}{n}\sin(nx) \tag{2.7}$$

Triangle Wave: This waveform shares some similarities with sawtooth waves, though instead of instantaneously returning to its minimum, it gradually returns at the same slope gradient, resembling a triangle. The triangle wave contains only odd harmonics, the magnitudes of which are proportional to the inverse square of the harmonic number, as can be seen in Figure 2.8. Equations 2.8 & 2.9 describe how triangle waveforms are constructed mathematically. (Tarr, 2018:93–96)

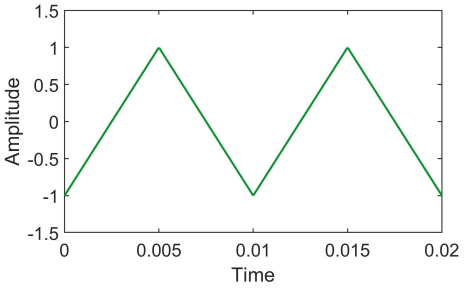

(a) Triangle wave in the time domain.

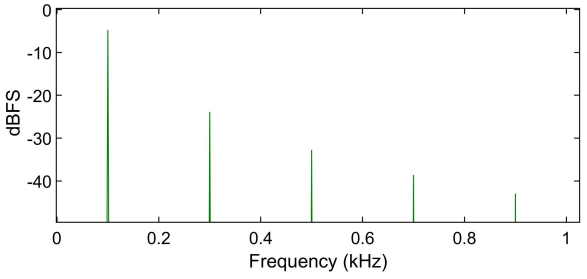

(b) Triangle wave in the frequency domain.

Figure 2.8: Triangle wave representations. (Tarr, 2018:93–95)

$$Triangle(x) = \frac{8}{\pi^2}\left(\sin(x) + \frac{1}{9}\sin(3x) + \frac{1}{25}\sin(5x) + ...\right) \tag{2.8}$$

$$Triangle(x) = \frac{8}{\pi^2}\sum_{n=1,3,5...}^{\infty}\frac{1}{n^2}\sin(nx) \tag{2.9}$$

Impulse Train: This periodic waveform is constructed digitally, when a single sample with an amplitude of 1 is followed by a series of samples with a value of 0. The pattern is then repeated and a periodic waveform is created (Figure 2.9a). The impulse train contains both odd and even integer related harmonics of the fundamental, all with equal magnitude to the fundamental (Figure 2.9b). (Tarr, 2018:96–99)

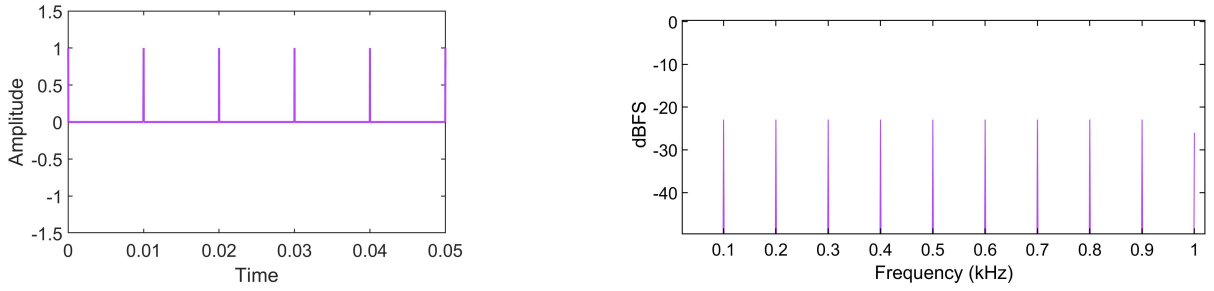

(a) Impulse train in the time domain.

(b) Impulse train in the frequency domain.

Figure 2.9: Impulse train representations. (Tarr, 2018:96–99)

2.1.5 The Decibel

The amplitude of a waveform is a measure of the strength of a sound, or the *quantity* of sound present. As sound is something that moves through time, the rate of *energy transfer* is of concern. Specifically, the magnitude of energy transferred per unit of time, or the number of joules per second (measured in watts) that are propagated. As sound is a spacial or three dimensional phenomenon, the rate of energy transfer is described with respect to area, this is known as *sound intensity*. Sound intensity can be defined as the net flow of acoustic energy in a sound field, measured in watts per square meter. The sound intensities encountered in the real world have enormous variances, in the order of a trillion (10^{12}) to one. For example, the threshold of human hearing is approximately 10^{-12} W/m^2, with pain being induced (because of loudness) at approximately 10 W/m^2. As this is a rather unwieldy range of values, a novel approach to measuring sound intensity is used instead. (White & Louie, 2005:19, 360; Howard & Angus, 2006:14–15)

The *Bel*[2] is a *logarithmic scale* that expresses the ratio of two intensities; its purpose is to mitigate the difficulties in working with large variations in intensity levels. Moreover, as the ratio of intensities produced by the Bel can be awkward to use in practice, it is divided into ten *decibels* (dB) for convenience. Coincidentally, the decibel closely corresponds to the human perception of *loudness* and therefore finds utility in many audio technology applications. A decibel is a unit that is 10 multiplied[3] by the logarithm (base 10) of the ratio of two quantities of intensity or power. Equation 2.10 describes how the *sound intensity level* (SIL) is derived from the ratio of the measured power density (I_{mes}) to a reference intensity[4] (I_{ref}) of 1 pW/m^2 (10^{-12} W/m^2). The result of Equation 2.10 does not refer to an absolute intensity, but a ratio of two different intensities, I_{mes} would be x dB above I_{ref}. Sound intensity level is a difficult

[2] Named after Alexander Graham Bell (1847-1922), the inventor of the telephone.
[3] The factor of 10 is added in order to accommodate the conversion of Bels into decibels.
[4] In this instance, the reference intensity is an approximation of the threshold of human hearing.

phenomenon to measure, instead *sound pressure level* (SPL) is commonly used; SPL can also be expressed in decibels.

It is important that a distinction be made between SIL and SPL. SIL refers to the acoustic energy transfer in a sound field, while SPL is the pressure differential between the compressions and rarefactions of a sound wave. This differential in pressure is used to quantify the *strength* of a particular sound. Acoustic power is proportional to the square of acoustic pressure[5], resulting in a modification of the defining equation, as seen in Equation 2.11.

Here P is the acoustic pressure, measured in micropascals (µPa); P_{ref} is assigned a value of 20 µPa, this is the approximated threshold of human hearing at 1 kHz. Therefore, if the pressure were to increase by a factor of 10, the intensity would increase by a factor of 100, resulting in an increase of 20 dB, as exemplified in Equation 2.11. (Everest & Pohlmann, 2014:19–23; Howard & Angus, 2006:16–18; Moore, 2012:10–11)

$$SIL(dB) = 10\log_{10}\left(\frac{I_{mes}}{I_{ref}}\right) \tag{2.10}$$

$$SPL(dB) = 10\log_{10}\left(\frac{P_{mes}}{P_{ref}}\right)^2 = 20\log_{10}\left(\frac{P_{mes}}{P_{ref}}\right) = 20\log_{10}\left(\frac{P_{mes}}{20\mu Pa}\right) \tag{2.11}$$

2.2 Foundations of Electronics

2.2.1 Basic Electrical Laws

Within all electronic circuits, there are three basic properties that are observed. These are *voltage* (V), *current* (I), and *resistance* (R), and are described below.

Voltage is the energy required to move a quantity of charge to a higher potential. Additionally, it can also be regarded as the energy released when a unit of charge moves from a higher potential to a lower potential. For this reason, voltage is also often referred to as *potential difference*. Voltage can be thought of as the force applied to cause a current to flow. (Horowitz & Hill, 2015:1–2; Laplante, 2005:735)

Current is the flow rate of electric charge through a discrete point in a circuit. Current is measured in *amperes* (A), 1 A is the equivalent of 1 coulomb of charge per second. Current is assigned an I or i symbol for equations. (Horowitz & Hill, 2015:2; Laplante, 2005:163)

Resistance is an opposition to the flow of current; the electrical current flowing through a point is proportional to the voltage across it. Resistance is measured in *Ohms*[6] and is assigned the Ω symbol as a unit of measure. (Horowitz & Hill, 2015:3–4; Laplante, 2005:588)

[5] The *Pascal* is used to measure pressure and is equal to one Newton per square metre (1 N/m^2).

[6] Named after German physicist Georg Simon Ohm, who discovered the laws relating voltage, current, and resistance.

The behaviour of voltage and current obey a particular set of physical laws. *Kirchoff's current law* states that there is a conservation of charge within a circuit. The sum of current entering a point (or component/node) in an electronic circuit equals the current exiting that point. Likewise, *Kirchoff's voltage law* states that the sum of all voltage drops within a closed circuit are equal to zero. (Horowitz & Hill, 2015:2)

Power (P) is the rate of time at which energy is expended or absorbed (or the ratio of energy transfer to time) by an electronic device; it is assigned the *watt* (W) as a unit of measure. Power can be related to voltage, current, and resistance. For example, 1 W of power is equivalent to the power dissipated by 1 Ω of resistance when 1 A of current flows through it. This relationship is exemplified in Equations 2.12, 2.13, & 2.14. (Alexander & Sadiku, 2012:10-11)

$$P = I.V \tag{2.12}$$

$$P = I^2.R \tag{2.13}$$

$$P = \frac{V^2}{R} \tag{2.14}$$

Ohm's law states that the voltage measured between two points in a circuit is directly proportional to the current flowing through those points (Equation 2.15). If the resistance is held at a constant value, then Equations 2.16, 2.17, & 2.18 can be used for calculations. (Alexander & Sadiku, 2012:30–31)

$$I \propto V \tag{2.15}$$

$$I = \frac{V}{R} \tag{2.16}$$

$$V = I.R \tag{2.17}$$

$$R = \frac{V}{I} \tag{2.18}$$

Current can flow within a conductor in two ways, namely *direct current* (DC), and *alternating current* (AC). DC is analogous to the flow of water, where the current moves in one direction only. The unidirectional flow of current from the positive to the negative terminal of a battery is an example of DC. Conversely, AC changes polarity periodically, which gives rise to the formation of a periodic waveform. An acoustic signal transduced into an electrical signal is an example of AC. (Alexander & Sadiku, 2012:7–12) Positive electrical current flows towards the point of lowest potential within a circuit. This point is known as ground and is often used as the reference point to measure voltages in electronic circuits. As ground is significant as a reference node in schematic diagrams, it is assigned a symbol, as illustrated in Figure 2.10. (Alexander & Sadiku, 2012:83)

Figure 2.10: Symbol for indicating ground. (IEEE Std 315, 1975:3.9.1)

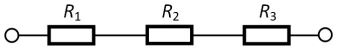

(a) Resistors in series.

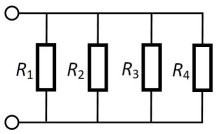

(b) Resistors in parallel.

Figure 2.11: Resistor configurations with symbol indicating resistor. (IEEE Std 315, 1975:2.1.1)

2.2.2 Resistance

The *resistor* is a component that is used to control the voltage and current in various stages of a circuit. Resistors function by dissipating power as heat and are often specified to be of a certain tolerance. Resistors can be connected in series or parallel, as demonstrated by Figure 2.11. For a series configuration, the total resistance is the sum of all the resistors, and is described in Equation 2.19. While resistors in a parallel configuration can be calculated using Equation 2.20. Resistors can also be used to create *voltage dividers* (Figure 2.12a) which are implemented in electronic circuits. For example, when provided a certain input voltage (V_{in}), a voltage divider delivers a portion of the input voltage as output voltage (V_{out}), this phenomenon is described by Equation 2.21. Voltage dividers can also be constructed from a *variable resistor* to make a *potentiometer* which is often implemented as volume and tone controls on audio devices. A potentiometer consists of an input at pin 1; with a variable output at pin 2, this is a attached to a *wiper* which is mechanically adjusted to give a desired output; pin 3 is usually connected to ground. The closer the wiper gets to pin 1, increased signal will be output to pin 2; conversely as the wiper approaches pin 3, the signal coming out of pin 2 will begin to attenuate. The schematic symbol is indicated in Figure 2.12b, Figure 2.12c shows the internal mechanism of a rotary potentiometer. (Horowitz & Hill, 2015:5–8)

$$R_{series} = R_1 + R_2 + R_3 + \ldots \tag{2.19}$$

$$\frac{1}{R_{parallel}} = \frac{1}{R_1} + \frac{1}{R_2} + \frac{1}{R_3} + \ldots \tag{2.20}$$

$$V_{out} = \frac{R_2}{R_1 + R_2}.V_{in} \tag{2.21}$$

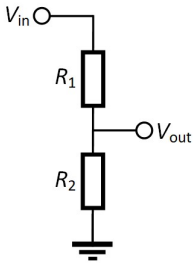

(a) Voltage divider circuit.

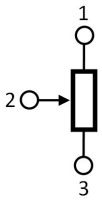

(b) Potentiometer symbol.

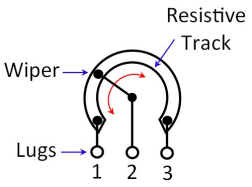

(c) Potentiometer construction.

Figure 2.12: Voltage dividers and potentiometers. (IEEE Std 315, 1975:2.1.3)

2.2.3 Capacitance

While the resistor is a common component amongst DC and AC circuits, circuits that employ AC can employ two passive further circuit components, the *capacitor* and the *inductor*. These components differ from resistors in that they store energy for use at a later time. A capacitor is a passive component that can store energy in an electric field; Figure 2.13 indicates the schematic symbol for the capacitor. Capacitance (C) is measured in *Farads*[7] and constructed from two closely spaced metal plates (usually aluminium foil) separated by an insulator or *dielectric*. A lead is attached to each piece of foil, and the foils and dielectric are wrapped around each other to make a compact component. The plates accumulate charge when a voltage is applied and become oppositely charged. Equation 2.22 describes this process mathematically; a capacitor with a voltage across its terminals has $+Q$ coulombs of charge on one plate and $-Q$ on the other. The charge on each conductor plate, and the voltage across each conductor, form a proportionality constant; this is by definition what capacitance is. The amount of capacitance of a capacitor depends primarily on its physical dimensions. (Alexander & Sadiku, 2012:216–217; Horowitz & Hill, 2015:18–20; Laplante, 2005:94)

$$Q = C.V \tag{2.22}$$

$$C = \frac{\epsilon.A}{d} \tag{2.23}$$

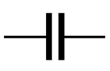

(a) Non-polarised.

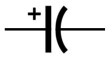

(b) Polarised.

Figure 2.13: Capacitor schematic diagram symbols. (IEEE Std 315, 1975:2.2.1-2.2.2)

[7] This unit of measure is named after renowned physicist Michael Faraday.

The following three factors determine the capacitance of a capacitor (described in Equation 2.23). The plate surface area (A); the larger the surface area, the greater the capacitance. The distance between the plates (d); a small distance results in higher capacitance. The permittivity[8] (ϵ) of the dielectric; higher permittivity results in increased capacitance.

If the voltage across a capacitor is time-invariant, no current will be able to flow through it; the capacitor is like an open circuit to DC. The capacitor will begin to charge if a DC voltage is connected across it, and resist abrupt changes in voltage. Ideal capacitors do not dissipate energy, and only consume energy when charging, and discharge energy when distributing power to the circuit. However, real-world capacitors have slight resistive properties and typically dissipate a small quantity of power. This phenomenon can be modelled as a resistor in parallel with an ideal capacitor. Like the resistor, capacitors can be configured in series or parallel. In series (Figure 2.14a) capacitance can be calculated by adding the reciprocal of the sum of the reciprocal of the individual capacitors (Equations 2.24 & 2.25). Capacitors in parallel (Figure 2.14b) can be calculated by summing the value of each individual capacitor (Equation 2.26). Interestingly, capacitors in parallel combine like resistors in series, and capacitors in series combine like resistors in parallel. (Horowitz & Hill, 2015:19–21)

$$\frac{1}{C_{total}} = \frac{1}{C_1} + \frac{1}{C_2} \tag{2.24}$$

$$C_{total} = \frac{C_1.C_2}{C_1 + C_2} \tag{2.25}$$

$$C_{total} = C_1 + C_2 + C_3 + ... + C_N \tag{2.26}$$

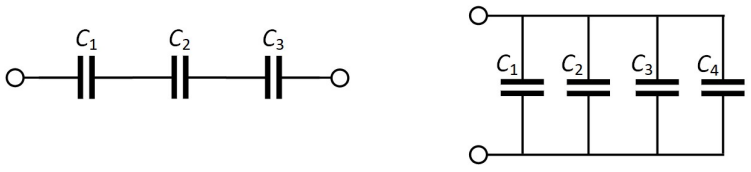

(a) Capacitors in series. (b) Capacitors in parallel.

Figure 2.14: Capacitors in series and parallel.

[8] This is how easily polarised the dielectric material between the plates is.

2.2.4 Inductance

Like the capacitor, the inductor is a passive component; inductors store energy in magnetic fields that are generated when current flows through them. Inductance (L) occurs when a conductor opposes the change of electric current flowing through it. Inductors are constructed from a coil of wire wound in a cylindrical shape around a core; although, all conductors exhibit a certain level of inductance. The unit of measurement used for inductance is the *Henry*[9] (H). If current passes through an inductor, the voltage across the inductor is directly proportional to the rate of change of current; or 1 H is equal to 1 volt-second per ampere. Like the capacitor, the inductance of an inductor depends its the physical properties and construction. With reference to Equation 2.27, inductance may be increased by increasing the cross sectional area (A), increasing the number of turns in the coil (N), reducing the length of coil (l), and by using a core with a high level of permeability (μ). The equivalent inductance of inductors connected in series (Figure 2.15a) is equal to the sum of all the individual inductances (Equation 2.28); while in parallel (Figure 2.15b) it is the reciprocal of the sum of the reciprocal of the individual inductances (Equations 2.29 & 2.30). It can be observed that inductors in series are calculated similarly to resistors in series, and inductors in parallel are calculated similarly to resistors in parallel. (Alexander & Sadiku, 2012:226-228)

$$L = \frac{N^2.\mu.A}{l} \tag{2.27}$$

$$L_{total} = L_1 + L_2 + L_3 + ... + L_N \tag{2.28}$$

$$\frac{1}{L_{total}} = \frac{1}{L_1} + \frac{1}{L_2} \tag{2.29}$$

$$L_{total} = \frac{L_1.L_2}{L_1 + L_2} \tag{2.30}$$

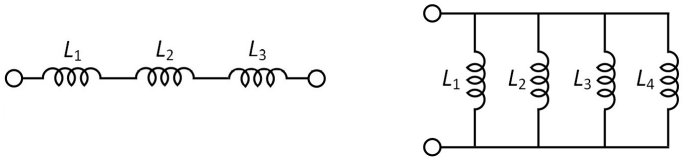

(a) Inductors in series. (b) Inductors in parallel.

Figure 2.15: Inductors in series and parallel, with schematic diagram symbol. (IEEE Std 315, 1975:6.2)

[9] This unit of measure is named after American scientist Joseph Henry.

2.2.5 Impedance

Impedance (Z) is the ratio of AC current to AC voltage; it is the ability of a circuit to conduct AC current for a particular AC voltage. Impedance can be thought of as AC *resistance*, where the resistance experienced by a current is a function of frequency. While resistance concerns only a particular *magnitude*, *impedance* affects both *magnitude* and *phase*; the behaviour of these circuits depends on voltage frequency. To understand the concept of impedance satisfactorily, a digression into the concept of *complex numbers* is necessary. These numbers have their origins in the notion of $\sqrt{-1}$ (or the square root of any negative number). While the *real numbers* exist on a horizontal number line, the *imaginary numbers* exist on another number line perpendicular to the real number line; both have their origin at the 0 (which is both imaginary and real). This gives rise to a set of axes, the *imaginary axis* and the *real axis*, this forms what is known as the *complex plane*, and every complex number corresponds to a point on the *complex plane*. Consequently, a complex number is a combination of a real number and an imaginary number, as represented in Equation 2.31. Equation 2.31 is the rectangular form of a complex number[10], $j = \sqrt{-1}$; z is the symbol for a complex number, with x the real part of z, and y the imaginary part of z. Moreover, in the context of complex numbers, x and y are not co-ordinates or locations (although there are some notable similarities), but the real and imaginary components of z on the *complex plane*. (Weisstein, 2002:493-494; Alexander & Sadiku, 2012:376-377)

$$z = x + jy \tag{2.31}$$

Due to the nature of impedance, it is represented as a complex value; resistance being the real component and *reactance* (X) the imaginary component. Both inductors and capacitors exhibit reactance, resulting in their voltage and current being 90° out of phase with each other. An inductive impedance has a current that follows behind the voltage, while a capacitive impedance has a voltage that follows behind the current. Impedance can be represented by a complex quantity in the rectangular form, as can be seen in Equation 2.32. The reactance is a magnitude (a positive value); a positive j value is associated with inductance, and a negative j value is associated with capacitance. Ohm's law can be adapted for use with impedance, Equation 2.33 can be used to calculate the inductive impedance, while Equation 2.34 can be used to calculate capacitive impedance.

$$Z = R \pm jX \tag{2.32}$$

$$\frac{V}{I} = j.\omega.L \tag{2.33}$$

$$\frac{V}{I} = \frac{1}{j.\omega.C} \tag{2.34}$$

[10] In the engineering sciences j is used in place of i so as to not confuse it with the symbol for electrical current.

$$X_C = \frac{1}{\omega.C} \tag{2.35}$$

Reactance can be thought of as a resistance that varies with frequency; it will increase in an inductor proportionally to an increase in frequency, and decrease in a capacitor proportionally to an decrease in frequency. This phenomenon can be elaborated upon in Equation 2.35 where it can be observed that a larger capacitance results in a lower reactance. If the value of a capacitor is doubled, the amount of current required to charge and discharge the capacitor at the same voltage swing within the same duration of time would also double. Doubling the frequency of the voltage (which doubles its rate of change), while keeping the value of the voltage constant, requires that the amount of current is also doubled, resulting in half the reactance. (Horowitz & Hill, 2015:40–42)

2.2.6 Filters

An important application of resistors, capacitors, and inductors is their ability to form frequency dependant voltage dividers, these are frequently used as *audio filter circuits*[11]. A filter circuit is designed to either pass or attenuate certain *frequencies of interest*, it is a frequency selective device. These *frequencies of interest* can be differentiated into either a *pass band*, or a *stop band*. A pass band is the range of the frequencies that are able to pass through the filter, while the stop band is the attenuated range of frequencies. An ideal pass band would separate from the stop band in a discrete section, in reality filters have a pass band that tapers off in the form of a slope. The *cutoff frequency* occurs when the signal first drops 3 dB below the nominal amplitude level of the filter as the frequency moves into the stop band; the *bandwidth* can be described as the range of the upper and lower bounds of the pass band. (Horowitz & Hill, 2015:48–50; Mcmanus, 2008:785–787)

The *frequency response* of a circuit describes the variation in behaviour depending on changes in input frequency; provided the amplitude of the input signal remains constant. These are typically represented in what is referred to as a *Bode plot*, these can be described as a graphical characterisation of a system's inherent frequency response, the plot includes both the magnitude and phase angle, an example is provided in Figure 2.16.

$$H(\omega) = \frac{V_{out}}{V_{in}} \tag{2.36}$$

The *transfer function* represented as $H(\omega)$ in Equation 2.36, and can be described as the ratio of frequency dependant output signal to input signal, it has both a magnitude and phase component. The *cut off frequency* is represented as ω_c, and the *centre frequency* is represented as ω_0, the point of which will be elaborated on in the following section. For simple RC circuits the cutoff frequency can be calculated using Equation 2.37. (Horowitz & Hill, 2015:48–50; Alexander & Sadiku, 2012:635; Laplante, 2005:73, 279)

[11] These types of filters are known as *passive filters*, an *active filter* would include an amplifier or active element in the circuit.

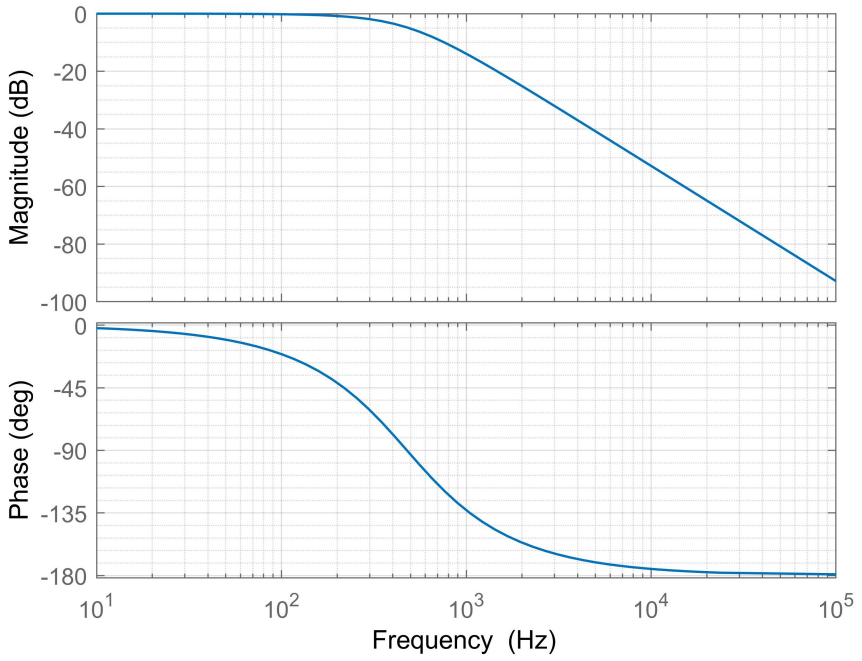

Figure 2.16: An example of a Bode plot diagram. (Mcmanus, 2008:707)

$$f_{3dB} = \frac{1}{2\pi.R.C} \tag{2.37}$$

There are four fundamental types of filters, these are described as follows.

Low Pass Filter: This filter type passes frequencies from DC, or the lowest frequency component of the signal, all the way up to ω_c. The transfer function of a low pass filter can be calculated using Equation 2.38 , while the circuit diagram and Bode plot can be seen in Figure 2.17. (Alexander & Sadiku, 2012:638–639)

$$H(\omega) = \frac{1}{1 + j\omega.R.C} \tag{2.38}$$

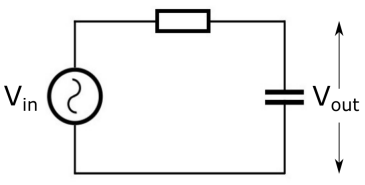

(a) Circuit diagram of a low pass filter.

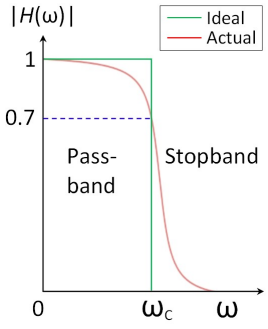

(b) Bode plot of a low pass filter.

Figure 2.17: Low pass filter.

High Pass Filter: This type of filter passes all frequencies above the cutoff frequency, the characteristics of which are the inverse of a low pass filter. The transfer function of a high pass filter can be calculated using the formula in Equation 2.39, while the circuit diagram and Bode plot can be seen in Figure 2.18. (Alexander & Sadiku, 2012:639)

$$H(\omega) = \frac{j\omega.R.C}{1+j\omega.R.C} \tag{2.39}$$

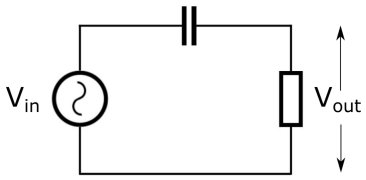

(a) Circuit diagram of a high pass filter.

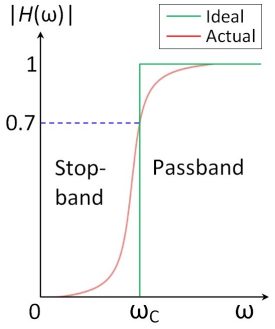

(b) Circuit diagram of a high pass filter.

Figure 2.18: High pass filter. (Alexander & Sadiku, 2012:639)

Band Pass Filter: These types of filters can be thought of as an amalgamation of low pass and high pass filters; and can be defined as a band that extends between two cut-off frequencies that are allowed to pass. This frequency band is given as $\omega_1 < \omega < \omega_2$ centred on a frequency of ω_0, which can be calculated from Equation 2.40; Equation 2.41 gives the formula of the transfer function of a band pass filter while the circuit diagram and Bode plot can be seen in Figure 2.19. (Alexander & Sadiku, 2012:639–640)

$$\omega_0 = \frac{1}{\sqrt{LC}} \tag{2.40}$$

$$H(\omega) = \frac{R}{R+j(\omega.L-1/\omega.C)} \tag{2.41}$$

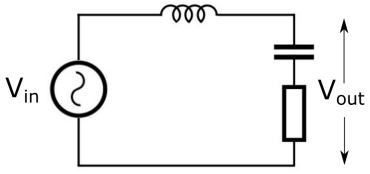

(a) Circuit diagram of a band pass filter.

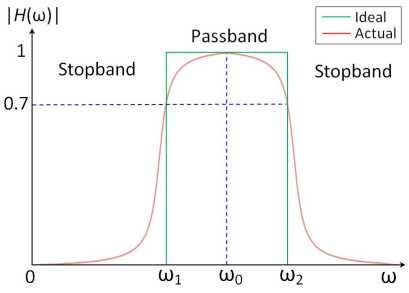

(b) Circuit diagram of a band pass filter.

Figure 2.19: Band pass filter. (Alexander & Sadiku, 2012:639–640)

Band Stop Filter: These are analogous to the inverse of a band pass filter, where a band of frequencies centred on ω_0 attenuates all frequencies within that particular band. Equation 2.42 is the formula of the transfer function of a band pass filter, while the circuit diagram and Bode plot can be seen in Figure 2.20. (Alexander & Sadiku, 2012:640–641)

$$H(\omega) = \frac{j(\omega.L - 1/\omega.C)}{R + j(\omega.L - 1/\omega.C)} \tag{2.42}$$

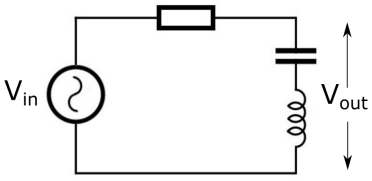

(a) Circuit diagram of a band stop filter.

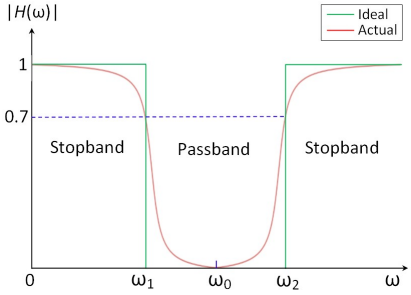

(b) Circuit diagram of a band stop filter.

Figure 2.20: Band stop filter. (Alexander & Sadiku, 2012:640–641)

2.2.7 Transformers

Whenever an electrical current flows through a conductor, a *magnetic field*[12], the strength of which corresponds to the amount of current flowing through the conductor. This magnetic field is known as *magnetic flux*; it emerges perpendicular to the flow of current through the conductor, with the direction of the flow of current influencing the *magnetic polarity*, which is the direction that the flux rotates around the conductor. If an AC current passes through a conductor, the instantaneous polarity and intensity of the flux will vary in proportion to the current and direction of the AC current. Similarly, if a conductor is exposed to a changing magnetic flux, a voltage will be induced across the conductor that is directly proportional to this rate of change. There is an inductive reactance between the induced voltage and the current already flowing through the conductor. The density of the magnetic flux generated by an inductor is directly proportional to the number of turns of wire that make up the inductor. The *magnetic flux density*[13] is affected by factors like the properties of the material in the flux's path, the physical dimensions of the inductor, and the nature of the coil winding. Therefore, if two coils are adjacent, AC current in one coil will induce AC voltage in the other coil; this is the basic principle behind the *transformer*. (Whitlock, 2008:275)

A transformer is constructed from two (or more) coils that are wound around a metallic core, these two coils are referred to as the *primary winding* and *secondary winding*. An AC voltage source is ordinarily connected to the primary winding, with the secondary winding connecting to the load of the circuit. Transformers are used primarily in three applications, namely *mains*

[12] "[M]agnetic force field where lines of magnetism exist." (Laplante, 2005:417)

[13] "[A] vector quantifying a magnetic field, so that a particle carrying unit charge experiences unit force when travelling with unit velocity in a direction perpendicular to the magnetic field characterised by unit magnetic flux density. It has the units of volt-seconds per square meter in the SI system of units." (Laplante, 2005:417)

power transmission, *power electronics*, and *impedance matching*[14] for signal transmission to ensure maximum power transfer.

When an AC voltage is applied across the primary winding, an AC voltage will subsequently appear across the secondary winding. The voltage across the secondary winding will correspond in multiples proportional to the turns ratio of the transformer, conversely the current flowing through the secondary will correspond in an inversely proportional manner, with power typically being conserved. A transformer with a primary winding of a 100 turns, and secondary of 50 turns, is considered a *step down transformer* with a ratio of $2:1$. If a voltage of 100 V is applied across the primary, 50 V will appear across the secondary. A transformer with a primary winding of a 100 turns, and secondary of 200 turns, is considered a *step up transformer* and has a ratio of $1:2$. If a voltage of 10 V is applied across the primary, 20 V would appear across the secondary. Furthermore, as transformers do not generate their own power, the available output power from the secondary winding of an ideal transformer is equivalent to the input power available at the primary; it must be noted that a real world transformer will dissipate a minuscule quantity of power. (Whitlock, 2008:275–276; Hurley & Wölfle, 2013:95–96)

Transformers *reflect* impedance from the primary winding to the secondary winding at the square of their turns ratio; this relationship is described in Equation 2.43, where Z_p is the primary impedance, Z_s is the secondary impedance, and $\frac{N_p}{N_s}$ the turns ratio (which is equivalent to the voltage ratio). If the aforementioned ideal $1:2$ transformer[15] has a $20\,\Omega$ load placed across its secondary winding, 1 A of current will flow from the secondary, and the transformer will dissipate 20 W of power. The primary will need to draw 2 A of current with an input voltage of 10 V, with the power equal to 20 W; from the perspective of the primary, the load appears to be $5\,\Omega$. While the voltage ratio of the transformer is $1:2$, the *impedance ratio* of the transformer would be $1:4$; a transformer thus converts both voltage and impedance. (Laplante, 2005:701; Alexander & Sadiku, 2012:574–577)

$$\frac{Z_p}{Z_s} = \left(\frac{N_p}{N_s}\right)^2 \tag{2.43}$$

In the ideal transformer example used previously, the wire used for the winding could have been an infinitely small diameter and could be wound around a core that is also infinitely small. In such a scenario, there would be enough primary inductance to provide the required excitation current, therefore the flux density would be unaffected by any load current. However, real transformers have to contend with *winding resistance*. Winding resistance occurs in both the primary and secondary winding and results in impaired performance such as voltage drops, loss of signal integrity in audio transformers, and overheating in power transformers. In order to mitigate the adverse effects of the winding resistance, the use of thicker wire, and fewer turns in the construction of the transformer can be employed, though these techniques often result in larger and more massive transformers. The effect of winding resistance can be modelled as a resistor (R_p) on the primary winding, and another resistor (R_s) on the secondary winding. (Whitlock, 2008:280–281)

[14] This is especially relevant to audio applications as often different devices with vastly differing input and output impedance will need to be interfaced with one another.

[15] With 10 V applied to the primary, there will be 20 V at the secondary.

Real transformers do not not have infinite primary inductance, a small *excitation current* will always flow through the primary winding when no load is connected to the secondary winding. If a load is connected across the secondary winding, current will pass through it, flowing in the opposite direction to the primary winding, and the magnetic flux will flow in opposition to the excitation flux, as illustrated in Figure 2.21. This results in a reduction of the impedance of the primary winding, causing additional current to be drawn from the source. This process reaches a point of equilibrium when the additional flux sufficiently matches the flux generated by the secondary. (Whitlock, 2008:275–277)

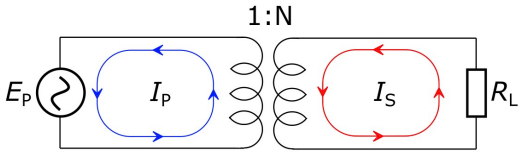

Figure 2.21: Load current nullifying the generation of flux . (Whitlock, 2008:277)

Excitation current and flux share an inverse relationship to frequency; if the primary winding of a transformer is held at a constant voltage (E_p), and the frequency is increased, the excitation current (I_p) and flux of the transformer will decrease linearly due to the primary inductance. If the voltage across the primary winding is held constant, the I_p and flux will halve in value if the frequency is doubled. As the transformer relies on the phenomenon of inductive reactance to function, I_p will be 90° out of phase with E_p and the secondary voltage (E_s). As the slew rate of a sine wave of constant amplitude, increases linearly with frequency, the rate of change of the flux stays constant. The slope or shape of the waveform is invariant as the frequency changes, as the voltage induced across the secondary winding is proportional to the slope (or rate of change) of the flux induced at the primary winding; resulting in the output voltage retaining its shape, hence the response is linear. (Whitlock, 2008:277)

All transformers are limited by a number of unavoidable parasitic elements; the interactions of which tend to react in a complex manner. Parasitic elements are simpler to mitigate on mains supplied power transformers, especially when compared to audio frequency transformers that cover the bandwidth of the human hearing range. Transformer designs that are optimised for low frequency response often result in a deterioration of high frequency response; likewise, designs that are optimised for high frequency response often exhibit a deterioration in low frequency response. It is optimal for a transformer to be designed with negligible levels of excitation current to avoid loading the source excessively. The excitation current at the primary winding can be reduced by increasing the value of inductance of the primary winding, as a considerable amount of inductance is required for a transformer to operate optimally at low frequencies. There are generally two methods to achieve this, increased turns could be used on the primary and secondary windings, although this is generally not always practically feasible. Another method would be to wind the primary and secondary coils around a highly magnetic *core*, which can increase the inductance by a factor of 10 000; a core can be any material placed inside a coil. (Whitlock, 2008:277-278)

Not all flux generated by a transformer is used, the flux that is generated by one winding is not always coupled to the other winding; uncoupled flux gives rise to an inductance on that particular winding in a phenomenon known as *leakage inductance*. As is the case with reflected

impedance, this inductance is reflected at the square of the turns ratio at the adjacent winding. The physical spacing and positioning of the primary and secondary windings determines the efficacy of the flux coupling. The most efficient means of achieving the lowest levels of leakage inductance is to wind both coils in close proximity on a common axis. *Interleaved windings* can also reduce leakage inductance, this technique involves layering the primary and secondary windings in multiple sections, resulting in a notable reduction in leakage inductance as the number of interleaves increases. Transformers are wound with fine, thinly insulated wire; as these wires are in close proximity to one another, *winding capacitances* can become problematic[16]. Capacitance can also arise between the primary and secondary windings, which can negatively affect the frequency response of a transformer. This can be remedied by placing a layer of shielding between the windings, a *Faraday shield*[17] can absorb the capacitative current that would typically flow between the windings. (Whitlock, 2008:281–283)

There are many similarities between electrical and magnetic circuits. For instance, the magnetic flux flows along a closed loop from one pole to another and always follows the path of least resistance. Within magnetic circuits, the *magnetising force*[18] (H) is analogous to voltage, which is directly proportional to *ampere turns*[19], and inversely proportional to the *flux path length* (l). The *flux density* (B) is the equivalent of electric current density, and corresponds to the density of flux lines per square unit of area. The relationship between field intensity and flux density can be plotted graphically as can be seen in Figure 2.22a, where the slope of the graph represents the *permeability* (μ) of the magnetic material, which is a measure of how magnetically conductive the core material is, the graph is known as a *hysteresis*[20] *loop* or BH loop. (Whitlock, 2008:278–279)

Generally non-magnetic materials such as air, plastic, aluminium, copper, brass, etc. have a permeability value of 1, while common ferro-magnetic materials such as steel have a permeability of approximately 300. Certain specialised materials can have permeability values that are far greater, for example, 4 % silicon steel has a permeability value of 5 000, while some alloys of nickel, iron, and molybdenum can have permeability ratings approaching 100 000. Materials that increase the permeability to such a degree vastly increase the concentration of magnetic flux and the inductance of the coil. The inductance of the coil increases with the square of the number of turns and has a directly proportional relationship to the permeability of the core. (Whitlock, 2008:278–279)

There are three general properties that describe the nature of a hysteresis loop; the flux density saturation points (B_{sat}), the slope of the BH curve (μ), and the coercive force (H_c). It can be observed from the hysteresis loops in Figure 2.22 that as the magnetising force is increased from 0, it eventually reaches a point where the flux density begins to taper off, any increase in

[16] This type of capacitance is also mitigated by using interleaved coils.

[17] "[A]n electrostatic (E field) shield made up of a conductive or partially conductive material or grid. A Faraday cage or screen room is effective for protecting inside equipment from outside radiated RF energies." (Laplante, 2005:252)

[18] This is also referred to as the *magnetic field intensity*

[19] This is the current flowing in the coil (I) multiplied by the number of turns (N).

[20] "(1) [T]he phenomenon that the magnetic state of a substance is dependent upon its magnetic history, so that its magnetisation for an increasing magnetising force differs from that for a decreasing magnetising force.(2) [T]he characteristic of magnetic materials that causes the trajectory of the flux density vs. field intensity curve as the intensity is increased to be different from that when the intensity is decreased, giving rise to a loss, which is proportional to the area enclosed by the two trajectories." (Laplante, 2005:335)

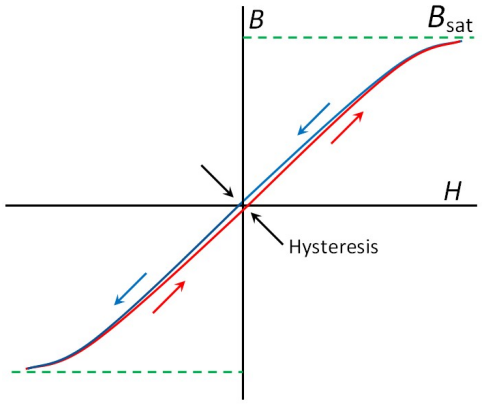

(a) Hysteresis loop of a magnetic core material. (Whitlock, 2008:278)

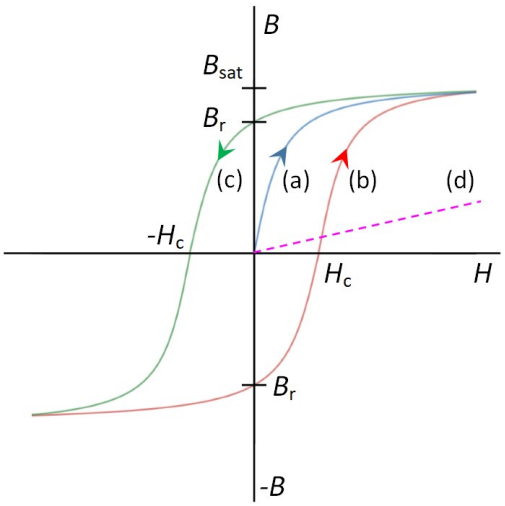

(b) Hysteresis loop of a highly hysteretic magnetic substance. (Hurley & Wölfle, 2013:9)

Figure 2.22: Examples of hysteresis loops.

the magnetising force above this point results in a negligible increase in the flux density. It is at this this point, that the magnetic material is said to *saturate*, as a result of this phenomenon the permeability of the magnetic core is reduced until it reaches full saturation, at this point it reaches the permeability of air. If a magnetising force is applied to a magnetic substance with a high level of hysteresis, it will remain magnetised even as the magnetising force is removed. High hysteresis magnetic substances are used in permanent magnets, and magnetic memory (or recording) devices; these substances tend to have wide or square hysteresis loops as illustrated in Figure 2.22b. In this example a completely demagnetised core has its flux density increased by increasing its magnetising force, this follows the curve indicated at (a) in the example. Once again the magnetising force saturates the flux density at B_{sat}, as the magnetising force is decreased, the flux density will follow the curve at (c). Eventually the magnetising force will reach its zero point, however there remains a residual flux density in the magnetic core material, this flux density is known as the *remanence*[21], indicated by B_r and -B_r in the diagram. For the flux density to once again reach a value of 0, a negative quantity of magnetising force is required, with -H_c commonly referred to as the *coercive force*. Eventually curve (c) will saturate again at -B_{sat}, a positive coercive force will need to be applied to return the core material to a zero flux value, this is indicated by curve (b) in the diagram. If the magnetising force is varied periodically, a fixed cyclical hysteresis loop pattern will occur. The line at (d) indicates what the BH curve would look like if there was no magnetic core material, observed to be highly linear but with a minutia of flux density, the inclusion of a magnetic core yields far greater values of flux density for a given magnetising force. The magnetic core material typically utilised in transformers has an inherently non-linear response, but can be considered approximately linear up until B_{sat}, but in the majority of designs B_{max} will be below this level. (Hurley & Wölfle, 2013:7–9; Whitlock, 2008:278–279)

[21] "(1) [I]n a ferromagnetic material, the value of the magnetic flux density when the magnetic field intensity is zero. (2) the magnetic induction (B) of a magnet after the magnetising field is removed and an air gap (hence self-demagnetising field) is introduced to the magnetic circuit. Also called retentivity or residual induction." (Laplante, 2005:586)

Conversely, specialised materials exist that are considered virtually non-hysteretic, these materials exhibit extremely low levels of remanant flux density once the magnetising force is removed. It is impossible to eliminate hysteresis completely, but its effects can be mitigated through the use of specialised metallic alloys. The hysteresis observed in transformers is problematic as the frequency response of the transformer becomes non-linear, resulting in harmonic distortion. At the centre of the hysteresis loops in Figure 2.22 is the zero signal point (the net magnetising force is 0) or what is known as the *magnetic operating point*. The arrows on each diagram indicate the direction that AC current will follow, with the amplitude of the AC being proportional to the magnitude of the loop. If an AC current increases in amplitude, it may approach the *saturation point* at the end of each hysteresis loop. The type of distortion that would be generated from an AC signal reaching the saturation points of a transformer would be odd order harmonic distortion, the properties of which will be discussed in Chapter 2.3.6. It is also possible for asymmetrical distortion to emerge in a transformer, for instance if a DC current flows through a winding, this would result in the centre point of the hysteresis loop shifting either up or down. This would result in one cycle of the waveform being closer to the saturation point, which would imply that one waveform cycle would clip before the other. If both sides of the signal saturate the transformer under these conditions, then even order distortion will be added to the odd order hysteresis distortion. This phenomenon can also occur if a DC current is inadvertently applied to either of the windings, this would have the effect of weakly magnetising the core. If this were to happen to a transformer with a narrow hysteresis loop, the residual magnetic field would be negligible on the removal of the DC current. A popular technique to reduce saturation when DC is present in the circuit, is to use narrow *air gaps* within the core of the transformer. These gaps have an extremely low permeability which serves to control the quantity of flux density within the entirety of the magnetic circuit. A drawback of using an air gap is that they reduce the overall inductance of the coil, this technique is particularly effective when there are large quantities of DC present within one of the coils. Transformers cores can be constructed out out numerous thin metallic sheets stacked together, the thin sheets are know as *laminations*. As high permeability materials are often also electrical conductors, minuscule AC voltages are induced from within the cross section of the core, these voltages cause eddy currents to flow. This results in a power loss known as *eddy current loss*, and can cause the core of the transformer to overheat. The laminations are typically all insulated from one another, the purpose of this is to mitigate the negative effects that may be caused by eddy current losses[22]. (Whitlock, 2008:278–280)

[22] "[A] circulating current in magnetic materials that is produced as a result of time-varying flux passing through a metallic magnetic material. [...] the energy wasted in sustaining undesirable eddy currents in an electrical conductor." (Laplante, 2005:222)

2.3 Signal Processing

2.3.1 Transduction

A *transducer* is a device that converts one form of energy into another. For example, acoustic waves can be transduced into an electric signal via a microphone's transducer; the signal can then be processed or stored on a medium. Another transducer can then convert the electrical signal back into sound energy; for example, a speaker driver can *transduce* electrical energy back into sound energy. The primary objective of many transducers is to ensure that the signal is reproduced accurately in another medium. The accuracy or acuity of the transduction process is known as its *fidelity*. A *signal processor* is a device that manipulates a signal in a particular way. Some examples encountered by audio professionals would typically be *microphone preamplifiers*, *equalisers*, and *dynamics processors*. An input signal will consist of amplitude, frequency, and phase information; it is contingent that a signal processor reproduces these properties accurately to function adequately. A signal is defined as desirable, transmitted information that has both intention and utility. However, signals are not the only constituent of transduced electrical energy, and phenomena such as *noise* and *distortion* emerge at various stages of transduction and signal processing. As they diminish the potential for fidelity, distortion and noise are generally considered objectionable traits. Therefore, the more electrical noise and distortion generated in a signal processor, the less fidelity the signal processor is considered to have. (Truax, 1984:7–8; ANSI S1.1-1994, 2005:7.04; Laplante, 2005:627,699)

2.3.2 Amplification

The electrical signal produced by a transducer, such as a microphone, is orders of magnitude below what is required for the majority of applications. A microphone with an internal impedance of 200 Ω will produce a voltage of 10 mV if presented with a moderate acoustic stimulus; this approximates to 1.8×10^{-8} W of power when connected to an 8 Ω speaker. An *amplifier* is therefore required to increase the input signal to a usable output level. The degree to which an amplifier increases (or decreases) an input signal is known as *gain*. Gain is a dimensionless unit, and can be defined as the ratio of an output signal variable to input signal variable of an audio system. (Patronis, 2008:703; White & Louie, 2005:18; Laplante, 2005:293)

Amplifiers can be categorised into four types, depending on the function they perform; these are *voltage amplifiers*, *current amplifiers*, *transconductance amplifiers*, and *transresistance amplifiers*. A voltage amplifier amplifies the voltage of an input signal into a corresponding output signal voltage. To function optimally, the input impedance of a voltage amplifier must be considerably higher than the source impedance of the input signal, and the output impedance of a voltage amplifier must be markedly lower than the load impedance connected to the output. The purpose of this is because the input signal needs to impart a maximum voltage on the amplifier input and impart a maximum voltage on the amplifier output load. A current amplifier amplifies the current of an input signal to a corresponding output signal current. Current amplifiers are associated with a low impedance input and a high impedance output. Transconductance amplifiers amplify the voltage of an input signal to a corresponding output signal current and have a high impedance input and a high impedance output. Finally, transresistance amplifiers amplify

an input signal current to a corresponding output signal voltage and have a low impedance input with a low impedance output. (Patronis, 2008:703)

Preamplifiers are a type of amplifier designed to handle low input signal levels, prevent noise generation, and connect to a myriad of other signal processing devices. A *power amplifier* is a voltage amplifier that can also deliver substantial quantities of electrical power and are usually the final amplification stage that connects to loudspeakers. Another property of amplifiers is their inherent input or output configuration. *Balanced* inputs are not connected directly to ground; the positive and negative cycles of the signal are electrically symmetrical to one another while referenced to ground. An amplifier input is *unbalanced* when one of its inputs are connected to ground (the input configuration is *single-ended*). Amplifiers can have any combination of balanced or unbalanced on their respective input and output stages. (Patronis, 2008:703–704)

Amplifiers can be further classified into a distinctive *class*. Different classes were designed in order to improve efficiency[23] and mitigate distortion in amplifiers. Each distinct class can be described as follows:

Class A : Refers to an amplifier that is constantly conducting current, even when there is no signal level present. Moreover, current will flow during both the positive and negative cycles of a waveform; the active component[24] will amplify the full 360°cycle. The average value of the current flow is relatively stable, even with a changing signal level. The signal modulates the current flow, increasing it and decreasing it in value; however, the current flow never reaches zero. The advantage of class A operation is a highly linear response, thereby negating the need for negative feedback; however, class A designs tend to be inefficient and are incapable of high output power. (White & Louie, 2005:302; Patronis, 2008:740)

Class B : Requires that the amplifier have two or more active amplification components. In effect, one component would amplify the positive cycle, and the other the negative cycle; each device amplifies exactly 180°. Class B operation is generally far more efficient than class A operation, but tends to suffer from excessive crossover distortion, as class B amplifiers struggle to switch between active components at low signal levels. (White & Louie, 2005:302-303; Patronis, 2008:740)

Class AB : Designed to mitigate the problems associated with class B operation. This configuration is similar in principle in to class B, except that both active amplification devices conduct current at low signal levels; the amplifier is in effect operating in class A at low signal levels. For class AB amplifiers, crossover distortion is reduced considerably, but this is at the expense of amplifier efficiency. (White & Louie, 2005:304; Patronis, 2008:740)

[23] The ability of an amplifier to convert the power it consumes to the power that it delivers to its load.
[24] This could be a transistor or valve.

2.3.2.1 Negative Feedback

The process of *feedback* involves taking a signal from an amplifier output and feeding it back into its input; the two signals will combine in either an additive or subtractive manner. Additive signals result in *positive feedback*[25], while subtractive signals result in *negative feedback* (NFB), or regeneration. NFB is often implemented in audio amplifiers to optimise their performance. Performance enhancements include: improved gain stability, frequency response, and input and output impedance levels; furthermore, there is a significant reduction in distortion. Figure 2.23 is a graphical representation of a basic feedback loop for a voltage amplifier with a transfer function[26] (A) with no feedback applied; the input signal is V_{in}, and V_{out} is the output signal. The *feedback path*, indicated in blue, has the transfer function (B). With the feedback loop connected to the input, an *error signal* (V_e) is formed; this determines the type of feedback required. When the feedback loop is closed, the overall gain is referred to as the *closed loop gain*, as opposed to the *open loop gain* which occurs when the loop is unconnected. The A is denoted as A' when NFB is applied, it can be calculated from the *universal feedback equation* (Equation 2.44). (Patronis, 2008:707; Blencowe, 2016:54-55)

$$A' = \frac{A}{1 + A.B} \tag{2.44}$$

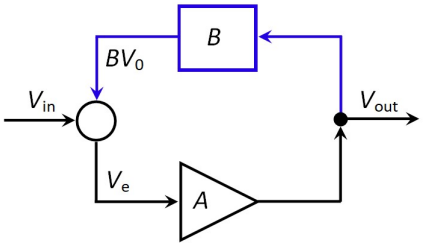

Figure 2.23: An example negative feedback loop. (Patronis, 2008:707)

The *gain reduction factor* (or *feedback factor*) is the absolute magnitude of the denominator of this equation, it is commonly referred to as the *feedback fraction*. The feedback will be negative when the gain reduction factor is more than one and positive when it is below one. For a NFB loop, the voltage level difference at the input will be attenuated due to destructive interference between the source signal and feedback signal, as the amplifier inverts the signal. The more NFB applied to the input (or the larger BV_0 becomes) the smaller the error of the amplifier will become. Eventually, the output signal will begin to match the input signal. However, the error can never be fully eradicated, as the NFB will completely nullify the input signal past a certain point. A feedback loop applied across a single gain stage is known as *local feedback*. *Global feedback* occurs when the feedback loop encompasses many gain stages, while *nested feedback* is the implementation of local and global feedback loops within the same overall system. (Patronis, 2008:707; Blencowe, 2016:54–55)

[25] This may cause an amplifier to self-oscillate.

[26] The *transfer function* of an amplifier is the mathematical relationship between the output signal and the input signal for a given steady state signal. (Patronis, 2008:704)

Generally, the reason for using NFB in audio amplification systems is to improve the *linearity* of an amplifier, as NFB reduces certain distortions by the value of the *feedback factor*. If an amplifier generates low order harmonic distortion, it will be fed back into the amplifier 180° out of phase with the input signal, nullifying itself when processed by the amplifier. However, more objectionable higher order harmonic distortion can emerge, as any distortion not removed by the NFB process will effectively be *redistorted*, despite an overall reduction of distortion in the system. Furthermore, NFB is ineffective at reducing crossover distortion because the amplifier gain is effectively zero in the crossover region (the feedback factor has no gain in this region). Feedback can also reduce amplifier noise, with the caveat that the amplifier gain will be reduced by the same quantity, resulting in the same SNR as an open loop configuration. (Blencowe, 2016:58)

2.3.3 Sampling

Analogue to digital converters (DAC) are devices that can *digitally encode* analogue signals. The process of *quantisation* involves assigning discrete *binary* values to analogue signal voltage levels. The *bit rate* is the number of possible discrete values that can be assigned to an amplitude. The digitised audio signal consists of a number of discrete time intervals known as the *sampling period* (T_s), this is the units of seconds per sample. The *sampling rate* ($F_s = \frac{1}{T_s}$) indicates the number of samples per second. As the amplitude is assigned a discrete value when sampled, digital signals are functions of discrete time. According to *Shannon's sampling theorem*, to accurately digitally encode a signal, the maximum sinusoidal frequency must be less than half of the sample rate. Therefore, if the highest frequency of an analogue signal is below the *Nyquist frequency* ($\frac{F_s}{2}$), no degradation will occur when it is digitally encoded. (Kadis, 2012:140–141; Laplante, 2005:605)

2.3.4 The Fourier Transform

It was observed, in Chapter 2.1.2, that all complex waves consist of a fundamental frequency with harmonics and partials of varying amplitudes, frequencies, and phases. A mathematician, Joseph Fourier (1768-1830), devised a technique to decompose complex waves into a series of sine waves of varying frequencies and phases, this is a process known as the *Fourier transform*[27]. (White & Louie, 2005:162–163)

The Fourier transform is a process for determining the quantity of a particular sinusoidal frequency present in a complex waveform; the purpose of which is to represent a waveform in the *frequency domain*. The Fourier transform is an algorithm that functions by multiplying a signal by a unit amplitude sine and cosine wave at each of its constituent points. The implementation of sine and cosine waves[28] allow both frequency and phase information to be extrapolated from the transformation process[29]. Subsequently, the results of the transformation process are averaged over an integer value of sinusoidal cycles. If no sine wave frequency is present in the original signal, the result will tend towards zero. However, if a sine wave frequency is present, its result will be proportional to its amplitude in the original signal. The Fourier transform will

[27] A *transform* is a process, that converts one form of data to another form of data. (Laplante, 2005:700)
[28] Sine and cosine waves are are orthogonal to one another.
[29] This is necessary as the sinusoids present in a complex wave could have different phase relationships.

return data in the form of a *spectrum* that can be used for analysis. If this operation is repeated for different sinusoids (whose period can divide the length of the original waveform an integer number of times), then computational redundancies will occur. If these are eliminated the process will become far simpler as the number of operations are reduced; this process is known as a *fast Fourier transform* (FFT). A problem arises if the signal's harmonics or partials are not exact multiples of the reciprocal of the waveform length. If the waveform does not start at the exact point that it ends and fails to loop back on itself perfectly, unwanted *artefacts* will appear in the spectrum. Artefacts are caused by square wave like jumps in the audio signal, these overshoots are called *jump discontinuities*. This error is caused by *asynchronous signal acquisition*, which is associated with a discontinuity in the signal analysis. (Cabot, 1997:9–10; Kadis, 2012:141–143)

To mitigate the effects of jump discontinuities, a *window* function is applied to the signal. This process entails fully attenuating a signal at its onset and end, resulting in the waveform becoming a *shaped burst*. Hence, the resulting spectrum is a *convolution* of the signal spectrum and the windowing function. Convolution is a mathematical operation that integrates an input signal with another function, resulting in an output function. The output signal is the input signal *convolved* with a particular *impulse response*. (Cabot, 1997:9–10; White & Louie, 2005:86; Laplante, 2005:148–149)

When in the digital domain, the FFT process is limited to a frequency range that is one half of the sample rate. As the FFT process produces a data set that is *amplitude vs frequency*, there will be half as many data points as the number of samples from the un-transformed input signal; these data points are known as *bins*. The FFT process is linear with regards to frequency; therefore, bins are all equal in width, and extend from 0 Hz up to half of the sample rate. If a digitised audio signal (sampled at 48 kHz) is 2048 samples in length, then an FFT of the signal will have 1024 amplitude values. Each bin is assigned to one of these 1024 amplitude values. The bandwidth of each bin can be found by dividing the Nyquist frequency of the signal (24 kHz) by 1024, which results in a bandwidth of approximately 23.4 Hz. (Metzler, 2005:70–71)

2.3.5 Distortion

The output signal of a perfectly *linear* audio system will change in proportion to a given input signal; the transfer characteristic such a system is represented in Figure 2.24. However, perfectly linear systems do not exist in reality, and all systems are subject to some imperfections and irregularities. Audio signal distortion is a phenomenon that permeates through all electronic signal processors. While signal distortion comes in many guises, it can generally be described as the addition of components or artefacts to a signal; or any alteration made to the amplitude, frequency, or phase of a signal. The distortion response of a system can also be represented as a *transfer characteristic curve*, which plots the output signal as a function of the input signal. (Laplante, 2005:207, 700; White & Louie, 2005:214–215)

Distortion can be divided into two main sub-categories, *linear distortion* and *non-linear distortion*. Linear distortion is characterised by changes to pre-existing components within the audio signal, with no new frequency components being introduced. Linear distortion results

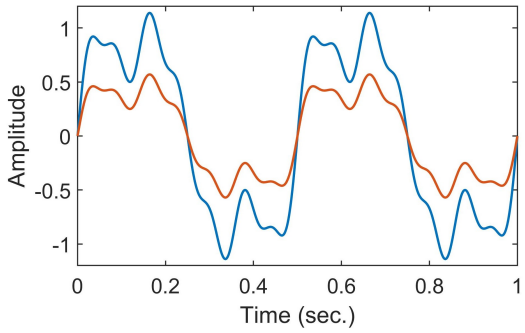

(a) An output signal that is twice the amplitude of the input signal.

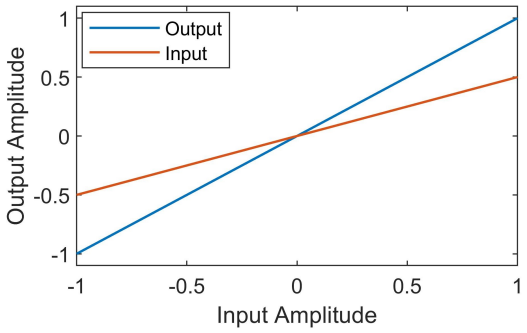

(b) The linear transfer characteristic of the two waveforms.

Figure 2.24: The effect of an increase in amplitude on a linear system.

in changes to the relative phases and/or amplitudes of frequencies within an audio signal. The transfer characteristic of a DUT that produces linear distortion, is characterised by a straight line (which is what the term *linear* refers to). The process of linear distortion results in changes to the shape of the audio signal waveform as a function of the signal constituents, not a function of signal level. Signal processors that exhibit linear distortion always exhibit it in the same way, it is always present; as opposed to non-linear distortion that varies depending on signal level changes. (Laplante, 2005:207, 700; White & Louie, 2005:214–215)

A common type of linear distortion is *phase distortion* or *phase shift*. Audio signal processors typically introduce a time delay, which is often not consistent at all frequencies; this results in a shift in phase over the frequency spectrum of the processed audio. Therefore, a signal processor may exhibit a flat frequency response curve despite producing a distorted waveform; phase distortion tends to affect transients more than steady state tones. For example, Figure 2.25a is a pseudo square wave, while Figure 2.25b demonstrates the effect of shifting the phase by -90° or $-\pi/2$ radians; it can observed that there is a marked change to the shape of the waveform. (Preis, 1976:346–347; White & Louie, 2005:287–288)

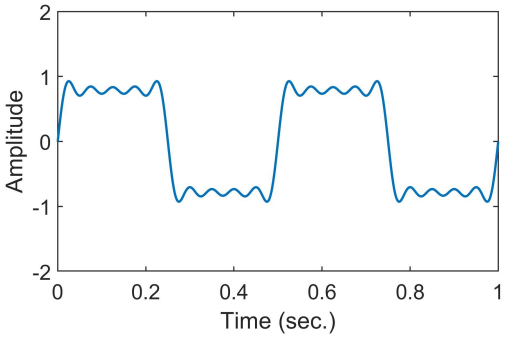

(a) A pseudo square wave constructed from odd harmonics up to the 9th harmonic.

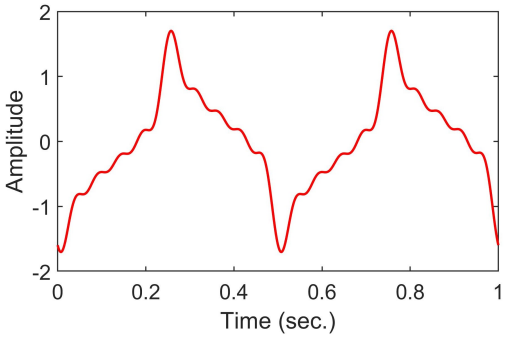

(b) A phase shift of 270° is applied to each harmonic, resulting in an altered waveform.

Figure 2.25: The effects of linear distortion on a complex waveform. (Preis, 1976:348)

Non-linear distortion is contingent on the introduction of frequency components *related* to the input signal in some manner. These frequency components are level (or amplitude) dependant, whereby an increase in level will increase new frequency components. Additionally, there may be changes to the phase and amplitude components of the original signal. Noise and other interference is generally not included as a form of distortion. There are a number of distinct types of non-linear distortion, these will be examined as follows. (Temme, 1992:233; Laplante, 2005:473)

2.3.6 Harmonic Distortion

Harmonic distortion arises from the *non-linear transfer characteristics* of a signal processing device. If a sine wave is input into a non-linear circuit, the output will contain frequency components that are integer multiples of the fundamental frequency; these manifest as additional harmonics. For example, a 100 Hz sine wave will produce harmonics at 200 Hz, 300 Hz and 400 Hz etc. For complex waveforms, harmonic distortion will arise at integer multiples of all the frequency components of the original complex waveform. Harmonic distortion can emerge in a number of forms, namely *even order distortion*, *odd order distortion*, or a combination thereof. Even order distortion contains only even integer multiples of the input signal, while odd order distortion contains only odd integer multiples of the input signal. (Laplante, 2005:318)

Distortion is typically a relative measurement that is referenced to the linear portion of an output signal in terms of amplitude and frequency. Standard tests for harmonic distortion ordinarily entail that a test tone be fed into the input of a DUT; partials of varying amplitudes will emerge, these can be measured in the resultant output signal (Temme, 1992:3). The standard test for harmonic distortion is referred to as *Total Harmonic Distortion* (THD), which Temme (1992:3) defines as the "[...] percentage of the power sum of all the harmonics to the power sum of all the harmonics plus the fundamental (i.e. amplitude normalisation)" while Metzler (2005:29) defines it as the: "[...] the square root of the sum of the squares of the individual harmonic amplitudes". THD can be calculated using Equation 2.45:

$$\text{THD} = \frac{100\sqrt{H_2^2 + H_3^2 \dots H_N^2}}{\sqrt{H_1^2 + H_2^2 + H_3^2 \dots H_N^2}} \tag{2.45}$$

Harmonic distortion manifests in a number of ways within the time domain. If a signal is applied to the input of an amplifier that is unable to provide the required voltage and/or current, the tops of the waveform will appear to be *peak limited*. This phenomenon is known as *clipping*, as the tops of the waveform appear to be clipped off. If both halves of the waveform are clipped in exactly the same shape, it is referred to as *symmetrical clipping*. *Hard clipping* occurs when the top of the waveform is cut off abruptly, resulting in a hard corner edge (the waveform and *transfer characteristic curve* are illustrated in Figures 2.26a & 2.26b). If a sine wave is peak limited enough then it will eventually begin to resemble a square wave. *Soft clipping* exhibits a gradual *compression* of the peaks of the waveform (the waveform and *transfer characteristic curve* are illustrated in Figures 2.26c & 2.26d). The spectrograms in Figures 2.26e & 2.26f display the subsequent harmonic makeup for each waveform clipping structure. Both hard and soft clipping produce odd order harmonics; hard clipping produces noticeably more harmonics

overall (with an emphasis on higher odd order harmonics), while soft clipping is generally limited to the addition the 3rd harmonic. (White & Louie, 2005:69–70; Tarr, 2018:157–159; Temme, 1992:3)

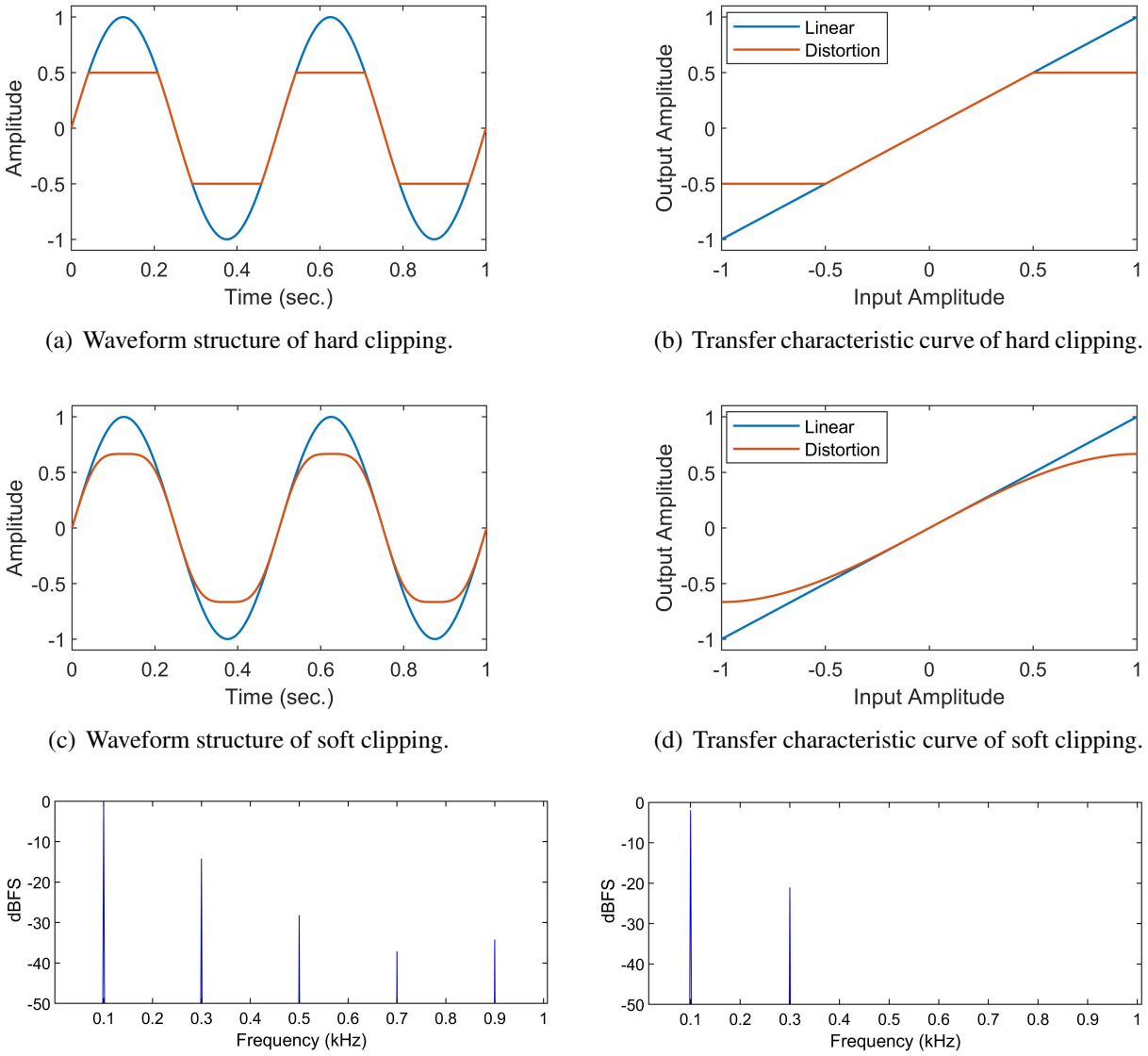

(a) Waveform structure of hard clipping.

(b) Transfer characteristic curve of hard clipping.

(c) Waveform structure of soft clipping.

(d) Transfer characteristic curve of soft clipping.

(e) Spectrogram of hard-clipped waveform.

(f) Spectrogram of soft-clipped waveform.

Figure 2.26: Hard and soft clipping. (Tarr, 2018:157–159)

If only a single half of the waveform is clipped, it is referred to as asymmetrical clipping. If the positive half of the wave is clipped it is positive *peak limited*, while if the bottom half is clipped it is negative peak limited (as seen in Figure 2.27a, the transfer characteristic curve is indicated in Figure 2.27b). Sine waves that have been asymmetrically clipped will generally produce even harmonics that are higher in magnitude than the constituent odd harmonics, as demonstrated in Figure 2.27e. Another common type of harmonic distortion is *crossover distortion*, which often manifests in class B and class AB amplifiers. As the signal in these types of amplifiers are shared by two or more active components, a discontinuity can arise when transferring the signal between the devices. This discontinuity occurs near the zero current region,

subsequently being more conspicuous at low signal levels (as illustrated in Figure 2.27c, the transfer characteristic curve is indicated in Figure 2.27d). Crossover distortion predominantly produces 2nd and 3rd order harmonic distortion products, as illustrated in Figure 2.27f. (White & Louie, 2005:69–70,358; Tarr, 2018:159–162; Temme, 1992:3)

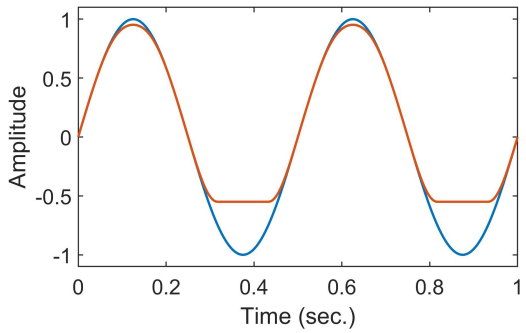

(a) Waveform structure of asymmetrical clipping.

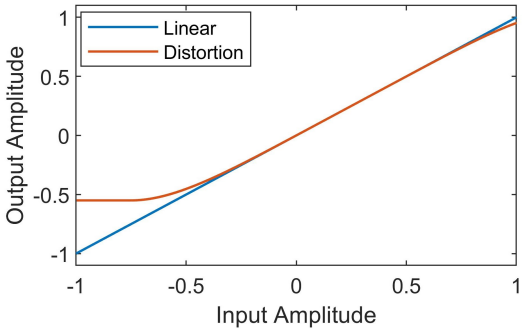

(b) Transfer characteristic curve of asymmetrical clipping.

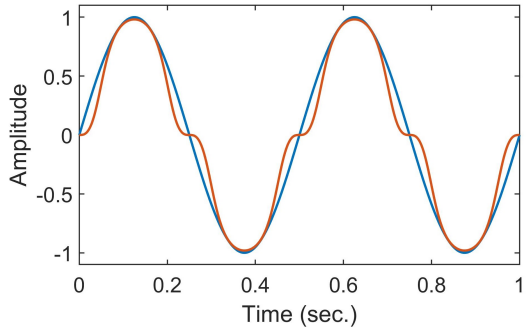

(c) Waveform structure of crossover distortion.

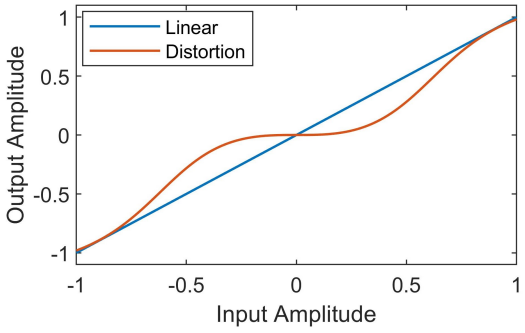

(d) Transfer characteristic curve of crossover distortion.

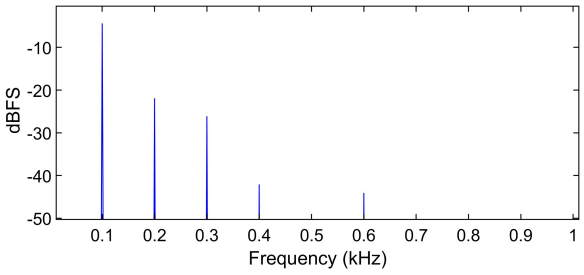

(e) Spectrogram of asymmetrical clipping.

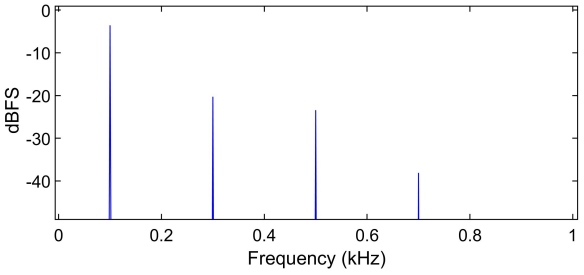

(f) Spectrogram of crossover distortion.

Figure 2.27: Asymmetrical clipping and crossover distortion. (Tarr, 2018:159–162)

2.3.7 Intermodulation Distortion

Intermodulation distortion (IMD) occurs when two frequencies *interact* in a phenomenon known as *amplitude modulation*. When IMD occurs, the lower frequency waveform is modulated by the higher frequency waveform, which results in the emergence of new frequency components. The IMD frequency relationships are indicated by Equation 2.46, where f_1 and f_2 are the test frequencies, and m and n are integers that extend to infinity. The order of IMD products is the sum of $m+n$, the result of which will give a number (or order) that is either even or odd[30]. Temme (1992:10) defines IMD order: "For intermodulation distortion and difference frequency distortion, the distortion order is equal to the sum of the absolute value of the frequency coefficients [...]."

$$m.f_1 \pm n.f_2 \tag{2.46}$$

To further clarify this point, in Figure 2.28a, two sine waves of 100 Hz and 800 Hz at equal amplitude are simultaneously input into a non-linear system, resulting in *side-band* distortion components arising in the output signal. The side-band frequencies are equal to the sum and difference of the upper frequency (800 Hz), and are integer multiples of the lower frequency. A variation of IMD known as *difference frequency distortion* (DFD) only considers frequency components that are subtracted from one another, and multiples of the differences between the test frequencies. DFD becomes apparent when two nearby frequencies of similar amplitude are input into a non-linear system (Figure 2.28b). Frequencies lower than the two input frequencies emerge, ascending from 100 Hz in 100 Hz intervals; the difference frequency amplitude decreases as the interval increases. (Laplante, 2005:625; Temme, 1992:10–11)

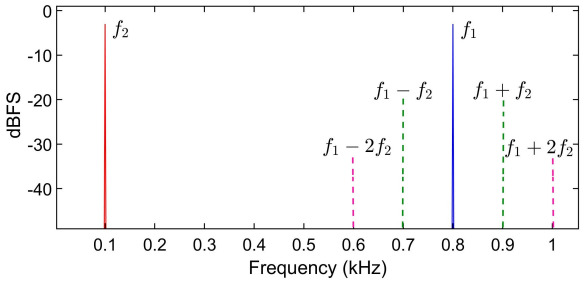

(a) IMD resulting from the interaction of an 100 Hz and 900 Hz input signal.

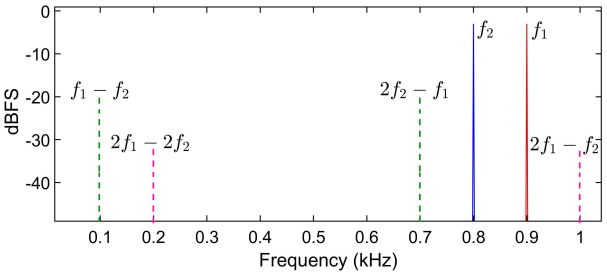

(b) DFD resulting from the interaction of a 800 Hz and 900 Hz input signal.

Figure 2.28: Intermodulation distortion. (Temme, 1992:10)

[30] Two standards for measuring IMD are the SMPTE RP120-1983 and DIN 45403.

2.3.8 Transient Intermodulation Distortion

Transient Intermodulation Distortion (TID) affects the transient response of an audio signal passing through a signal processor; TID generally manifests in two ways. When a signal with a sharp step response (like a square wave) is input into an amplifier, and the amplifier is unable to match the rapid change of the input signal, a momentary *compression* of the amplitude envelope occurs. TID is related to deficits in the *slew rate*[31] of active components within the amplifier. Audio devices have a maximum slew rate (which is the highest rate they can operate before distortion is induced), this limits the high frequency and high amplitude capabilities of all audio signal processors. TID can also manifest as a *ringing* type phenomenon on the edge of waveforms, and resembles a short overshoot with a steep transient. This form of TID is caused by time delays within the amplifier. A square wave could have some of its higher frequency harmonics delayed, resulting in a phase shift of those harmonics. TID tends to affect signals with steep slopes that are high in amplitude and contain high frequencies. However, low amplitude and low frequency signals tend to remain unaffected. TID can therefore affect the timbre of high frequency signals; White & Louie (2005:404) claim that if a cymbal is struck and recorded at close range, there would be an increase of low frequencies, resulting in a *muddying* or *thickening* of the sound. Linsey-Hood (2009:214) describes the qualitative effects of TID on audio material as having a *tizziness* or *overly-bright* quality. (Crowhurst, 1959:2–119; White & Louie, 2005:356, 404; Jung *et al.*, 1979:59–60)

[31] "[...] the rate of variation of an AC voltage in terms of volts per second." (Laplante, 2005:635)

2.4 Perception

2.4.1 Psychoacoustics

The field of *psychoacoustics* investigates the complex relationship between physical sounds and the physiological and psychological perception processes. Sound and its properties are well established within the sciences, and a variety of acoustical properties are assigned units of measure that are either logarithmic or linear. For example, frequency is a linear scale measured in Hertz, while pitch is a logarithmic measure of the same phenomenon, although neither of these scales accurately depict the human perception of acoustical stimuli. (Parncutt, 1989:19)

Sound intensity and loudness should not be equivocated, as the human auditory system's perception of loudness varies with frequency. The *phon* is the unit of measure that has been designated to the perception of *loudness*, and is derived from multiple empirical experiments on human subjects. If a nominal tone is perceived to be as loud as a test tone of 1000 Hz at 60 dB, it is said to have a loudness of 60 phons. The perceived loudness is measured for the frequency range of human hearing, and collated into the *equal loudness contours*, which are depicted in Figure 2.29[32]. Zwicker & Fastl (2007:19) claims that this test has a high level of reproducibility, and is within the range of approximately 3 dB for most people. The accuracy of the equal loudness curves has improved over the decades, with the latest iteration being the ISO 226:2003 standard. It has been found that human beings are most sensitive to frequencies around 3.5 kHz; this implies that people are able to hear this frequency at an extremely low intensity, approximately -8 dB_{SPL}. At this level all frequencies, besides a narrow band adjacent to 3.5 kHz, would be inaudible. At the two opposite ends of the graph in Figure 2.29, sounds become increasingly difficult to hear at lower levels. The *threshold in quiet* is a function that displays the minimum audible amplitude of a particular frequency, any sound that falls below this threshold will be inaudible, even if it can be measured with recording/measuring equipment; the threshold in quiet is represented as the 0 phon line in Figure 2.29. It can be inferred from Figure 2.29 that the frequency response of human hearing mechanism becomes more linear with increasing loudness. The amplitude resolution of the ear is, in a best case scenario, approximately 0.25 dB; although under some circumstances it can be higher, at approximately 0.5 dB to 1 dB. (Davis, 2007:748; Zwicker & Fastl, 2007:203–204; White & Louie, 2005:154–155)

2.4.1.1 Masking and Critical Bands

(ANSI S1.1-1994, 2005:12.29) defines *masking* as "The process by which the threshold of one sound is raised by the presence of another (masking) sound". The phenomenon of masking occur in two forms, namely simultaneous and non-simultaneous. Simultaneous masking occurs when a sound masks another concurrently, Zwicker & Zwicker (1991:116) explains this phenomenon via an analogy:

> An example for the simultaneous condition would be the case where we have a conversation with our [neighbour] while a loud truck passes by. In this case our conversation is severely disturbed. To continue our conversation successfully we have to raise our voice to produce more speech power and greater loudness.

[32] This set of curves is also often referred to as the *Fletcher-Munson* curves, named after the scientists who devised the experiment.

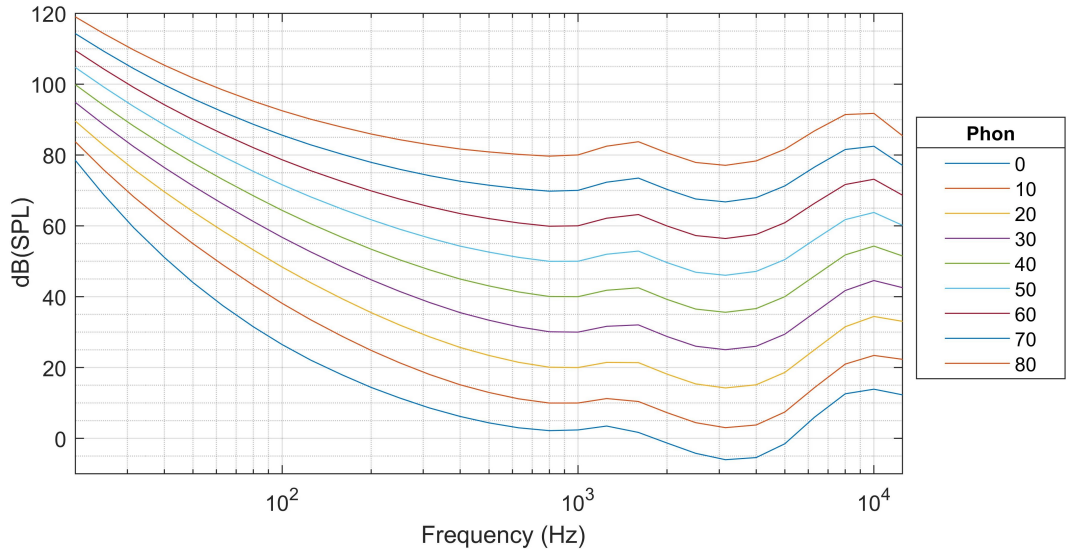

Figure 2.29: ISO 226:2003 Normal equal-loudness-level contours. (Hummersone, 2020)

Non-simultaneous masking occurs in the form of *post-masking*; when in the presence of a test signal, a masking tone is stopped abruptly, the test signal will continue to be masked for a short duration of time. The *masking threshold* is the minimum sound pressure level a particular sound needs to be in order to be audible in the presence of a masker. This level is usually always above the threshold in quiet, and is equivalent to the threshold in quiet when the frequencies of the two sounds are dissimilar. The *threshold of audibility* of a sinusoidal signal in the presence of a narrow band noise masker, is at a certain amplitude, unaffected by an increase in the bandwidth of the noise masker. (Zwicker & Zwicker, 1991:116–117,121)

The next key concept is that of *critical bands*, these are analogous to a set of *auditory filters* which act as a function of the movement of *basilar membrane*, an organ of the inner ear. The basilar membrane is analogous to a spectrum analyser, in that certain frequencies excite the basilar membrane in a particular region more so than other frequencies. These excitations do not occur at discrete locations, but instead occur over minute areas; these areas of excitation are what give the auditory system its frequency resolution. The areas of excitation that frequencies act upon correspond to what is referred to as critical bands, which have been assigned a unit of measurement known as the *Bark*. Critical bands are added together in such a way that the lower critical band coincides with, or overlaps the lower limit of the next higher critical band. The critical band rate increases in increments of 100 Hz up until 500 Hz, above 500 Hz the critical band rate increases exponentially; there are 24 critical bands in total. The interaction of sound energies within the same critical band, can result in *beating*, *roughness*, and *masking effects*; while there is no interaction of sound energies in differing critical bands. (Zwicker & Fastl, 2007:117, 158–159; Zwicker & Zwicker, 1991:116–117)

2.4.2 Distortion: Perceptual Considerations

The perception of non-linear distortion is a complex phenomenon, as the human hearing system is also non-linear. Therefore, trying to ascertain what types of non-linear distortion the ear can perceive and the means of scaling such perceptions is an arduous task. Masking is one of the primary mechanisms that affect our ability to perceive non-linear distortion. It has no equivalent in linear systems theory does not occur outside of the human hearing system. There are two fundamental properties of masking that need to be taken into account. Firstly, masking occurs in both directions around a sound; with the slope biased towards higher frequencies. Secondly, masking effects increase considerably with increasing excitation level; the higher the amplitude of the masker, the more of the frequency spectrum it is able to mask. Geddes & Lee (2003b:6) proposes three *distortion perception principles*. Firstly, upper distortion frequency components are less likely to be perceptible (as they will be masked) than lower frequency distortion components, this is due to the above mentioned biased *slope*. Next, distortion components that lie closer to the test sound, are less likely to be perceived due to the taper of the masking effect. These distortion components are more likely to be located in the masker's *strong* area the closer they are to the masker. Finally, distortion components are more likely to be perceptible at lower sound levels; this is because masking increases with signal level. (Geddes & Lee, 2003b:5–6)

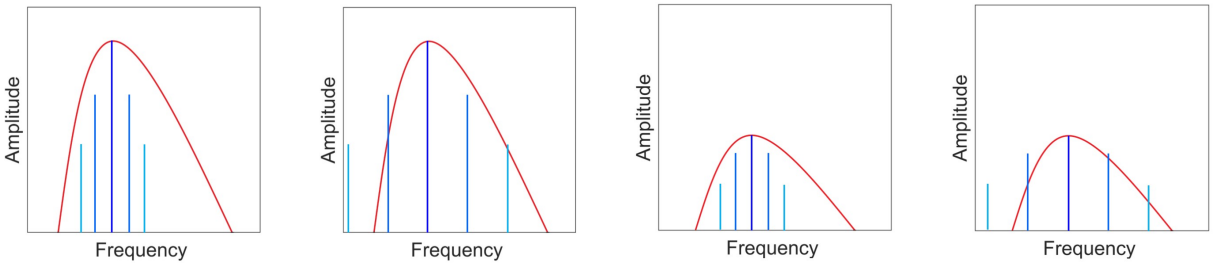

(a) Low order non-linearity with a high signal level.

(b) High order non-linearity with a high signal level.

(c) Low order non-linearity with a low signal level.

(d) High order non-linearity with a low signal level.

Figure 2.30: Masking of non-linear harmonic distortion components. (Geddes & Lee, 2003b:6)

Consider Figure 2.30, four tones are presented in different contexts, a low order non-linearity and a high order non-linearity, each corresponding to a low signal level and high signal level respectively. It can be observed that lower order distortion products tend to be masked to a greater degree than higher order distortion products, with increasing signal levels exacerbating the masking of lower order distortion products. Higher order distortion is generally not masked and non-linear components at low signal levels will be more audible than those at higher signal levels. There is no interaction between odd and even harmonics, odd orders only generate odd harmonic content, and even orders only generate even order content. An n^{th} order non-linearity is responsible for generating n^{th} order harmonic components, as well as the harmonic components below it. Pure tones generate harmonics that are above the fundamental of the input signal, and multiple tones generate an n^{th} order non-linearity at $\pm n$ multiplied by the modulation frequency and every other value of n below it. (Geddes & Lee, 2003b:5–6)

2.4.3 Timbre

Timbre is considered a highly complex concept, and there appears to be no consensus regarding the precise definition of timbre. Generally, timbre is defined as the attribute of an auditory sensation whereby a listener can identify that two sounds with the same loudness and pitch are different (ANSI S1.1-1994, 2005:12.09). Krumhansl (1989:44) is critical of the standard definitions of timbre and argues that they fail to explain the residual differences we hear between two different sounds. Acoustic measurements in the form of a spectral energy distribution and amplitude envelopes are far too complex to infer or isolate any viable timbral information. Acoustic measurements lack the ability to translate what acoustical properties are perceptually relevant; conceivably, only a small subset influence the perception of timbre. There is also an implicit assumption that timbre is autonomous and independent of the other dimensions of sound. It can be inferred that spectral energy distributions are inherently related to pitch, with amplitude envelopes related to duration. (Krumhansl, 1989:44)

The harmonics produced by distortion share the same timbral properties as the harmonics produced by musical instruments. Hamm (1973:272) notes that the harmonic constituents of the sound produced by a musical instrument can affect its timbre, a phenomenon well understood by artisan musical instrument makers. Timbre itself is primarily influenced by the first few harmonics, with each harmonic having a unique timbral characteristic. Furthermore, combinations of harmonics can also alter the perception of a particular harmonic. There is a perceptible distinction between odd order and even order harmonics. Odd order harmonics are said to have a *stopped* or *covered* timbre, while even order harmonics are said to have a *choral* or *singing* characteristic. For individual harmonics, the 2^{nd} harmonic, which is the harmonic most likely to be masked, infuses an audible *fullness* and *body* on the timbre. The 3^{rd} harmonic is said to *blanket* the timbre and can a make a sound appear softer under certain circumstances, if a 5^{th} is added to sound with a strong 3^{rd}, a harsh *metallic* quality is produced. If a strong 3^{rd} and strong 2^{nd} are combined, then the *covered* quality is reduced; if a 4^{th} and 5^{th} harmonic are added, the timbre is imbued with a *horn* like quality. Higher order harmonics above the 7^{th} are what gives a sound *bite* or *edge*, if these are balanced with the fundamental, the sound can reinforce the fundamental with a sharp attack. As the upper harmonics are not musically related, high levels may cause a timbre to become objectionable. (Hamm, 1973:272)

2.5 The Valve

The *thermionic valve* is a device that contains electrodes sealed within an airtight vacuum glass enclosure[33]. A voltage applied to one electrode can change the amplitude of a current passing through another electrode. In contrast to the resistor, inductor, and capacitor, the valve is an active circuit component. This means valves are able to *amplify* signals, and therefore requires a supply of power to operate optimally. In an active device a *source* controls the flow of energy provided by a power supply into a *load*. Valves operate by means of a phenomenon known as *thermionic emission*. If substance is heated above that of the ambient environment, electrons that would usually be bound to the nucleus of an atom become free. Moreover, within a vacuum, electrons are attracted to positively charged electrodes. (Langford-Smith, 1963:1; Blencowe, 2016:97–98)

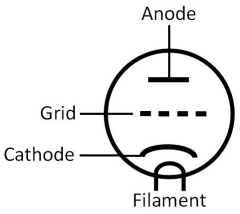

Figure 2.31: A valve with three electrodes, known as a triode. (IEEE Std 315, 1975:7.2–7.3)

The glass envelope of the valve contains a set of electrodes, each designed to perform a specialised task. A *triode* is a three electrode valve found in many audio signal processors (the schematic symbol for a triode is indicated in Figure 2.31). The constituent electrodes of a triode can be described as follows:

Cathode (k): The function of this electrode is to provide a source of free electrons; it is coated with a specialised chemical that readily emits electrons when heated. The cathode is *negatively charged*, as electrons flow from a negative to a positive (in this case the *anode* or *plate*). The cathode is heated to approximately 777° C, while at this temperature electrons boil off the cathode and form an *electron cloud*, known as *space charge*. Without an external influence, the space charge will become too dense and repel any further electrons from boiling off of the cathode. The *heater* (or *filament*) is a double helix filament similar to an incandescent light bulb. Its purpose is to provide a source of thermal energy for the cathode. The metal cathode sleeve usually encapsulates the heater filament as proximity increases heat transfer. The heater is insulated from the cathode, and does not act as a source of electrons[34]. Furthermore, it is not involved in the signal processing function of the valve and is generally omitted from schematics. The heater is supplied by a low voltage, high current power supply[35]. (Langford-Smith, 1963:4–5; Blencowe, 2016:100–102)

[33] Some early designs used a metal enclosure.
[34] Although under certain circumstances it can be a source of unwanted hum if connected to a AC power supply.
[35] Standard values for most audio valves are approximately 6.3 V at 300 mA and 12.6 V at 150 mA, this equates to a dissipation of approximately 1.89 W.

Anode (a): The anode (also referred to as the *plate*) is a positively charged electrode. Its purpose is to attract and receive electrons from the space charge that originates at the cathode. The number of electrons striking the surface of the anode affects its ability to pass current, as this can generate substantial amounts of heat. This limitation can cause the *thermal emission* of electrons from the anode surface and cause any gas stored within the anode to be released. If the anode voltage becomes negative, it will repel the space charge, and no current will flow. The anode can be darkened to aid with the radiation of heat and thus prevent damage. (Langford-Smith, 1963:5; Blencowe, 2016:98–99)

Control Grid (g): The flow of electrons within a valve can be manipulated by the control grid. This electrode is constructed from a fine wire wrapped around supporting side-rods. It is placed in close proximity to the cathode to maximise its efficacy. (Langford-Smith, 1963:5; Blencowe, 2016:99–100)

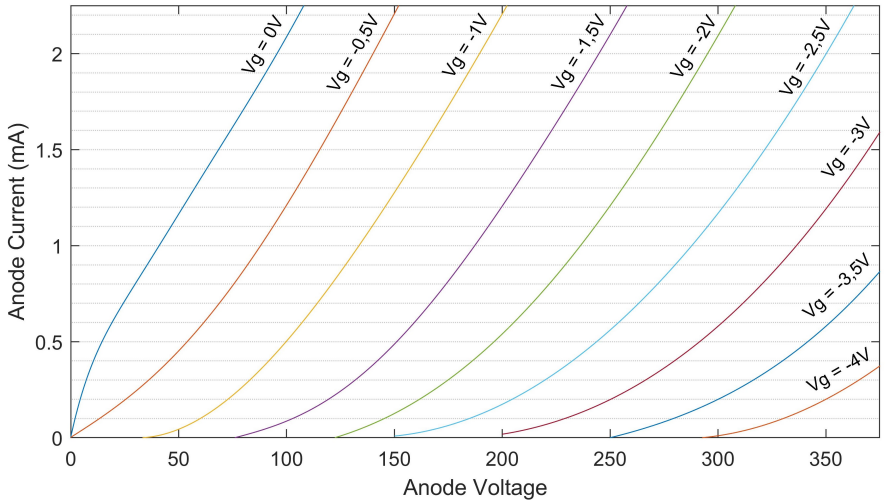

Figure 2.32: Static anode characteristics, with control grid curves of type ECC83/12AX7 triode valve. (Jones, 2012:75)

The control grid will attract electrons in the space charge when a positive voltage is applied. However, most electrons pass around the control grid, and become captured in the anodes electric field. A negative voltage across the control grid repels electrons, reducing the flow of space charge. The electron flow is nullified when the voltage drops below a certain threshold, even with a positive voltage across the anode. Therefore, valves are limited by the amount of current they can pass. The valve has reached its *saturation point* once this value is exceeded in a phenomenon known as the *cutoff*. Due to the control grid's close proximity to the cathode, a change in the grid voltage has a far more significant effect on the anode current than a similar change in anode voltage. Consequently, this results in a wide range of possible anode currents for a given anode voltage, contingent on whatever grid voltage is applied. Therefore, a triode is able to convert a voltage change at the control grid, to a change in power across a *load*[36] connected to the anode. In principle this allows an audio signal (that modulates the control grid) to be *amplified* at the anode. More precisely, the valve itself does not amplify the applied grid to

[36] This could be as simple as a resistor, or a transformer coupled loudspeaker.

cathode voltage; the amplified voltage across the load impedance is caused by the valve controlling the power available from the power supply. The manner in which the power is controlled is determined by the *operating conditions* and *characteristics* of the valve, and the topology of the circuit. (Blencowe, 2016:114–115)

The control grid voltage allows a range of anode currents per anode voltage value. This phenomenon, the *static anode characteristics*, can be modelled as the *control grid curves* (Figure 2.32). The graph represents the relationship between anode current (I_a) and anode voltage (V_a) for differing control grid to cathode voltages (V_{gk}). Figure 2.32 specifically gives the control grid curves for arguably the most ubiquitous preamplifier valve, the ECC83/12AX7[37]. There are a range of different valve types, each with differing internal properties; these valves will have differing sets of curves. (Blencowe, 2016:115–117)

The *valve coefficients* are a set of parameters or constants[38] that characterise the AC operation of a valve, contingent on a specified *operating point*, and are defined as follows:

Amplification Factor (μ): Under ideal operating conditions, this is the highest voltage amplification that the valve can provide.[39]. In other words, it is the ratio of the incremental change in anode voltage to the incremental change in control grid voltage in the opposite direction[40]. Amplification factor corresponds to the horizontal separation of control grid curves on the anode characteristic curves graph. This concept is described by Equation 2.47. (Langford-Smith, 1963:13; Jones, 2012:73–75)

$$\mu = \frac{\Delta V_a}{\Delta V_g} \tag{2.47}$$

Transconductance (g_m)[41]: This is the incremental change in anode current per incremental change in control grid voltage. To clarify, if all other voltages remain constant, it is the ability of a grid voltage to change an anode current. Transconductance corresponds to the vertical separation of control grid curves on the anode characteristic graph. This concept is described by Equation 2.48. (Langford-Smith, 1963:14; Jones, 2012:75)

$$g_m = \frac{\Delta I_a}{\Delta V_g} \tag{2.48}$$

[37] ECC83 is the European designation, while 12AX7 is the USA designation.
[38] Blencowe (2016:117) notes that this term is "somewhat optimistic", and should only be thought of as applying to *ideal* valves.
[39] This ideal would be a load with infinite resistance.
[40] The phase of the amplified waveform is reversed; an increase in control grid voltage would result in a reduction in anode voltage, and *vice versa*.
[41] The valve coefficients are dynamic AC parameters, it is convention that they are assigned lowercase letters.

Anode Resistance (r_a) : This is the incremental change in anode voltage per incremental change in anode current, for which there is a non-linear relationship. The anode resistance corresponds to the inverse of the slope of the tangent of the control grid curve; whereby a steeper slope implies lower anode resistance. This concept is described by Equation 2.49. (Langford-Smith, 1963:14; Jones, 2012:75)

$$r_a = \frac{\Delta V_a}{\Delta I_a} \tag{2.49}$$

These parameters are related by *van der Bijl's* equations[42], which are outlined as follows:

$$\mu = g_m \,.\, r_a \tag{2.50}$$

$$g_m = \frac{\mu}{r_a} \tag{2.51}$$

$$r_a = \frac{\mu}{g_m} \tag{2.52}$$

2.5.1 The Common Cathode Triode Amplifier

Valves require an external electronic circuit to configure their operation and function optimally. Furthermore, a *bias* voltage supply is required to set an *operating point*. Valves operate best at high voltages and low currents. Figure 2.33 demonstrates a circuit with an HT[43] supply that is 350 V relative to ground; this is a typical value for most valve circuits. The circuit illustrated in Figure 2.33 has an anode load resistor R_l (175 kΩ) that connects the HT supply (+350 V) to the anode. The anode conditions are modulated by V_{gk}, an AC voltage source with an A_{pp} value of 8 V; Ohm's law gives an to I_a value of 2 mA.

The anode current for any anode voltage that uses an HT of 350 V and R_l of 175 kΩ can be observed by placing a *loadline*[44] on the anode characteristics graph (Figure 2.34). If R_L or HT are changed, the loadline would have to be recalculated. The loadline in Figure 2.34 intersects the V_{gk} curves at discrete locations and allows the anode voltage for various values of V_{gk} to be calculated. While this first example serves as an adequate introduction, it is far from ideal. A negative voltage swing of 4 V on V_{gk} would cause V_a to increase from 72 V to 332 V; a voltage difference of 260 V. As gain can be defined as the ratio of input voltage to output voltage, it can

[42] The author wishes to note that Hendrik van der Bijl was South African and an alumni of Stellenbosch University; van der Bijl played a key role in the development of the valve and made many contributions to the sciences. For more information on his life and achievements, please see https://www.iol.co.za/news/the-vision-that-gave-sa-power-1231822 [Visited 2019-11-08].

[43] This stands for *high tension*, but is also sometimes referred to as the *B+*.

[44] This line is straight because Ohm's law is a linear equation.

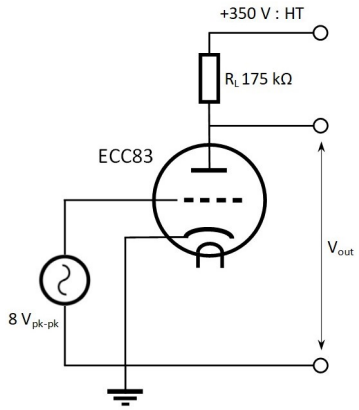

Figure 2.33: A simple common cathode amplifier. (Jones, 2012:66–67)

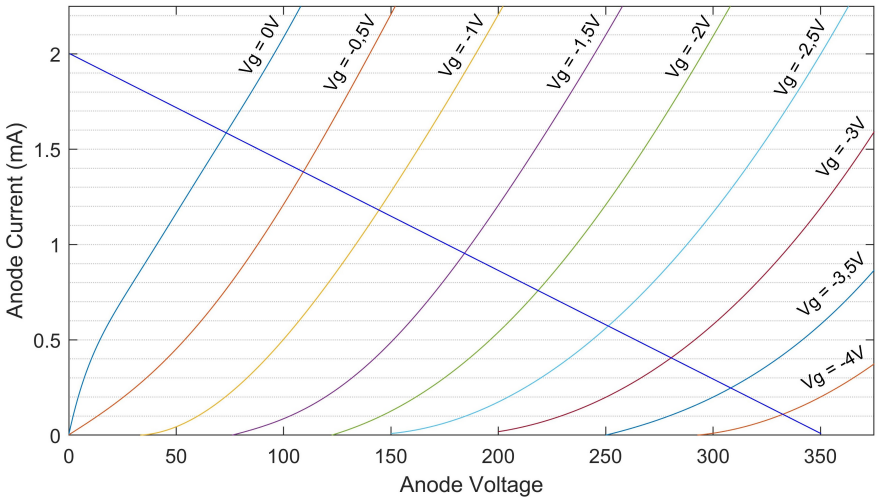

Figure 2.34: The loadline added to control grid curves. (Jones, 2012:66–67)

be calculated to be 65. The problem arises when the AC voltage applied to V_{gk} swings positive. There is limited space on the loadline (in Figure 2.34) as V_a approaches 0 V, this will cause a heavily distorted signal on V_a. (Jones, 2012:65–67)

A large anode current will flow if no *bias voltage* is applied between the control grid and ground ($V_{gk} = 0$). The current flow is limited by the quantity of electrons available at the cathode. However, a bias voltage (referred to as the *operating point*) can be applied to turn the valve *more off* for optimal operation. In effect, this regulates the quantity of electrons that flow from the cathode. It is important that the chosen bias voltage enables the most linear amplification of both sides of the waveform. The operating point sets the *quiescent* conditions, or the *no signal* conditions of the amplifier; this point will occur somewhere along the loadline. The output signal is superimposed on the DC voltage from the HT supply. A *coupling capacitor* is connected to the anode and will allow an AC signal to pass, but block DC from the HT supply. With reference to Figure 2.35, a battery can be used to apply a negative DC bias voltage to the control grid via a grid resistor R_g. The purpose of this is to prevent the short circuiting the AC voltage source; there is also a coupling capacitor (C_g) to prevent the short circuiting of the battery. The choice of an optimal operating point is limited by several factors. First, in Figure

2.34, note that as V_a increases, the grid curves become closer together and more curved[45]. This is exacerbated as V_a gets closer to the HT voltage, and approaches a region of non-linearity. The supply of current will gradually decrease and the signal will become distorted, this is known as the *cutoff region.* Conversely, as the control grid is made more positive towards the opposite end of the loadline, *positive grid current* $V_{gk(\max)}$ occurs. At a certain point the control grid will no longer repel electrons emitted by the cathode, instead it attracts electrons and behaves akin to a new anode. This results in an attenuation of the positive peaks of the audio signal, resulting in asymmetrical clipping. The problem of $V_{gk(\max)}$ varies from valve to valve, but is normally considered to be at approximately -1 V (the exact value will be provided the valve datasheet). The valve datasheet provides many important limiting values, such as the maximum allowed anode dissipation (the internal electrodes are at risk of melting). Other important values are the maximum DC and AC ($V_{a(b)}$) voltages that can be continuously applied to the anode. (Jones, 2012:68–70)

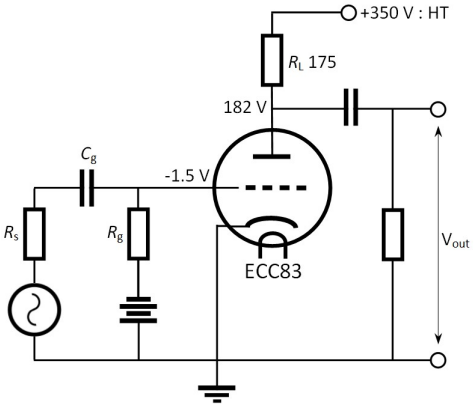

Figure 2.35: Grid bias voltage applied using a battery. (Jones, 2012:68)

Circuit designers are faced with the problem of whether to select an operating point that allows for either maximum voltage swing or maximum linearity. For example, to bias for a maximum voltage swing a V_a of 225 V could be selected, this would result in the anode voltage swinging up to 300 V and down to 150 V, this could be set via a grid bias of -2.1 V. Conversely, due to the unequal gain on each half of the wave cycle, biasing for linearity requires that the circuit designer be cognisant of the triodes tendency to produce 2nd order harmonic distortion. To avoid this, an operating point must be selected where the grid lines are equidistant on either side of the operating point. From Figure 2.34 it can be inferred that for a V_a of 182 V, a bias voltage of -1.5 V would satisfy this requirement. (Jones, 2012:70–71)

The next step of the circuit design process is to determine the AC *conditions* of the gain stage. Firstly, the *voltage amplification* (A_v) of the valve circuit will need to be calculated, the formula for this is provided in Equation 2.53[46]. If a V_a of 182 V with a bias voltage of -1.5 V are observed on the loadline in Figure 2.34, a 0.5 V change in either direction on the control

[45] Any part of the grid curve that is straight will result in linear operation, and any part that is curved will result non-linear operation.

[46] It must be noted that while the equation is the same to that of μ, A_v occurs along the loadline.

grid line would result in a V_a of 220 V and 148 V respectively. These values are inserted into the formula (Equation 2.54[47]) giving an A_v of -72 . (Jones, 2012:71)

$$A_v = \frac{V_{out}}{V_{in}} = \frac{\Delta V_a}{\Delta V_g} \tag{2.53}$$

$$A_v = \frac{220\,\text{V} - 148\,\text{V}}{1\,\text{V} - 2\,\text{V}} = -72 \tag{2.54}$$

As linearity has been chosen as the primary goal of this example, the maximum undistorted voltage swing will need to be determined. If either side of the selected operating point of -1.5 V is observed, the positive grid current occurs at approximately 148 V. To the right of the operating point there is no limit until V_a = HT; however, the output voltage cannot swing as far negative as it can positive. Therefore, the maximum undistorted peak to peak voltage swing is twice the value of the operating point to the positive grid current limit (the first limit encountered); this corresponds to 72 $V_{pk\text{-}pk}$. It is convention for AC signals to be expressed as RMS values, and the maximum undistorted output signal is calculated to be approximately 25 V_{rms}. If this value is deemed to be insufficient, another operating point can be selected by adjusting the values of the HT and R_L. (Jones, 2012:71)

The anode circuit of a triode can be modelled as a voltage source coupled through a series resistance in parallel with R_l, as demonstrated in Figure 2.36. As r_a is a dynamic AC parameter, r_{out} will also be a dynamic parameter. The r_a of the circuit given in Figure 2.35 can be calculated with Equation 2.49, where the values of ΔV_a and ΔI_a can be found by drawing a tangent on the grid curve of the selected operating point, as demonstrated in Figure 2.37. Recall that r_a corresponds to the *gradient* of the slope of this tangent. Therefore, the lower bound of the tangent provides one set of current and voltage values, while the upper bound provides the other set[48]. Equation 2.49 allows r_a to be calculated, note that it is common practice to leave the denominator in milliamps, as this allows the automatic output of a value in kiloohms; the answer is provided below in Equation 2.55. Now that the value of r_a has been established, r_{out} can be calculated (resistors in parallel) resulting in a value of 47 kΩ (Equation 2.56). Jones (2012:72) notes that this is considered to be a high value of r_{out} as high μ valves tend to exhibit high values of r_a. (Jones, 2012:72–71; Blencowe, 2016:118–119)

$$r_a = \frac{\Delta V_a}{\Delta I_a} = \frac{382\,\text{V} - 121\,\text{V}}{4\,\text{mA} - 0\,\text{mA}} = 65\,\text{k}\Omega \tag{2.55}$$

$$r_{out} = \frac{r_a . R_l}{r_a + R_l} = \frac{65\,\text{k}\Omega \times 175\,\text{k}\Omega}{65\,\text{k}\Omega + 175\,\text{k}\Omega} = 47\,\text{k}\Omega \tag{2.56}$$

[47] The negative symbol used in this equation indicate that the amplifier inverts the output signal.

[48] With regards to the upper bound of V_a as seen in Equation 2.55, Jones (2012:73) recommends drawing a line perpendicular to the V_a axis from where the tangent meets the top of the graph, while both Langford-Smith (1963:15–16) & Blencowe (2016:118–119) use slightly different methods, these ultimately achieve the same result.

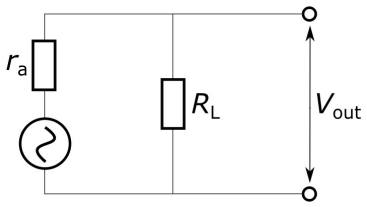

Figure 2.36: Equivalent circuit model of a triode's anode circuit.

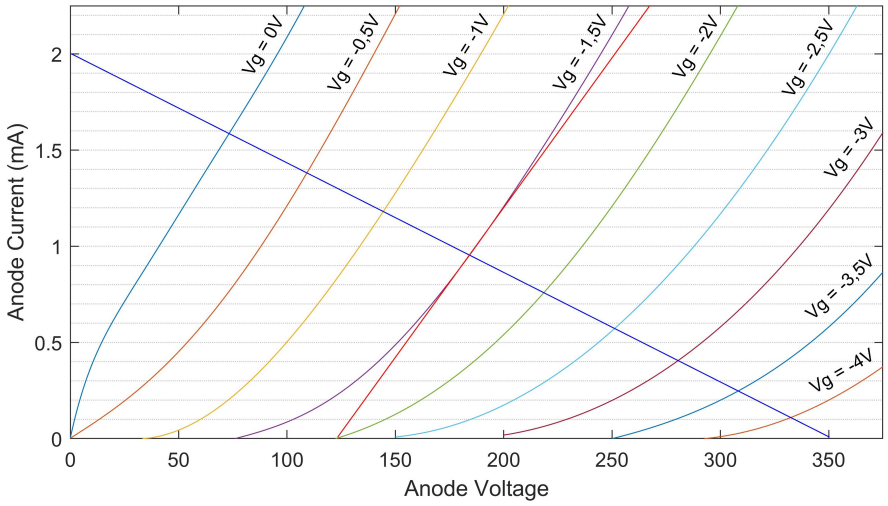

Figure 2.37: Anode load resistance tangent.

The value of μ can now be determined by placing a horizontal line across the operating point; hypothetically, doing this would give R_L an infinite value. Using the formula provided in Equation 2.47, and inserting the values of the horizontal line intersection of the grid lines, the upper and lower bounds of V_a and V_g can be determined (Equation 2.57). Note that the negative signs of the grid voltage curve can be ignored. Now that the values of μ and r_a have been established, it is possible to calculate A_v. Equation 2.58 provides a valuable means to compare values for errors. The loadline method gave A_v a value of 72, whereas the formula gave a value of 73, a negligible difference. (Jones, 2012:74)

$$\mu = \frac{\Delta V_a}{\Delta V_g} = \frac{233\,\text{V} - 133\,\text{V}}{2\,\text{V} - 1\,\text{V}} = 100 \tag{2.57}$$

$$A_v = \mu\left(\frac{R_L}{R_L + r_a}\right) = 100\left(\frac{175\,\text{k}\Omega}{175\,\text{k}\Omega + 65\,\text{k}\Omega}\right) = 73 \tag{2.58}$$

Following from the previous two examples, it appears as if g_m can be calculated by placing a vertical line[49] on the intersection of the operating point, and the change in anode current measured at the intersection of the grid lines. However, this method is problematic as the difference in current is greater from the -1.5 V to -1 V than from the -1.5 V to -2 V grid lines.

[49] This indicates that V_a is held constant.

Moreover, measuring the average of the grid lines from -1 V to -2 V gives an incorrect approximation. This problem can be overcome by using Equation 2.51, as the values of r_a and μ have previously been established, Equation 2.59 gives a result of 1.54 mA/V. Blencowe (2016:117) notes that as a valve ages the value of r_a tends to increase, g_m tends to decrease, while μ generally tends to remain unchanged and decreases only slightly. (Jones, 2012:75–76; Blencowe, 2016:120–121)

$$g_m = \frac{\mu}{r_a} = \frac{100}{65\,\text{k}\Omega} = 1.54\,\text{mA/V} \tag{2.59}$$

2.5.2 Cathode Bias

The implementation of batteries, or another power supply to bias a valve gain stage is highly impractical. In practice the most common method of biasing can be seen in Figure 2.38, where a *cathode bias resistor* (R_k) is placed between the cathode and ground. A *grid-leak resistor* (R_g) is placed between the control grid and ground. Therefore, the control grid is now at 0 V, thus making an input coupling capacitor redundant. The purpose of R_g is to create a path for electrons to flow through to discharge positive ions within the valve. The ions arise due to residual gas particles within the valve that have become positively charged due to the flow of electrons between the cathode and plate. Subsequently, there will always be some degree of *leakage current* that flows from the control grid to ground. The R_g is ordinarily assigned a large resistance value as a potential divider is formed with the output resistance of the previous stage. This results in a small loss of gain, which can add up through gain stages. A further benefit of a large value of R_g is economical, in that it permits the use of a low value coupling capacitor to connect to the following stage. Moreover, low value coupling capacitors tend to be smaller in size, which is beneficial if limited space is available. The R_k resistor is located between the cathode and ground, meaning anode current will now have to flow through it. Consequently, a voltage drop will form across R_k and the cathode will therefore be at a higher potential than the control grid. As an operating point has already been selected, the current that will flow through the resistor can be determined; it is equivalent to the anode current. To calculate the value of R_k used in the circuit in Figure 2.38, Equation 2.60 gives the anode current value of 0.96 mA; Equation 2.61 gives an R_k of 1.56 kΩ, which would bias the valve to its required operating point. (Jones, 2012:77–78, 80–83)

$$I_a = \frac{HT - V_a}{R_L} = \frac{350\,\text{V} - 182\,\text{V}}{175\,\text{k}\Omega} = 0.96\,\text{mA} \tag{2.60}$$

$$R_k = \frac{1.5\,V}{0.96\,\text{mA}} = 1.56\,\text{k}\Omega \tag{2.61}$$

The implementation of a resistor to set the operating point causes *cathode degeneration*; this can be either beneficial or problematic depending on the requirements of the design. Cathode degeneration occurs as the result of the grid voltage modulating the cathode voltage, and therefore the DC operating point. The grid voltage causes a change in plate current which causes a change in plate voltage. However, the plate current now also has to flow through R_k. Therefore,

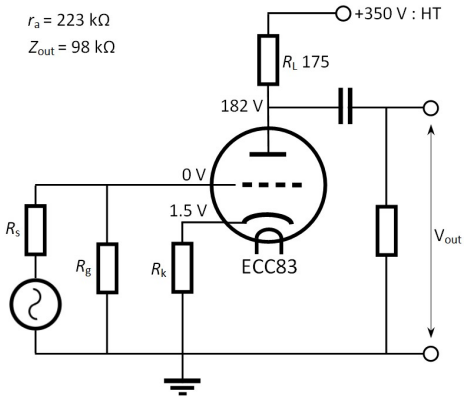

Figure 2.38: Cathode bias circuit without bypass capacitor.

as the anode current rises the cathode voltage will increase, and *vice versa*. This implies that a change in grid voltage results in a change in cathode voltage, and V_{gk} will be less than the applied signal voltage alone. The valve amplifies the difference between the grid and cathode voltage, the valve now has less signal to amplify. This results in lower gain, greater *headroom*, and lower levels of distortion. Cathode degeneration is a form of negative feedback, thus the universal feedback equation can be used to calculate any changes to gain; Equation 2.62 demonstrates that the gain is now considerably reduced. Another parameter that is affected by the introduction of negative feedback is the anode resistance, this can be calculated using Equation 2.63, which gives a value of 223 kΩ. The value of r_a has increased substantially from 65 kΩ to 223 kΩ. When placed in parallel with R_l the output impedance becomes 98 kΩ, a notable increase from 47 kΩ. (Jones, 2012:78–79)

$$A_{fbk} = \frac{A_0}{1+\beta.A_0} = \frac{72}{1+(1.56/175)\ \times\ 72} = 44 \tag{2.62}$$

$$r'_a = r_a + (\mu+1).R_k = 65 + (100+1) \times 1.56\text{k}\Omega = 223\,\text{k}\Omega \tag{2.63}$$

While in some instances negative feedback may be wanted, it reduces the gain of the system. With the addition of a *cathode bypass capacitor* (C_k) as seen in Figure 2.39, the gain can be fully restored by eliminating negative feedback at R_k. The C_k allows the AC signal to pass directly to ground, while maintaining a constant DC voltage at R_k. As a low pass filter is now formed with the output resistance of the cathode, C_k must have minimal reactance so that it allows all desired AC frequencies to pass. If the capacitance is too small only higher frequencies will pass, thereby creating a treble boost type of effect[50]. To calculate the cathode resistance, Equation 2.64 is used, giving a value of 2.38 kΩ, which in parallel with R_k gives a total of 942 Ω for r'_k. In order to select a value of C_k, consideration must be given to the lowest frequency of concern. It is generally accepted that the low frequency threshold of human hearing is 20 Hz. It must also be noted that there are likely various other gain stages throughout the amplifier, each with varying levels of filtering that can accumulate over the various stages.

[50] This phenomenon is taken advantage of in many guitar amp circuits to tune the frequency response.

Besides the goal of achieving a linear frequency response in the amplification process, the phase and transient response also require careful attention. These can be effected by a factor of 10 times the filter cut off frequency. Another problem is that *electrolytic capacitors* are often used as cathode bypass capacitors. These tend to have a rather poor tolerance and an unstable value that shifts with age. Jones (2012:80) recommends choosing a filter cut off value of 1 Hz to mitigate the aforementioned problems. Equation 2.65 demonstrates how to calculate the value of capacitance required for a low frequency cut off at this frequency. While the relationship between the gain, the frequency response, and value of capacitance can be rather unintuitive; the *shelved* response of the curve of the frequency response is easily approximated, as can be seen in Figure 2.40. The frequency at which the gain begins to increase from its lowest threshold (its unbypassed level) is given by Equation 2.66. (Jones, 2012:79–81)

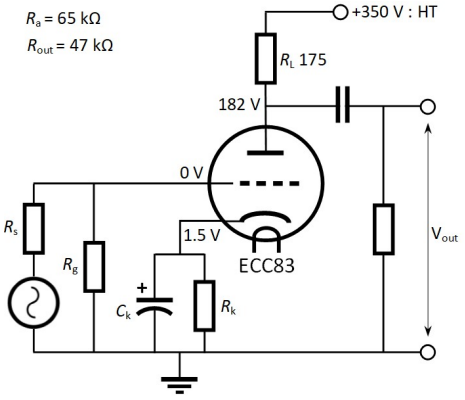

Figure 2.39: Cathode bias circuit with bypass capacitor.

$$r_k = \frac{R_L + r_a}{\mu + 1} = \frac{175 + 65}{100 + 1} = 2.38\,\text{k}\Omega \tag{2.64}$$

$$C_k = \frac{1}{2\pi.f.r'_k} = \frac{1}{2\pi \times 1 \times 942\,\Omega} \approx 170\ \mu\text{F} \tag{2.65}$$

$$f_{low} = \frac{1}{2\pi.R_k.C_k} \tag{2.66}$$

2.5.3 Miller Capacitance

Within the triode valve there are a number of electrodes separated by a vacuum. Whenever two electrodes are closely separated by an insulator, capacitance will develop across them; these are known as the *inter-electrode capacitances*. These capacitances are considered undesirable, of greatest concern is the grid to anode capacitance (C_{ga}), and the grid to cathode capacitance (C_{gk}). These are modelled as components in Figure 2.41. Current will flow into these capacitances as if they were real components, as demonstrated by the equivalent circuit in Figure 2.42.

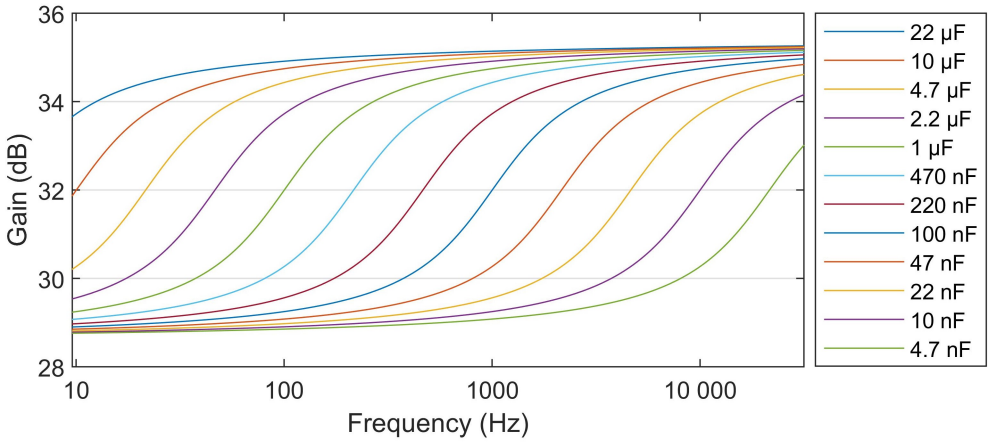

Figure 2.40: An approximation of the of various values of cathode bypass capacitor on the frequency response of the output signal. (Blencowe, 2016:142)

This phenomenon is exacerbated by what is known as the *Miller effect*[51], whereby the capacitance of C_{ga} is increased by approximately the same value as the gain. To elaborate, if the gain of the stage is 73 and a +1 V signal is introduced, V_a would drop by 73 V, resulting in a signal voltage of 74 V appearing across C_{ga}. This invariably results in a capacitive load that is a factor of 60 greater than the C_{ga} already present. This is known as *Miller capacitance*, which can be calculated with Equation 2.67. For the aforementioned values the miller capacitance is found to be approximately 115 pF, equating to a high frequency -3 dB point of 29 kHz[52]. While this high frequency attenuation is above the threshold of human hearing, it can become problematic as the capacitive effect can accumulate over many stages. Additionally, there are usually stray capacitances that emerge within a circuit that can exacerbate the high frequency attenuation. (Jones, 2012:83–84)

$$C_{\text{Miller}} = (A+1).C_{ga} = (73+1) \times 1.6 \text{ pF} = 115 \text{ pF} \tag{2.67}$$

While this high frequency attenuation is above the upper limit of human hearing, it can become problematic as the capacitive effect can accumulate over many stages. Furthermore, there are usually stray capacitances that emerge within a circuit that can exacerbate the high frequency attenuation. Jones (2012:84–85) suggests a number of ways that input capacitance problems can be mitigated:

i Reduce the output resistance of the previous stage. This can be done by using a valve with a lower output resistance; however, these valves tend to have a much lower gain. Another option is to use a some kind of impedance conversion device like a transformer or current buffer.

ii Screening the grid support rods would lower C_{ga} significantly. These *beamed grid* triodes tend to be designed only for radio UHF and other non-audio applications.

[51] This phenomenon is named after renowned electrical engineer John Milton Miller, who discovered it in the 1920s.

[52] The value of C_{gk} is 1.6 pF which would be added to this to find the total input capacitance, but C_{gk} has little effect on the -3 dB point of 29 kHz as it is such a low value.

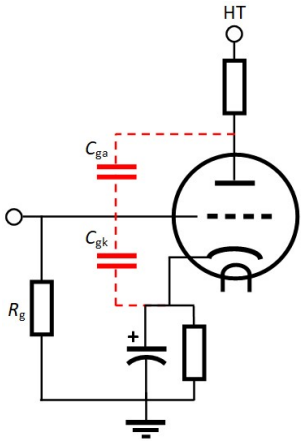

Figure 2.41: Inter-electrode capacitances as hypothetical components.

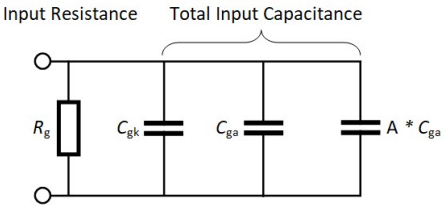

Figure 2.42: Equivalent circuit representing inter-electrode capacitances.

iii Using valves with extra electrodes that screen the grid from the anode. These are known as *tetrodes* and pentodes. However, these valves require more complex circuits, which take up more space, and are more likely to be microphonic than triode valves.

iv Reduce the gain of the circuit. This is not always desirable, as additional gain stages would be required to make up for the lost gain.

2.5.4 Valve Buffer Stages

While valves are ordinarily used as voltage gain amplifiers, they can also be used in unity gain buffer stages; although they perform poorly at this task. A buffer stage is used to isolate two stages within a circuit to minimise the interaction between them. They are characterised by a low output impedance and a high input impedance. The term *unity gain buffer* is a somewhat of a misnomer, as the gain provided is fractionally less than 1; any more and it would be considered an amplifier. Before the concept of unity gain buffer can be examined, a digression into two underlying, but related, concepts must be made. A *constant current source* (CCS) can be defined as a supply of energy that is inserted into a load that has a terminal connected to ground; an example of this would be a battery. A *constant current sink* controls the properties of an external energy source, though it supplies no energy of its own. (Jones, 2012:107–109)

According to Jones (2012:107–109), the performance of a constant current source or sink is determined by the following three characteristics:

DC Accuracy: The efficacy of a source or sink to manipulate current under varying conditions.

Voltage Compliance: The range of voltage that a source or sink can manipulate current.

Output Resistance: Ideally, the output resistance is infinite; however, these devices are constrained by power dissipation limitations.

Constant current/voltage sources/sinks are used to enhance the AC performance of a circuit. An ideal constant voltage source has zero resistance to AC, meaning that an infinite AC current flowing it through results in no voltage across it. In reality, these devices are considered *approximations*, and are subject to limitations. Examples of a real world constant voltage source would be a *voltage regulator*[53], other examples would include the reservoir capacitor found in most power supplies (an example of a source), and the cathode bypass capacitor (an example of a sink). Conversely, an ideal constant current source/sink has infinite resistance to AC, even with infinite voltage across it, no AC current will be able to flow through it. Traditionally, large inductors known as *chokes* have been used to approximate ideal constant current sources/sinks; chokes are often found in the power supply of large power amps (an example of a source), and are used to resist changes in current, additionally the inductance of the primary winding of an audio output transformer (an example of a sink) also shares this property. While passive devices have typically been used in many older designs, these have their limitations; modern designs use active components to approximate ideal sources and sinks more accurately. (Jones, 2012:107–109)

2.5.5 The Cathode Follower

The *cathode follower*[54] is a simple valve buffer circuit, that is depicted in Figure 2.43. The output signal of a buffer has to approximately replicate, or output, an exact copy of the input signal. The output signal is said to *follow* the input signal; hence, they are often referred to as *followers*. Valve gain stages suffer from high output impedance, thus the purpose of the cathode follower is impedance conversion. The cathode follower has no voltage gain[55], its function is to provide *current gain* amongst a variety of other useful properties. The basic principle behind a cathode follower is that a signal is inserted into V_{gk} in much the same way as a common cathode amplifier. However, the key difference is that the load resistor is placed between the cathode and ground. Subsequently, the output of the stage is taken from the cathode. If a positive signal is applied to the grid, the valve will raise its conduction and more current flow through R_k. This causes the voltage across the load R_k and V_{gk} to rise and fall sympathetically; therefore, the stage is non-inverting. The output voltage cancels out most of the input voltage, leaving only a fraction of the original input voltage to be amplified. The counteractive relationship of the input to output voltage results in *cathode current degenerative feedback*, the entirety of the output voltage cancels out a significant majority of the input voltage. Consequently, the cathode follower has 100 % negative feedback. The concession for approximate unity gain is

[53] These are semiconductor devices that are used to regulate or maintain a voltage at a specified value, typically they are used to remove power supply ripple and noise from a DC power source. (Laplante, 2005:736)

[54] The cathode follower was developed by Anthony Winther in 1925, but perfected by Alan Blumlein in around 1934.

[55] The voltage gain is fractionally below unity gain.

an improved performance in distortion and bandwidth, a notably higher input resistance (usually approximately 500 MΩ), and a lower output resistance (ordinarily around 1 kΩ or less). These are all qualities required of a competent buffer stage. (Langford-Smith, 1963:316–317; Blencowe, 2016:247–248; Jones, 2012:103–104)

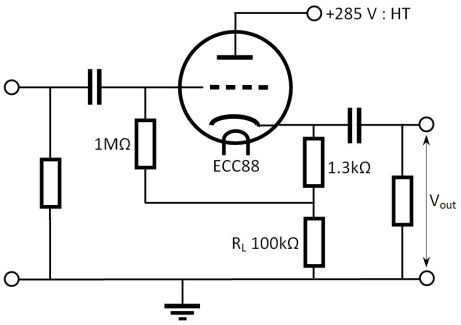

Figure 2.43: Simple cathode follower circuit. (Jones, 2012:104)

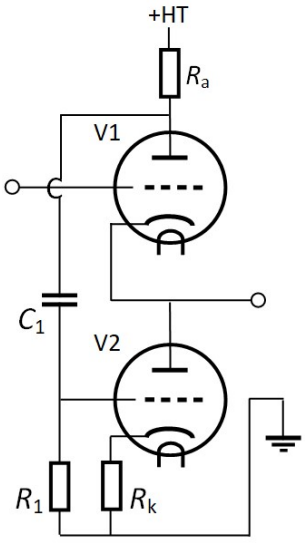

Figure 2.44: White cathode follower. (Blencowe, 2016:281)

An enhanced version of the cathode follower is the *White cathode follower*[56] (WCF). This is a *compound cathode follower*, as two triodes are used in conjunction in a buffer circuit. The supplied HT voltage will be shared approximately equally between the two anodes. The circuit configuration is similar to a standard cathode follower, V_2 aids V_1 in providing a source of current to deliver to the load. Thus the WCF can be thought of as a push-pull amplifier, or as White (1941:1) claims "[...] analogous to a class B amplifier." (Blencowe, 2016:281; White, 1941:1)

With reference to Figure 2.44, it is common practice to employ a low value anode resistor for V_1. This produces an inverted signal that is inserted into the grid of V_2 via C_1. V_2 and V_1 are in anti-phase with each other; hence, when V_2 conducts more, V_1 will conduct less, and

[56] Named after Eric White who patented it in 1941. (White, 1941:1)

vice versa. The external load will therefore be supplied by the difference in anti-phase currents supplied by V_1 and V_2, and the quiescent current shared by both valves. This process results in increased output power and substantially reduced output impedance. The WCF can be thought of as a small power amplifier, but is prone to distortion when used for this purpose. If the WCF is used to drive a high impedance load, the circuit can be designed to minimise distortion. When the anode resistance is equal to the output impedance, divided by the amplification factor of the lower triode ($R_a = Z_l/\mu_2$), the current flowing through V_2 will become constant and function like a true CCS. Blencowe (2016:283) notes that the optimised value for R_a in a WCF is approximately 1.3 kΩ, but finds through empirical measurement that distortion is reduced up until a R_a value of between 4 kΩ to 8 kΩ. The formula for the output resistance of a WCF is provided in Equation 2.68 (note the numerical subscript refers to the upper (1) or lower (2) triode). (Blencowe, 2016:281–284)

$$R_o = \frac{(r_{a1} + R_a).(R_k + r_{a2})}{(\mu_1 + 1).(r_{a2} + R_k) + (\mu_1 + 1).\mu_2.R_a + r_{a1} + R_a} \tag{2.68}$$

2.5.6 Valve Distortion

It can be observed in Figure 2.37 that the grid curves adjacent to the bias point are not evenly spaced. As they become more negative, they become closer and more concave. For a 1 V_{pp} input signal on the grid, the output signal at the anode would have a positive cycle with more headroom than the negative cycle. This results in a non-linear transfer function and asymmetrical clipping. The effect of this is harmonic distortion dominated by the 2nd harmonic; a common characteristic of triode valves. When the signal is increased further, the distortion will increase as the grid curves become closer together. Moreover, if the operating point becomes more negative, the transfer characteristic will become more non-linear. This phenomenon is referred to as *cutoff clipping*, as the valve can no longer supply more power, even if the grid becomes more negative. Cutoff clipping is characterised by a soft compression of the peak. It does not happen at a discrete point, but over a broad area as the input signal swings negative. (Blencowe, 2016:130–133)

On the other hand, the headroom of the positive peak is limited by how much current the triode can pass. As the grid voltage becomes more positive, it will begin to approach the voltage of the cathode. This will cause the electrons from the space charge to become more attracted to the grid than the anode[57]; this phenomenon is known as *grid current limiting*. The clipping structure produced by grid current limiting is *soft* in nature and also does not occur at a discrete point; however, it is certain to occur before $V_{gk} = 0$. (Blencowe, 2016:134–135)

The selection of the operating point typically determines whether cutoff clipping or grid current limiting occurs first. If the valve is *cold biased*, or if the selected operating point is more negative in value (closer to the cutoff region), then the valve will go into cutoff clipping before grid current limiting. Conversely, if the valve is *warm biased*, or the selected operating point is closer to the zero grid curve, then grid current limiting will occur first. (Blencowe, 2016:133–135)

[57] Blencowe (2016:134) notes that this would be akin to placing a diode between the grid and cathode.

Chapter 3

Research & Experimental Design

3.1 Research Overview

REGARDING the academic study of music production, Zagorski-Thomas & Frith (2012:7–8) claims that research comes from a broad range of disciplines, because of the complex technical and aesthetic nature of the music production process. In terms of methodological approaches, Zagorski-Thomas & Frith (2012) notes that musicologists typically employ a form of *content analysis* to analyse musical scores, and prescribes a similar approach to analysing *recordings*:

> There are now a multitude of possible visual representations of digital files that can be used to create graphic interpretations of audio phenomena: waveforms, spectrograms, chromagrams, onset detection, inharmonicity detection - the list is endless and relates specifically to features that you may want to study. But that is the key: the methodology for textual [content] analysis relies on identifying and measuring given features in the text (Zagorski-Thomas & Frith, 2012:7–8).

Audio content analysis involves the extraction of information from audio signals. For example, an audio recording stored on digital media is *content*. The extracted information is known as *metadata*, and can be defined as data about (audio) data. Metadata can encompass any information that permits a meaningful description or explanation of raw audio data. Nowadays, attempts are made for the automatic extraction of all viable data from audio recordings. This includes formal, perceptual, musical, and technical metadata. (Lerch, 2012:1)

Quantitative research is an approach to empirical inquiry that collects, analyses, and produces data in numerical form as opposed to narrative form. Quantitative research is deductive in nature and requires that a researcher be objective, and dissociate themselves from any preconceived notions they might have about the research. The primary concern of quantitative researchers is *validity*, where *internal validity* is the accuracy of the research variables that are being measured. Likewise, *external validity* is how *repeatable* the research is, or how *generalisable* it is to a larger sample size. (Donmoyer, 2008:713; Miller, 2008:909–910)

Exploratory experimentation is implemented in order to explore phenomena without employing an explicit hypothesis, or be motivated by a specific theoretical approach. The exploratory experimental approach is not bound by a hypothesis or theory. The goals can either be *practical*, in that a researcher can learn how to manipulate a phenomenon, or *theoretical*, in which a conceptual framework for future research can be developed. (Waters, 2007:3–5)

This research employed an *exploratory experiment* in order to generate *quantitative data*, which was analysed in the form of *audio content analysis*. The nature of the aforementioned concepts guided the approach to empirical research adopted for this thesis, and provided a framework most appropriate to attaining the stated objectives.

Laplante (2018:87) recommends the following structure for reporting on the results of experiments. Firstly, one should state the necessity for experimentation, and then provide an in depth description of the methodologies employed. This should be followed by the results, the interpretation of results, and finally the conclusions. These steps should ensure the repeatability and validity of the experiments conducted.

3.2 Data Measurement and Analysis Instrumentation

Measurement is a tool that allows us to describe, differentiate, explain, predict, diagnose, and process the myriad of the phenomena we encounter when enquiring into the world around us. Measurements help to mitigate ambiguity and inconsistency when describing phenomena. Tal (2020) defines measurement as "[...] an activity that involves interaction with a concrete system with the aim of representing aspects of that system in abstract terms". While Pedhazur & Schmelkin (1991:17) define measurement as "[...] mapping a set of objects onto a set of numbers, such that there is isomorphism between the objects measured and the numbers assigned to them". With the aforementioned conceptualisation of measurement in mind, powerful measurement instrument tools and techniques must be selected to ensure that the research is conducted with a high degree of rigour. MATLAB was be employed as an analysis tool as its advanced scientific computing features make it an excellent instrument for the measurement and analysis of audio data. (Tarr, 2018:3)

Within the MATLAB software environment, digital audio signals are represented as an *array* of numbers. Monophonic audio signals thus have an array of one column, and a multitude of rows. These represent unique samples, each at a regular interval of time. The value of the numbers within the rows indicates the amplitude value of discrete samples. The *Audio Toolbox* provides a particular set of *functions* that allow MATLAB to interact with digital audio files. For example, in order to load an audio file into MATLAB, one could use the `audioread` function. This function stores the audio data within a *column vector*[1], with the sample rate of the audio file being allocated into a *scalar*[2] *variable*[3]. In order to make use of the `audioread` function a particular programming syntax[4] is used. (Tarr, 2018:21–23)

[1] A column vector is a two dimensional array in which the row is omitted, as it has only one index value (Butterfield & Ngondi, 2016:matrix).

[2] "A number comprising a single value (such as an integer or real number), as opposed to a complex number (containing two scalars) or a vector (which is a scalar only in the special case of its containing one number)." (Butterfield & Ngondi, 2016:scalar)

[3] "A unit of storage that can be modified during program execution, usually by assignment or read operations. A variable is generally denoted by an identifier or by a name." (Butterfield & Ngondi, 2016:variable)

[4] "The rules defining the legal sequences of symbolic elements in a language. The syntax rules define the form of the various constructs in the language, but say nothing about the meaning of these constructs. Examples of constructs are: expressions, procedures, and programs (in the case of programming languages) and terms, well-formed formulas, and sentences (in the case of logical languages)." (Butterfield & Ngondi, 2016:syntax)

Listing 3.1: Basic audio commands.

```
Fs = 44100;
x = 'example.wav';
[y,Fs] = audioread(x);
sound(y,Fs);
xOut = 'exampleOut.wav'
audiowrite(xOut,y,Fs);
```

In Listing 3.1 an audio file `'example.wav'` is assigned to the variable `x`. The variable `y` contains the samples of the signal in an array, with the variable `Fs` containing the sampling rate of the file as it is stored on the computer. The `sound` function can then play back the selected audio file. The audio data can then be edited or manipulated within MATLAB, and the resultant data saved back into an audio file by using the `audiowrite` command. This is demonstrated by the variable `xOut`, which is used to assign the output file name.

The DSP *System Toolbox* provides tools for analysing digital audio signal processing systems, the primary instruments used for this research were the system objects; `dsp.TimeScope` and the `dsp.SpectrumAnalyser`. The `dsp.TimeScope` system object is used to display and analyse time domain signals, akin to an oscilloscope. While the `dsp.SpectrumAnalyser` system object can be used to display and analyse the frequency spectrum properties of time domain signals. For the experiments, the `dsp.TimeScope` system object was configured with the code in Listing 3.2:

Listing 3.2: Time domain render.

```
Fs = 44100;
a = audioread('TestFile1.wav');
b = audioread('TestFile2.wav');
c = audioread('TestFile3.wav');
scope = dsp.TimeScope('NumInputPorts',3,
'ShowLegend',true,
'SampleRate',Fs, 'TimeSpan',5,'Position'
,[60 375 350 400],
'ChannelNames',{'TestFile1','TestFile2',
'TestFile3'});
scope(a,b,c)
```

In Listing 3.2, three audio test files are loaded into matlab using the `audioread` function, and each is assigned to a variable. The next section of code defines the parameters of this instance of `dsp.TimeScope`, which is configured to have three input ports for three channels of input signals. The `'ShowLegend',true` statement will result in a *legend* being included with the render of the waveform, this will display the unique colours and names of each channel. The `'SampleRate',Fs` provides the sample rate data for `dsp.TimeScope`, which in this instance is defined by `Fs = 44100`. The `'TimeSpan',5` statement, sets the time span to 5 seconds, and `'Position',[60 375 350 400]` sets the position and dimensions of the rendered plot. The names to be used by the legend are assigned by the `'ChannelNames'` statement. Finally, the `scope(a,b,c)` initialises `dsp.TimeScope` to begin rendering the three audio files with the set parameters. (Matlab, 2020a:4-1285–4-1298)

The `dsp.SpectrumAnalyser` system object was configured with the code in Listing 3.3 for the experiments:

Listing 3.3: Spectrum render.

```
Fs = 44100;
a = audioread('TestFile1.wav');
SA = dsp.Spectrumanalyser('SampleRate',Fs,'Method','Filter bank',...
'SpectrumType',"Power", 'SpectrumUnits','dBFS',...
'PlotAsTwoSidedSpectrum',false,'YLimits',[-60 0];
SA.RBWSource = 'property';
SA.RBW = 1;
for Iter = 1:100
    SA(a);
end
release(SA);
```

Once again an audio file is loaded at a particular sample rate; the spectrum parameters are then configured by the `SA` variable. The `'Method','Filter bank'` sets the spectrum estimation method to the *filter bank*[5] technique. The `'SpectrumType',"Power"` statement configures `dsp.SpectrumAnalyser` to function as a *power spectrum*[6]. While the next statement `'SpectrumUnits','dBFS'` instructs the system object `dsp.SpectrumAnalyser` to output the spectrum data as dBFS[7] units, note that any harmonic partials will be returned on the dBc scale, that is they are represented as a power relative to a *carrier frequency*, which in this case would be the magnitude of the fundamental. The `'PlotAsTwoSidedSpectrum',false` statement sets the spectrum as single sided, so as to not return any redundant negative frequency data. The `'YLimits',[-60 0]` statement configures `dsp.SpectrumAnalyser` to only display frequency data above -60 dB, as this was assumed to be the practical dynamic range of the devices under test[8]. (Matlab, 2020a:4-1203–4-1223, Matlab, 2020b:24-34)

In order to configure the frequency resolution of the spectrum, adjustments must be made within the user interface of the `dsp.SpectrumAnalyser` window, or from within the code by using the `SA.RBWSource = 'property'` statement; this enables the user to select a *resolution bandwidth*. The resolution bandwidth (RBW) is the smallest frequency interval that can be resolved. As high levels of acuity were a requirement for this research, the RBW was set to 1 Hz by the `SA.RBW = 1` statement. The `dsp.SpectrumAnalyser` window has a *distortion measurements* feature, this initiates the *distortion measurements* panel which provides the user with harmonic distortion values in the form of frequency and magnitude data. The sinusoidal frequency with the highest magnitude is designated the fundamental, with other frequencies as harmonics. A *for loop* is then used to run the spectrum analyser a hundred times and return

[5] The filter bank technique is selected over the alternative Welch technique, as it has a higher level of precision, which comes at the expensive of greater computational power. (Matlab, 2020b:16-62)

[6] Matlab (2020b:16-14) defines this as: "The power spectrum (PS) of a time-domain signal is the distribution of power contained within the signal over frequency, based on a finite set of data. The frequency-domain representation of the signal is often easier to analyse than the time-domain representation[...] The goal of the power spectral estimation is to estimate the power spectrum of a signal from a sequence of time samples."

[7] White & Louie (2005:97) defines these as: "The absolute digital signal level referenced to full scale on a digital level detector."

[8] Note: the primary DUT measured hum at 100 Hz at approximately -70 dBFS at its maximum gain setting.

the average of the iterations via the `for Iter = 1:100` statement. Finally, the spectrum analyser is commanded to analyse the variable with the given set of properties in `SA(a)`; with `end` terminating the *for loop*. The `dsp.SpectrumAnalyser` window is then initiated with the `release(SA)` statement. (Matlab, 2020b:24-33–24-34)

In certain instances an entire spectrum may not be required. The DSP toolbox can be used to extract harmonic distortion data as numerical values as indicated in the Listing 3.4. In this example, `r` returns total harmonic distortion data in dBc as a real value scalar, `harmpow` returns the power of individual harmonics in in dBc, while `harmfreq` returns the frequencies of the individual harmonics. The command `thd` then computes the harmonic distortion data for `a` at the sample rate `Fs`, the `10` value indicates that `thd` should return power and frequency data up to the 10^{th} harmonic. The next line `format shortg` sets the maximum length of returned code to five digits. The last line of code, `round(harmpow,1)`, returns the power values of the first ten harmonics, rounded to the first decimal digit, in a column array, with the fundamental at the top in descending order to the 10^{th} harmonic.

Listing 3.4: Harmonic distortion values.

```
Fs = 44100;
a = audioread('TestFile1.wav');
[r, harmpow,harmfreq] = thd(a,Fs,10);
format ShortG;
round(harmpow,1)
ans =
         -4.4
        -26.1
        -15.1
        -27.5
          -22
          -30
        -28.7
        -33.8
          -36
        -39.2
```

3.3 Synthesis of Audio Test Files

In order to adequately test the experimental devices, a series of test tones is required. Periodic signals with known harmonic properties will be used in the experiment. The method behind synthesising a periodic waveform in MATLAB is described in Listing3.5.

Listing 3.5: Sine wave

```
Fs = 44100;
Ts = (1/Fs);
t = 0:Ts:5;
f = 110;
sn = sin(2*pi*f*t);
audiowrite('SineWaveTest.wav',sn,Fs,'BitsPerSample',16)
```

```
x = audioread("SineWaveTest.wav");
```

The first line, `Fs = 44100` declares the sampling rate of the synthesised periodic waveform, this is set to 44 100 Hz as this is the standard sampling rate for CD quality audio. The next parameter to be declared, `Ts = (1/Fs)` is the sample period, while `t = 0:Ts:5` sets the time duration of the periodic waveform to 5 seconds. The frequency of the periodic waveform is set to a pitch of A2 or frequency of 110 Hz by `f = 110`. The sine wave is generated by `sn = sin(2*pi*f*t)`, using the properties of the variables `f` and `t`. The last line of code writes the audio to a data file using the `audiowrite` command, this is followed by the name of the file being encoded `'SineWaveTest.wav'`, `'BitsPerSample',16);` sets the bit rate to 16 bit, the standard bit-rate of CD quality audio. The code to construct a sawtooth, square, and triangle wave share similarities, while the code for an impulse train differs in that individual samples are generated at regular intervals. The resultant waveforms and spectrums can be seen in Chapter 2.1.4; the MATLAB code used to generate each audio test file is included in Listings 3.6–3.9: (Tarr, 2018:80–99)

Listing 3.6: Sawtooth wave.

```
Fs = 44100;
Ts = (1/Fs);
t = 0:Ts:5;
f = 110;
st = sawtooth(2*pi*f*t + pi);
audiowrite('SawWaveTest.wav',st,Fs,'BitsPerSample',16)
x = audioread("SawWaveTest.wav");
```

Listing 3.7: Square wave.

```
Fs = 44100;
Ts = (1/Fs);
t = 0:Ts:5;
f = 110;
sq = square(2*pi*f*t);
audiowrite('SquareWaveTest.wav',sq,Fs,'BitsPerSample'16);
x = audioread("SquareWaveTest.wav");
```

Listing 3.8: Triangle wave.

```
Fs = 44100;
Ts = (1/Fs);
t = 0:Ts:5;
f = 110;
tr = sawtooth(2*pi*f*t + pi/2,0.5);
audiowrite('TriWaveTest.wav',tr,Fs,'BitsPerSample',16)
x = audioread("TriWaveTest.wav");
```

Listing 3.9: Impulse train.

```
Fs = 44100;
Ts = (1/Fs);
t = 0:Ts:5;
f = 100;
it = zeros(size(t));
period = round(Fs/f);
it(1:period:end) = 1;
audiowrite('ImpulseTrainTest.wav',tr,Fs,'BitsPerSample',16)
x = audioread("ImpulseTrainTest.wav");
```

3.4 Triode Anode Characteristics Analysis Process

The static anode characteristics are critical for the analysis of the gain stages of the primary DUT. While this is normally conducted somewhat crudely by hand with a pencil and ruler, MATLAB is able to plot the static anode characteristics with a far higher degree of acuity. Furthermore, the bias point, DC loadline, and valve constants can also be calculated with the generated plot values. To derive the control grid curves, MATLAB's *polynomial curve fitting* function `polyfit`, was used to trace the curves from the original valve datasheets[9]. A series of horizontal x (V_a) and vertical y (I_a) co-ordinate values were input into an array. The `polyfit` function then finds the closest coefficients of a polynomial that best fits the data points. The function `linspace` then sets the upper and lower bounds of curve, and divides the curve into a series of equally spaced *elements*, and `polyval` is implemented to evaluate data points absent in the original arrays. Listing 3.10 provides the code for the grid curve of $V_{gk} = -0.5$ for the 12AX7 valve, `x05` and `y05` are assigned to V_a and I_a respectively. Polyfit will approximate a curve with the data entered in `pf05 = polyfit(x05,y05,5)`. The polynomial degree of 5 was found heuristically to be the best approximation for the $V_{gk} = -0.5$ grid curve. The command `ls05 = linspace(0,250,10000)` sets the range of the curve, from 0 V to 250 V, and the number of equally spaced data points, which is 10 000. The command `pv05 = ... polyval(pf05,ls05)` then evaluates the unknown points, and the plot render is initiated by the `plot(ls05,pv05)` command. (Gilat, 2017:38, 269–271; Matlab, 2020c:6-11)

Listing 3.10: 12AX7 $-0.5V_{gk}$ grid curve.

```
x05 = [0 25 50 75 100 125 150 175 200 225 250];
y05 = [0 .2 .45 .8 1.2 1.65 2.3 2.7 3.25 3.9 4.5];
pf05 = polyfit(x05,y05,5);
ls05 = linspace(0,250,10000);
pv05 = polyval(pf05,ls05);
xt = 120;
yt = 1;
str = 'Vg = -0.5V';
text(xt,yt,str)
```

[9] The values used to make this code were taken from the relevant GENERAL ELECTRIC data sheets of each valve, see 12AX7 (1954) and 12AY7 (1954).

```
plot(ls05,pv05)
```

Following from this, an analysis of the triode gain stage provided in Figure 3.1 can be demonstrated using MATLAB code. The DC loadline is a gradient plotted between two points, with the x-axis origin being the HT value when I_a is zero, and I_a the y-axis origin when V_a is zero; I_a is calculated using Ohm's law across the R_L. The R_L has a value of 100 kΩ and an HT voltage of 250 V, equating to a maximum I_a of 2.5 mA. Therefore, in the code in Listing 3.11, the DC loadline is drawn from 250 V on the x-axis to 2.5 mA on the y-axis[10]; `linspace` then assigns 10 000 equally spaced data points to the rendered line.

Listing 3.11: DC load line.

```
dc = linspace(0+2.5i, 250+0i, 10000);
plot(dc)
```

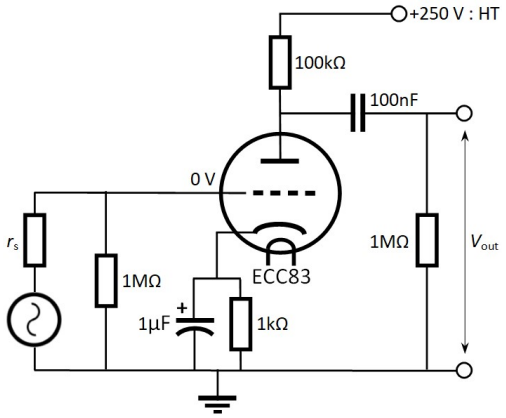

Figure 3.1: 12AX7 Triode gain stage for demonstration purposes.

To find the bias point as well as the quiescent V_a and I_a values, the techniques covered in Chapter 2.5.1 can be employed to calculate the *cathode loadline*. If the hypothetical R_k is given as 1 kΩ, then the V_a and I_a can be calculated at two values of V_{gk} using Ohm's law. In this instance, a V_{gk} of 0.5 V and 1.5 V appear to be optimal (see Equations 3.1 & 3.2).

$$I = \frac{V_g}{R_k} = \frac{0.5}{1000} = 0.5\,\text{mA} \tag{3.1}$$

$$I = \frac{V_g}{R_k} = \frac{1.5}{1000} = 1.5\,\text{mA} \tag{3.2}$$

The cathode loadline must then be plotted between the points where I_a is 0.5 mA and V_{gk} is 0.5 V, to the point where I_a is 0.5 mA and V_{gk} is 0.5 V. This is where using MATLAB's plot

[10] Anode current is represented as an imaginary number, hence the i symbol in the code.

function is advantageous as it provides the V_a values at these two points[11], which are observed as 54 V and 117.5 V respectively. The code for drawing this line employs a similar methodology to the DC loadline and can be seen in Listing 3.12.

Listing 3.12: Cathode load line.

```
cll = linspace(54+.5i, 217.5+1.5i, 10000);
plot(cll)
```

The point at which the DC loadline and cathode loadline intersect is the bias point, at this point the MATLAB plot will give us the quiescent I_a, which is 1.05 mA and the quiescent V_a, which is 144.6 V. It can be seen from the graph that the bias point sits somewhere on the DC loadline between the 1 V V_{gk} curve and the 1.5 V V_{gk} curve. In order to best approximate its value, `linspace` can be used to divide this portion of the line into 10 equally spaced lengths, where it can be observed that the bias point appears to be approximately 1.15 V. The code for this process is shown in Listing 3.13:

Listing 3.13: Operating point.

```
plot(144.6, 1.054, 'x');
text(xt,yt,str)
```

In order to determine the anode resistance r_a, a tangent must be drawn at the point where V_{gk} intersects the bias point, or at its closest approximation; r_a is the gradient of this tangent. The tangent was calculated heuristically in MATLAB and is plotted in the code in Listing 3.14, with Equation 3.3 giving a resultant r_a of 60.6 kΩ.

Listing 3.14: Anode resistance tangent.

```
tng = linspace(72.8+0i, 250+2.915i, 10000);
plot(tng)
```

$$r_a = \frac{\Delta V_a}{\Delta I_a} = \frac{160\,\text{V} - 120\,\text{V}}{1.43\,\text{ma} - 0.77\,\text{ma}} \approx 60.6\,\text{k}\Omega \tag{3.3}$$

The amplification factor (μ) is calculated by measuring the change in V_a as a ratio of the change in V_{gk}, while I_a is maintained at a constant; the quiescent anode current in this example is 1.05 mA. The MATLAB plot provides us with easy access to the V_a and V_{gk} values, and μ is calculated to be 100 (Equation 3.4). The mutual conductance (g_m) can be calculated by measuring the change in I_a as a ratio of the change in V_{gk}, while V_a is maintained at a constant, the quiescent anode voltage, which in this example is 144.6 V. Once again the MATLAB plot provides easy access to the I_a and V_{gk} values, and g_m is calculated to be 1.66 mA/V (Equation 3.5).

[11] This is accomplished by simply zooming in on the point of interest and clicking on it, MATLAB then displays the x and y co-ordinates respectively.

$$\mu = \frac{\Delta V_a}{\Delta V_g} = \frac{191\,\text{V} - 91\,\text{V}}{1.5\,\text{V} - 0.5\,\text{V}} = 100 \tag{3.4}$$

$$g_m = \frac{\Delta I_a}{\Delta V_g} = \frac{2.09\,\text{mA} - 0.43\,\text{mA}}{1.5\,\text{V} - 0.5\,\text{V}} \approx 1.66\,\text{mA/V} \tag{3.5}$$

The properties of the cathode circuit can also also analysed. The internal cathode resistance r_k is calculated to be 1.59 kΩ (Equation 3.6), which in parallel with an R_k of 1 kΩ gives a total resistance of the cathode (r'_k) to be approximately 614 Ω. From the schematic it can be seen that C_k is 1 µF which allows the frequency response of the cathode bypass circuit to be calculated (Equation 3.7). Furthermore, the output impedance of the stage can now also be calculated using Equation 3.8.

$$r_k = \frac{R_L + r_a}{\mu + 1} = \frac{100\,\text{k}\Omega + 60.6\,\text{k}\Omega}{100 + 1} \approx 1.59\,\text{k}\Omega \tag{3.6}$$

$$f_{\text{-3dB}} = \frac{1}{2\pi . C_k . r'_k} = \frac{1}{2\pi \times 0.000001\,F \times 680\,\Omega} \approx 234\,\text{Hz} \tag{3.7}$$

$$Z_{\text{out}} = \frac{R_a \times r_a}{R_a + r_a} = \frac{100 \times 60.6}{100 + 60.6} \approx 37.73\ \text{k}\Omega \tag{3.8}$$

The filter network created by the C_g and R_g can now be calculated, $f_{\text{-3dB}}$ is given as 1.53 Hz according Equation 3.9. The AC loadline can now be calculated, as seen in Equation 3.10 this gives a $R_{a(\text{AC})}$ of 90.9 kΩ. This can be integrated with the quiescent V_a and I_a of the operating point to give the maximum I_a and V_a values, thus providing values required for the AC loadline, as seen in Equations 3.11 & 3.12; with the code included in Listing 3.15. The parameters derived and measured above can then be generated into a graph by MATLAB, as seen in Figure 3.2; the code for the plot can be seen in Appendix A.1.

$$f_{-\text{3dB}} = \frac{1}{2\pi . C_g . (Z_{out} + R_g)} = \frac{1}{2\pi \times 0,0000001 \times 1037730} \approx 1.53\,\text{Hz} \tag{3.9}$$

$$R_{a(\text{AC})} = \frac{R_a \times R_g}{R_a + R_g} = \frac{100 \times 1000}{100 + 1000} \approx 90.9\,\text{k}\Omega \tag{3.10}$$

$$I_{a(\text{Max})} = I_a + \frac{V_a}{R_{a(\text{AC})}} = 1.05 + \frac{144.6}{90.9} \approx 2.65\,\text{mA} \tag{3.11}$$

$$V_{a(\text{Max})} = V_a + I_a \times R_{a(\text{AC})} = 144.6 + 1.05 \times 90.9 \approx 240.04\,\text{V} \tag{3.12}$$

Listing 3.15: AC loadline.

```
ac = linspace(0+2.65i, 240.04+0, 10000);
plot(ac)
```

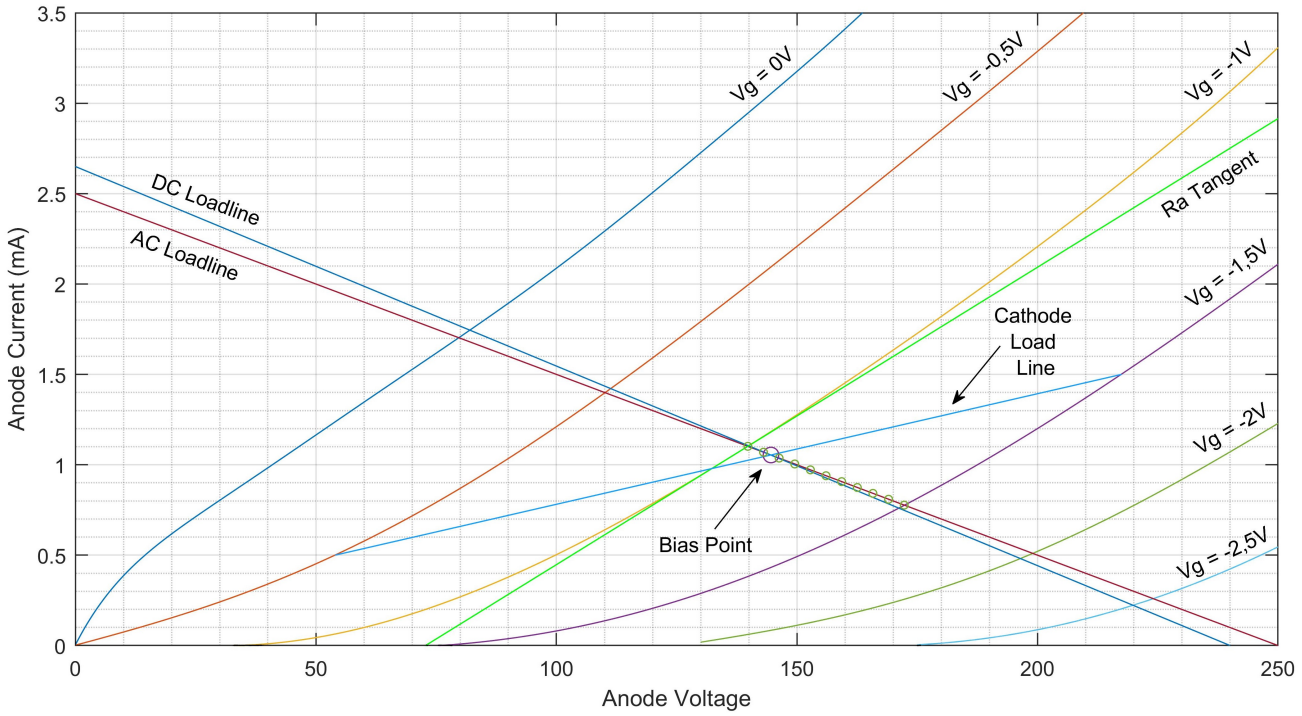

Figure 3.2: Characteristics of example circuit.

3.5 Experiment Processes

Distortion tests have historically been devised to measure the overall quantity of distortion generated by a DUT. These historical tests are problematic for analysing signal colouration as this is not the purpose for which they were designed; thus, it is reasonable to acknowledge that they are ineffective at this task. Therefore, a series of experiments were devised to ameliorate these distortion tests, with the intention of exploring the unique distortion profiles of each DUT. The experiments were designed to examine each DUT's response to changes in sine and complex waves in both the time and spectral domains.

3.5.1 Experiment 1: Time Domain Analysis of the Clipping Structure of Sine waves.

The aim of Experiment 1 was to examine how the nature of each DUT's clipping structure emerges with an increasing signal level in the time domain; permitting the analysis of the differences and similarities between devices. Firstly, sine waves of varying amplitudes were input into each DUT. The amplitude of the sine wave was adjusted to be at the point where the highest harmonic partial after the fundamental was approximately 15 dBc to 16 dBc. From there the

input signal was attenuated in 5 dB increments using the PROTOOLS' *trim* plugin. The value of harmonic level was selected as a *control* in order to adequately compare the results of each DUT. It is reasonable to presume that this is approximately the maximum level of distortion likely to be used in an audio production studio. The files were then simultaneously loaded into `dsp.TimeScope`; the `'NumInputPorts',7` parameter permits seven audio files to be loaded into `dsp.TimeScope`. The code initiates a window that displays approximately one wavelength from the steady state region of each waveform, and can be seen in Listing 3.16.

Listing 3.16: Clipping structure code.

```
Fs = 44100;
a = audioread("0.wav");
k = audioread("-5.wav");
u = audioread("-10.wav");
e1 = audioread("-15.wav");
o1 = audioread("-20.wav");
y1 = audioread("-25.wav");
i2 = audioread("-30.wav");

scope = ...
    dsp.TimeScope('NumInputPorts',7,'ShowLegend',true,'SampleRate',Fs,
'TimeSpan',0.012,'Position',[60 375 350 400],
'ShowLegend',true,
'ChannelNames',{'0db','-5dB','-10dB','-15dB','-20dB','-25dB','-30dB'});

scope(a,k,u,e1,o1,y1,i2)
```

3.5.2 Experiment 2: Harmonic Distortion as a Function of Input Level

The objective of Experiment 2 was to observe how the levels of harmonic distortion partials evolved depending on an increasing input level. This experiment was inspired by Hamm (1973:270–271), who produced noteworthy experiment results, but was unfortunately limited by the measurement technology available to him at the time. Experiment 2 was conducted in the digital domain and used discrete values for the amplitude of the test files. Once again, sine waves of varying amplitudes were inserted into each plugin. The test input signal with the highest amplitude was selected, contingent on the next highest harmonic partial magnitude being approximately 15 dBc to 16 dBc below the fundamental. From there the input signal was attenuated in 0.5 dB increments from 0 dB to -30 dB using the PROTOOLS' *trim* plugin. Once each file had been processed, the `harmpow` command (from Listing 3.4) was used to extract harmonic distortion data for the first 10 harmonics in each file; the values of which were stored in a matrix.

The values of this matrix were then used to construct a graph that shows the harmonic distortion components as a function of the input level. The y-axis indicates the input signal level (ISL), with the straight blue line showing the linear input amplitude of the test signal. The x-axis displays the output amplitude of the processed test signal fundamental and harmonics. To improve the legibility of the graph, the fundamental and each harmonic was given a unique

colour. Furthermore, odd and even harmonics were each assigned a unique symbol, with odd harmonic data points indicated by an x symbol, and even harmonic data points indicated by an ○; the fundamental's data points are assigned to a Δ.

3.5.3 Experiment 3: Time Domain & Frequency Domain Analysis of Harmonic Distortion & Clipping Structure on Complex Waves.

The objective of Experiment 3 was to analyse the effects of harmonic distortion on complex waveforms and observe the characteristics of any TID that may be generated. The implementation of complex waves should allow the researcher to distinguish between linear and nonlinear distortions that emerge; something not always possible with sine waves.

The complex waveforms were synthesised in MATLAB (The code is outlined in Chapter 3.3), and input into each DUT. The results were plotted in the time domain with `dsp.TimeScope`, and an integrated spectrum was created for the processed files of the same waveform type in `dsp.SpectrumAnalyser`.

3.6 The Primary Device Under Test

Designed by Scott Hampton as a DIY project which was published in *Tape-Op* (Hampton, 2002), and based on his *SilverBox 4*[12] and *HVTP2* microphone preamplifier. Hampton is now the proprietor of HAMPTONE[13], a company that manufactures bespoke signal processors for recording studio applications. This device was chosen because of its popularity, both as a product and project for DIY enthusiasts. Furthermore, Hampton not only includes a great deal of technical information about the design, but also succinctly elaborates on his design philosophy and aesthetic goals. The microphone preamplifier was designed to manifest the *soft clipping* qualities associated with valves and transformers; the nature of which is of primary concern to this research. Moreover, the design permits using two different types of valve in the V1 position; a 12AY7[14] or 12AX7 valve may be used, thus allowing for a greater quantity of data to be generated and analysed. The 12AY7 is Hampton's preferred valve, and states that it has a particular "very soft roll-over, and generates almost no odd harmonics when biased properly - making it, in my opinion, the choice for the gain stages", though Hampton adds that the 12AX7A is "sonically [...] less forgiving". (Hampton, 2002:42)

Hampton's microphone preamplifier implements two gain stages, one for each of the two halves of a dual triode. The circuit employs a buffer stage, referred to by Hampton (2002:42) as a *totem pole output buffer*, however according to Blencowe (2016:281–282) and Jones (2012:114–115) this circuit topology is in actual fact a WCF. Hampton (2002:43–44) suggests some recommended modifications to improve the performance of the device. Most notable is the interpolation of another WCF after the first gain stage; both of the WCF's share the same design. This is advantageous as the lower output impedance permits the usage of a lower value gain attenuation potentiometer; it is possible to reduce this value from 100 kΩ to 5 kΩ. The

[12] This unit is reviewed at: https://tapeop.com/reviews/gear/55/silverbox-4-tube-preamp/ [Visited 2020-04-26].
[13] See http://hamptone.com/ [Visited 2020-04-26].
[14] In this thesis the term 12AY7 includes all special versions of this valve, this includes the 6027A and 12AY7A.

WCF employs 12AU7[15] valves, these are well suited to this task as they can supply high levels of current.

Self (2015:341) notes that it is best practice to have the resistance value of a potentiometer as low as possible in audio applications (contingent on the preceding stage's output impedance); as lower resistance potentiometers are less susceptible to noise, hum, and other types of parasitic phenomenon. Additionally, a stepped attenuator has been implemented to supersede the more conventional volume potentiometer. Hampton claims that stepped attenuators are purely resistive, while volume potentiometers add unwanted reactance to the signal. Moreover, as the stepped attenuators have discrete gain reduction values, there is improved *channel matching*, which is an especially useful feature when implemented in a multi-channel device such as this. (Hampton, 2002:43–44)

As the schematic provided is rather unwieldy, it has been truncated into two separate parts, with the letters A, B, and C indicate concatenation points. Figure 3.3 shows the first schematic of the device, there is a balanced XLR input that connects to an input transformer with a ratio of 1 : 10. Hampton (2002:42) notes that using a high quality input transformer is of critical importance; accordingly, this device uses a SOWTER 9045[16]. The input transformer then connects to the first triode gain stage (V1A) this is then DC coupled to the WCF V2. V2 connects to the stepped attenuator via a 2.2 µF coupling capacitor (the schematic is continued in Figure 3.4). The stepped attenuator then connects to the second gain stage, V1B; which is DC coupled to the next WCF, V3. The WCF then connects to the output transformer, a STUDER 1 : 4 input transformer that has been used in reverse, thus providing the required 4 : 1 output ratio.

For the experiments, an XLR cable was modified to include a voltage divider or L-pad. This attenuated the signal from the DAC by 40 dB, to match the signal level output of a typical microphone. The L-pad also served to adjust the output impedance of the DAC to 150 Ω for compatibility with the input impedance of the microphone preamplifier. The DAC used for the experiments was a TASCAM US-1x2, and the output signal was taken from the RCA line out. The switched attenuator was set to -12 dB to balance the generation of harmonic distortion evenly between the two gain stages. While the software emulators readily achieved a highest harmonic level of -15 dBc, the primary DUT was unable to achieve this level. As the input signal was increased past a certain point, the primary DUT readily generated more crossover distortion as opposed to the desired peak compression. Therefore, an unfortunate limitation of the research was that the clipping structure of the primary DUT could not be observed for the very highest signal levels.

[15] The European equivalent code is ECC82.

[16] SOWTER is a company that manufactures audio transformers in the UK. https://www.sowter.co.uk/ [Visited 2020-04-29].

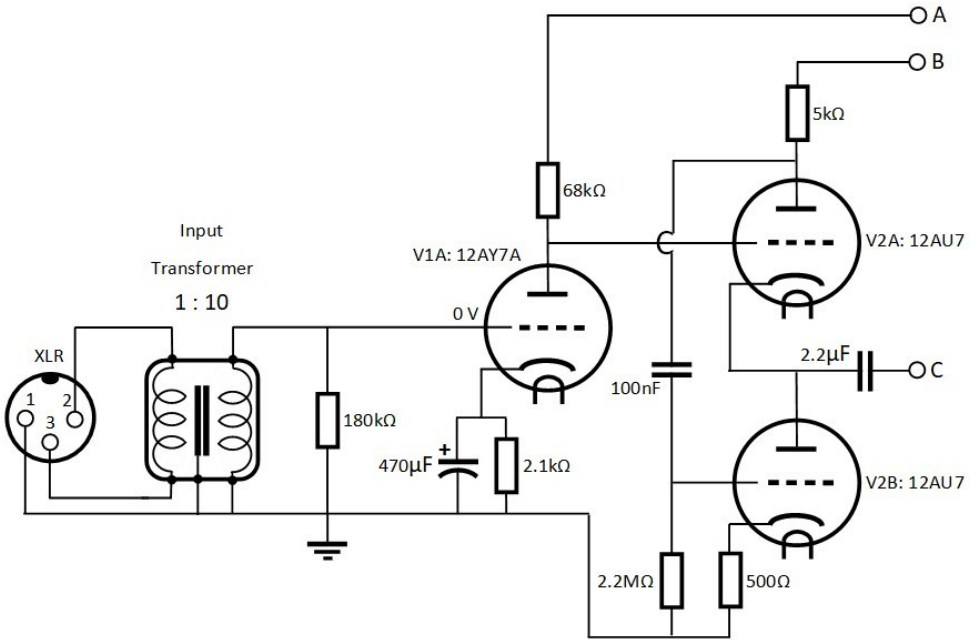

Figure 3.3: Schematic of primary DUT part 1.

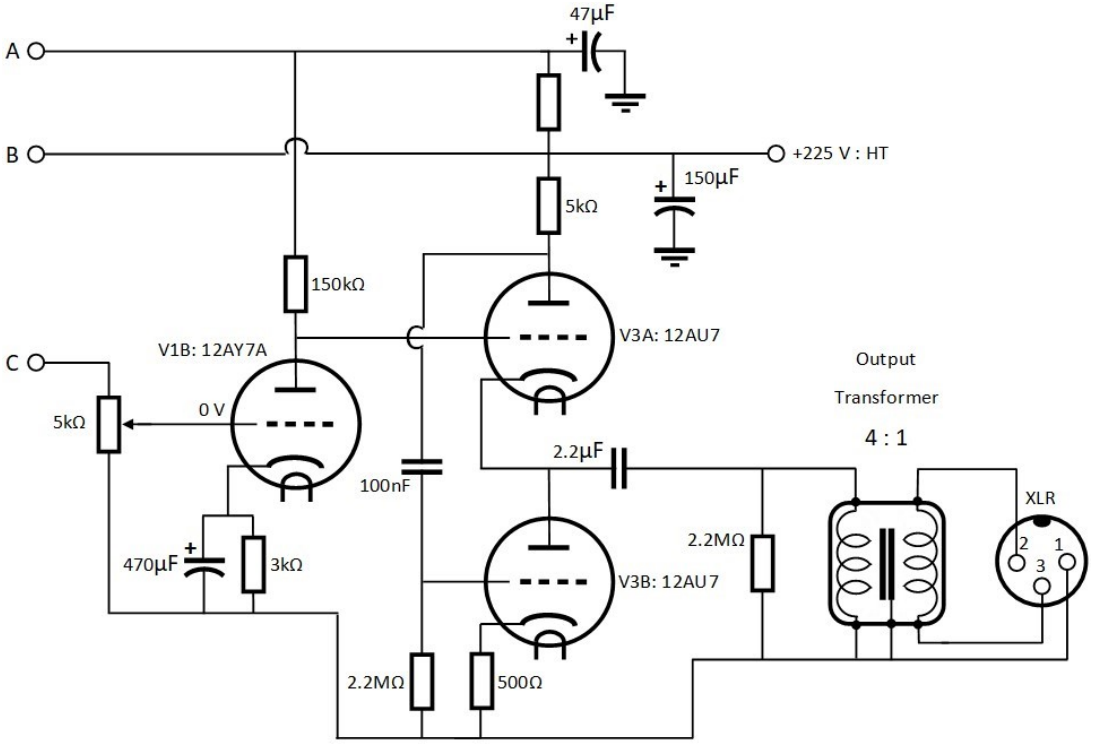

Figure 3.4: Schematic of primary DUT part 2.

3.7 The Secondary Devices Under Test

The secondary DUTs consist of three software plugins that can be used with most DAW software. These plugins function to emulate the signal colouration induced by a valve signal processor. While there are a multitude of software companies that offer such plugins, three were chosen arbitrarily based on their apparent popularity in popular media. Demo versions of each plugin

were used, because of their high cost. These offer the same performance, but are only usable for a short time period.

To ensure that the results of the study were as generalisable as possible, and given that each plugin is unique, presumably with its individual sonic character, certain control measures were implemented. Each plugin comes with a variety of unique parameters and controls, these were not used as they fall outside the scope of the research. Each plugin was configured as similarly as possible, the goal was to isolate just the saturation effect of the triode without any extraneous processing influencing the processed waveform. The plugins were configured to saturate in such a way that the highest harmonic partial power level was approximately 15 dBc below the fundamental.

3.7.1 PLUGIN ALLIANCE: BlackBox

The PLUGIN ALLIANCE Black Box is a software emulator of a device of the same name developed by BRAINWORX. This plugin emulates both the audio transformers and the 12AX7 triode of the device. While the plugin includes many interesting features, the plugin was configured to emphasise the character of the triode saturation. During the experiments, it tended to clip the output channel, the *output* parameter was reduced to 40 % to avoid this problem. To mitigate overloading the pentode stage and ensure that the triode stage was overloaded sufficiently, the pentode control was increased to 70 % to satisfy the required harmonic distortion levels. (Plugin Alliance, 2020)

Figure 3.5: PLUGIN ALLIANCE: Black Box User Interface [screen shot]. (Plugin Alliance, 2020)

3.7.2 IZOTOPE: Ozone Exciter Triode

The IZOTOPE Ozone Exciter is a multiband type saturation plugin that emulates a variety of *vintage* audio technologies, but not any device in particular. Of the two valve emulations available, the triode emulation was selected as it best suits the purposes of the research. The saturation *amount* control was set to 10.0 with the *mix* control set to 100 %, to achieve the desired level of harmonic distortion. The *oversampling* control was enabled as this is claimed to improve the quality of the emulation. Multi-band processing is an available feature; however, only a single

band was used over the entire usable frequency range. The additional bands were superfluous to the scope of the research. (Izotope, 2017)

Figure 3.6: IZOTOPE: Ozone Exciter User Interface [screen shot]. (Izotope, 2017)

3.7.3 SOUNDTOYS: Radiator

The SOUNDTOYS Radiator is an emulator designed to mimic the sonic character of the ALTEC 1567A valve mixer. This device is often associated with the Motown era of the early 1960s, it has regained popularity with modern popular music artists and producers. The plugin can emulate the different input impedance responses of microphone or line levels. *Line* was chosen as it had the most linear response according to its supplied bode plot. To achieve the desired level of harmonic distortion, the *input control* was set to +4 dB, the *mix* control set to 100%. Interestingly, this device also emulates the noise properties of the original device; nevertheless, this feature was also considered beyond the scope of the research and was disabled. (Soundtoys, 2015)

Figure 3.7: SOUNDTOYS: Radiator User Interface [screen shot]. (Soundtoys, 2015)

Chapter 4

Results & Analysis

4.1 Analysis of Gain Stages: Primary DUT.

THE analysis begins with an analysis of each common cathode gain stage of the primary DUT. This will be done according to the techniques outlined in Chapter 2.5.1. Firstly the DC operating conditions will be determined. This will be followed by the calculation of A_v, r_a, μ, and g_m for each gain stage. Finally, the properties r_k and f_{low} will be analysed. Two small signal triodes have been selected for investigation. The 12AY7 for which the circuit was designed, and the 12AX7, a higher gain triode pin compatible with the 12AY7. MATLAB has been implemented to plot the anode characteristic curves and respective loadlines, the code for which is included in Appendix A.

4.1.1 V1A:12AY7 Characteristics

The first step required to analyse this gain stage is to calculate the DC loadline. This can be done with Ohm's law, whereby it can be calculated that with an R_L of 68 KΩ and an HT of approximately 212 V, there is a maximum I_a of 3.1 mA. The DC loadline is therefore plotted from 212 V on the x-axis to 3.1 mA on the y-axis, as can be seen in Figure 4.1. The bias voltage is not provided in the schematic but can be calculated by using a *cathode loadline* superimposed on the grid curves, as R_k is given as 2.1 kΩ. The cathode loadline is selected to pass between V_{gk} = 3 V and V_{gk} = 2 V. Now that R_k is known, the cathode loadline can be calculated using Equations 4.1 & 4.2 and plotted on the anode characteristics graph in Figure 4.1. Consequently, the operating point is observed to be approximately 2.47 V, with a quiescent I_a of 1.17 mA at a V_a of 131.8 V. The first parameter that can now be determined is V_a, which is taken at points on the 2 V and 3 V grid curve, as seen in Equation 4.3, thus equating to an A_v of approximately 27. The next step is to calculate the AC parameters. The anode resistance r_a (Equation 4.4)[1], amplification factor μ (Equation 4.5)[2], and lastly, the mutual conductance g_m (Equation 4.6).

$$I = \frac{V_g}{R_k} = \frac{3\,\text{V}}{2100\,\Omega} \approx 1.43\,\text{mA} \tag{4.1}$$

[1] The tangent line required to calculate this value has been included in Figure 4.1.
[2] This is based on a constant current of 1.17 mA.

$$I = \frac{V_g}{R_k} = \frac{2\,\text{V}}{2100\,\Omega} \approx 0.95\,\text{mA} \tag{4.2}$$

$$A_v = \frac{\Delta V_a}{\Delta V_g} = \frac{146\,\text{V} - 119\,\text{V}}{2\,\text{V} - 3\,\text{V}} \approx -27 \tag{4.3}$$

$$r_a = \frac{\Delta V_a}{\Delta I_a} = \frac{125\,\text{V} - 110\,\text{V}}{1.53\,\text{mA} - 1.08\,\text{mA}} \approx 33.33\,\text{k}\Omega \tag{4.4}$$

$$\mu = \frac{\Delta V_a}{\Delta V_g} = \frac{154\,\text{V} - 113\,\text{V}}{3\,\text{V} - 2\,\text{V}} \approx 41 \tag{4.5}$$

$$g_m = \frac{\mu}{r_a} = \frac{41}{33.33\,\text{k}\Omega} \approx 1.23\,\text{mA/V} \tag{4.6}$$

The internal cathode resistance r_k is calculated to be 2.41 kΩ (Equation 4.7), which in parallel with an R_k of 2.1 kΩ gives a total resistance of the cathode ($r\prime_k$) to be 1.12 kΩ. According to the schematic C_k is 470 µF, which allows the frequency response of the cathode circuit to be calculated (Equation 4.8). This equates to 0.3 Hz, well below the infrasonic frequency threshold of human hearing.

$$r_k = \frac{R_L + r_a}{\mu + 1} = \frac{68\,\text{k}\Omega + 33.33\,\text{k}\Omega}{41 + 1} \approx 2.41\ \text{k}\Omega \tag{4.7}$$

$$f_{low} = \frac{1}{2\pi . C_k . r'_k} = \frac{1}{2\pi \times 0.00047\,\text{F} \times 1120\,\Omega} \approx 0.3\,\text{Hz} \tag{4.8}$$

4.1.2 V1A:12AX7 Characteristics

The cathode loadline is selected to pass between $V_{gk} = 1\,V$ and $V_{gk} = 1.5\,V$ using Equations 4.9 & 4.10. Along with the DC loadline, these are plotted on the anode characteristics graph in Figure 4.2. Consequently, the operating point is observed to be approximately 1.47 V, giving a quiescent I_a of 0.7 mA at a V_a of 163.6 V. The next parameter that can be determined is A_v, which equates to approximately 54.2 (Equation 4.11). The AC parameters can be calculated as follows, the r_a (Equation 4.12)[3], μ (Equation 4.13)[4], and g_m (Equation 4.14).

[3] The tangent line required to calculate this value has been included in Figure 4.2.
[4] This is based on a constant current of 0.76 mA.

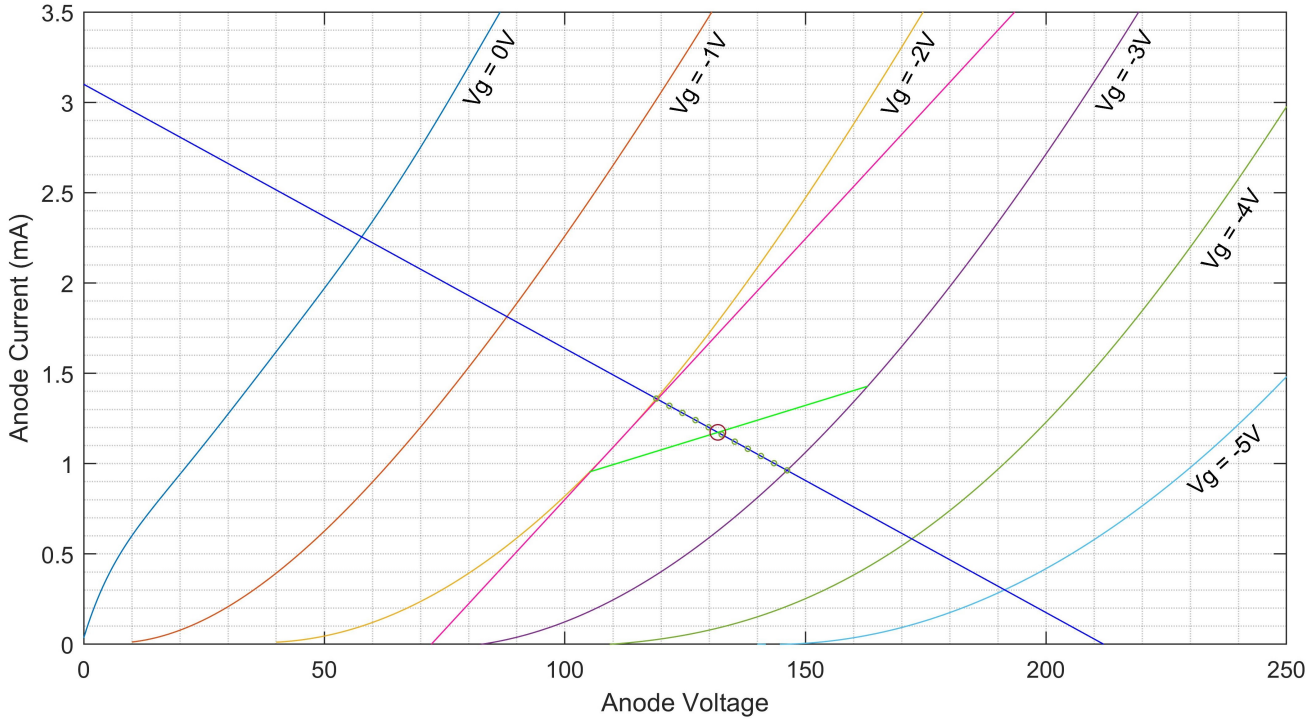

Figure 4.1: V1A:12AY7 Triode Anode Characteristics.

$$I = \frac{V_g}{R_k} = \frac{1.5\,\text{V}}{2100\,\Omega} \approx 0.71\,\text{mA} \tag{4.9}$$

$$I = \frac{V_g}{R_k} = \frac{1\,\text{V}}{2100\,\Omega} \approx 0.47\,\text{mA} \tag{4.10}$$

$$A_v = \frac{\Delta V_a}{\Delta V_g} = \frac{165.4\,\text{V} - 138.3\,\text{V}}{1\,\text{V} - 1.5\,\text{V}} \approx -54.2 \tag{4.11}$$

$$r_a = \frac{\Delta V_a}{\Delta I_a} = \frac{180\,\text{V} - 150\,\text{V}}{0.89\,\text{mA} - 0.47\,\text{mA}} \approx 71.42\,\text{k}\Omega \tag{4.12}$$

$$\mu = \frac{\Delta V_a}{\Delta V_g} = \frac{215.1\,\text{V} - 114.8\,\text{V}}{2\,\text{V} - 1\,\text{V}} \approx 100.3 \tag{4.13}$$

$$g_m = \frac{\mu}{r_a} = \frac{100.3}{71.42\,\text{k}\Omega} \approx 1.4\,\text{mA/V} \tag{4.14}$$

The internal cathode resistance r_k is calculated to be 1.38 kΩ (Equation 4.15), which in parallel with an R_k of 2.1 kΩ gives a total resistance of the cathode r_k' to be approximately 833 Ω. The frequency response of the cathode circuit is calculated in Equation 4.16.

$$r_k = \frac{R_L + r_a}{\mu + 1} = \frac{68\,\text{k}\Omega + 71.42\,\text{k}\Omega}{100.3 + 1} \approx 1.38\,\text{k}\Omega \tag{4.15}$$

$$f_{low} = \frac{1}{2\pi.C_k.r_k^{'}} = \frac{1}{2\pi \times 0.00047\,\text{F} \times 833\,\Omega} \approx 0.4\,\text{Hz} \tag{4.16}$$

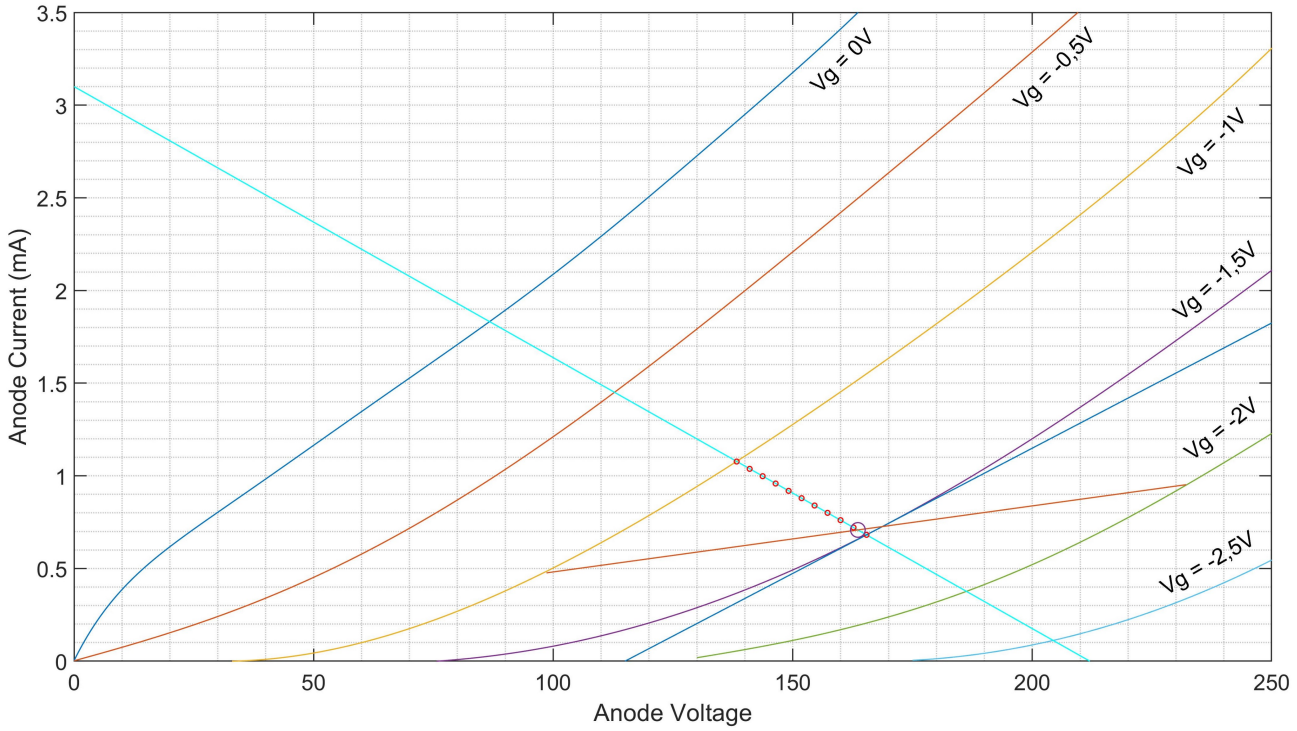

Figure 4.2: V1A:12AX7 Triode Anode Characteristics.

4.1.3 V1B:12AY7 Characteristics

Now that the operating conditions for the first gain stage have been analysed, attention can be turned to the 2nd gain stage, V1B. The cathode loadline is selected to pass between $V_{gk} = 2V$ and $V_{gk} = 3V$. The cathode loadline can be calculated using Equations 4.17 & 4.18 and plotted on the anode characteristics graph in Figure 4.3. The operating point can be observed to be approximately 2.64 V, with a quiescent I_a of 0.75 mA at a V_a of 107.8 V. The next parameter that can be determined is A_v, which equates to approximately 30.43 (Equation 4.19). The AC parameters can be calculated as follows; r_a (Equation 4.20)[5], μ (Equation 4.21)[6], and g_m (Equation 4.22).

$$I = \frac{V_g}{R_k} = \frac{3\,\text{V}}{3000\,\Omega} = 1\,\text{mA} \tag{4.17}$$

[5] The tangent line required to calculate this value has been included in Figure 4.3.
[6] This is based on a constant I_a of 0.78 mA.

$$I = \frac{V_g}{R_k} = \frac{2\,\text{V}}{3000\,\Omega} \approx 0.66\,\text{mA} \tag{4.18}$$

$$A_v = \frac{\Delta V_a}{\Delta V_g} = \frac{130.1\,\text{V} - 99.67\,\text{V}}{2\,\text{V} - 3\,\text{V}} \approx -30.43 \tag{4.19}$$

$$r_a = \frac{\Delta V_a}{\Delta I_a} = \frac{110\,\text{V} - 90\,\text{V}}{1.05\,\text{mA} - 0.58\,\text{mA}} \approx 42.55\,\text{k}\Omega \tag{4.20}$$

$$\mu = \frac{\Delta V_a}{\Delta V_g} = \frac{137.5\,\text{V} - 97.3\,\text{V}}{3\,\text{V} - 2\,\text{V}} \approx 40 \tag{4.21}$$

$$g_m = \frac{\mu}{r_a} = \frac{40}{42.55\,\text{k}\Omega} \approx 0.94\,\text{mA/V} \tag{4.22}$$

The internal cathode resistance (r_k) is calculated to be 4.69 kΩ (Equation 4.23), which in parallel with the R_k of 3 kΩ which gives a total resistance of the cathode r'_k to be approximately 1.83 kΩ. The frequency response of the cathode circuit is provided in Equation 4.24.

$$r_k = \frac{R_L + r_a}{\mu + 1} = \frac{150\,\text{k}\Omega + 42.55\,\text{k}\Omega}{40 + 1} \approx 4.69\ \text{k}\Omega \tag{4.23}$$

$$f_{low} = \frac{1}{2\pi . C_k . r'_k} = \frac{1}{2\pi \times 0.00047\,\text{F} \times 1830\,\text{k}\Omega} \approx 0.18\ \text{Hz} \tag{4.24}$$

4.1.4 V1B:12AX7 Characteristics

The cathode loadline is selected to pass between $V_{gk} = 1\,V$ and $V_gk = 1.5\,V$. The cathode loadline can be calculated using Equations 4.25 & 4.26 and plotted on the anode characteristics graph in Figure 4.4. Consequently, the operating point is observed to be approximately 1.45 V, with a quiescent anode current of 0.49 mA at a V_a of 144.5 V. The next parameter that can be determined is A_v, which equates to approximately 66.2 (Equation 4.27). The AC parameters can be calculated as follows; r_a (Equation 4.28)[7], μ (Equation 4.29)[8], and g_m (Equation 4.30).

$$I = \frac{V_g}{R_k} = \frac{1.5\,\text{V}}{3000\,\Omega} = 0.5\,\text{mA} \tag{4.25}$$

[7] The tangent line required to calculate this value has been included in Figure 4.4.
[8] This is based on a constant current of 0.76 mA.

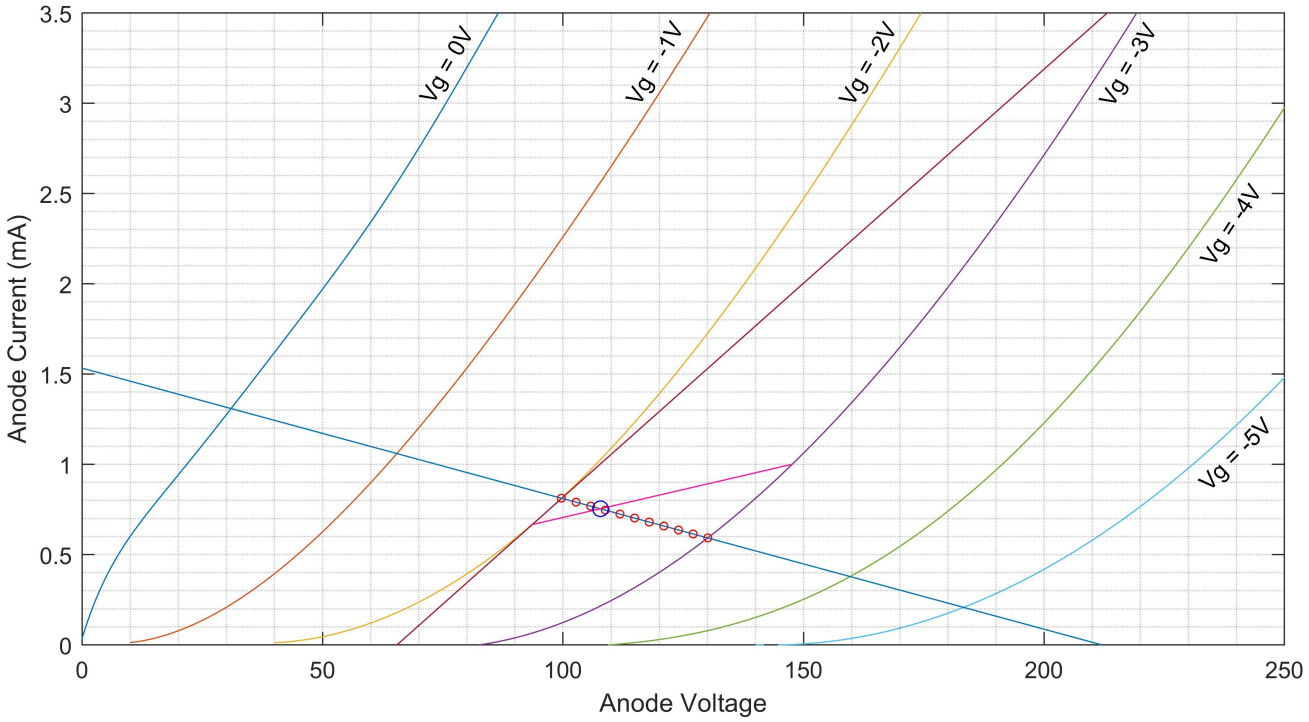

Figure 4.3: V1B:12AY7 Triode Anode Characteristics.

$$I = \frac{V_g}{R_k} = \frac{1\,\text{V}}{3000\,\Omega} \approx 0.33\,\text{mA} \tag{4.26}$$

$$A_v = \frac{\Delta V_a}{\Delta V_g} = \frac{147.6\,\text{V} - 114.5\,\text{V}}{1\,\text{V} - 1.5\,\text{V}} \approx -66.2\,\text{V} \tag{4.27}$$

$$r_a = \frac{\Delta V_a}{\Delta I_a} = \frac{160\,\text{V} - 140\,\text{V}}{0.61\,\text{mA} - 0.38\,\text{mA}} \approx 86.96\,\text{k}\Omega \tag{4.28}$$

$$\mu = \frac{\Delta V_a}{\Delta V_g} = \frac{197.1\,\text{V} - 98.86\,\text{V}}{2\,\text{V} - 1\,\text{V}} \approx 98.24 \tag{4.29}$$

$$g_m = \frac{\mu}{r_a} = \frac{98.24}{86.96\,\text{k}\Omega} \approx 1.13\,\text{mA/V} \tag{4.30}$$

The properties of the cathode circuit can also be analysed, the internal cathode resistance r_k is calculated to be 2.39 kΩ (Equation 4.31), which in parallel with an R_k of 3 kΩ gives the total resistance of the cathode r_k' to be approximately 1.33 kΩ. The frequency response of the cathode circuit is given in Equation 4.32.

$$r_k = \frac{R_L + r_a}{\mu + 1} = \frac{150\,\text{k}\Omega + 86.96\,\text{k}\Omega}{98.24 + 1} \approx 2.39\ \text{k}\Omega \tag{4.31}$$

$$f_{low} = \frac{1}{2\pi.C_k.r_k'} = \frac{1}{2\pi \times 0.00047\,\mathrm{F} \times 1330\,\mathrm{k\Omega}} \approx 0.3\,\mathrm{Hz} \tag{4.32}$$

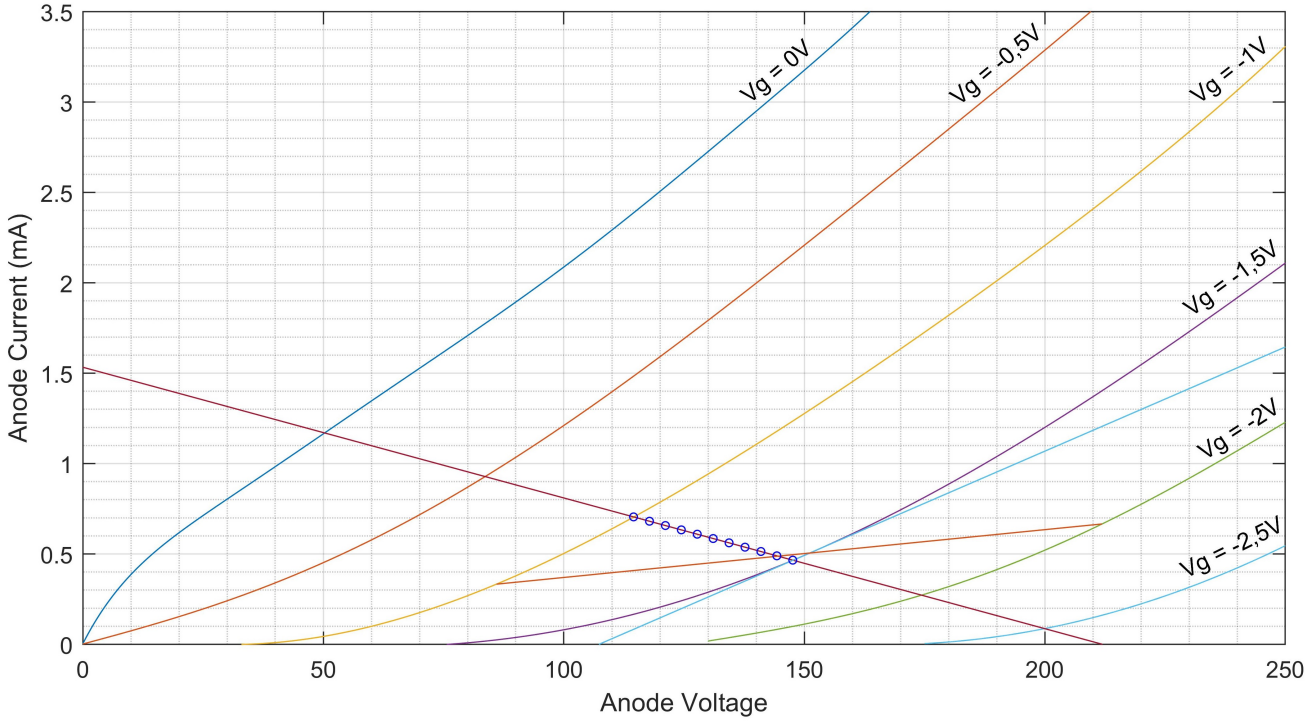

Figure 4.4: V1B:12AX7 Triode Anode Characteristics.

4.1.5 Summary of Results

Summary of Results				
Property	V1A:12AY7	V1A:12AX7	V1B:12AY7	V1B:12AX7
Operating Point	-2.47 V	-1.47 V	-2.64 V	-1.45 V
Quiescent V_a	131.8 V	163.6 V	107.8 V	144.5 V
Quiescent I_a	1.17 mA	0.7 mA	0.75 mA	0.49 mA
Voltage Amplification A_v	-27	-54	-30	-66
Anode Resistance r_a	33.33 kΩ	71.42 kΩ	42.55 kΩ	86.96 kΩ
Amplification Factor μ	41	100.3	40	98.24
Mutual Conductance g_m	1.23 mA/V	1.4 mA/V	0.94 mA/V	1.13 mA/V
Cathode Resistance r_k	2.41 kΩ	1.38 kΩ	4.69 kΩ	2.39 kΩ
Cathode Resistance r_k'	1.12 kΩ	0.83 kΩ	1.83 kΩ	1.33 kΩ

4.2 Experiment 1: Time Domain Analysis of the Clipping Structures of Sine Waves

4.2.1 Results of Experiment

The audio files used in this experiment are stored as hyperlinks in Appendix E; the results of the experiment for each device are included in the relevant appendices below

- PLUGIN ALLIANCE - Black Box: See Appendix B.1
- IZOTOPE Ozone - Exciter Triode: See Appendix B.2
- SOUNDTOYS - Radiator: See Appendix B.3
- V1:12AY7: See Appendix B.4
- V1:12AX7: See Appendix B.5

4.2.2 Analysis of Results

The results of Experiment 1 indicate significant differences between the clipping structure of each device. Firstly, it can be observed that the Black Box clipped the test signal quite abruptly on the positive peak from approximately -5 dB, while remaining relatively unaffected at -10 dB. This would imply that notable peak compression occurs from approximately -10 dB to 0 dB. The negative peak was marginally wider, with the zero crossing point occurring fractionally earlier and ending fractionally later with the increasing amplitude of the test signal. The negative peak generates greater levels of peak compression, this was especially noticeable on the -10 dB wave. An interesting observation was that the 0 dB line was *compressed* below that of the -5 dB line, although by a trivial amount. Another difference between the positive and negative peaks was that the positive peak had a higher amplitude, just short of 0.75, whilst the negative peak had an amplitude of around -0.65. Overall, the Black Box tended to induce a quasi-square wave shape in the clipping structure of the input signal as the amplitude was increased; the clipping structure was approximately symmetrical in nature.

The Ozone Triode was observed to induce a *sawtooth* like shape in the clipping structure of the input signal as the amplitude increased. The angle of the slope was far more acute than the horizontal clip of the Black Box. Peak compression appeared quite distinctly at approximately -10 dB on the positive peak, implying that peak compression begins upwards of -15 dB. The negative cycle began peak compression at a lower input level, where the -15 dB signal was already noticeably distorted when compared to its positive cycle counterpart. Much like the Black Box, the Ozone Triode also had a *wider* negative cycle. Although, the clipping structure of the negative cycle of the Ozone Triode was markedly different when compared to the positive cycle, and displayed distinct asymmetrical clipping with an increasing input signal amplitude. The negative cycle displayed a higher level of peak compression than the positive cycle, with the 0 dB input signal reaching an apex at an amplitude just greater than 0.75. The amplitude of the negative cycle is notably lower, reaching an amplitude just below -0.5. The -10 dB, -5 dB, and 0 dB lines all were all at approximately the same amplitude level and had a similar

slope gradient from when the negative cycle begins to ascend to the zero crossing. Another noteworthy observation were the *sharp edges* of the waveform distortion, a phenomenon not present in the other devices.

The positive cycle of the Radiator manifested a soft peak compression with increasing amplitude. The positive cycle did not develop any particular sawtooth or square wave shape. However, the negative cycle had a tendency towards a square wave shape, similar to that of the Black Box. The positive cycle began gentle peak compression between -15 dB and -10 dB. Interestingly, the negative cycle began peak compression in a narrower band. For example, the -10 dB had negligible levels of peak compression but developed considerable peak compression by -5 dB. Additionally, the negative cycle output level attenuated with increasing input signal level past a certain point. This was demonstrated by the 0 dB signal, which measured an amplitude of approximately 0.4, and the -10 dB signal which measured an amplitude close to 0.475.

Turning now to the primary DUT, severe crossover distortion can be observed in the test results of both the 12AY7 and 12AX7 valves. Interestingly, the amplitude of the -5 dB and lower signal for both valves was significantly less than the software DUT's. For the -5 dB and lower signals on the 12AY7, there appeared to be mild asymmetrical clipping, with the negative peak slightly lower in amplitude than the positive peak. This would suggest that the operating points selected by Hampton (2002) for the 12AY7 gain stage are effective. The 0 dB signal did not appear to have significant peak compression or any easily observable clipping structure. This would imply that the amount of harmonic distortion selected for the initial level was mostly comprised of crossover distortion. The 12AX7 generated more prominent asymmetrical clipping, with a compressed and elongated positive cycle and a shorter but less compressed negative cycle. It was observed in the analysis of the 12AX7 gain stages that the operating points were closer to the cutoff area of the valve, and could explain the discrepancy in peak compression between the two valves. While the 12AX7 has a higher voltage gain that the 12AY7, its output signal levels were slightly below those of the 12AY7, with the 0 dB signals producing equivalent amplitude and clipping structure.

4.3 Experiment 2: Harmonic Distortion as a Function of Input Level

4.3.1 Results of Experiment

The raw harmonic distortion data and the audio files used for this experiment are included as hyperlinks in Appendix E. The MATLAB code listings for each experiment on each device are included in the relevant appendices below:

- PLUGIN ALLIANCE - Black Box: See Appendix C.1.1
- IZOTOPE - Ozone Exciter Triode: See Appendix C.1.2
- SOUNDTOYS - Radiator: See Appendix C.1.3
- V1:12AY7: See Appendix C.1.4
- V1:12AY7: See Appendix C.1.5

The graphical representations of the experiment for each device are included in the relevant appendices below:

- PLUGIN ALLIANCE - Black Box: See Appendix C.2.1
- IZOTOPE - Ozone Exciter Triode: See Appendix C.2.2
- SOUNDTOYS - Radiator: See Appendix C.2.3
- V1:12AY7: See Appendix C.2.4
- V1:12AY7: See Appendix C.2.5

4.3.2 Analysis of Results

The results of Experiment 2 produced some surprising findings. While the nature of the research was exploratory, which implies the lack of any explicit hypothesis, there remained assumptions about the outcome of the experiments. For instance, it was assumed that the harmonic distortion values would increase linearly with increasing input magnitude, however this was not what was observed. For the secondary DUT's, the magnitude of the harmonics fluctuated in *cycloid* wave like patterns, appearing to increase and decrease in magnitude at random. These patterns become more erratic as the harmonic order increased, and with lower order harmonics generally behaving more linearly. Another point of interest was that the magnitude of the fundamental was higher than the ISL, but with increasing ISL began to taper off until it becomes horizontal, eventually falling below the magnitude of the ISL. At the point where the fundamental begins to taper, a considerable increase in the magnitude of harmonic distortion is observed.

The Black Box had an output signal level (OSL) with a fundamental approximately 8 dB more in magnitude than the ISL at -30 dB. Both signals increased linearly until the ISL reaches -15 dB, at this point the OSL fundamental begins to taper off, dropping below the ISL when it reaches -5.5 dB. Initially, the 2^{nd} harmonic was predominant but drops off sharply as the ISL approaches -17 dB. It is overtaken by the 3^{rd} harmonic which follows a quasi-logarithmic curve until its maximum measure value at -15 dBc. Additionally, the 2^{nd} harmonic tapers off and does not increase by much past the -29 dB to -26 dB band. The 2^{nd} harmonic is overtaken by the 5^{th} harmonic which increases abruptly in magnitude from about the -12 dB ISL mark, after completing one cycloid. Interestingly, this phenomenon is also shared by the other harmonics (except the 3^{rd} harmonic), after one cycloid is completed there is a rapid increase in magnitude until the 0 dB mark is reached. The Black Box tended to produce, or emphasise, predominantly lower order odd harmonics, with the 3^{rd} harmonic being the most dominant, followed by the 5^{th}.

The Ozone Triode had an output signal with a fundamental with approximately 2 dB more magnitude than the input signal when at -30 dB. The fundamental tapers off at -14 dB ISL and becomes fully saturated from -6 dB ISL onwards. The harmonic distortion of this device was dominated by the 2^{nd} harmonic, which increases somewhat linearly from -60 dB to -15 dB, with a gradient that is steeper than both the ISL and OSL fundamental. This suggests that this device induces greater 2^{nd} harmonic distortion with increasing ISL. The cycloid behaviour of the upper harmonics components are far less distinct in this device and displayed more random

behaviour. The 3rd harmonic increases quickly from the -14 dB ISL mark, reaching a level of -30 dB. It then slopes off at the -14 dB ISL point eventually reaching a level of -45 dB when the ISL reaches 0 dB. Subsequently, it is overtaken by the 4th, 5th, and 7th harmonic. This suggests that signals with a high amplitude could have less 3rd harmonic distortion than lower amplitude signals. Another notable difference between the Ozone Triode and Black Box is that the final distribution of harmonics of the Black Box are closely grouped, whereas for the Ozone Triode this distribution is wider.

The Radiator also had an output signal fundamental with approximately 2 dB more magnitude than the input signal when at -30 dB. However, the fundamental tapers off far sooner at -8 dB ISL and becomes saturated from the -9 dB ISL point, but does gradually increase by 1 dB by the 0 dB ISL point. The graph suggests that the Radiator produces the least harmonic distortion of the secondary DUT's, with the first harmonic distortion component only appearing just after -20 dB ISL. This device tended to be dominated by 2nd harmonic distortion. Although, much like what occurred with the Black Box, the 2nd harmonic drops in magnitude after it is briefly overtaken by the 3rd harmonic; however, the effect is far less pronounced. The 2nd harmonic recovers to take over the 3rd harmonic at -6.5 dB ISL, here the 4th harmonic also increases and overtakes the 3rd harmonic at -2 dB ISL. The cycloid behaviour of the upper harmonics is more erratic than the Black Box, but not quite as erratic as the Ozone Triode.

The 12AY7 and 12AX7 had a fundamental significantly below the ISL, this is possibly due to differences and limitations in the experiment process when compared to the software plugins. Both valves presented moderate levels of 2nd order harmonics, followed by even lower levels of 3rd order harmonics. Once the ISL reaches -2.5 dB, the crossover distortion emerges and a multitude of harmonics quickly increase in magnitude. At this point there is a sharp increase in the magnitude of the fundamental of the 12AX7 valve, corresponding to the *expansion* encountered in Experiment 1; after this point its fundamental tapers off in magnitude. This phenomenon is subtle in the 12AY7 valve, which also developed a tapering off of its fundamental at this point. It is interesting to note that, with the exception of the 3rd harmonic of the 12AX7 valve, the harmonics appear to not exhibit the cycloid like behaviour of the software emulators. Moreover, the harmonics of the 12AY7 and 12AX7 appear to increase linearly with signal level when compared to software emulators.

4.4 Experiment 3: Time Domain & Frequency Domain Analysis of Harmonic Distortion & Clipping Structures of Complex Waves

4.4.1 Results of Experiment

The graphical representations of the experiment for each device are included in the relevant appendices below:

- Sawtooth Waves: See Appendix D.1
- Square Waves: See Appendix D.2
- Triangle Waves: See Appendix D.3
- Impulse Train: See Appendix D.4

4.4.2 Analysis of Results

4.4.2.1 Sawtooth Wave Analysis

Much like what was observed in Experiment 1, the Black Box developed a square wave like distortion of the waveform, this phenomenon affected the positive cycle more so than the negative cycle, which retains a sawtooth like shape. The general clipping structure of the waveform is marginally asymmetrical, with no TID compression of the initial transient. Traces of TID ringing were observed on the steep edge of the wave.

The Ozone Triode retained a semblance to the original test signal, the negative cycle being more peak compressed than the positive cycle; indicating asymmetrical clipping. This device produced considerable TID compression of the initial transient (more so than the other DUT's), taking approximately 70 ms to reach a stable amplitude. This device had no observable evidence of TID ringing on the transients.

Much like the Black Box, the Radiator also produced a square like clipping structure, but with a greater degree of asymmetry. The negative cycle developed a strong square wave like characteristic. While the positive cycle maintained a likeness to the sharper sawtooth. The Radiator displayed a milder TID compared to that of the Ozone Triode, taking approximately 20 ms to reach a stable amplitude. This device exhibited the most TID ringing on the transients.

The 12AY7 retained a similar appearance to the original sawtooth wave, but with a convex slope. There was pronounced TID ringing on the transients, as well as asymmetrical clipping, and notable peak compression of the positive cycle of the wave. These phenomena were all exacerbated for the 12AX7, whereby the positive peaks were more compressed than the 12AY7. The negative peaks displaying a moderately higher amplitude with a slope more convex than the 12AY7. Interestingly, neither valve produced crossover distortion for this waveform type.

The combined spectrum of the three software emulator test signals indicated a close resemblance to the original sawtooth test signal for the upper harmonics. However, there was a disparity for the first three harmonics where there were conspicuous differences in the levels

for each device. The Black Box had the highest magnitude fundamental, but the lowest 2nd harmonic magnitude of the devices, followed by the strongest 3rd harmonic. The Black Box then tends to alternate between slightly increased odd and slightly decreased even harmonics for the remainder of the spectrum. The 12AY7 and 12AX7 did not deviate markedly from the sawtooth test signal.

4.4.2.2 Square Wave Analysis

As observed previously, the Black Box tends to distort the test waveforms into quasi-square waves. It was therefore not surprising that the results of this test indicate that it retained many of its original characteristics, although a negligible amount of asymmetrical clipping was observed. No TID compression was observed, but noticeable TID ringing on the edges of the waveform was evident.

Surprisingly, the Ozone Triode distorted the square wave into a quasi-sawtooth wave. While the vertical sides of the square wave are retained, a sawtooth *edge* has been superimposed on the peak of each square wave. The positive peaks had a marginally higher amplitude, reaching a level of about 0.9, with the negative peak reaching about 0.75; indicating asymmetrical clipping. The Ozone Triode displayed notable TID compression of the initial transient, again taking approximately 70 ms to reach a stable amplitude. TID ringing on the edges of the waveform were evident, but not to the same degree as the other secondary DUT's.

The Radiator also produced quasi-sawtooth wave distortion, but to a far less extent than the Ozone Triode. The waveform exhibits TID compression of the transient, taking approximately 20 to 30 ms to stabilise in amplitude. The amplitude of the positive cycles gradually decline from 0.65 to 0.45 after the recovery from the initial compressed transient, this takes place over a period of approximately 60 ms. This device once again displays the highest levels of TID ringing on the edges of the waveform.

The 12AY7 generated severe crossover distortion, producing a clipping structure that vaguely resembles a sawtooth wave. The clipping structure was approximately symmetrical, and there was moderate TID ringing on the edges of the waveform. The 12AX7 generated crossover distortion for the first few cycles, before disappearing. The negative cycle bore some similarities to that of the Ozone Triode and had a *squarer* positive cycle that the 12AY7. If it were not for the crossover distortion, it could be inferred that the 12AY7 would likely share a similar clipping structure with the Ozone Triode.

The combined spectrum of the three software emulators yielded no noteworthy deviation from the original test signal. The harmonics for each device taper off in approximately the same manner as the square wave test pattern. While the Ozone Triode did indicate some low level even harmonics, these are well below the level of the surrounding harmonics and can be considered redundant. The valves produced additional even harmonics, these tended to generally be lower in magnitude than the software emulators. It can also be observed that the valves generated relatively strong levels of 3rd harmonic when compared to the Ozone Triode and Radiator, but still falling well short of those generated by the Black Box.

4.4.2.3 Triangle Waves Analysis

The Black Box produced similar results once again, a tendency to distort into quasi-square waves, and no TID compression. The clipping structure is now symmetrical, however, the top of the waveform was not horizontally peak compressed and had a similar gradient to its previous results. No TID ringing was evident, likely due to triangle waves not having *hard* transient edges like sawtooth and square waves.

The Ozone Triode displayed TID compression of about 70 ms, with no TID ringing evident. The clipping structure was strongly asymmetrical, and the negative wave cycle resembled a quasi-sawtooth wave. The positive cycle retained a mild similarity to the original triangle wave.

The Radiator displayed TID compression of about 20 ms to 30 ms, with no TID ringing evident. The clipping structure was strongly asymmetrical, the negative wave cycle distinctly resembled a quasi-square wave. The positive cycle appears rounded off, much like a quasi-sine wave.

The 12AY7 did not exhibit any explicit clipping, although the shape of the waveform is noticeably distorted. The 12AY7 waveform cycle peaks at approximately 0.45, while the negative cycle peaks marginally lower at approximately -0.43. On the other hand, the 12AX7 exhibited compression of its positive peak, and the waveform peaks rather erratically, ranging from 0.25 to just below 0.2. The negative waveform cycle bares a strong resemblance to the negative waveform cycle of the 12AY7. Unlike the prior examples, neither triode generated any crossover distortion.

Regarding the software emulators, the triangle wave spectrum produced arguably the most interesting results of the spectrum analysis tests of Experiment 3. Both the Ozone Triode and Radiator added considerable levels of 2^{nd} order harmonic distortion at -15 dB, with the Black Box adding a lessor but still relevant -25 dB. The Black Box increased 3^{rd} order harmonic distortion levels when compared to the test signal, while the Ozone Triode and Radiator showed reduced levels. All devices indicated similar levels of 4^{th} order harmonic distortion. The Ozone Triode drops sharply from the 7^{th} harmonic, with the Black Box following the test signal closely, with the Radiator adding moderate even order harmonic distortion.

The triodes also produced some interesting results, the 12AY7 produced lower levels of even harmonics and higher levels of odd harmonics than the 12AX7. The 12AY7 harmonics also appeared to have erratic values, while the 12AX7's harmonics tapered off in a noticeably more linear fashion until the 6^{th} harmonic. At this point the odd harmonics taper off at a slightly higher value than the preceding even harmonic.

4.4.2.4 Impulse Train Analysis

The impulse train test allowed for a closer examination of the TID response of each DUT. The Black Box displayed no TID compression of the transient but did exhibit pronounced TID ringing well into the negative cycle, reaching an amplitude of -0.2. There appears to be a *sidelobe* around each waveform, this is likely a TID artefact.

The Ozone Triode produced a noticeably compressed transient that took approximately 70 ms to reach a stable amplitude. The TID ringing was far less pronounced than the ringing induced by the Black Box. The amplitude of the TID ringing appears to be directly proportional to

the amplitude of the impulse. There was a small DC offset after each impulse that gradually returned to the zero point, this is potentially also a TID artefact.

The Radiator developed TID ringing in the negative cycle that was similar in amplitude to the Black Box, but its impulse only reached a maximum amplitude of 6.4. Once again the ringing appears to be proportional to the impulse amplitude. The DUT produced a compressed transient that took approximately 30 ms to reach a stable amplitude.

The 12AY7 produced moderate levels of TID ringing on the negative cycles and generally produced an impulse train as expected. On the other hand, the 12AX7 produced highly compressed peaks, most likely caused by the valve being biased close to the cutoff area.

For the results of the spectrum it was decided to use the entire frequency range of the spectrum, as this waveform type lends itself to this kind of analysis. The bandwidth of the spectrum was set to display magnitudes between -65 dB and -35 dB, as this enables a closer examination of each device's harmonic characteristics. Both the Radiator and Black Box had the least flat harmonic frequency response, with the radiator exhibiting a substantial *hump* in the treble region from 16 kHz to 18 kHz. The two triodes generated the flattest harmonic frequency response, with the Ozone Triode not far behind. The frequency response of the triodes were probably limited by Miller capacitances, as well as winding capacitances in the input and output transformers. All the devices have a high frequency response that slopes off above 18 kHz, well above the hearing range of most adult humans.

4.5 Discussion

4.5.1 Experiment 1

The secondary DUTs all produced distinct clipping structures that were readily distinguishable. The primary DUT did not induce considerable peak compression, where even the 0 dB input signal retained its sine wave like form before the effects of the crossover distortion appear. The Black Box produced the most symmetrical clipping structures, as well as the most odd order harmonics. This might be because of the emulation of a *pentode* valve generating a different distortion profile than a triode. Another peculiarity were the hard edges observed on the Ozone Triode waveform (these could be DSP errors), a phenomenon not observed for the other devices.

The secondary DUT clipping structures demonstrate a tendency to distort waveforms to approximately resemble sawtooth, square, and triangle waves with increasing signal level. The Black Box tended to morph a sine wave into a square wave, and the Ozone Triode tended to morph a sine wave into a sawtooth wave. While the Radiator altered the sine wave in an interesting way; the positive cycle tended to resemble a triangle wave, while the negative cycle tended to resemble a square wave. This phenomenon was also encountered in Experiment 3, where the Black Box appeared to morph the sawtooth wave into a square wave like shape, and the Ozone Triode morphed a square wave into a sawtooth like shape. The tendency to morph into another waveform shape corresponded to changes in the harmonic composition of the test signals in Experiment 3. This suggests that, for different devices, the timbre of an audio waveform could differentiate past a certain signal level. In Experiment 1, for example, low level signals were generally indistinguishable. However, as the signal amplitude is increased, each DUTs distortion characteristics emerge.

4.5.2 Experiment 2

The results of this experiment suggest that valves generate distortion that is *dynamic*, with levels of harmonics that change according to input levels. It was found that the software emulators had harmonics that increased and decreased in magnitude in peculiar cycloid wavelike patterns. Conversely, the harmonics generated by the primary DUT appeared to increase linearly as the input signal increased, until the emergence of the crossover distortion. This suggests a potential discrepancy between hardware and software devices. While not conclusive, it does make this phenomenon a prime candidate for further research.

In Experiments 1 & 2 it was observed that the Ozone Triode produced a notable level of 2^{nd} order harmonics on a sine wave, although in Experiment 3 it only added an iota of 2^{nd} order harmonics to the already pre-existing 2^{nd} order harmonics. This phenomenon suggests harmonic distortions are not necessarily linearly additive and appear to emerge readily on *simpler* waveforms (that are more sine wave like), while for complex waveforms, the accumulation of harmonics declines past a certain point. The waveform type also appeared to influence the harmonics that were generated. For example, the Ozone Triode and Radiator both produced significantly more 2^{nd} order harmonics[9] for the triangle wave test than for the square wave test.

[9] Both the square wave and triangle test signals contain no even harmonics.

Concerning the primary DUT, it was observed in Experiments 1 & 2 that as crossover distortion was induced, the signal level increased abruptly in amplitude, corresponding with an abrupt increase in harmonics. This led not only a considerable distortion of transients on audio material but also an *expansion* thereof. Conceivably, this could create an expansion effect similar to that of a *transient designer*, where the transients of an audio signal can be manipulated or exaggerated in a defined way.

It is also conceivable that the crossover distortion could be perceived as being objectionable by audio professionals, and this is especially likely for the steady state part of a waveform. The crossover distortion was an unfortunate limitation, but as it only affected the highest signal level, its impact on the findings was moderately insignificant. This problem likely arises because of the WCF after the first gain stage being unable to drive a somewhat low 5 kΩ load impedance at high signal levels. Changing the variable gain control to a higher value might resolve this issue. It is reasonable to assume that crossover distortion would likely not affect most audio material, as the steady state would normally be well below the point where it is induced. For both the 12AY7 and 12AX7 valves, this is between -2 dB and -3 dB. Before the emergence of the crossover distortion, the primary DUT exhibited a clear absence of higher order harmonics. It predominantly generated the 2^{nd} harmonic, followed by a much lower 3^{rd} harmonic; this corresponds with the findings made by Hamm (1973).

4.5.3 Experiment 3

The impulse response test provided insight into the harmonic response over the entire available frequency range for each DUT. For instance, the Radiator tended to increase the magnitude of high frequency harmonics over 10 kHz, and the Black Box attenuated lower frequency harmonics that descend from 4 kHz. The other DUTs exhibited a relatively flat harmonic response. Overall, Experiment 3 produced the least interesting results. While the DUTs appeared to have their inherent waveform and harmonic components altered, it did not provide any significant inferences that could not be made from the other experiments. With this in mind, the results support the notion that harmonic distortion generated by valve DUTs is not linearly additive.

4.5.4 Summary

MATLAB proved effective as a tool for the calculation of the operating point and coefficients of a valve gain stage. It was demonstrated that the 12AX7 valve was not optimal for V1 position of the primary DUT. This was substantiated by the high peak compression of the positive waveform cycles observed in its results. While the static anode curves generated in MATLAB provide a higher level of acuity, the code was laborious to use. This makes the analysis or design of a gain stage effective, but arduous to implement. The process could be optimised through the development of a standalone software application, whereby a user could input a set of variables and the application would calculate the optimal operating point for maximum linearity. MATLAB has a *compiler*[10] that allows for the creation of standalone applications for home or internet use with MATLAB code. As the static anode curves are an approximation, with small variances between valves, one could envisage the development of a device able to automatically

[10] See https://www.mathworks.com/products/compiler.html for more information. [Accessed 21-01-2021]

measure the static anode curves for individual valves by employing a micro-controller, such as an ARDUINO. This device would allow for the customisation of circuits to optimise them for particular valves.

The gist of the preceding analysis and discussion is that each DUT produced distinct distortion characteristics and thus fulfils the primary objective. Following from this, the secondary objectives were partially fulfilled, in that the distortion characteristics were measured with high acuity and validity, with the aid of MATLAB. However, any inherent differences in distortion character between software devices and hardware devices produced intriguing yet inconclusive results. The analysis and discussion provided succinct insight into the research questions, and the distortion characteristics of the DUTs were delineated. Questions regarding differences in distortion profiles and variations in software and hardware devices were also addressed.

Chapter 5

Conclusion

THE audio studio is a complex environment, having developed on the contingency of technological progress. It is perhaps ironic that a precursor technology such as the valve is so revered by so many audio professionals. It was this phenomenon that was the initial impetus for conducting this research. This is a complex problem that can be explored from multiple perspectives and subject areas. The focal point of this thesis was the distortion characteristics of valves. It is distortion that gives rise to the so called *euphonic* signal colouration that is the purported reason for their popularity. Despite its exploratory nature, the research was definitive in finding that different types of signal processors produce a unique profile of distortions. Moreover, the extent and manner to which this occurred surpassed prior assumptions. The findings intimate that different valve signal processors can impart idiosyncratic signal colouration on audio material under certain conditions.

The key objective of this research was to devise and evaluate techniques for the analysis of distortion characteristics. Then implement these techniques in a series of experiments. An improved method of analysis could significantly refine our understanding of signal colouration, bridging the divide between quantitative measurement and qualitative experience. Subsequently, three experiments were designed, specifically for the analysis phase. Experiment 1 yielded insight into the evolution of peak compression (or clipping structure) at different signal levels for each DUT. Experiment 2 then examined how the magnitudes of harmonics evolve at different signal levels for each DUT. While Experiment 3 investigated the effects of distortion on complex waves, of concern was the subsequent changes to the preexisting harmonic constituents of complex waves. All three experiment procedures yielded intriguing results despite minor limitations. The findings intimate the possibility that hardware and DSP emulators have dissimilar distortion characteristics. However, because of the paucity of sample DUTs and crossover distortion present in the primary DUT, nothing conclusive can be asserted; further research could examine this more comprehensively.

The most significant implication of this thesis is that an audio signal can have its harmonic composition altered in a myriad ways by a valve signal processor. There are likely scenarios where harmonics may increase above a masking threshold when processed by such a device. Therefore, a musical instrument producing a tone could produce certain harmonics below a masking threshold. When processed by a valve, these harmonics could increase above the masking threshold, due to constructive interference caused by additional harmonics arising from non-linear distortion. If the 2^{nd} harmonic rises above the masking threshold of an audio

signal, its subsequent timbre could potentially develop a *fullness* and *body* not present before, in accordance with the assertions of Hamm (1973:272). Conversely, if an n^{th} harmonic generated by a signal processor is out of phase with an n^{th} harmonic already present in an audio signal. Destructive interference could cause the harmonic to drop below the masking threshold, potentially also resulting in a change in timbre.

As this thesis was *holistic* in its approach to analysing the DUTs, further research could examine distortion emerging at discrete stages. For example, distortion measurements could be made at the input transformer, first gain stage, buffer stage, etc. Such an approach would enable researchers to gain insight into the emergence of distortion at discrete stages of a DUT. This would facilitate a more comprehensive analysis of the complexity of the distortion emergence processes. Based on the findings of this thesis, it is difficult to make any qualitative judgements concerning signal colouration, nor can any inferences be made as to the reasons some find valve distortion *euphonic*. However, this thesis demonstrates that it is indeed possible to examine the more salient features of distortion. Further research could correlate individual distortion measurement characteristics with pyschoacoustical phenomena, thus stimulating and strengthening academic discourse on the aesthetics of signal colouration in professional audio practice.

Appendices

Appendix A

Static Anode Characteristics MATLAB code

Listing A.1: Demonstration Circuit

```
%Graph Labels and Settings
grid minor;hold;xlabel('Anode Voltage');ylabel('Anode Current (mA)');
axis([0,250,0,3.5]);set(gcf,'position',[60 375 800 400]);
title('12AX7 Triode Anode Characteristics')

%Grid Curves
x0 = [0 10 20 30 40 50 60 75 90 100 110 120 130 140 150 175 200];
y0 = [0 .35 .66 .82 1 1.15 1.35 1.67 1.9 2.1 2.3 2.5 2.7 2.97 3.15 ...
    3.8 4.5];
pf0 = polyfit(x0,y0,8);
ls0 = linspace(0, 200, 10000);
pv0 = polyval(pf0,ls0);
xt = 120;
yt = 1;
str = 'Vg = 0V';
text(xt,yt,str)
plot(ls0,pv0)

x05 = [0 25 50 75 100 125 150 175 200 225 250];
y05 = [0 .2 .45 .8 1.2 1.65 2.3 2.7 3.25 3.9 4.5];
pf05 = polyfit(x05,y05,5);
ls05 = linspace(0,250,10000);
pv05 = polyval(pf05,ls05);
xt = 120;
yt = 1;
str = 'Vg = -0,5V';
text(xt,yt,str)
plot(ls05,pv05)

x1 = [25 50 75 100 125 150 175 200 225 250];
y1 = [0 .05 .225 .5 .8 1.4 1.65 2.2 2.75 3.3];
```

```
pf1 = polyfit(x1,y1,5);
ls1 = linspace(35,250,10000);
pv1 = polyval(pf1,ls1);
xt = 120;
yt = 1;
str = 'Vg = -1V';
text(xt,yt,str)
plot(ls1,pv1)

x15 = [75 100 125 150 175 200 225 250 275];
y15 = [0 .075 .25 .5 .8 1.2 1.65 2.1 2.6];
pf15 = polyfit(x15,y15,5);
ls15 = linspace(75,250,10000);
pv15 = polyval(pf15,ls15);
xt = 120;
yt = 1;
str = 'Vg = -1,5V';
text(xt,yt,str)
plot(ls15,pv15)

x2 = [125 150 175 200 225 235 250];
y2 = [0  .1 .3 .5 .85 1 1.225];
pf2 = polyfit(x2,y2,4);
ls2 = linspace(130,250,10000);
pv2 = polyval(pf2,ls2);
xt = 120;
yt = 1;
str = 'Vg = -2V';
text(xt,yt,str)
plot(ls2,pv2)

x25 = [175 200 225 250];
y25= [0 .1 .255 .55];
pf25 = polyfit(x25,y25,2);
ls25 = linspace(175,250,10000);
pv25 = polyval(pf25,ls25);
xt = 120;
yt = 1;
str = 'Vg = -2,5V';
text(xt,yt,str)
plot(ls25,pv25)

%DC Loadline
dc = linspace(0+2.5i, 250+0i, 10000);
xt = 20;
yt = 3;
str = 'DC Loadline';
text(xt,yt,str)
plot(dc)

%AC Loadline
ac = linspace(0+2.65i, 240.04+0, 10000);
xt = 20;
```

```
yt = 3;
str = 'AC Loadline';
text(xt,yt,str)
plot(ac)

%ra tangent
tan = linspace(72.8+0i, 250+2.915i, 10000);
xt = 20;
yt = 3;
str = 'ra Tangent';
text(xt,yt,str)
plot(tan)

%Cathode Load Line
cll = linspace(54+.5i, 217.5+1.5i, 10000);
xt = 20;
yt = 3;
str = 'Cathode Load Line';
text(xt,yt,str)
plot(cll)

%Bias Point
plot(144.6, 1.054, 'o');
vgk = linspace(139.8+1.102i, 172.3+.7766i, 11);
plot(vgk,'o')
xt = 20;
yt = 3;
str = 'Bias Point';
text(xt,yt,str)
```

Listing A.2: V1A: 12AY7 Triode Anode Characteristics

```
% Graph Labels and Settingss
grid minor;hold;xlabel('Anode Voltage');ylabel('Anode Current (mA)');
axis([0,250,0,3.5]);set(gcf,'position',[60 375 800 400]);
title('V1A: 12AY7 Triode Anode Characteristics');

%Grid Curves
x0 = [0 1 2 3 5 10 15 20 25 30 40 50 60 70 80 90 100 110 120 130];
y0 = [0 .1 .24 .29 0.38 .56 .78 .88 1.19 1.3 1.55 1.99 2.35 2.75 ...
    3.2 3.65 4.1 4.55 5 5.5];
pf0 = polyfit(x0,y0,8);
ls0 = linspace(0, 130, 10000);
pv0 = polyval(pf0,ls0);
xt = 120;
yt = 2.9;
str = 'Vg = 0V';
text(xt,yt,str)
plot(ls0,pv0)

x1 = [5 10 15 20 30 40 50 60 70 80 90 100 110 120 130 140 150 160];
y1 = [0 .01 .04 .09 .21 .4 .61 .89 1.19 1.55 1.9 2.25 2.65 3.05 3.5 ...
```

```
    3.9 4.35 4.85];
pf1 = polyfit(x1,y1,4);
ls1 = linspace(10,170,10000);
pv1 = polyval(pf1,ls1);
xt = 164;
yt = 2.9;
str = 'Vg = -1V';
text(xt,yt,str)
plot(ls1,pv1)

x2 = [40 45 50 60 70 80 90 100 110 120 130 140 150 160 170 180 190 ...
    200 210];
y2 = [.01 .02 .04 .11 .3 .37 .57 .81 1.08 1.4 1.7 2.1 2.5 2.9 3.3 ...
    3.7 4.2 4.65 5.1];
pf2 = polyfit(x2,y2,4);
ls2 = linspace(40,220,10000);
pv2 = polyval(pf2,ls2);
xt = 208;
yt = 2.9;
str = 'Vg = -2V';
text(xt,yt,str)
plot(ls2,pv2)

x3 = [65 70 75 80 85 90 95 100 110 120 130 140 150 160 170 180 190 ...
    200 210 220 230 240 250 260];
y3= [-0.2 0 .01 .02 0.25 .06 .075 .12 .23 .36 .54 .75 1.1 1.3 1.6 ...
    2.0 2.35 2.7 3.1 3.6 4 4.45 4.9 5.3];
pf3 = polyfit(x3,y3,3);
ls3 = linspace(70,280,10000);
pv3 = polyval(pf3,ls3);
xt = 231;
yt = 2.9;
str = 'Vg = -3V';
text(xt,yt,str)
plot(ls3,pv3)

x4 = [100 105 110 120 130 140 150 160 170 180 190 200 210 220 230 ...
    240 250 260 270 280 290 300];
y4 = [-.02 -.01 .01 .04 .08 .15 .25 .37 .53 .75 1 1.25 1.45 1.85 ...
    2.2 2.6 3 3.4 3.8 4.25 4.7 5.15];
pf4 = polyfit(x4,y4,4);
ls4 = linspace(95,350,10000);
pv4 = polyval(pf4,ls4);
xt = 231;
yt = 2.1;
str = 'Vg = -4V';
text(xt,yt,str)
plot(ls4,pv4)

x5 = [130 135 140 145 150 160 170 180 190 200 210 220 230 240 250 ...
    260 270 280 290 300 310 320 330];
y5 = [-.01 0 .01 .02 .03 .06 .1 .18 .27 .4 .55 .75 .95 1.2 1.5 1.8 ...
    2.1 2.45 2.8 3.2 3.65 4.05 4.5];
```

```
pf5 = polyfit(x5,y5,2);
ls5 = linspace(140,350,10000);
pv5 = polyval(pf5,ls5);
xt = 231;
yt = 0.9;
str = 'Vg = -5V';
text(xt,yt,str)
plot(ls5,pv5)

%DC Loadline
dc = linspace(0+3.1i, 212+0i, 10000);
xt = 20;
yt = 3;
str = 'DC Loadline';
text(xt,yt,str)
plot(dc)

%ra Tangent
tan = linspace(72.25+0i, 193.5+3.5i, 10000);
xt = 20;
yt = 3;
str = 'ra Tangent';
text(xt,yt,str)
plot(tan)

%Cathode Load Line
xt = 20;
yt = 3;
str = 'Cathode Load Line';
text(xt,yt,str)
plot([105.1 162.9], [0.9538 1.428])

%Bias Point
vgk = linspace(119+1.36i, 146.2+.9626i, 11);
plot(vgk,'o')
plot(131.8, 1.173, 'o');
xt = 20;
yt = 3;
str = 'Bias Point';
text(xt,yt,str)
```

Listing A.3: V1A: 12AX7 Triode Anode Characteristics

```
% Graph Labels and Settings
grid;hold;xlabel('Anode Voltage');ylabel('Anode Current (mA)');
axis([0,250,0,3.5]); set(gcf,'position',[60 375 800 400]);
title('V1A: 12AX7 Triode Anode Characteristics')

%Grid Curves
x0 = [0  10 20 30 40 50 60 75 90 100 110 120 130 140 150 175 200];
y0 = [0 .35 .66 .82 1 1.15 1.35 1.67 1.9 2.1 2.3 2.5 2.7 2.97 3.15 ...
    3.8 4.5];
```

```
pf0 = polyfit(x0,y0,8);
ls0 = linspace(0, 200, 10000);
pv0 = polyval(pf0,ls0);
xt = 120;
yt = 1.9;
str = 'Vg = 0V';
text(xt,yt,str)
plot(ls0,pv0)

x05 = [0 25 50 75 100 125 150 175 200 225 250];
y05 = [0 .2 .45 .8 1.2 1.65 2.3 2.7 3.25 3.9 4.5];
pf05 = polyfit(x05,y05,5);
ls05 = linspace(0,250,10000);
pv05 = polyval(pf05,ls05);
xt = 120;
yt = 1.9;
str = 'Vg = -0,5V';
text(xt,yt,str)
plot(ls05,pv05)

x1 = [25 50 75 100 125 150 175 200 225 250];
y1 = [0 .05 .225 .5 .8 1.4 1.65 2.2 2.75 3.3];
pf1 = polyfit(x1,y1,5);
ls1 = linspace(35,250,10000);
pv1 = polyval(pf1,ls1);
xt = 120;
yt = 1.9;
str = 'Vg = -1V';
text(xt,yt,str)
plot(ls1,pv1)

x15 = [75 100 125 150 175 200 225 250 275];
y15 = [0 .075 .25 .5 .8 1.2 1.65 2.1 2.6];
pf15 = polyfit(x15,y15,5);
ls15 = linspace(75,250,10000);
pv15 = polyval(pf15,ls15);
xt = 120;
yt = 1.9;
str = 'Vg = -1,5V';
text(xt,yt,str)
plot(ls15,pv15)

x2 = [125 150 175 200 225 235 250];
y2 = [0  .1 .3 .5 .85 1 1.225];
pf2 = polyfit(x2,y2,4);
ls2 = linspace(130,250,10000);
pv2 = polyval(pf2,ls2);
xt = 120;
yt = 1.9;
str = 'Vg = -2V';
text(xt,yt,str)
plot(ls2,pv2)
```

```
x25 = [175 200 225 250];
y25= [0 .1 .255 .55];
pf25 = polyfit(x25,y25,2);
ls25 = linspace(175,250,10000);
pv25 = polyval(pf25,ls25);
xt = 120;
yt = 1.9;
str = 'Vg = -2,5V';
text(xt,yt,str)
plot(ls25,pv25)

%DC Loadline
b = linspace(0+3.1i, 212+0i, 10000);
xt = 20;
yt = 3;
str = 'DC Loadline';
text(xt,yt,str)
plot(b)

%ra Tangent
tan = linspace(115+0i, 250+1.825i, 10000);
xt = 20;
yt = 3;
str = 'ra Tangent';
text(xt,yt,str);
plot(tan);

%Cathode Load Line
cll = linspace(98.6+.4763i, 232.1+.952i, 10000);
xt = 20;
yt = 3;
str = 'Cathode Load Line';
text(xt,yt,str)
plot(cll)

%Bias Point
plot(163.6, 0.7079, 'x');
vgk = linspace(138.3+1.077i, 165.4+.6815i, 11);
plot(vgk,'o')
xt = 20;
yt = 3;
str = 'Bias Point';
text(xt,yt,str)
```

Listing A.4: V1B: 12AY7 Triode Anode Characteristics

```
% Graph Labels and Settings
grid minor;hold;xlabel('Anode Voltage');ylabel('Anode Current (mA)');
axis([0,250,0,3.5]);set(gcf,'position',[60 375 800 400]);
title('V1B: 12AY7 Triode Static Anode Characteristics');

%Grid Curves
```

```
x0 = [0 1 2 3 5 10 15 20 25 30 40 50 60 70 80 90 100 110 120 130];
y0 = [0 .1 .24 .29 0.38 .56 .78 .88 1.19 1.3 1.55 1.99 2.35 2.75 ...
    3.2 3.65 4.1 4.55 5 5.5];
pf0 = polyfit(x0,y0,8);
ls0 = linspace(0, 130, 10000);
pv0 = polyval(pf0,ls0);
xt = 120;
yt = 1.9;
str = 'Vg = 0V';
text(xt,yt,str)
plot(ls0,pv0)

x1 = [5 10 15 20 30 40 50 60 70 80 90 100 110 120 130 140 150 160];
y1 = [0 .01 .04 .09 .21 .4 .61 .89 1.19 1.55 1.9 2.25 2.65 3.05 3.5 ...
    3.9 4.35 4.85];
pf1 = polyfit(x1,y1,4);
ls1 = linspace(10,170,10000);
pv1 = polyval(pf1,ls1);
xt = 164;
yt = 1.9;
str = 'Vg = -1V';
text(xt,yt,str)
plot(ls1,pv1)

x2 = [40 45 50 60 70 80 90 100 110 120 130 140 150 160 170 180 190 ...
    200 210];
y2 = [.01 .02 .04 .11 .3 .37 .57 .81 1.08 1.4 1.7 2.1 2.5 2.9 3.3 ...
    3.7 4.2 4.65 5.1];
pf2 = polyfit(x2,y2,4);
ls2 = linspace(40,220,10000);
pv2 = polyval(pf2,ls2);
xt = 208;
yt = 1.9;
str = 'Vg = -2V';
text(xt,yt,str)
plot(ls2,pv2)

x3 = [65 70 75 80 85 90 95 100 110 120 130 140 150 160 170 180 190 ...
    200 210 220 230 240 250 260];
y3= [-0.2 0 .01 .02 0.25 .06 .075 .12 .23 .36 .54 .75 1.1 1.3 1.6 ...
    2.0 2.35 2.7 3.1 3.6 4 4.45 4.9 5.3];
pf3 = polyfit(x3,y3,3);
ls3 = linspace(70,250,10000);
pv3 = polyval(pf3,ls3);
xt3 = 231;
yt3 = 1.9;
str = 'Vg = -3V';
text(x3,y3,str)
plot(ls3,pv3)

x4 = [100 105 110 120 130 140 150 160 170 180 190 200 210 220 230 ...
    240 250 260 270 280 290 300];
y4 = [-.02 -.01 .01 .04 .08 .15 .25 .37 .53 .75 1 1.25 1.45 1.85 ...
```

```
    2.2 2.6 3 3.4 3.8 4.25 4.7 5.15];
pf4 = polyfit(x4,y4,4);
ls4 = linspace(95,250,10000);
pv4 = polyval(pf4,ls4);
xt = 231;
yt = 2.1;
str = 'Vg = -4V';
text(xt,yt,str)
plot(ls4,pv4)

x5 = [130 135 140 145 150 160 170 180 190 200 210 220 230 240 250 ...
    260 270 280 290 300 310 320 330];
y5 = [-.01 0 .01 .02 .03 .06 .1 .18 .27 .4 .55 .75 .95 1.2 1.5 1.8 ...
    2.1 2.45 2.8 3.2 3.65 4.05 4.5];
pf5 = polyfit(x5,y5,2);
ls5 = linspace(140,250,10000);
pv5 = polyval(pf5,ls5);
xt = 231;
yt = 0.9;
str = 'Vg = -5V';
text(xt,yt,str)
plot(ls5,pv5)

%ra Tangent
tan = linspace(65.5+0i, 213.15+3.5i, 10000);
xt = 20;
yt = 3;
str = 'ra Tangent';
text(xt,yt,str);
plot(tan);

%DC Loadline
dc = linspace(0+1.533i, 212+0i, 10000);
xt = 20;
yt = 3;
str = 'DC Loadline';
text(xt,yt,str);
plot(dc);

%Cathode Load Line
plot([93.57 147.6], [0.666 1]);
xt = 20;
yt = 3;
str = 'Cathode Load Line';
text(xt,yt,str)

%Bias Point
vgk = linspace(99.67+0.8123i, 130.1+.5923i, 11);
plot(vgk,'o');
plot(107.8, 0.7537, 'o');
xt = 20;
yt = 3;
str = 'Bias Point';
```

```
text(xt,yt,str)
```

Listing A.5: V1B: 12AX7 Triode Anode Characteristics

```
% Graph Labels and Settings
grid;hold;xlabel('Anode Voltage');ylabel('Anode Current (mA)');
axis([0,250,0,3.5]);set(gcf,'position',[60 375 800 400]);
title('V1B: 12AX7 Triode Anode Characteristics')

%Grid Curves
x0 = [0 10 20 30 40 50 60 75 90 100 110 120 130 140 150 175 200];
y0 = [0 .35 .66 .82 1 1.15 1.35 1.67 1.9 2.1 2.3 2.5 2.7 2.97 3.15 ...
    3.8 4.5];
pf0 = polyfit(x0,y0,8);
ls0 = linspace(0, 200, 10000);
pv0 = polyval(pf0,ls0);
xt = 120;
yt = 2.9;
str = 'Vg = 0V';
text(xt,yt,str)
plot(ls0,pv0)

x05 = [0 25 50 75 100 125 150 175 200 225 250];
y05 = [0 .2 .45 .8 1.2 1.65 2.3 2.7 3.25 3.9 4.5];
pf05 = polyfit(x05,y05,5);
ls05 = linspace(0,250,10000);
pv05 = polyval(pf05,ls05);
xt = 120;
yt = 2.9;
str = 'Vg = -0,5V';
text(xt,yt,str)
plot(ls05,pv05)

x1 = [25 50 75 100 125 150 175 200 225 250];
y1 = [0 .05 .225 .5 .8 1.4 1.65 2.2 2.75 3.3];
pf1 = polyfit(x1,y1,5);
ls1 = linspace(35,250,10000);
pv1 = polyval(pf1,ls1);
xt = 120;
yt = 2.9;
str = 'Vg = -1V';
text(xt,yt,str)
plot(ls1,pv1)

x15 = [75 100 125 150 175 200 225 250 275];
y15 = [0 .075 .25 .5 .8 1.2 1.65 2.1 2.6];
pf15 = polyfit(x15,y15,5);
ls15 = linspace(75,250,10000);
pv15 = polyval(pf15,ls15);
xt = 120;
yt = 2.9;
str = 'Vg = -1,5V';
```

```
text(xt,yt,str)
plot(ls15,pv15)

x2 = [125 150 175 200 225 235 250];
y2 = [0  .1 .3 .5 .85 1 1.225];
pf2 = polyfit(x2,y2,4);
ls2 = linspace(130,250,10000);
pv2 = polyval(pf2,ls2);
xt = 120;
yt = 2.9;
str = 'Vg = -2V';
text(xt,yt,str)
plot(ls2,pv2)

x25 = [175 200 225 250];
y25= [0 .1 .255 .55];
pf25 = polyfit(x25,y25,2);
ls25 = linspace(175,250,10000);
pv25 = polyval(pf25,ls25);
xt = 120;
yt = 2.9;
str = 'Vg = -2,5V';
text(xt,yt,str)
plot(ls25,pv25)

%DC Loadline
dc = linspace(0+1.533i, 212+0i, 10000);
xt = 20;
yt = 3;
str = 'DC Loadline';
text(xt,yt,str);
plot(dc);

%ra Tangent
tan = linspace(107.3+0i, 250+1.645i, 10000);
xt = 20;
yt = 3;
str = 'ra Tangent';
text(xt,yt,str);
plot(tan);

%Cathode Load Line
plot([86.02 211.9], [.333 .666]);
xt = 20;
yt = 3;
str = 'Cathode Load Line';
text(xt,yt,str)

%Bias Point
vgk = linspace(147.6+0.4658i, 114.5+.7051i, 11);
plot(vgk,'o');
xt = 20;
yt = 3;
```

```
str = 'Bias Point';
text(xt,yt,str);
```

Appendix B

Results of Experiment 1

B.1 PLUGIN ALLIANCE: Black Box Clipping Structure

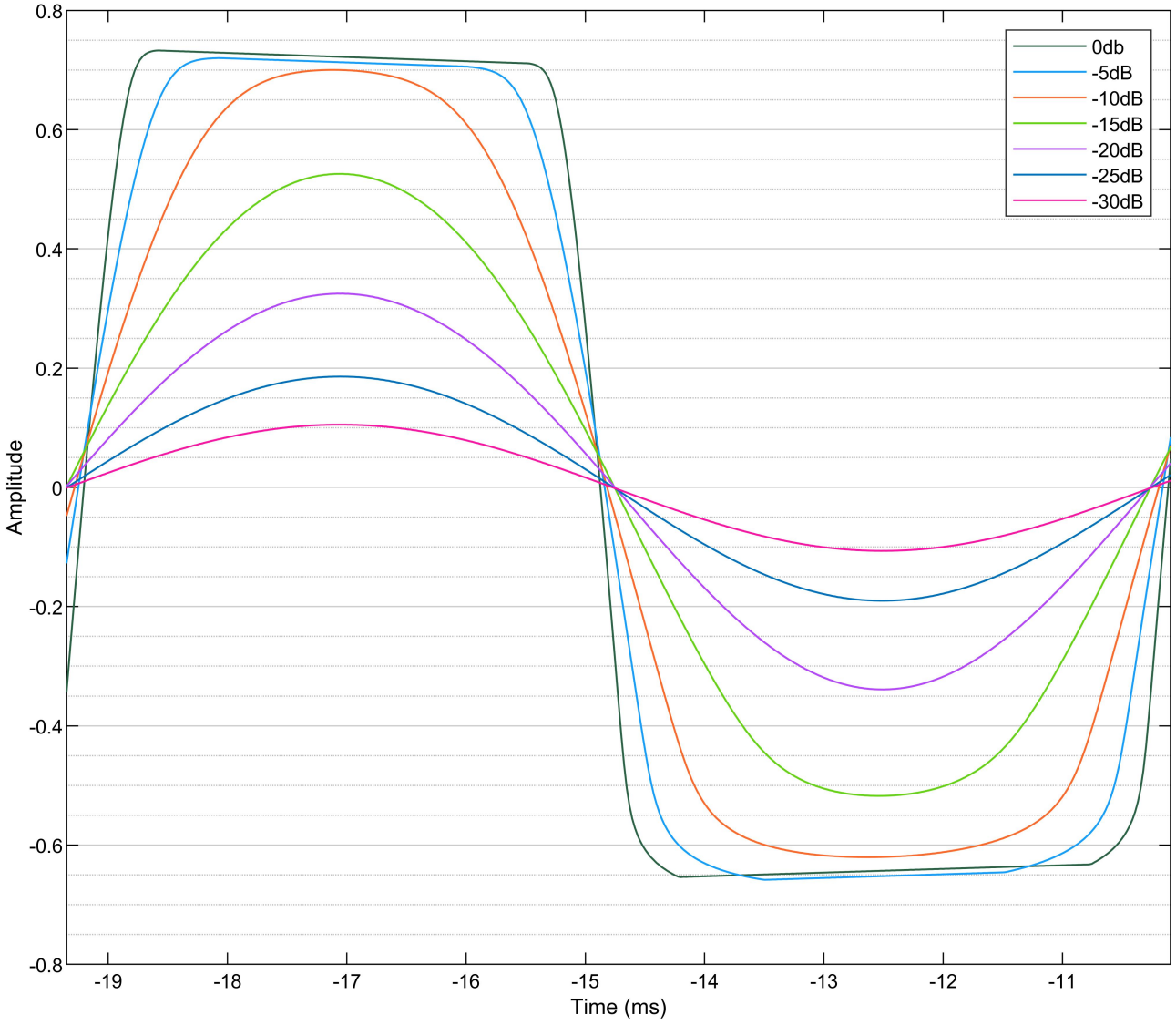

Figure B.1: Oscillogram of PLUGIN ALLIANCE: Black Box clipping structure, increasing incrementally in 5 dB steps.

B.2 IZOTOPE: Ozone Triode Clipping Structure.

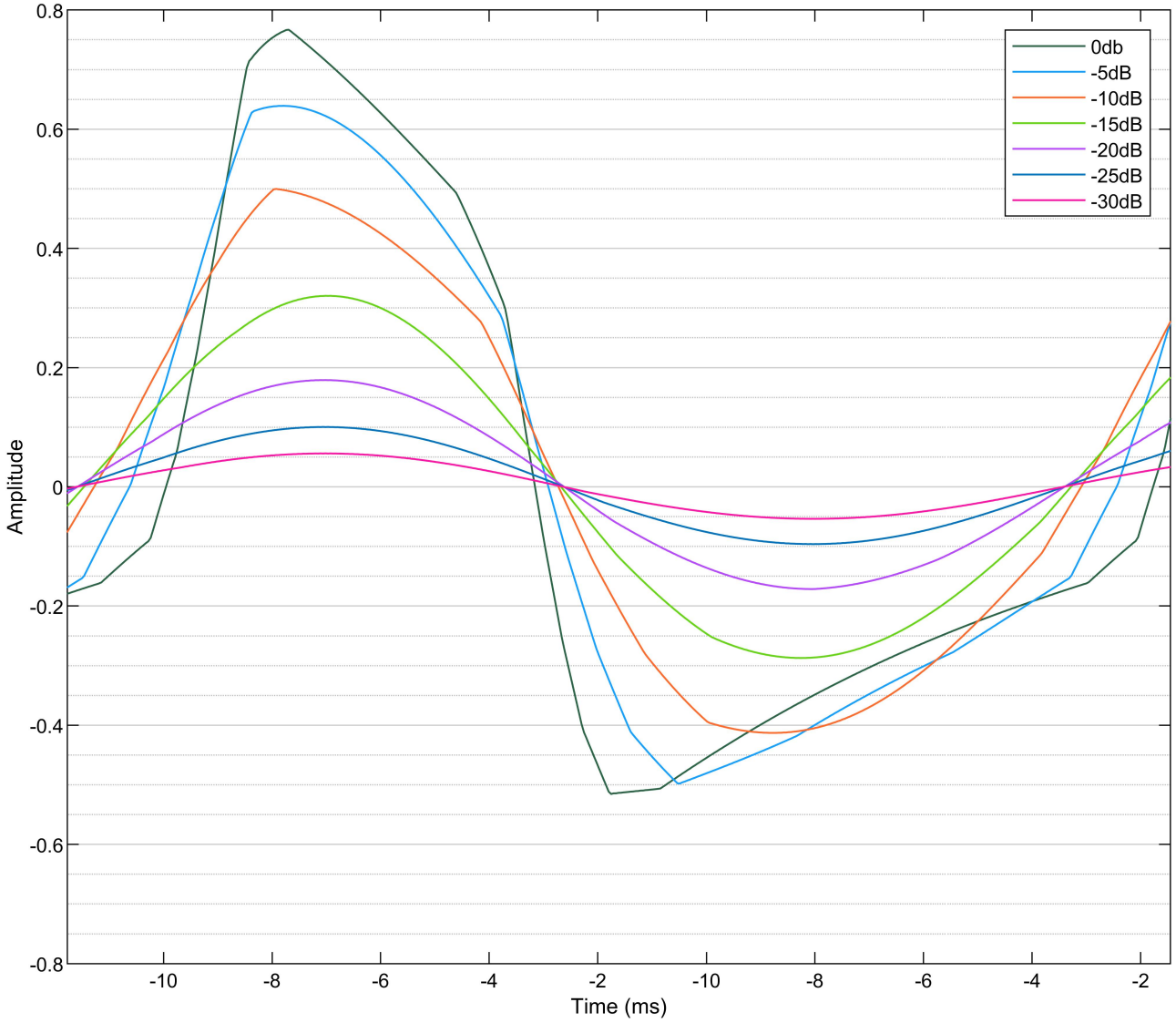

Figure B.2: Oscillogram of IZOTOPE: Ozone Triode clipping structure, increasing incrementally in 5 dB steps.

B.3 SOUNDTOYS: Radiator Clipping Structure

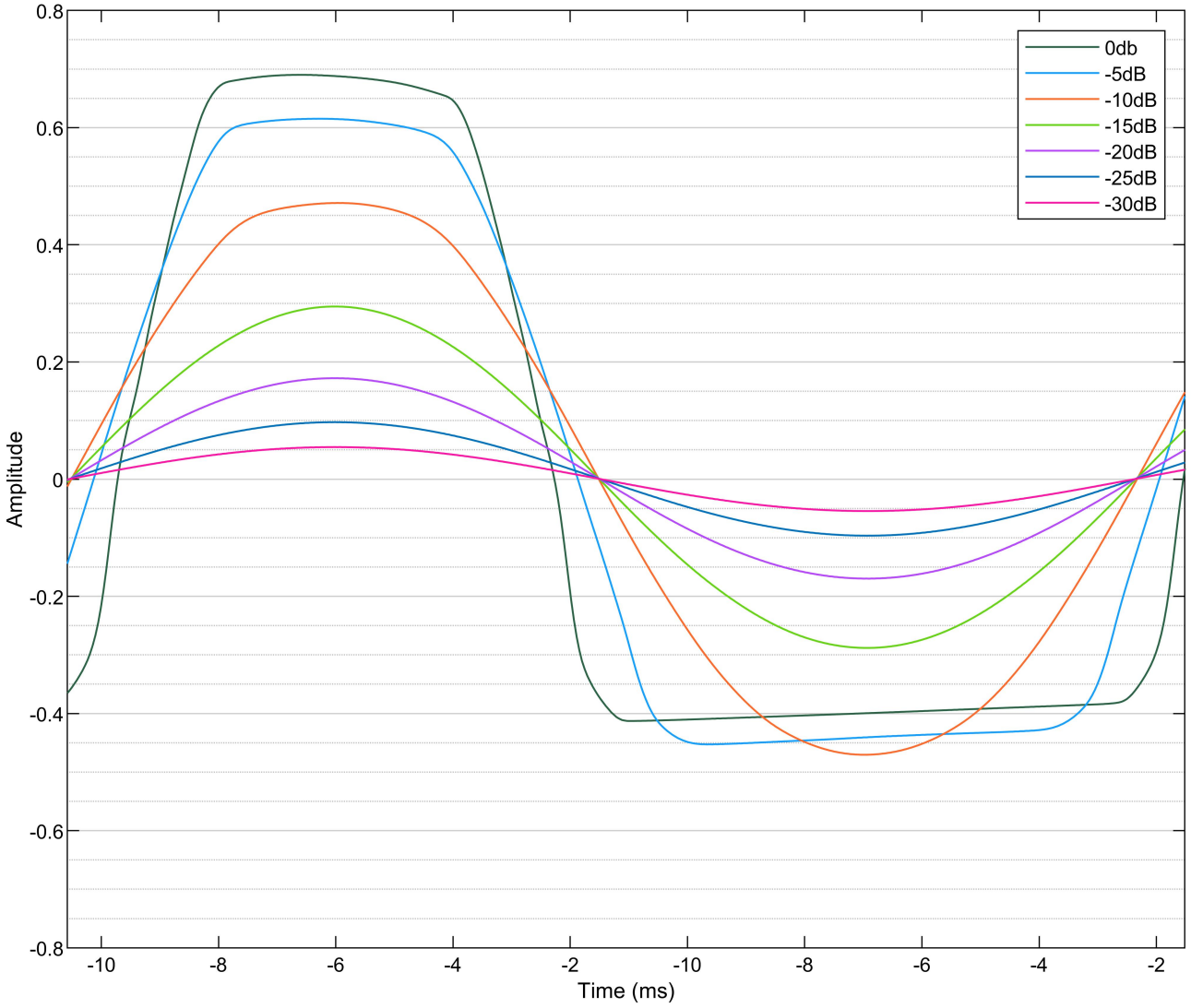

Figure B.3: Oscillogram of SOUNDTOYS: Radiator clipping structure, increasing incrementally in 5 dB steps.

B.4 V1:12AY7 Clipping Structure

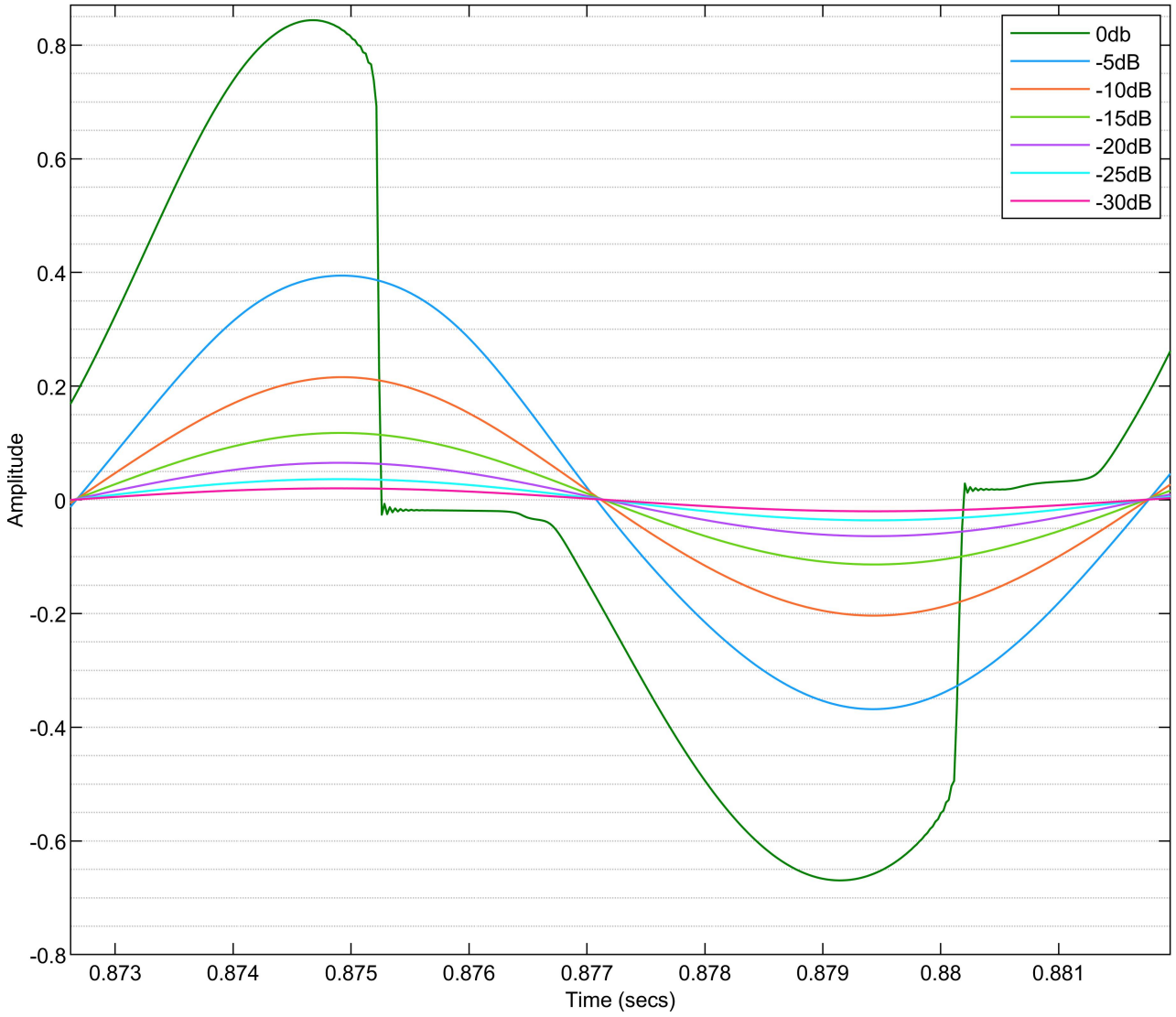

Figure B.4: Oscillogram of V1:12AY7 clipping structure, increasing incrementally in 5 dB steps.

B.5 V1:12AX7 Clipping Structure

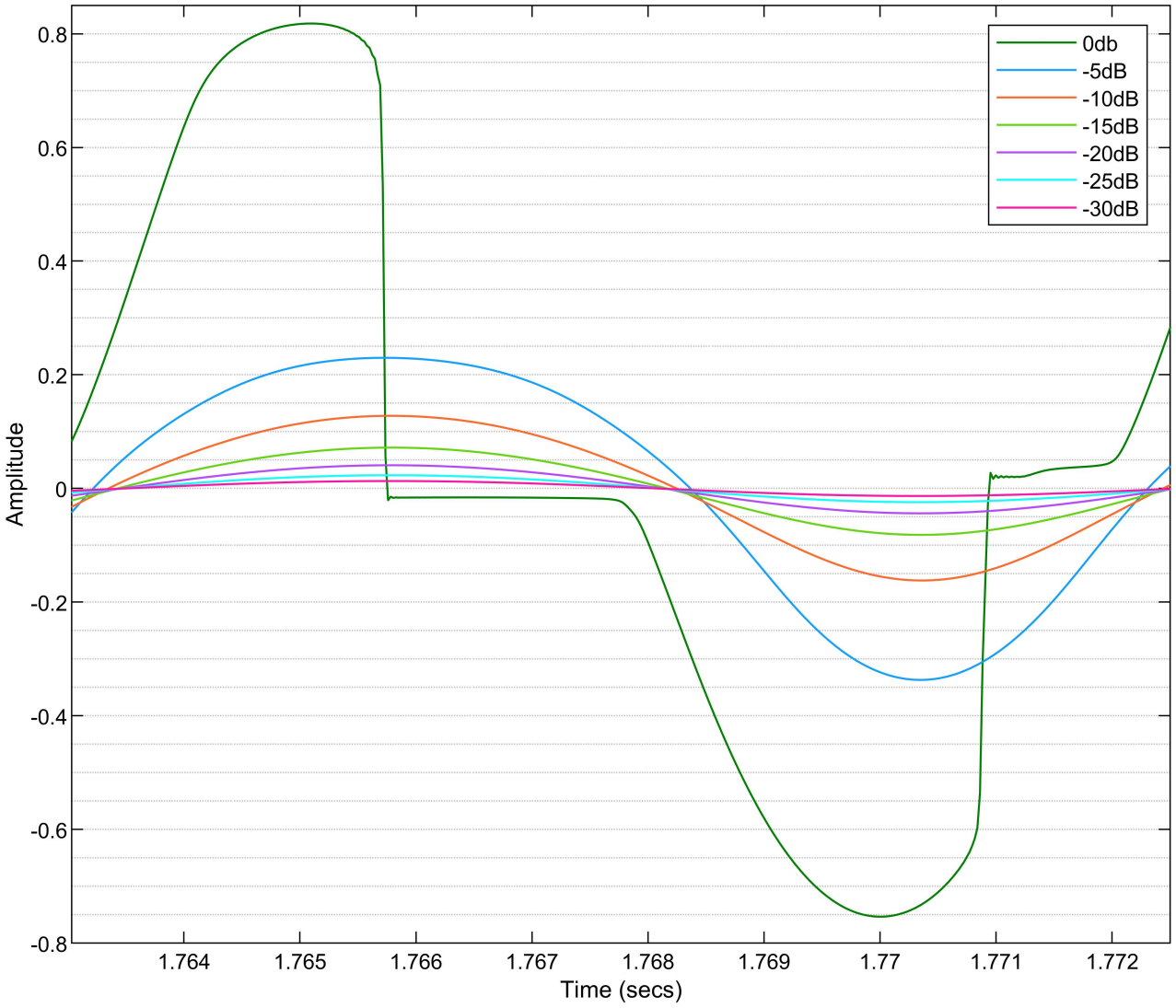

Figure B.5: Oscillogram of V1:12AX7 clipping structure, increasing incrementally in 5 dB steps.

Appendix C

Results of Experiment 2

C.1 MATLAB code

C.1.1 PLUGIN ALLIANCE Black Box

Listing C.1: PLUGIN ALLIANCE: Black Box Experiment

```
grid; hold; xlabel('Input Signal Level');ylabel('Output Signal ...
    Level');axis([-30,0,-60,0]);title('BlackBox Harmonic ...
    Distortion');set(gcf,'position',[60 375 800 400]);

x = [0 -0.5 -1 -1.5 -2 -2.5 -3 -3.5 -4 -4.5 -5 -5.5 -6 -6.5 -7 -7.5 -8 -8.5 ...
    -9 -9.5 -10 -10.5 -11 -11.5 -12 -12.5 -13 -13.5 -14 -14.5 -15 -15.5 -16 ...
    -16.5 -17 -17.5 -18 -18.5 -19 -19.5 -20 -20.5 -21 -21.5 -22 -22.5 -23 ...
    -23.5 -24 -24.5 -25 -25.5 -26 -26.5 -27 -27.5 -28 -28.5 -29 -29.5 -30];

ys = x;
plot(x,ys,'-','MarkerSize',4);

y = [-4.4 -4.4 -4.4 -4.4 -4.4 -4.4 -4.4 -4.5 -4.5 -4.5 -4.6 -4.6 -4.7 -4.7 ...
    -4.8 -4.9 -5 -5.1 -5.2 -5.3 -5.5 -5.7 -5.9 -6.1 -6.4 -6.6 -6.9 -7.2 -7.5 ...
    -7.8 -8.2 -8.5 -8.9 -9.3 -9.7 -10.2 -10.6 -11.1 -11.6 -12.1 -12.6 -13.1 ...
    -13.6 -14 -14.5 -15 -15.5 -16 -16.5 -17 -17.5 -18 -18.5 -19 -19.5 -20 ...
    -20.5 -21 -21.5 -22 -22.5];
plot(x,y,'*-','MarkerSize',3);

y2 = [-25.4 -25.7 -26.1 -26.5 -26.8 -27.1 -27.4 -27.7 -27.9 -28.1 -28.3 ...
    -28.5 -28.6 -28.7 -28.8 -28.8 -28.8 -28.9 -29 -29.3 -29.8 -30.5 -31.4 ...
    -32.6 -34.1 -36.1 -38.6 -42.2-47.8 -62.3 -53.6 -48.2 -44.9 -43.3 -42.6 ...
    -42.5 -42.9 -43.4 -44.2 -45.1 -46 -46.9 -47.9 -48.9 -49.9 -50.9 -51.9 -53 ...
    -54 -55 -56 -57 -58 -59 -60 -61 -62 -63.1 -64.1 -65.1 -66.1];
plot(x,y2,'o-','MarkerSize',3);

y3 = [-14.9 -15 -15.1 -15.2 -15.4 -15.5 -15.7 -15.9 -16.2 -16.5 -16.8 -17.2 ...
    -17.6 -18.1 -18.6 -19.2 -19.8 -20.5 -21.3 -22.1 -23 -23.9 -24.9 -26 -27.2 ...
    -28.4 -29.8 -31.3 -33 -34.9 -37 -38.9 -41.5 -44.5 -47.6 -50.8 -53.9 -56.8 ...
    -59.4 -61.8 -63.9 -65.9 -67.7 -69.5 -71.2 -72.8 -74.4 -76 -77.6 -79.1 ...
    -80.7 -82.3 -83.8 -85.4 -86.9 -88.5 -89.9 -91.3 -92.7 -94.1 -95.5];
plot(x,y3,'x-','MarkerSize',5);

y4 = [-26.6 -27 -27.5 -28 -28.5 -29 -29.5 -30.1 -30.6 -31.1 -31.7 -32.3 -33 ...
    -33.8 -34.8 -36.2 -38.2 -40.9 -45 -52.8 -61.7 -49 -44.7 -42.5 -41.2 -40.6 ...
    -40.5 -40.9 -41.7 -42.9 -44.6 -46.2 -48.9 -52.2 -56.2 -60.9 -66.1 -71.8 ...
    -78.2 -85.7 -96.1 -115.2 -100.8 -98.8 -98.9 -99.7 -100.7 -101.6 -102.8 ...
    -104.2 -105.7 -107 -109.1 -111.5 -114.4 -120.5 -126.4 -147.4 -130.4 ...
    -126.4 -125.9];
plot(x,y4,'o-','MarkerSize',3);

y5 = [-21.5 -21.7 -22 -22.3 -22.7 -23.2 -23.7 -24.3 -25 -25.7 -26.6 -27.6 ...
    -28.6 -29.7 -30.9 -32.2 -33.8 -35.4 -37.3 -39.3 -41.5 -44.2 -47.7 -52.9 ...
    -64 -62.2 -54.4 -51.4 -50 -49.7 -50.2 -51.1 -53 -55.7 -59.1 -63 -67.5 ...
```

```
    -72.2 -76.9 -81.5 -86 -90.5 -94.8 -99.1 -103.2 -106 -108.8 -111.6 -114.1 ...
    -116.8 -119.8 -124.1 -131.7 -130.8 -122.7 -120.7 -119.9 -123 -125.1 ...
    -125.7 -126.1];
plot(x,y5,'x-','MarkerSize',5);

y6 = [-28.6 -29.3 -30 -30.8 -31.6 -32.5 -33.5 -34.6 -35.8 -37.2 -39 -41.3 ...
    -44.7 -50.7 -79 -52 -46.8 -44.1 -42.7 -42 -41.9 -42.3 -43.1 -44.4 -46.1 ...
    -48.5 -51.9 -56.8 -66.2 -72.6 -63.1 -61.2 -61 -62.4 -65.1 -68.7 -73.1 ...
    -77.9 -82.9 -87.9 -93.1 -98.3 -103.3 -107.7 -111.1 -113.6 -116.4 -119.6 ...
    -124.7 -132.8 -132.4 -124.2 -121.2 -118.9 -119.6 -120.4 -122.6 -123.4 ...
    -125.7 -127.8 -126.9];
plot(x,y6,'o-','MarkerSize',3);

y7 = [-27.7 -28.2 -28.7 -29.4 -30.1 -31 -32 -33.1 -34.3 -35.7 -37.1 -38.7 ...
    -40.4 -42.3 -44.8 -47.8 -51.2 -55.8 -64.6 -68.8 -58.2 -54.1 -51.9 -50.8 ...
    -50.4 -50.8 -51.9 -53.8 -56.8 -61.4 -69.3 -86.8 -74.7 -71.7 -72.6 -75.3 ...
    -79.2 -83.9 -88.9 -93.9 -98.9 -103.9 -109.2 -116.4 -130.5 -129.7 -134.6 ...
    -129.9 -127.8 -125.1 -122.1 -120.6 -121.2 -121.1 -123 -129.2 -134.7 ...
    -137.8 -131.9 -131.9 -131.9];
plot(x,y7,'x-','MarkerSize',5);

y8 = [-31.6 -32.6 -33.8 -35 -36.5 -38.2 -40.2 -42.8 -46.5 -52.9 -78 -52.8 ...
    -47.5 -45 -43.9 -43.5 -43.5 -44.1 -45.2 -46.8 -48.9 -51.8 -56.1 -63.4 ...
    -81.9 -63.8 -60 -58.9 -59.4 -61.3 -64.8 -69 -78.1 -97.9 -84 -84.2 -87 ...
    -91.2 -95.9 -100.9 -106.4 -112.6 -121.1 -137 -142.5 -131.2 -125.2 -124.3 ...
    -122.3 -120.7 -120.2 -121.3 -121 -124 -130.8 -132 -132.7 -135.6 -132.4 ...
    -133.5 -132.5];
plot(x,y8,'o-','MarkerSize',3);

y9 = [-34.5 -35.2 -36 -37 -38.1 -39.4 -40.7 -42.2 -43.7 -45.4 -47.3 -49.7 ...
    -53 -58 -65.7 -81.6 -63 -57.6 -54.7 -53.1 -52.3 -52.4 -53.2 -54.8 -57.5 ...
    -61.8 -69.9 -82 -69.5 -67.3 -68.1 -70.2 -75.1 -83.2 -99.1 -98.3 -96.9 ...
    -100.4 -105.1 -110.1 -114.1 -116.7 -119.2 -124.5 -133.5 -129 -126.1 ...
    -124.3 -123.3 -124.1 -125.6 -132 -143.5 -137.4 -142.8 -132.8 -122.6 ...
    -131.3 -134.5 -132.8 -135.5];
plot(x,y9,'x-','MarkerSize',5);

y10 = [-35.7 -37.3 -39.2 -41.4 -44.4 -48.6 -56.2 -66.4 -52.8 -48.3 -46 -45 ...
    -44.8 -45.3 -46.1 -47.3 -49.3 -51.9 -55.5 -61.1 -74.6 -68.4 -62 -59.8 ...
    -59.3 -60.2 -62.6 -66.8 -74.8 -90.7 -77.1 -76 -78 -83.2 -91.9 -104.5 ...
    -117.1 -112.6 -114.9 -117 -119.4 -122.2 -131 -129.8 -124.4 -122.2 -121.8 ...
    -121.7 -123.1 -125.5 -125.6 -130 -136.6 -145.7 -139.9 -132.1 -135.5 ...
    -132.9 -136.4 -134.9 -136.2];
plot(x,y10,'o-','MarkerSize',3);

legend('Input Signal','Fundamental','2^{nd} Harmonic','3^{rd} ...
    Harmonic','4^{th} Harmonic','5^{th} Harmonic','6^{th} Harmonic','7^{th} ...
    Harmonic','8^{th} Harmonic','9^{th} Harmonic','10^{th} Harmonic');
```

C.1.2 IZOTOPE: Ozone Exciter Triode

Listing C.2: IZOTOPE Ozone Triode Experiment

```
grid; hold; xlabel('Input Signal Level');ylabel('Output Signal ...
    Level');axis([-30,0,-60,0]);title('Izotope ...
    Triode');set(gcf,'position',[60 375 800 400]);

x = [0 -0.5 -1 -1.5 -2 -2.5 -3 -3.5 -4 -4.5 -5 -5.5 -6 -6.5 -7 -7.5 -8 -8.5 ...
    -9 -9.5 -10 -10.5 -11 -11.5 -12 -12.5 -13 -13.5 -14 -14.5 -15 -15.5 -16 ...
    -16.5 -17 -17.5 -18 -18.5 -19 -19.5 -20 -20.5 -21 -21.5 -22 -22.5 -23 ...
    -23.5 -24 -24.5 -25 -25.5 -26 -26.5 -27 -27.5 -28 -28.5 -29 -29.5 -30];

ys = x;
plot(x,ys,'-','MarkerSize',3);

y = [-8.3 -8.3 -8.3 -8.3 -8.2 -8.2 -8.3 -8.3 -8.3 -8.3 -8.4 -8.5 -8.6 -8.7 ...
    -8.8 -9 -9.1 -9.2 -9.4 -9.6 -9.8 -10.1 -10.4 -10.7 -11 -11.3 -11.6 -12 ...
    -12.4 -12.9 -13.4 -13.8 -14.3 -14.8 -15.3 -15.8 -16.2 -16.7 -17.2 -17.7 ...
    -18.2 -18.7 -19.2 -19.7 -20.2 -20.7 -21.2 -21.7 -22.2 -22.7 -23.2 -23.7 ...
    -24.2 -24.7 -25.2 -25.7 -26.2 -26.7 -27.2 -27.8 -28.3];
plot(x,y,'*-','MarkerSize',3);

y2 = [-15.2 -15.4 -15.7 -16.1 -16.5 -16.9 -17.3 -17.8 -18.4 -19 -19.7 -20.4 ...
    -21.1 -21.9 -22.8 -23.7 -24.8 -25.9 -27.2 -28.5 -29.6 -30.2 -31 -31.8 ...
    -32.6 -33.5 -34.4 -35.2 -35.6 -36.3 -37.1 -38 -38.9 -39.9 -40.9 -42 -43.2 ...
    -44.6 -45.9 -47.4 -48.7 -49.8 -50.4 -50.9 -51.4 -52 -52.5 -53 -53.6 -54.1 ...
    -54.7 -55.2 -55.7 -56.3 -56.9 -57.4 -58 -58.6 -59.2 -59.8 -60.4];
plot(x,y2,'o-','MarkerSize',3);

y3 = [-45.1 -40.6 -37.6 -35.5 -33.9 -32.7 -31.8 -31.1 -30.6 -30.3 -30.1 ...
    -29.9 -29.7 -29.7 -29.8 -30.2 -30.7 -31.6 -32.8 -34.2 -35.5 -36.1 -37 ...
    -38.3 -40 -42.4 -45.9 -51.2 -56.5 -57.7 -57.9 -58.2 -58.7 -59.3 -60.1 ...
    -61.2 -62.7 -64.8 -68.1 -74.6 -82.2 -70.5 -69.7 -69.8 -69.9 -70 -70.1 ...
    -70.2 -70.3 -70.4 -70.5 -70.6 -70.7 -70.8 -70.9 -71 -71.1 -71.2 -71.3 ...
    -71.5 -71.6];
plot(x,y3,'x-','MarkerSize',5);

y4 = [-24.2 -24.5 -24.8 -25.2 -25.7 -26.3 -26.9 -27.7 -28.5 -29.3 -30 -30.8 ...
    -31.9 -33.3 -34.7 -36.2 -37.6 -38.7 -39.2 -39.2 -39.7 -41.5 -43.6 -45.8 ...
    -48.2 -50.3 -52.1 -54 -60.8 -68.1 -78 -80.1 -71.2 -67.9 -66.7 -66.7 -68.1 ...
    -71.9 -86 -74.3 -68 -65.1 -65.2 -65.7 -66.3 -66.9 -67.6 -68.2 -68.8 -69.5 ...
    -70.2 -70.9 -71.7 -72.4 -73.3 -74.1 -75.1 -76.1 -77.1 -78.3 -79.6];
plot(x,y4,'o-','MarkerSize',3);

y5 = [-29.1 -30.2 -31.3 -32.6 -34 -35.6 -37.4 -39.3 -41.6 -44.1 -46.7 -49.7 ...
    -50.8 -50.1 -48.5 -46.6 -45.2 -44.5 -45 -47.2 -49.6 -48.8 -48.1 -47.7 ...
    -47.9 -49.1 -52.4 -61.7 -71.5 -68.3 -70.7 -74.5 -82.4 -87.4 -75.7 -71 ...
    -68.2 -66.5 -65.6 -65.7 -68 -72.9 -74.4 -74.6 -74.7 -74.8 -75 -75.1 -75.2 ...
    -75.4 -75.5 -75.7 -75.9 -76.1 -76.3 -76.5 -76.7 -77 -77.3 -77.6 -78];
plot(x,y5,'x-','MarkerSize',5);
```

```
y6 = [-51.5 -49.4 -47.7 -46.5 -45.8 -45.3 -45 -44.9 -45.1 -46 -48.8 -55.2 ...
    -67.3 -63 -59.2 -59.8 -63.9 -68.7 -68.4 -57.6 -51 -50.4 -50.9 -52.2 ...
    -54.5-57.4 -59.5 -59.1 -63.5 -66.6 -67.4 -69.2 -72.8 -81.8 -81.1 -71.6 ...
    -67.5 -65.5-64.9 -65.8 -67.8 -71.8 -73.7 -74.4 -75.1 -75.9 -76.7 -77.6 ...
    -78.5 -79.5 -80.6-81.7 -83 -84.5 -86.1 -88.1 -90.6 -93.8 -98.8 -110.1 ...
    -106.5];
plot(x,y6,'o-','MarkerSize',3);

y7 = [-37.5 -38.4 -39.4 -40.5 -41.7 -43 -44.5 -46.2 -48.1 -50.1 -52.1 -51.4 ...
    -50.2 -49.5 -49.2 -50 -52.9 -60.4 -71.9 -67.4 -66.8 -68.3 -75 -66.7 -59 ...
    -55.1 -54.4 -58.7 -75.6 -78.3 -73.5 -70.6 -68.7 -67.6 -67.2 -67.4 -68.6 ...
    -71.1 -76.2  -91.1 -103.8 -79.9 -77.8 -78 -78.1 -78.3 -78.5 -78.7 -79 ...
    -79.2 -79.5 -79.7 -80 -80.4 -80.8 -81.2 -81.7 -82.2 -82.8 -83.5 -84.3];
plot(x,y7,'x-','MarkerSize',5);

y8 = [-41.8 -43.6 -45.6 -47.8 -50.1 -52.3 -53.6 -53.1 -50.8 -48 -46.5 -46.5 ...
    -47.4 -48.9 -51.4 -54.5 -56.3 -54.6 -51.4 -50.9 -56 -62 -97.2 -64.8 -62.2 ...
    -64.7 -72.7 -74.4 -101.8 -85.5 -82.8 -74 -70 -67.8 -66.8 -66.9 -68.3 ...
    -71.3 -76.9 -84.8 -93.7 -82.5 -80.6 -81.6 -82.6  -83.7 -85 -86.3 -87.9 ...
    -89.7 -92 -94.8 -98.8 -106 -119.3 -103.4 -98.3 -95.4 -93.4 -91.9 -90.8];
plot(x,y8,'o-','MarkerSize',3);

y9 = [-58.2 -61.4 -64 -66.5 -68.5 -63.4 -57.5 -53.5 -51.4 -51.2 -53.9 -57 ...
    -58.7 -59.1 -56.6 -53.2 -50.9 -50.8 -54.4 -62.4 -60.8 -61.4 -60.5 -59.8 ...
    -61.4 -72.3 -64.1 -60.8 -66.7 -69.2 -68.5 -68.5 -69.1 -70.6 -73.4 -78.7 ...
    -92.4 -89.4 -92.8 -82.6 -76 -78.2 -80.6 -80.8 -81.1 -81.3 -81.6 -81.9 ...
    -82.3 -82.6 -83.1 -83.5 -84 -84.6 -85.3 -86 -86.9 -87.9 -89.1 -90.6 -92.4];
plot(x,y9,'x-','MarkerSize',5);

y10 = [-53.7 -55.8 -58.7 -62.9 -67.9 -68.8 -65.2 -60 -56.4 -55.6 -57.7 -64.3 ...
    -78 -61.7 -58.1 -59.3 -67.2 -68.6 -71.6 -57.9 -56.9 -55.9 -57 -61.4 -78.3 ...
    -68.2 -68.7 -73.5 -96.5 -71.5 -69.6 -68.8 -69.1 -70.4 -73.5 -79.4 -96.6 ...
    -90 -95.8 -90.2 -81.1 -82.7 -87.5 -88.9 -90.6 -92.5 -95 -98.2 -103 -114 ...
    -111.4 -103 -98.9 -96.4 -94.6 -93.4 -92.3 -91.6 -91.1 -90.8 -90.7];
plot(x,y10,'o-','MarkerSize',3);

legend('Input Signal','Fundamental','2^{nd} Harmonic','3^{rd} ...
    Harmonic','4^{th} Harmonic','5^{th} Harmonic','6^{th} Harmonic','7^{th} ...
    Harmonic','8^{th} Harmonic','9^{th} Harmonic','10^{th} Harmonic');
```

C.1.3 SOUNDTOYS: Radiator

Listing C.3: SOUNDTOYS Radiator Experiment

```
grid; hold; xlabel('Input Signal Level'); ylabel('Output Signal ...
    Level');axis([-30,0,-60,0]);title('Radiator Harmonic ...
    Distortion');set(gcf,'position',[60 375 800 400]);

x = [0 -0.5 -1 -1.5 -2 -2.5 -3 -3.5 -4 -4.5 -5 -5.5 -6 -6.5 -7 -7.5 -8 -8.5 ...
    -9 -9.5 -10 -10.5 -11 -11.5 -12 -12.5 -13 -13.5 -14 -14.5 -15 -15.5 -16 ...
    -16.5 -17 -17.5 -18 -18.5 -19 -19.5 -20 -20.5 -21 -21.5 -22 -22.5 -23 ...
    -23.5 -24 -24.5 -25 -25.5 -26 -26.5 -27 -27.5 -28 -28.5 -29 -29.5 -30];

ys = x;
plot(x,ys,'-','MarkerSize',4);

y = [-7.3 -7.2 -7.2 -7.2 -7.2 -7.2 -7.2 -7.2 -7.2 -7.3 -7.3 -7.4 -7.5 -7.5 ...
    -7.6 -7.7 -7.9 -8.1 -8.3 -8.6 -9 -9.5 -9.8 -10.2 -10.7 -11.1 -11.6 -12.1 ...
    -12.6 -13.1-13.5 -13.9 -14.4 -14.9 -15.4 -15.9 -16.4 -16.9 -17.3 -17.8 ...
    -18.3 -18.8 -19.3 -19.8 -20.3 -20.8 -21.3 -21.8 -22.3 -22.8 -23.3 -23.8 ...
    -24.3 -24.8 -25.3 -25.8 -26.3 -26.8 -27.3 -27.8 -28.3];
plot(x,y,'^-','MarkerSize',3);

y2 = [-15.9 -16.2 -16.6 -17 -17.5 -17.9 -18.4 -19 -19.6 -20.3 -21.1 -22.1 ...
    -23.4 -24.9 -26.5 -28.6 -31.5 -35 -38.7 -42.8 -46.3 -48.3 -46.5 -45.5 ...
    -45.6 -46.5 -47.7 -48.9 -50.2 -51.3 -52.4 -53.2 -54.1 -54.9 -55.7 -56.5 ...
    -57.3 -58.2 -59.1 -60 -61 -62 -63.1 -64.1 -65.2 -66.3 -67.3 -68.4 -69.4 ...
    -70.5 -71.5 -72.5 -73.6 -74.6 -75.6 -76.7 -77.7 -78.7 -79.8 -80.8 -81.8];
plot(x,y2,'o-','MarkerSize',3);

y3 = [-27.6 -26.8 -26.2 -25.5 -24.8 -24.5 -24.3 -24.1 -24 -24 -24.1 -24.4 ...
    -24.8 -25.2 -25.9 -27 -28.7 -30.8 -33.2 -35.7 -37.8 -39.7 -42.8 -46.6 -50 ...
    -52.1 -53.6 -55 -56.5 -58.1 -59.5 -60.5 -61.7 -62.7 -63.6 -64.5 -65.4 ...
    -66.5 -67.6 -68.8 -70.1 -71.4 -72.9 -74.3 -75.8 -77.2 -78.7 -80.2 -81.6 ...
    -83.1 -84.6 -86 -87.5 -88.9 -90.4 -91.9 -93.3 -94.8 -96.2 -97.7 -99.1];
plot(x,y3,'x-','MarkerSize',5);

y4 = [-22.5 -22.8 -23.2 -23.7 -24.3 -25.1 -26.2 -27.3 -28.5 -30 -31.9 -34.5 ...
    -38.4 -43 -48.1 -59 -58.1 -63.8 -57.7 -52.3 -50.8 -51.8 -57 -67.8 -80 ...
    -73.7 -76.3 -82.5 -104.9 -84.7 -80.1 -78.9 -78.9 -80.2 -82.5 -86 -91.1 ...
    -98.9 -128.6 -103.1 -99.3 -98.4 -98.8 -99.9 -101.4 -102.9 -104.4 -105.9 ...
    -107.5 -109.1 -110.6 -111.8 -113.9 -116 -117.3 -118.6 -120.7 -122 -125 ...
    -125.8 -127.2];
plot(x,y4,'o-','MarkerSize',3);

y5 = [-35.3 -37.9 -41.5 -47.6 -53.9 -47.8 -43.4 -41.7 -41 -41 -41.5 -42.9 ...
    -45.8 -52.3 -59.1 -47.9 -44.5 -43.2 -45.1 -47.3 -49.2 -50.5 -53.8 -61.2 ...
    -75.4 -86.1 -86.2 -87.2 -84.2 -81.1 -79.1 -78.4 -78.5 -79.4 -81 -83.3 ...
    -86.3 -89.8 -93.6 -97.9 -102.9 -107.9 -112.5 -116 -117.1 -117.8 -120.4 ...
    -120.6 -122.7 -123 -123.9 -126.1 -127.8 -127.7 -128.2 -129.7 -129.5 ...
    -131.5 -130.8 -135.2 -133.7];
```

```
plot(x,y5,'x-','MarkerSize',5);

y6 = [-33.8 -33.9 -34.4 -35 -36 -37.9 -41.1 -45.5 -53.5 -59.2 -47.9 -43.5 ...
    -41.3 -41.1 -43.1 -45.4 -50 -54.2 -57.6 -57.4 -56.2 -56.7 -59.9 -66.9 ...
    -84.4 -79.3 -77.1 -77.3 -78.8 -81.7 -87.1 -94.7 -103.7 -93.3 -91.1 -91.3 ...
    -92.9 -95.1 -97.7 -101.1 -105.1 -109.8 -114.7 -118.7 -121.1 -122.6 -123.9 ...
    -126.4 -127.4 -131 -131.7 -135.5 -139.5 -138.1 -140.9 -137.9 -142.5 ...
    -141.2 -143.6 -141.8 -150.5];
plot(x,y6,'o-','MarkerSize',3);

y7 = [-39.3 -42.4 -47.2 -58.2 -54.9 -47 -43.5 -42.7 -42.6 -43.6 -45.5 -48.9 ...
    -56.6 -66.7 -54.8 -54.5 -59.2 -65.2 -61.1 -63.3 -62.9 -60.3 -59.7 -64.1 ...
    -73.3 -81 -80.5 -81.6 -84.2 -87.4 -93.1 -104.1 -108.8 -102.1 -84.8 -83.9 ...
    -101.8 -103.4 -105.8 -109.6 -115 -124 -141.4 -128.3 -128.8 -128.8 -131.8 ...
    -132.7 -135.4 -134.6 -135.4 -135.5 -137.1 -147.7 -139.4 -150.7 -139.3 ...
    -150.1 -144.5 -147.3 -140.1];
plot(x,y7,'x-','MarkerSize',5);

y8 = [-45.4 -44.5 -44.5 -45 -46.7 -50.3 -58.7 -58.7 -49.8 -46.5 -44.7 -44.4 ...
    -46 -49.7 -56.6 -71.8 -66.1 -67 -72.2 -70.9 -73.7 -68 -66.1 -68.3 -73.7 ...
    -81 -88 -104.3 -93.3 -88.6 -88 -88.8 -91 -94.6 -99.8 -106.9 -116.1 -135.4 ...
    -119.1 -117.4 -119.9 -125.6 -145.5 -135.1 -133.3 -132.2 -136.6 -142.3 ...
    -142.4 -141 -145.4 -145 -147.9 -149.8 -143.2 -143.5 -145.8 -146.2 -151.2 ...
    -145.1 -154.1];
plot(x,y8,'o-','MarkerSize',3);

y9 = [-53 -65.7 -54.1 -47.8 -44.6 -42.7 -41.4 -41.7 -42.2 -44.1 -47.7 -54 ...
    -71.6 -61.9 -71.3 -65.9 -59.9 -61 -68.8 -63.4 -64.3 -70.8 -74.7 -72.8 ...
    -84.7 -84.2 -82.9 -86.6 -93.8 -122.4 -98.9 -96.7 -96.4 -98.4 -102.4 ...
    -108.5 -116.2 -132.2 -124.8 -119.6 -120.3 -122.4 -126 -130.1 -136 -137.1 ...
    -133.6 -150.8 -134.1 -139.7 -141.7 -146.6 -145.9 -147.5 -144.9 -138.2 ...
    -143.9 -146.4 -141.9 -149.6 -141];
plot(x,y9,'x-','MarkerSize',5);

y10 = [-43.9 -42.9 -42.8 -42.9 -43.9 -45.8 -48.8 -55.5 -64.7 -58.6 -54.7 ...
    -56.7 -69 -60.1 -56 -55.4 -59.5 -65.8 -73.4 -63.7 -65 -70.9 -87.7 -83.5 ...
    -84 -88 -87.6 -87.3 -89 -92.8 -98.7 -105.7 -125.1 -110.5 -110.1 -112.8 ...
    -114.8 -117.7 -123.1 -151 -127.4 -125.6 -131.5 -139.2 -142.5 -143.3 ...
    -144.9 -145 -148.1 -145.7 -146.3-139.5 -147.7 -148.3 -138 -144.1 -150.2 ...
    -141.8 -140.7 -149.8 -149.5];
plot(x,y10,'o-','MarkerSize',3);

legend('Input Signal','Fundamental','2^{nd} Harmonic','3^{rd} ...
   Harmonic','4^{th} Harmonic','5^{th} Harmonic','6^{th} Harmonic','7^{th} ...
   Harmonic','8^{th} Harmonic','9^{th} Harmonic','10^{th} Harmonic');
```

C.1.4 V1:12AY7

Listing C.4: V1: 12AY7

```
grid;hold;xlabel('Input Signal Level');ylabel('Output Signal Level'); ...
    axis([-30,0,-60,0]);title('V1 - 12AY7 Harmonic Distortion'); ...
    set(gcf,'position',[60 80 700 700]);

x = [0 -0.5 -1 -1.5 -2 -2.5 -3 -3.5 -4 -4.5 -5 -5.5 -6 -6.5 -7 -7.5 -8 -8.5 ...
    -9 -9.5 -10 -10.5 -11 -11.5 -12 -12.5 -13 -13.5 -14 -14.5 -15 -15.5 -16 ...
    -16.5 -17 -17.5 -18 -18.5 -19 -19.5 -20 -20.5 -21 -21.5 -22 -22.5 -23 ...
    -23.5 -24 -24.5 -25 -25.5 -26 -26.5 -27 -27.5 -28 -28.5 -29 -29.5 -30];

ys = x;
plot(x,ys,'-','MarkerSize',4);

y = [-7 -7.10 -7.20 -7.40 -7.90 -8.80 -9.30 -9.80 -10.3 -10.9 -11.4 -11.9 ...
    -12.4 -13 -13.5 -14 -14.5 -15.1 -15.6 -16.1 -16.6 -17.1 -17.7 -18.2 -18.7 ...
    -19.2 -19.7 -20.2 -20.7 -21.3 -21.8 -22.3 -22.8 -23.3 -23.8 -24.3 -24.8 ...
    -25.7 -25.8 -26.3 -26.8 -27.3 -27.8 -28.3 -28.8 -29.3 -29.8 -30.3 -30.8 ...
    -31.3 -31.8 -32.3 -32.8 -33.3 -33.8 -34.3 -34.8 -35.2 -35.8 -36.3 -36.9];
plot(x,y,'^-','MarkerSize',3);

y2 = [-28.2 -28.2 -28.6 -29.2 -33.7 -36.6 -37.3 -37.6 -37.8 -38.2 -38.8 ...
    -39.3 -40.1 -40.7 -41.5 -42.3 -43.3 -44.1 -45.2 -46 -47 -47.9 -48.9 -49.9 ...
    -50.8 -51.8 -52.9 -53.7 -54.7 -55.6 -56.6 -57.6 -58.7 -59.5 -60.5 -61.4 ...
    -62.5 -64.3 -64.4 -65.2 -66.4 -67.3 -68.3 -69.4 -70.3 -71.2 -72.3 -73.2 ...
    -74.3 -74.8 -76.1 -77.2 -78.3 -79.2 -80.3 -81.3 -82.3 -83.1 -84.2 -85.3 ...
    -86.5];
plot(x,y2,'o-','MarkerSize',3);

y3 = [-18.2 -19.4 -21.3 -23.9 -38 -46 -49 -51.3 -52.8 -53.4 -53.5 -53.3 ...
    -53.4 -53.5 -54 -54.6 -55.5 -56.4 -57.4 -58.5 -59.7 -60.9 -62.1 -63.4 ...
    -64.6 -66 -67.3 -68.6 -70 -71.4 -72.7 -74.1 -75.6 -77 -78.5 -79.9 -81.4 ...
    -84.1 -84.4 -86 -87.5 -89.2 -90.8 -92.4 -94.1 -95.9 -97.7 -99.5 -101.4 ...
    -103.5 -105 -106.8 -108.2 -109.8 -111.5 -113.6 -114.6 -116.9 -117.6 -119 ...
    -119.9];
plot(x,y3,'x-','MarkerSize',5);

y4 = [-26.8 -27.7 -29.7 -33.5 -43.3 -44.4 -46.4 -48.4 -50.5 -52.8 -55.4 ...
    -58.2 -61.3 -64.4 -67.6 -70.7 -74.1 -76.6 -79.7 -81.6 -83.7 -85.3 -87 ...
    -88.7 -90 -91.9 -93.8 -94.7 -96 -97.1 -98.9 -99.6 -101.1 -101.9 -103.1 ...
    -104.2 -105.3 -107.7 -108.3 -108.7 -110.1 -111.4 -112.7 -115.1 -116.3 ...
    -116.2 -118.6 -121.6 -122.6 -124 -127.3 -126.9 -125.4 -135.8 -133.5 -135 ...
    -136.2 -142.2 -139.3 -137.8 -136.6];
plot(x,y4,'o-','MarkerSize',3);

y5 = [-24.6 -25.3 -26.6 -28.6 -39.9 -48.2 -50 -51.6 -53.4 -55.3 -57.4 -59.7 ...
    -62.2 -64.9 -67.7 -70.4 -73 -75.7 -78.2 -80.6 -83.1 -85.4 -87.6 -89.8 ...
    -91.9 -93.8 -95.5 -97.7 -99.5 -101.4 -103.7 -106.6 -108.8 -111.7 -109.6 ...
    -115 -113.3 -119.3 -117.1 -117.2 -130.5 -122.2 -123.3 -126.6 -118.1 ...
```

```
    -116.8 -125 -121.1 -118.5 -120.4 -118.2 -120.2 -123.4 -132.3 -126.8 ...
    -122.4 -120.3 -120.5 -122.3 -138.3 -140];
plot(x,y5,'x-','MarkerSize',5);

y6 = [-28.6 -29.1 -30.4 -33.2 -52 -67.7 -66.6 -66.3 -66.8 -67.9 -69.6 -72 ...
    -75 -79 -83.7 -89.5 -95.5 -106 -110.3 -106 -105.2 -106.6 -108.5 -112.1 ...
    -114.2 -113.2 -114.8 -116.5 -117.3 -119.2 -116.5 -118 -120 -119.4 -119.8 ...
    -120.8 -123.7 -124.8 -126.6 -126.4 -127.3 -127.7 -132.4 -130.4 -139.9 ...
    -133.6 -144.6 -143.2 -137.2 -138.1 -139.9 -131.3 -135.2 -143.3 -144 ...
    -143.4 -137.6 -139.1 -135.3 -140.7 -139.4];
plot(x,y6,'o-','MarkerSize',3);

y7 = [-31.4 -31.8 -32.2 -32.9 -46.8 -62.8 -67.5 -72.7 -79.3 -86.8 -88.2 ...
    -87.4 -89.2 -92.5 -97.2 -101.9 -103.2 -104.2 -105 -106.2 -107.6 -109.4 ...
    -110.4 -112.2 -113.5 -115.4 -115.6 -118.4 -121.4 -124.4 -126.9 -125.8 ...
    -129.5 -132.4 -132.4 -134.6 -132.7 -130.8 -134 -132.9 -127.6 -135.3 ...
    -129.6 -138.9 -135.8 -133.8 -136.2 -134.7 -134 -141.1 -141.7 -139 -140.2 ...
    -148.3 -148.8 -142.9 -133.1 -136.8 -146 -142.1 -135.5];
plot(x,y7,'x-','MarkerSize',5);

y8 = [-29.9 -30.7 -31.9 -34.2 -52.9 -67.6 -71 -75.1 -81 -90.6 -96.9 -89.9 ...
    -89.3 -90.3 -92.7 -95.5 -98.9 -102.6 -106.4 -110.3 -113.6 -114.3 -115.2 ...
    -115.7 -118.9 -121.4 -125.3 -135.8 -133.5 -136.9 -131.4 -132.9 -138 -136 ...
    -134.4 -136.6 -135.8 -139.4 -136.7 -136.7 -142.1 -134.8 -148.3 -140 -136 ...
    -144.8 -140.7 -149.6 -140.3 -140.6 -134.3 -136.6 -137.5 -136.2 -136.8 ...
    -133.2 -138.8 -140.9 -141.1 -141.7 -139];
plot(x,y8,'o-','MarkerSize',3);

y9 = [-36.7 -38.5 -39.3 -38.2 -51.7 -74 -74.9 -76.8 -79.7 -84 -90.4 -101.3 ...
    -105.3 -101.8 -102.7 -105.4 -108.7 -112 -114.3 -115.9 -118.5 -122.2 ...
    -130.7 -133.2 -134.4 -133.7 -131.3 -134 -135.3 -132.4 -142.3 -131.3 ...
    -138.1 -129.1 -130.5 -144.4 -139.2 -134.8 -145 -141 -134.1 -140.9 -142.5 ...
    -131.5 -146.5 -142.3 -145.3 -147.4 -133.3 -137.4 -148.4 -140.8 -135.2 ...
    -142.8 -135.7 -140.3 -138.6 -146.2 -141.6 -140.1 -142.4];
plot(x,y9,'x-','MarkerSize',5);

y10 = [-30.7 -31.7 -33.4 -35.6 -55.7 -82.2 -81.3 -81.1 -82.1 -84.4 -88.1 ...
    -93.4 -100.1 -108.5 -113.7 -116.9 -121.8 -124.3 -126.8 -118.3 -116.7 ...
    -118.7 -124.8 -132.5 -124.7 -127.2 -130.3 -128.9 -126.3 -134.5 -128.9 ...
    -132 -130.5 -128.7 -129.7 -129.3 -131.1 -130 -129.5 -129.1 -129.2 -129.9 ...
    -131.8 -130.7 -128.4 -127.7 -131.2 -128.4 -129.1 -129.9 -129.3 -127.9 ...
    -127.7 -128.7 -130.2 -126.6 -131.7 -133 -128.8 -128.5 -131.7];
plot(x,y10,'o-','MarkerSize',3);

legend('Input Signal','Fundamental','2^{nd} Harmonic','3^{rd} ...
    Harmonic','4^{th} Harmonic','5^{th} Harmonic','6^{th} Harmonic','7^{th} ...
    Harmonic','8^{th} Harmonic','9^{th} Harmonic','10^{th} Harmonic');
```

C.1.5 V1:12AX7

Listing C.5: V1: 12AX7

```
grid; hold;xlabel('Input Signal Level');ylabel('Output Signal ...
    Level');axis([-30 0 -60 0]);title('V1 - 12AY7 Harmonic ...
    Distortion');set(gcf,'position',[60 80 700 700]);

x = [0 -0.5 -1 -1.5 -2 -2.5 -3 -3.5 -4 -4.5 -5 -5.5 -6 -6.5 -7 -7.5 -8 -8.5 ...
    -9 -9.5 -10 -10.5 -11 -11.5 -12 -12.5 -13 -13.5 -14 -14.5 -15 -15.5 -16 ...
    -16.5 -17 -17.5 -18 -18.5 -19 -19.5 -20 -20.5 -21 -21.5 -22 -22.5 -23 ...
    -23.5 -24 -24.5 -25 -25.5 -26 -26.5 -27 -27.5 -28 -28.5 -29 -29.5 -30];

ys = x;
plot(x,ys,'-','MarkerSize',4);

y = [-6.8 -6.9 -7 -9.8 -10.7 -11.3 -11.8 -12.4 -12.9 -13.5 -14.1 -14.7 -15.2 ...
    -15.8 -16.4 -17 -17.6 -18.2 -18.8 -19.4 -19.9 -20.5 -21.1 -21.6 -22.2 ...
    -22.7 -23.2 -23.8 -24.3 -24.8 -25.4 -25.9 -26.4 -26.9 -27.4 -28 -28.5 -29 ...
    -29.5 -30 -30.5 -31 -31.5 -32 -32.5 -33,-33.5 -34 -34.5 -35,-35.5 -36 ...
    -36.5 -37 -37.5 -38 -38.5 -38.9 -39.5 -40 -40.6];
plot(x,y,'^-','MarkerSize',3);

y2 = [-19.3 -20.2 -21.9 -22.7 -23.5 -24.1 -24.9 -25.6 -26.4 -27.2 -28.1 -29 ...
    -29.9 -30.9 -31.9 -33 -34 -35.1 -36.2 -37.3 -38.5 -39.5 -40.6 -41.7 -42.8 ...
    -43.8 -44.9 -46 -47 -48.1 -49.1 -50.2 -51.2 -52.3 -53.3 -54.3 -55.3 -56.3 ...
    -57.4 -58.4 -59.4 -60.4 -61.4 -62.4 -63.4 -64.4 -65.4 -66.4 -67.4 -68.4 ...
    -69.5 -70.5 -71.5 -72.5 -73.5 -74.5 -75.5 -76.3 -77.5 -78.5 -79.7];
plot(x,y2,'o-','MarkerSize',3);

y3 = [-18 -18.9 -20.5 -44.3 -55.2 -68.1 -58.4 -52.8 -50.2 -48.7 -47.9 -47.5 ...
    -47.6 -47.9 -48.4 -49.1 -50.1 -51.1 -52.2 -53.4 -54.6 -55.8 -57.1 -58.4 ...
    -59.7 -61.1 -62.4 -63.9 -65.3 -66.7 -68.2 -69.7 -71.1 -72.6 -74 -75.5 -77 ...
    -78.5 -80 -81.4 -83 -84.5 -86.1 -87.6 -89.2 -90.9 -92.5 -94.1 -95.8 -97.5 ...
    -99.3 -101.1 -102.9 -104.9 -106.8 -108.7 -111 -112.7 -115.8 -116.8 -118.3];
plot(x,y3,'x-','MarkerSize',5);

y4 = [-26 -27.3 -29.8 -40.6 -43.3 -44.8 -46.8 -49 -51.5 -54.4 -58.1 -62.9 ...
    -69.9 -86.5 -76.1 -72 -70.7 -70.7 -71.3 -72.2 -73.4 -74.8 -76.2 -77.7 ...
    -79.4 -81.2 -83 -84.9 -86.9 -88.8 -90.9 -93 -95 -97 -99 -100.9 -102.9 ...
    -105 -107 -109 -111.3 -112.9 -114.9 -117.7 -121.9 -121.2 -124.3 -126.2 ...
    -125.7 -130.3 -132.5 -134.6 -134.5 -149 -136.5 -145.3 -144.7 -136 -138.8 ...
    -135 -143.6];
plot(x,y4,'o-','MarkerSize',3);

y5 = [-28.3 -27 -25.5 -50.7 -49 -49.3 -49.8 -50.6 -51.6 -52.9 -54.5 -56.4 ...
    -58.6 -61 -63.5 -66.1 -68.7 -71.2 -73.6 -76 -78.4 -80.8 -83.4 -86.3 -88.9 ...
    -91.5 -94.3 -97 -98.8 -101.4 -102.9 -105.4 -107.8 -110.2 -114.1 -116.4 ...
    -118.7 -119.6 -127.4 -131 -140.2 -128.7 -122.8 -127.6 -130.8 -123.1 ...
    -120.4 -124.9 -124.2 -128.8 -121.8 -124.8 -120.7 -138.7 -126.4 -121.6 ...
    -119.8 -130.6 -130.1 -122.9 -123.9];
```

```
plot(x,y5,'x-','MarkerSize',5);

y6 = [-25.2 -26.1 -27.9 -53.8 -62.9 -67.6 -86.6 -73.8 -69.2 -67.5 -67.2 -68 ...
    -69.5 -71.7 -74.5 -77.7 -81.1 -84.4 -87.6 -90.6 -93.7 -97 -100.6 -105.7 ...
    -110.8 -116.3 -125.2 -130.9 -142.3 -131.1 -132.6 -136.2 -134.7 -136.2 ...
    -134.6 -142.2 -135.2 -138.4 -143.5 -136.3 -146.1 -146.1 -140.9 -132.9 ...
    -145.9 -143.6 -138.2 -136.4 -141.2 -133.5 -136.2 -137.8 -139 -137.5 ...
    -141.2 -139.3 -145.3 -132.5 -136.3 -133.2 -134.9];
plot(x,y6,'o-','MarkerSize',3);

y7 = [-41.3 -43 -39.3 -54.9 -55.7 -57.2 -59.3 -61.8 -64.8 -68.4 -72.9 -78.4 ...
    -84.6 -90.8 -94.9 -97.1 -98.5 -101 -104.9 -111.9 -117.4 -113.8 -113.9 ...
    -115.7 -119.1 -128 -149.5 -126.3 -125.1 -126.1 -123.2 -127.9 -130.5 ...
    -131.4 -133.8 -137.1 -129.4 -131.5 -127.9 -127.3 -131.7 -132 -129.7 ...
    -134.3 -135.2 -131.5 -135.2 -135.4 -148.2 -140.2 -141.6 -135.5 -142.5 ...
    -144.2 -142.9 -132.9 -151.7 -130.2 -133.5 -137.7 -134.9];
plot(x,y7,'x-','MarkerSize',5);

y8 = [-27.8 -28 -29 -67.5 -73.9 -71.5 -69.9 -70.3 -71.8 -74.3 -78.1 -83.6 ...
    -91.7 -108.2 -106.3 -106.2 -111.3 -121.1 -123.9 -122.6 -117.5 -116.2 ...
    -116.3 -116.7 -118.5 -123.7 -129.8 -132.2 -148.3 -133.4 -133.4 -137.4 ...
    -138.5 -140.1 -140.3 -143.9 -143.9 -132.8 -143.7 -145.3 -142.4 -148.2 ...
    -142.7 -134.8 -135.6 -136.3 -136.7 -140.7 -130.9 -143.6 -143.9 -142 ...
    -140.2 -147.3 -150.1 -140.3 -137.3 -145.7 -134.3 -131.4 -143.3];
plot(x,y8,'o-','MarkerSize',3);

y9 = [-38.5 -41.9 -47.1 -62.2 -66.5 -69.8 -75.6 -84.3 -97.5 -89.2 -88.4 ...
    -91.4 -97.8 -113.6 -112.1 -113.1 -121.1 -114 -111.2 -112.6 -117 -126.4 ...
    -131.1 -119.9 -120.3 -120.2 -121.1 -122.7 -124.4 -125.1 -135 -143.4 ...
    -138.1 -131.5 -140.8 -139.7 -139.5 -142.8 -132.4 -143.3 -143.9 -141.7 ...
    -139.9 -137.7 -141.2 -131.2 -141.7 -155.1 -145.1 -148 -134.9 -139.8 ...
    -137.2 -142.6 -141 -140.7 -143 -146.1 -141 -145.6 -131.3];
plot(x,y9,'x-','MarkerSize',5);

y10 = [-32.4 -32.3 -31.7 -84.1 -73.2 -74.5 -77.2 -81.6 -89.1 -109.7 -94.8 ...
    -93.3 -96.1 -102.7 -119.9 -115.5 -116.9 -130.9 -120.5 -118.9 -120.8 ...
    -121.7 -124.2 -128.6 -129.5 -127.3 -128.5 -130.3 -133.3 -129.2 -131.8 ...
    -131.7 -130.8 -127.6 -130.4 -128.1 -130.1 -130.5 -128.3 -129.7 -131 ...
    -131.8 -133.9 -131.7 -129 -129.2 -129.4 -129.9 -130.2 -129 -127.8 -130.4 ...
    -129.3 -134.4 -131.8 -129.7 -131.8 -134.8 -129.4 -130.1 -129.2];
plot(x,y10,'o-','MarkerSize',3);

legend('Input Signal','Fundamental','2^{nd} Harmonic','3^{rd} ...
    Harmonic','4^{th} Harmonic','5^{th} Harmonic','6^{th} Harmonic','7^{th} ...
    Harmonic','8^{th} Harmonic','9^{th} Harmonic','10^{th} Harmonic');
```

C.2 Graphical Representations of Experiment 2

C.2.1 PLUGIN ALLIANCE: Black Box

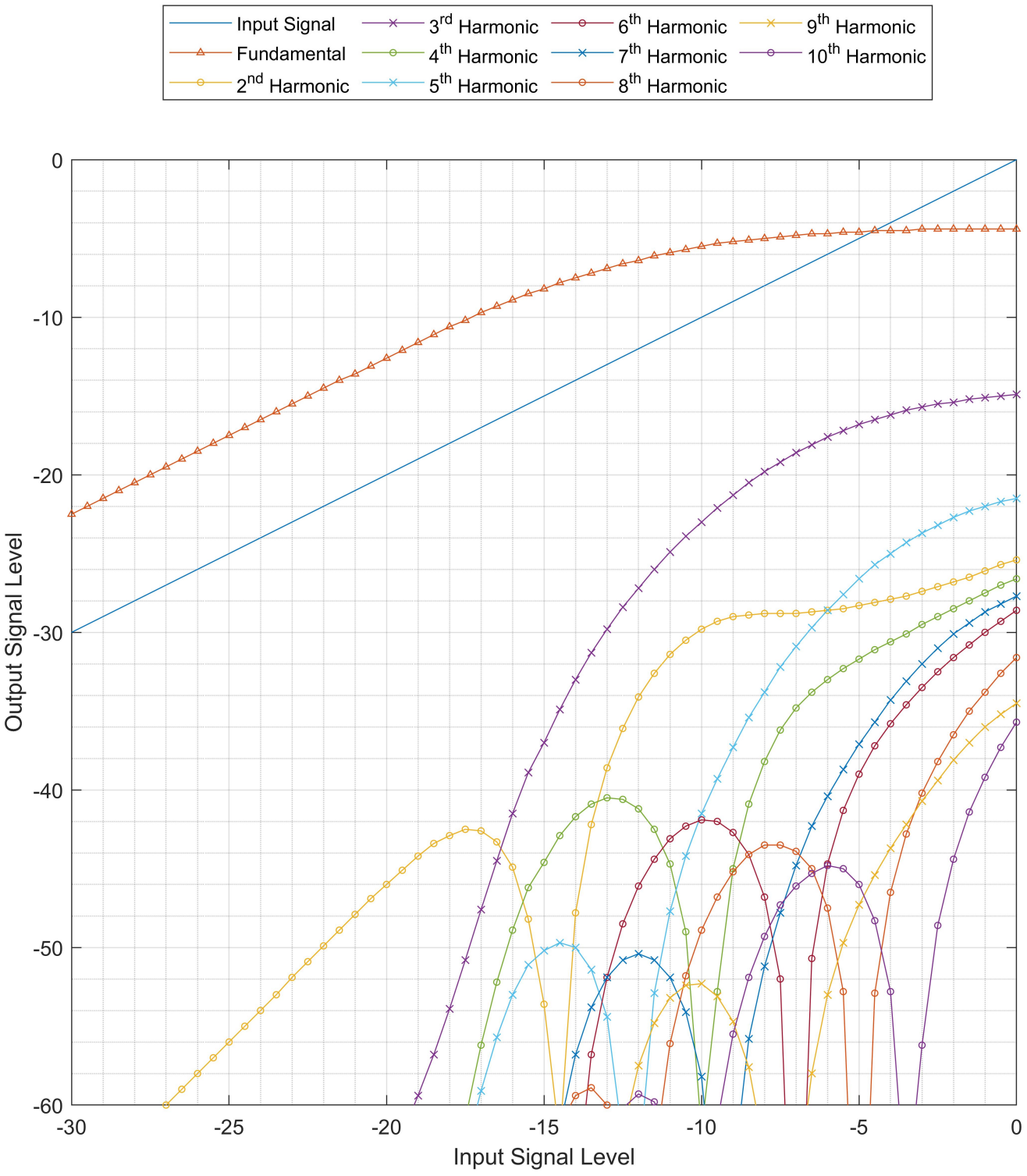

Figure C.1: PLUGIN ALLIANCE: Black Box Harmonic Distortion

C.2.2 IZOTOPE: Ozone Exciter Triode Harmonic Distortion

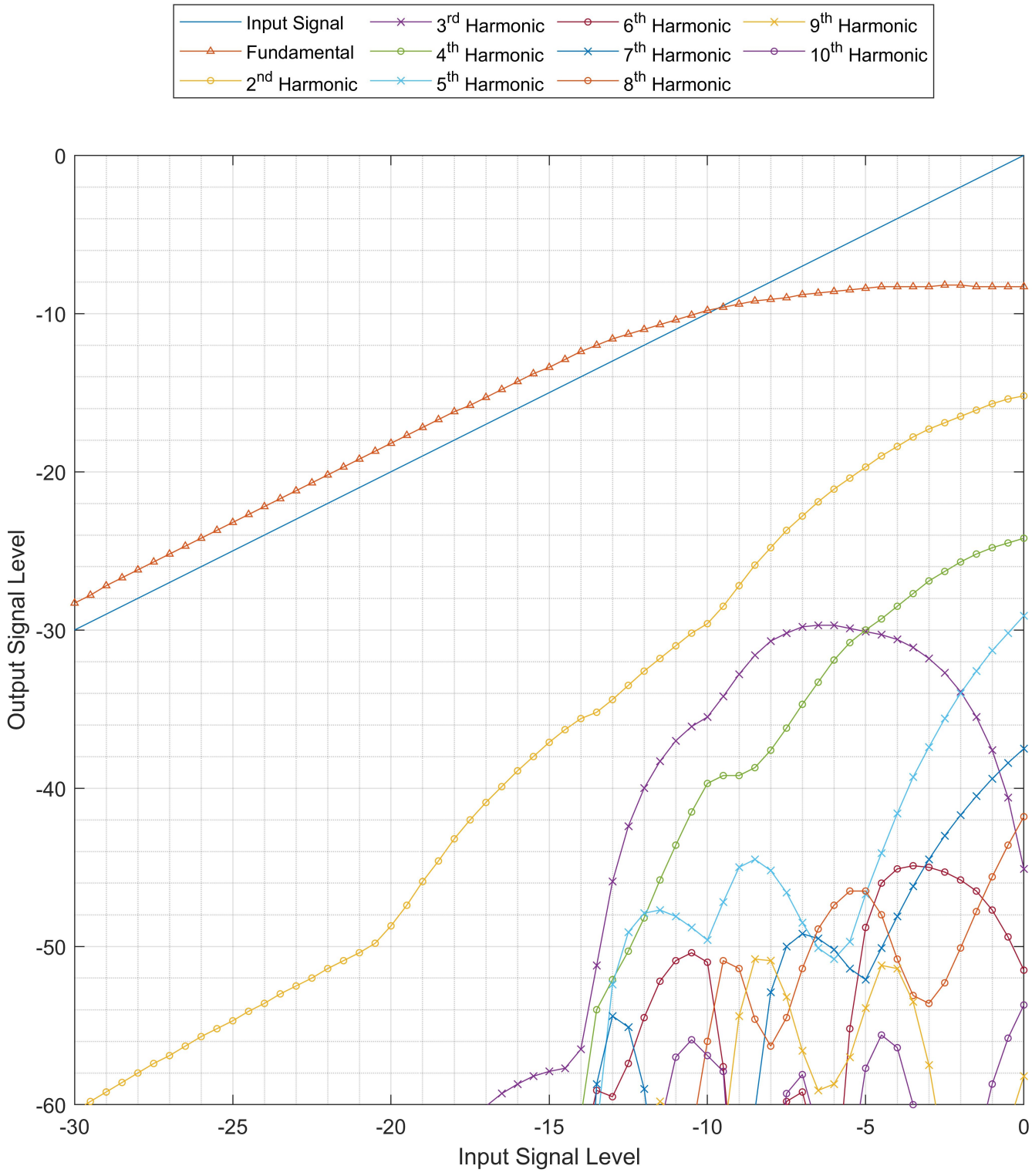

Figure C.2: IZOTOPE: Ozone Triode Harmonic Distortion

C.2.3 SOUNDTOYS: Radiator Harmonic Distortion

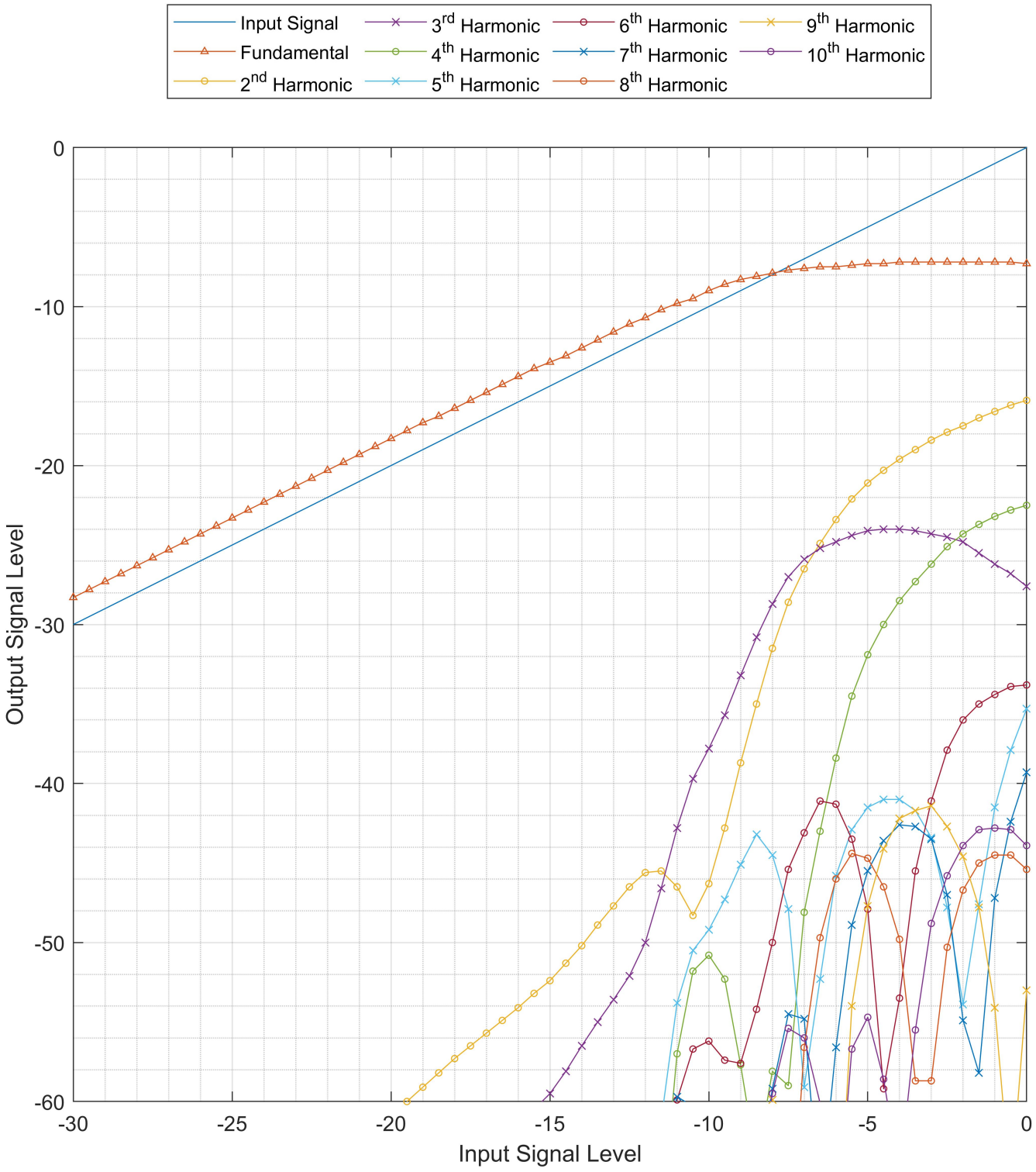

Figure C.3: SOUNDTOYS: Radiator Harmonic Distortion

C.2.4 V1:12AY7

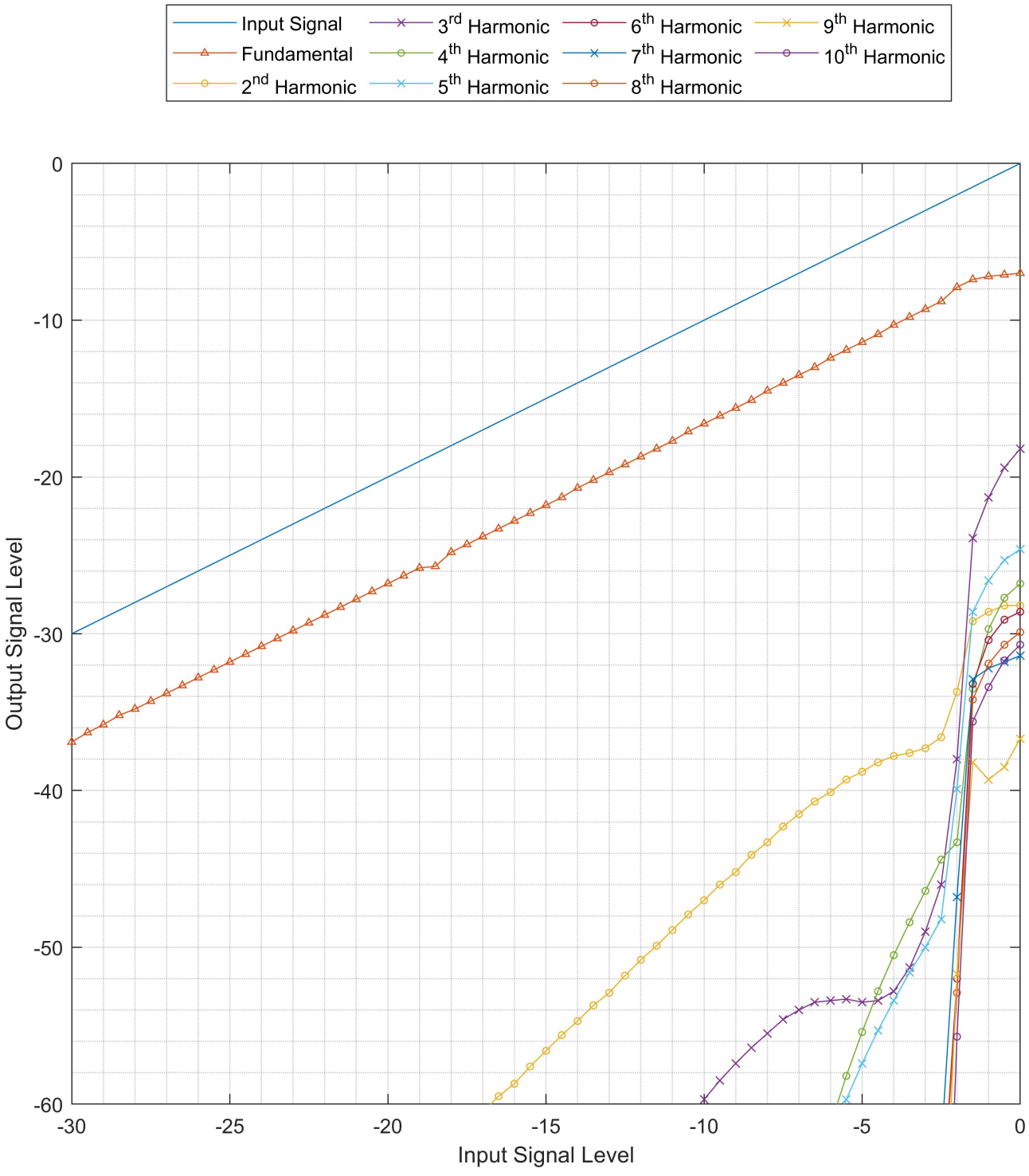

Figure C.4: V1:12AY7 Harmonic Distortion

C.2.5 V1:12AX7

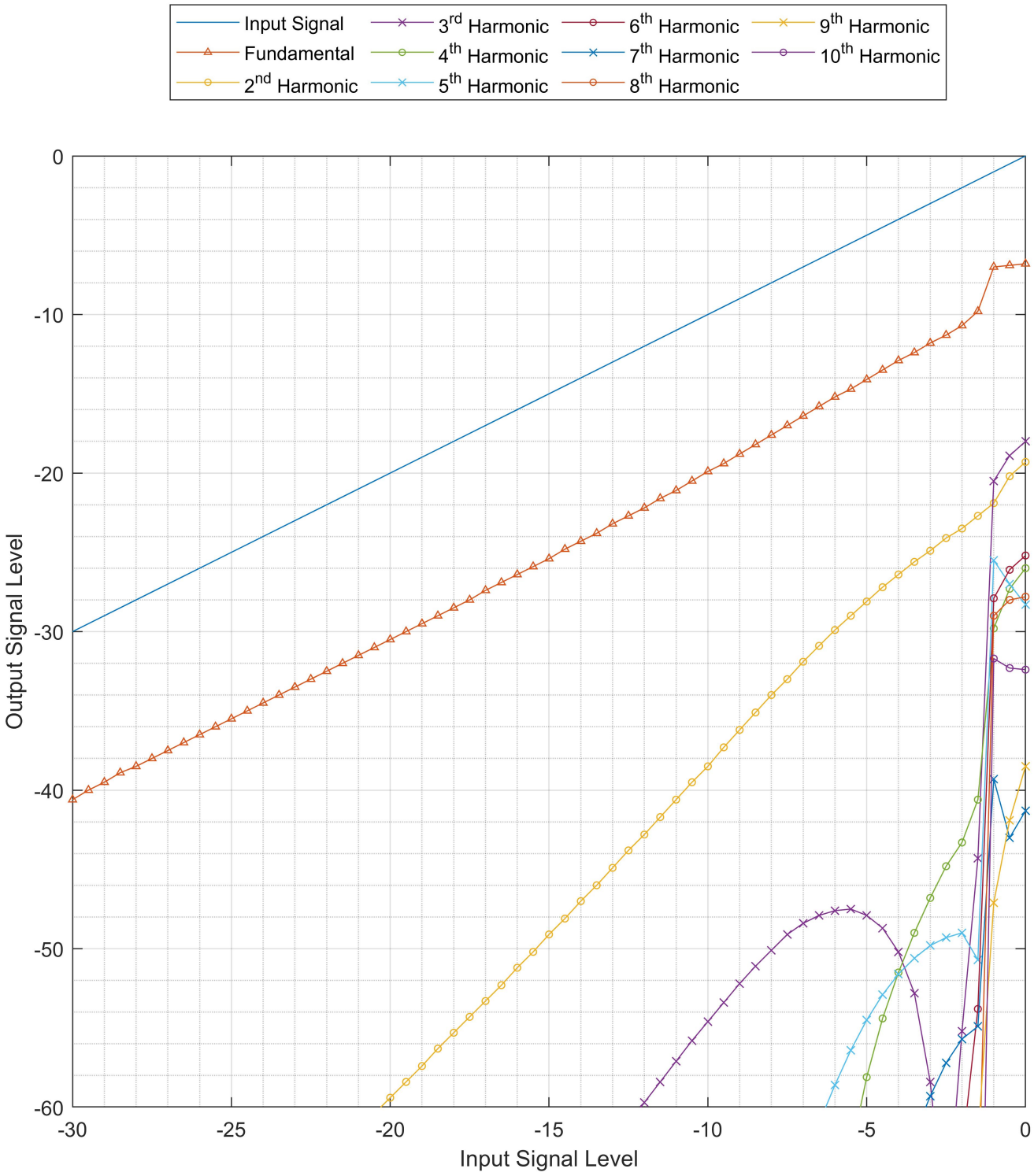

Figure C.5: V1:12AX7 Harmonic Distortion

Appendix D

Results of Experiment 3

D.1 Sawtooth Waves

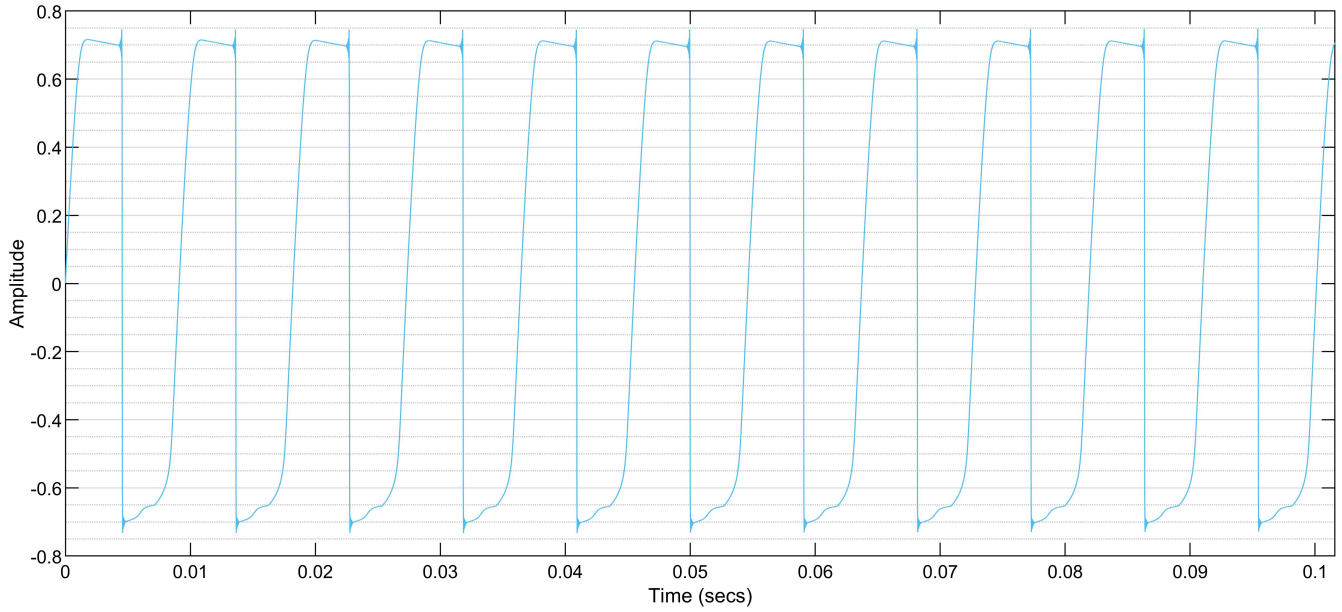

Figure D.1: Black Box - Sawtooth Wave.

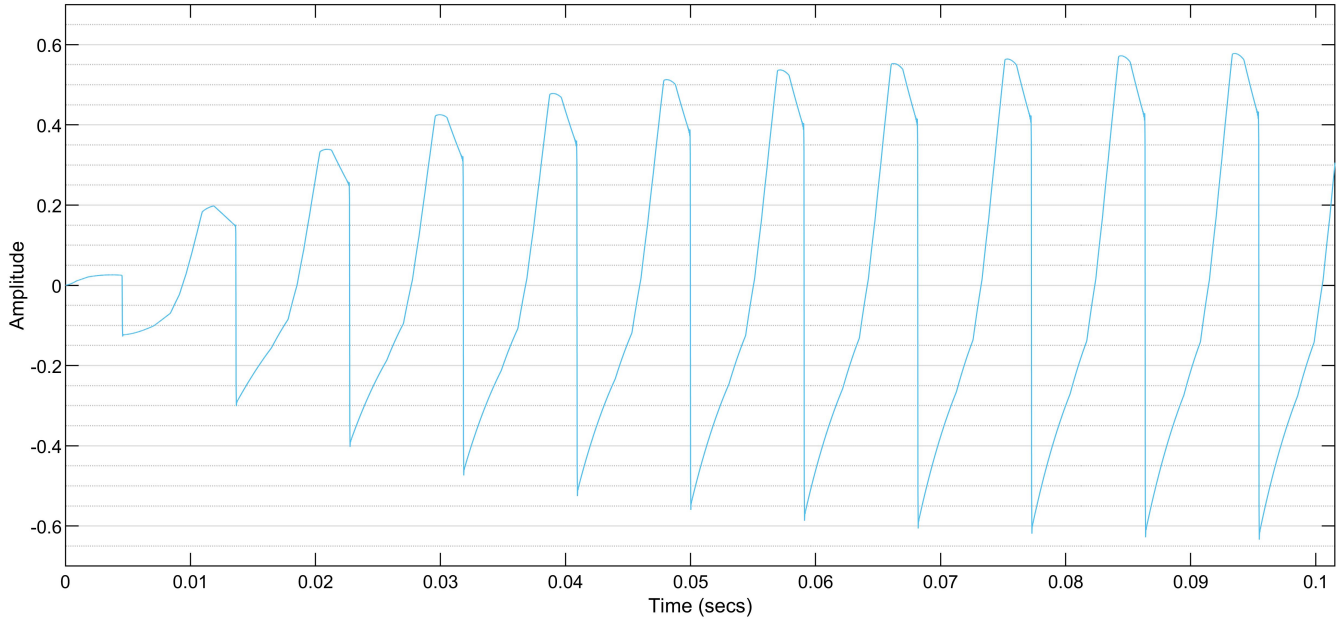

Figure D.2: Izotope Triode - Sawtooth Wave.

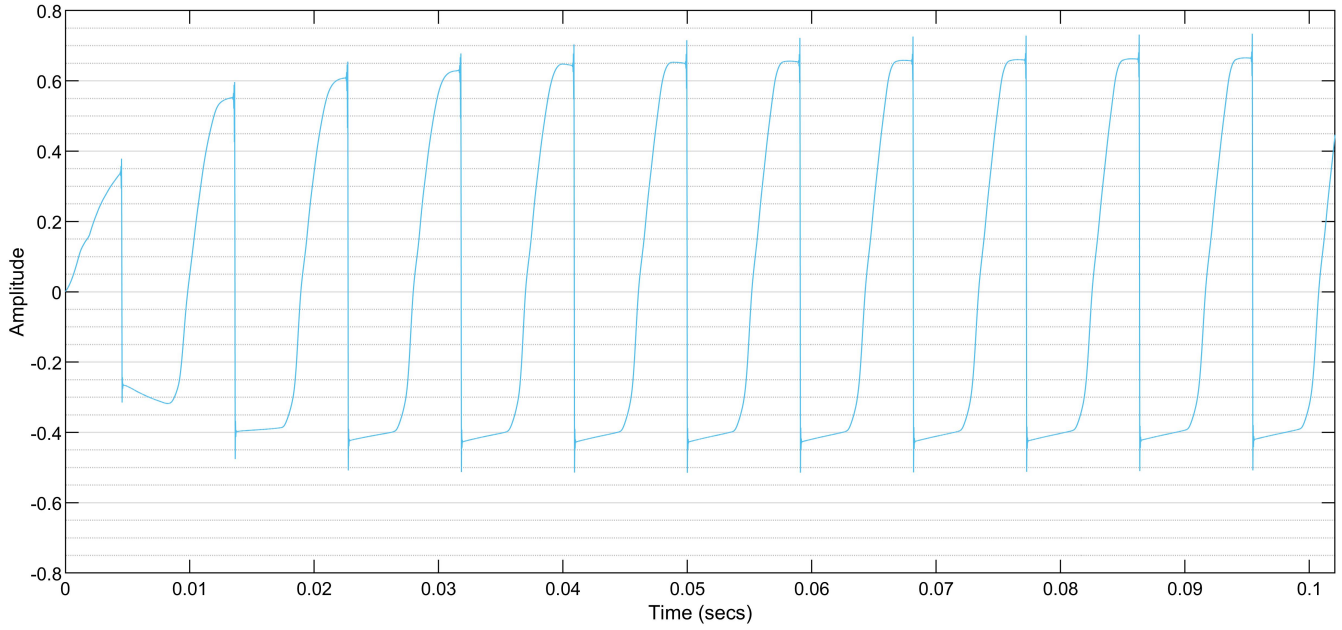

Figure D.3: Soundtoys Radiator - Sawtooth Wave.

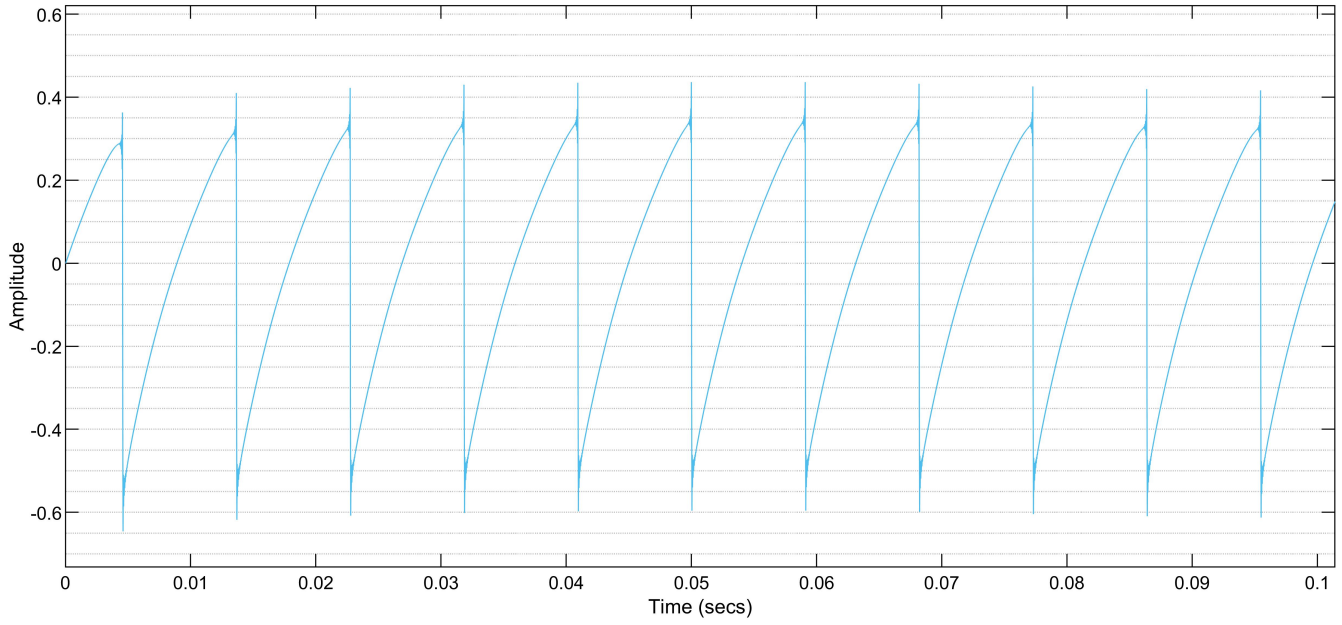

Figure D.4: 12AY7 - Sawtooth Wave.

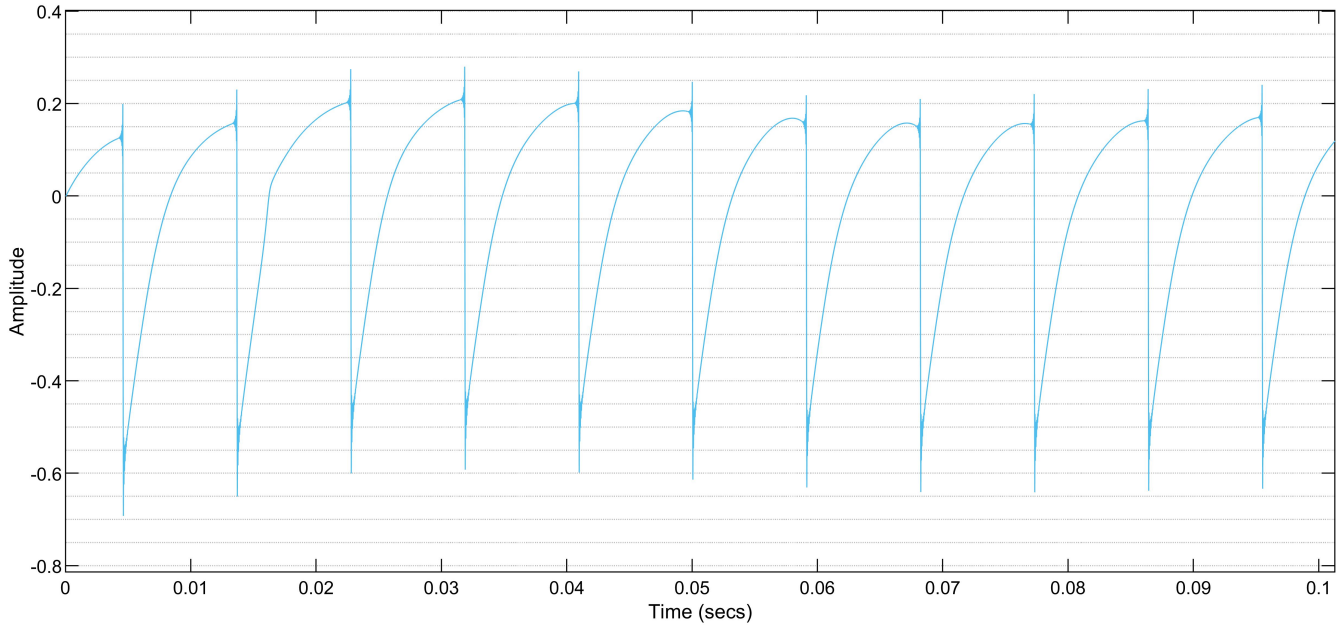

Figure D.5: 12AX7 - Sawtooth Wave.

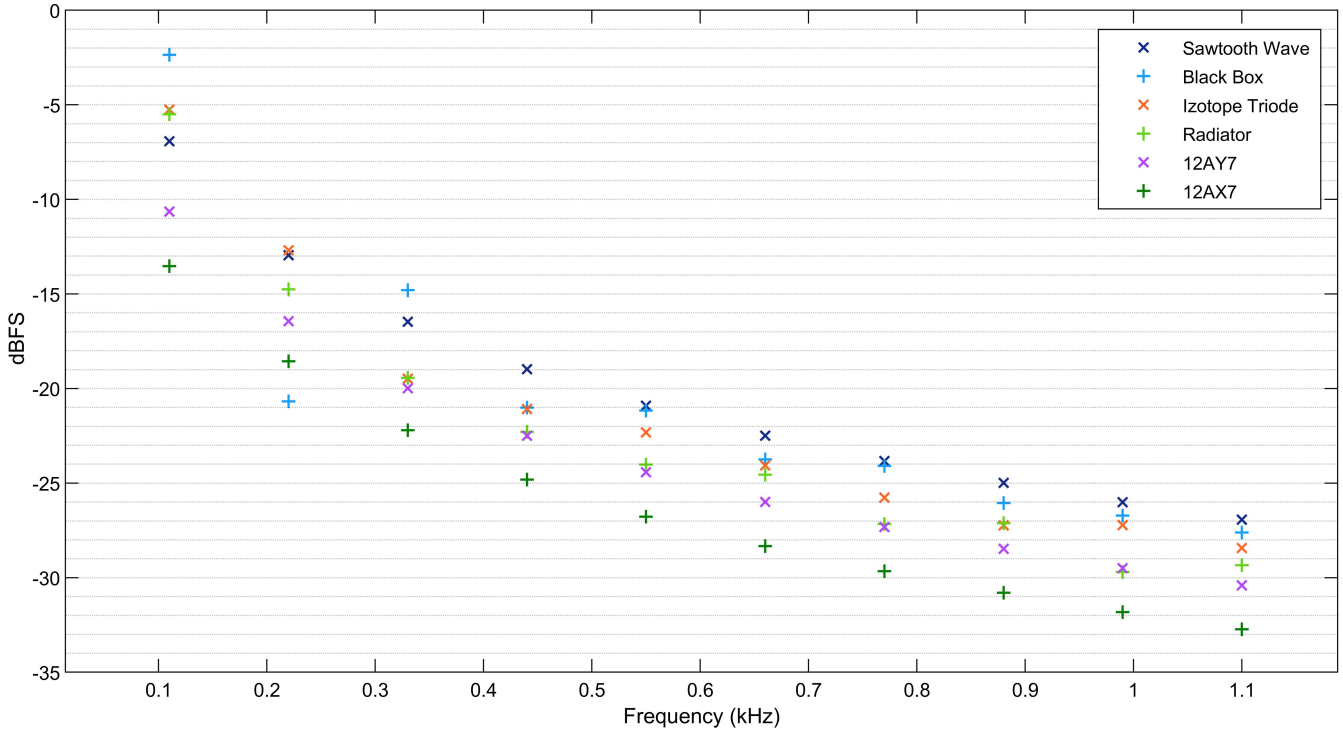

Figure D.6: Combined spectrum of each device's response to sawtooth waveforms.

D.2 Square Waves

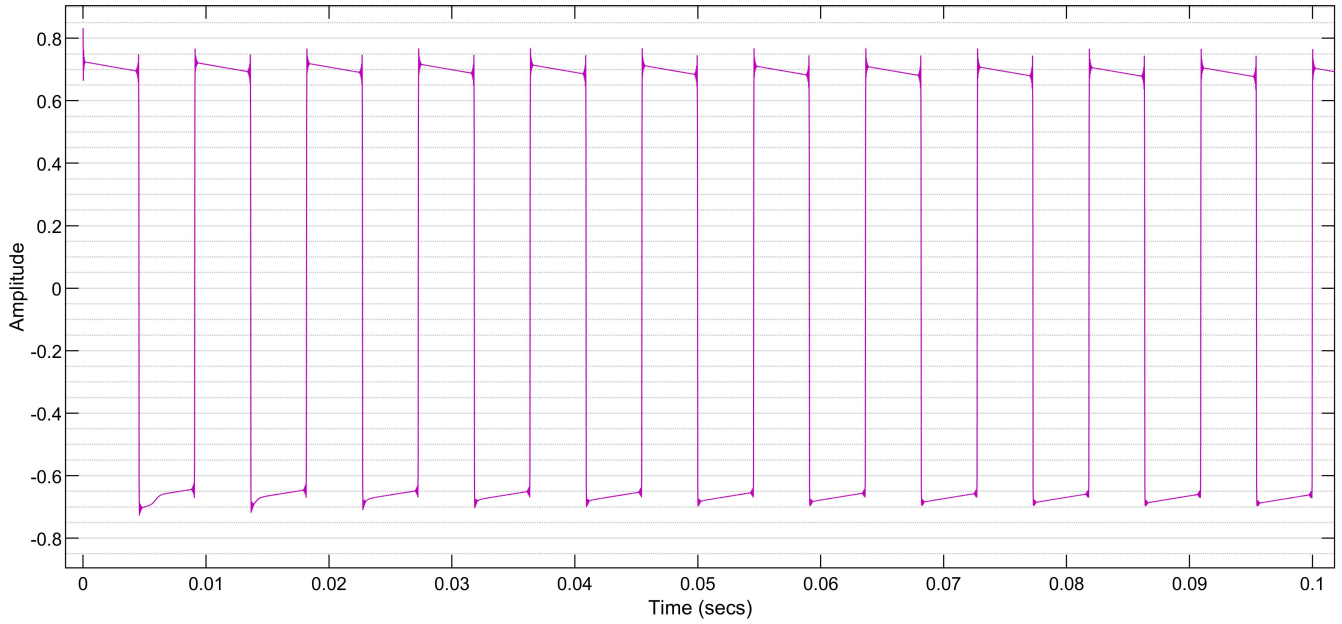

Figure D.7: Black Box - Square Wave.

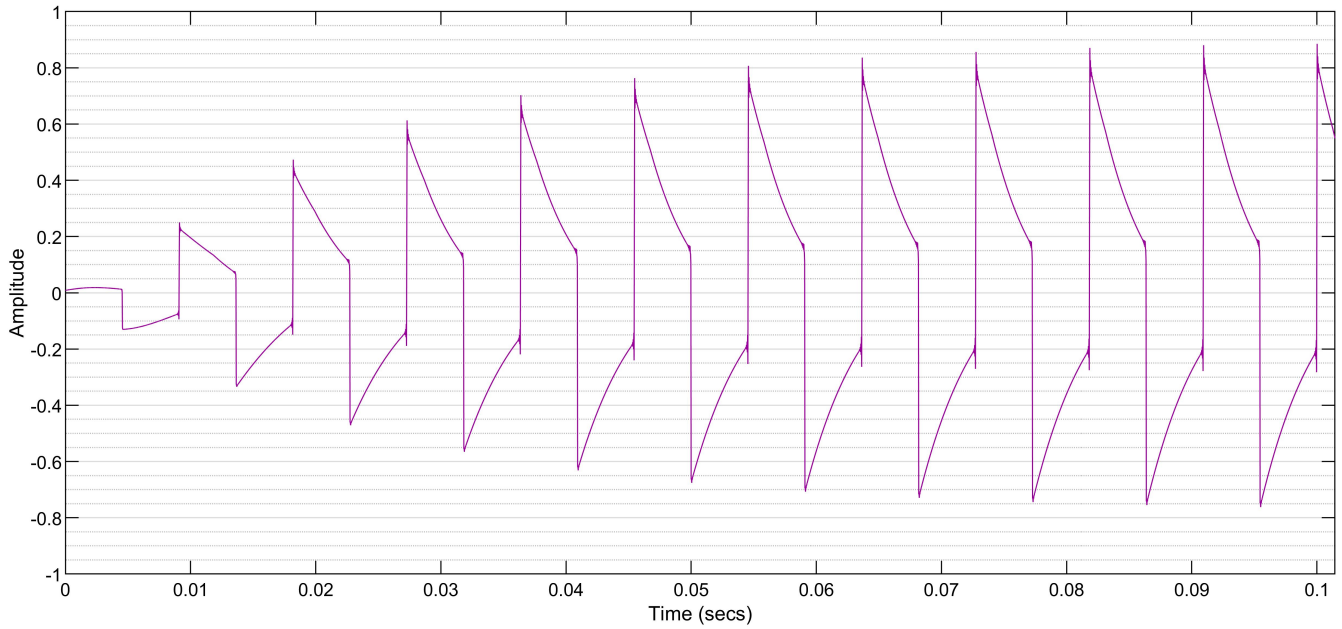

Figure D.8: Izotope Triode - Square Wave.

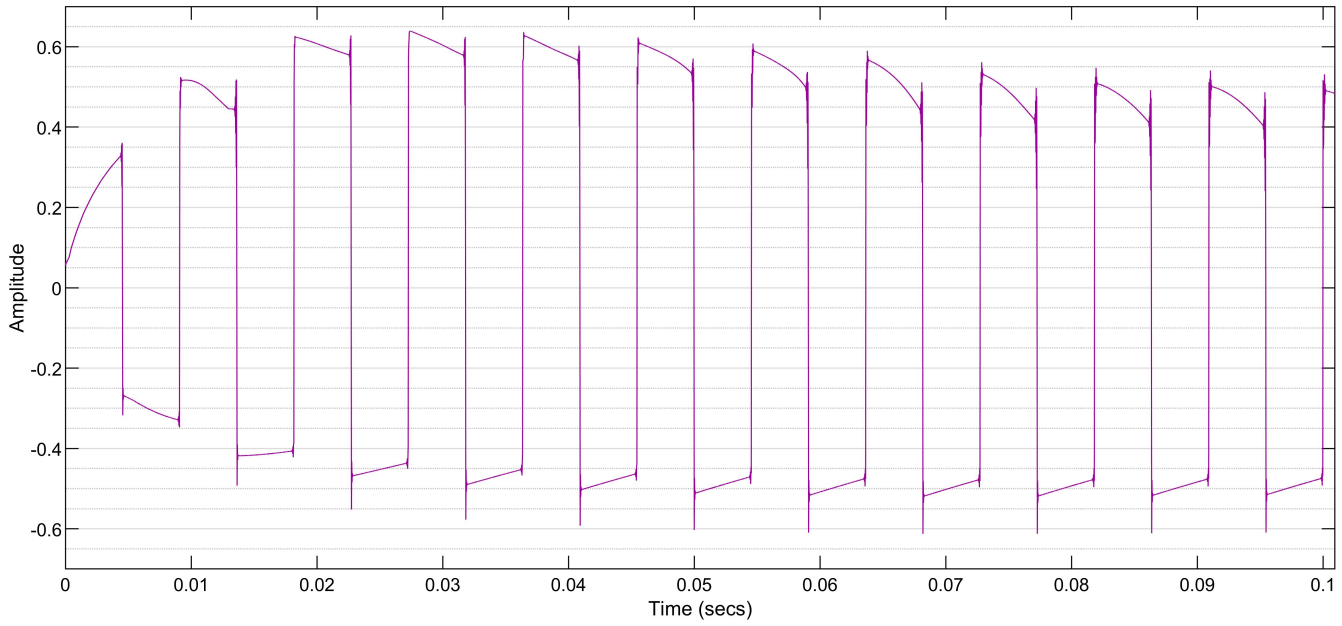

Figure D.9: Soundtoys Radiator - Square Wave.

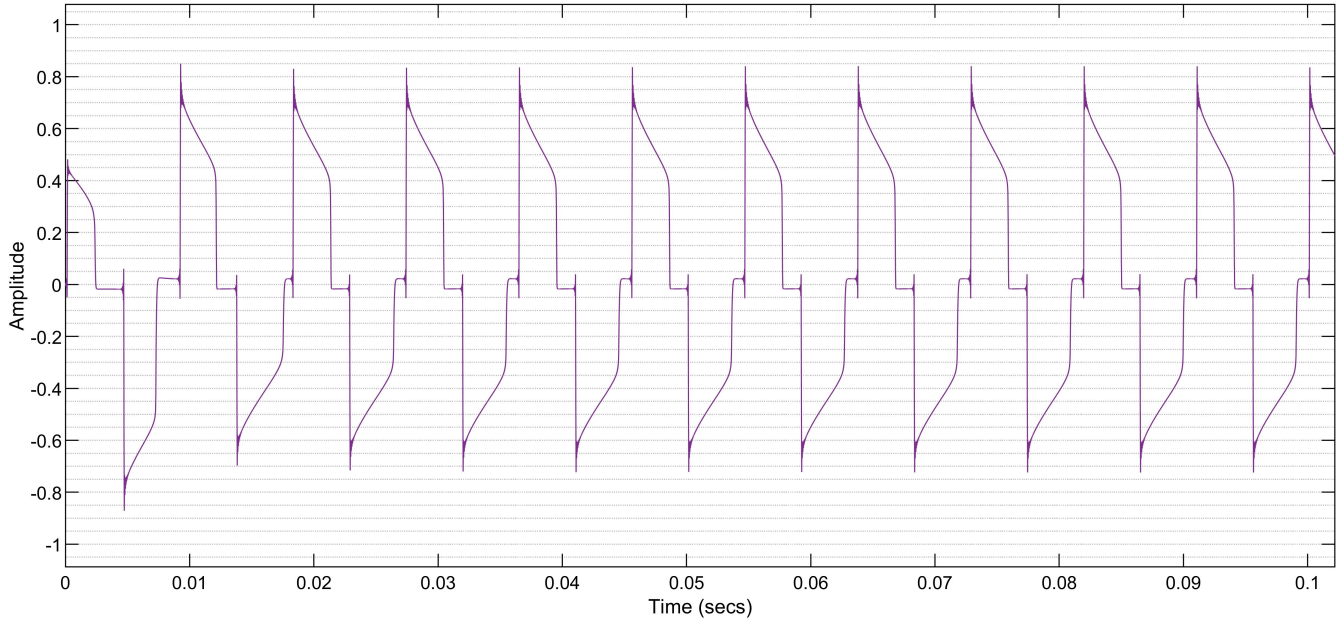

Figure D.10: 12AY7 - Square Wave.

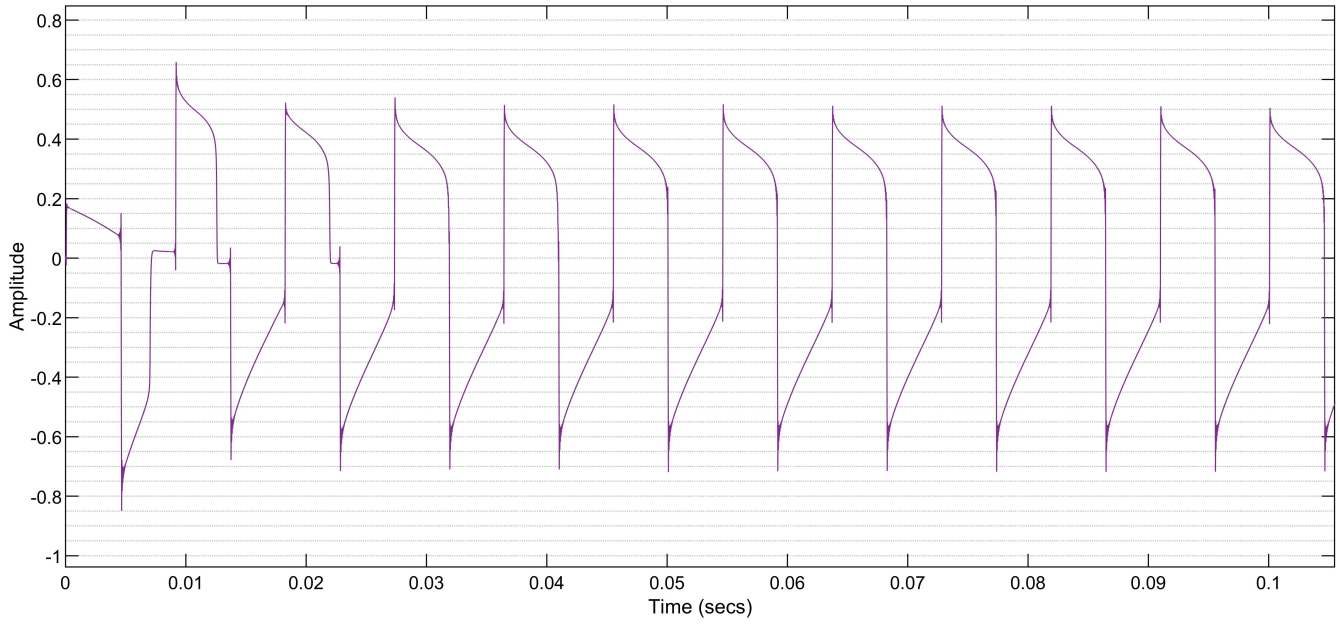

Figure D.11: 12AX7 - Square Wave.

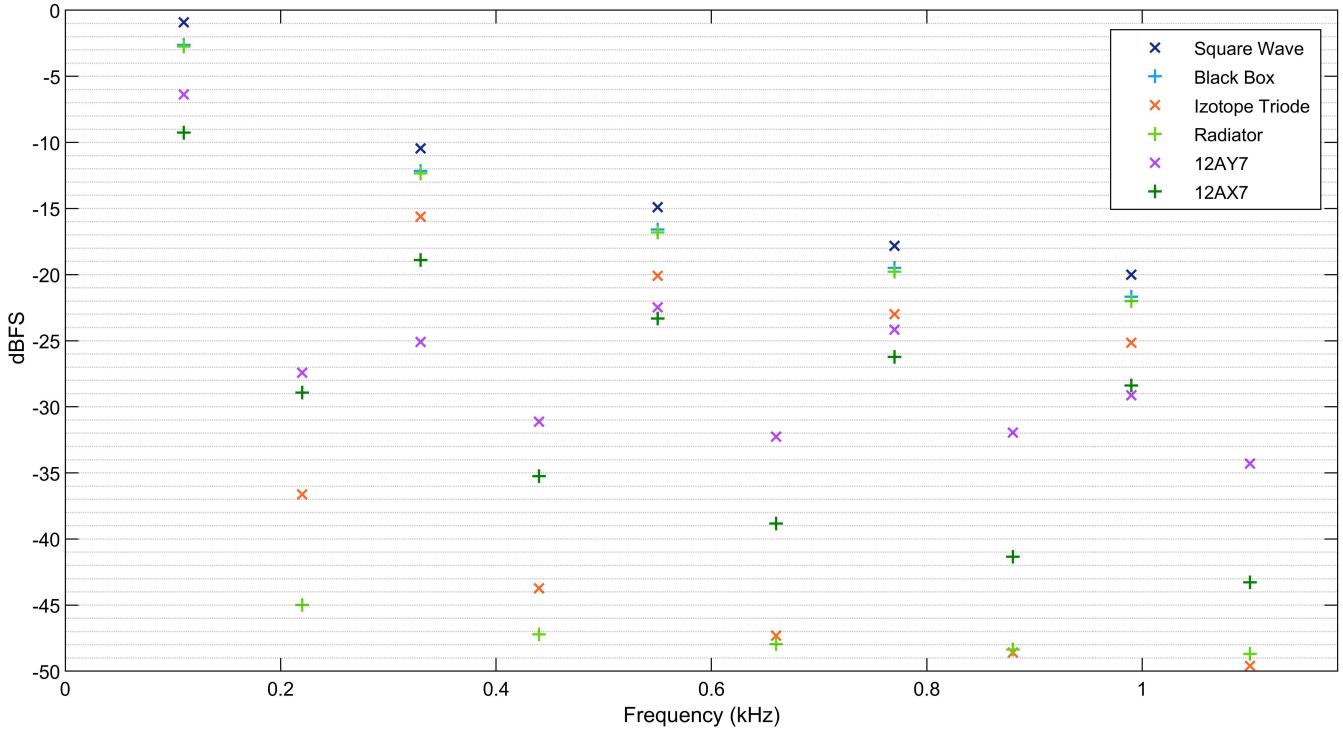

Figure D.12: Combined spectrum of each device's response to square waves.

D.3 Triangle Waves

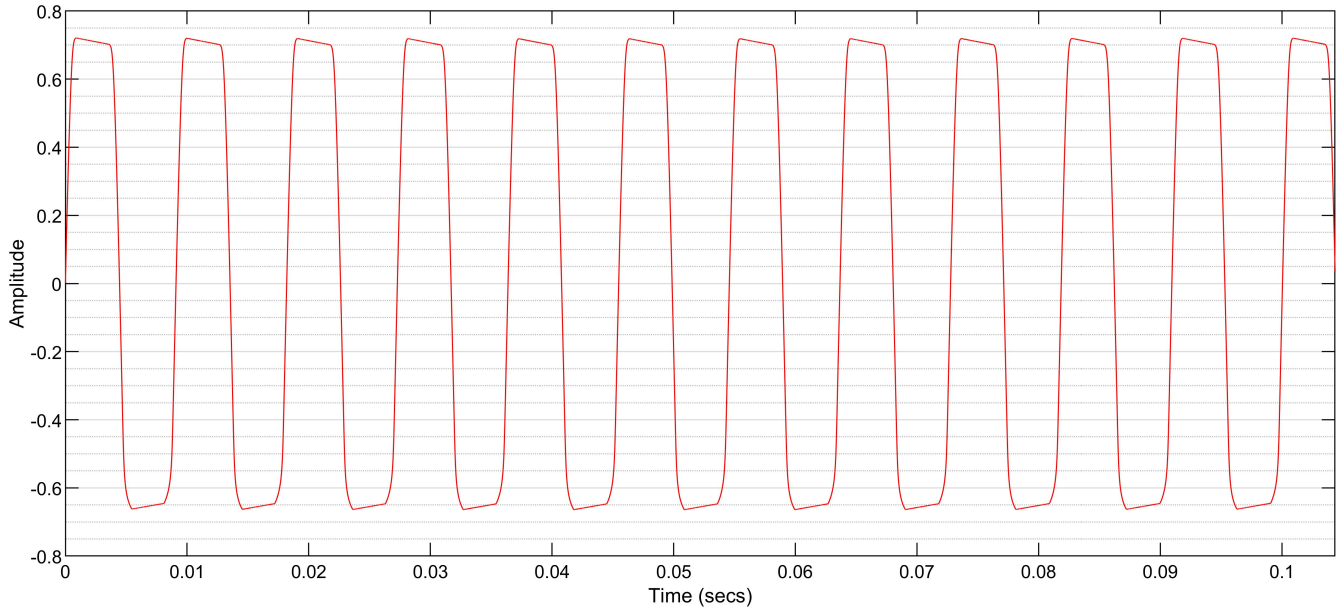

Figure D.13: Black Box - Triangle Wave.

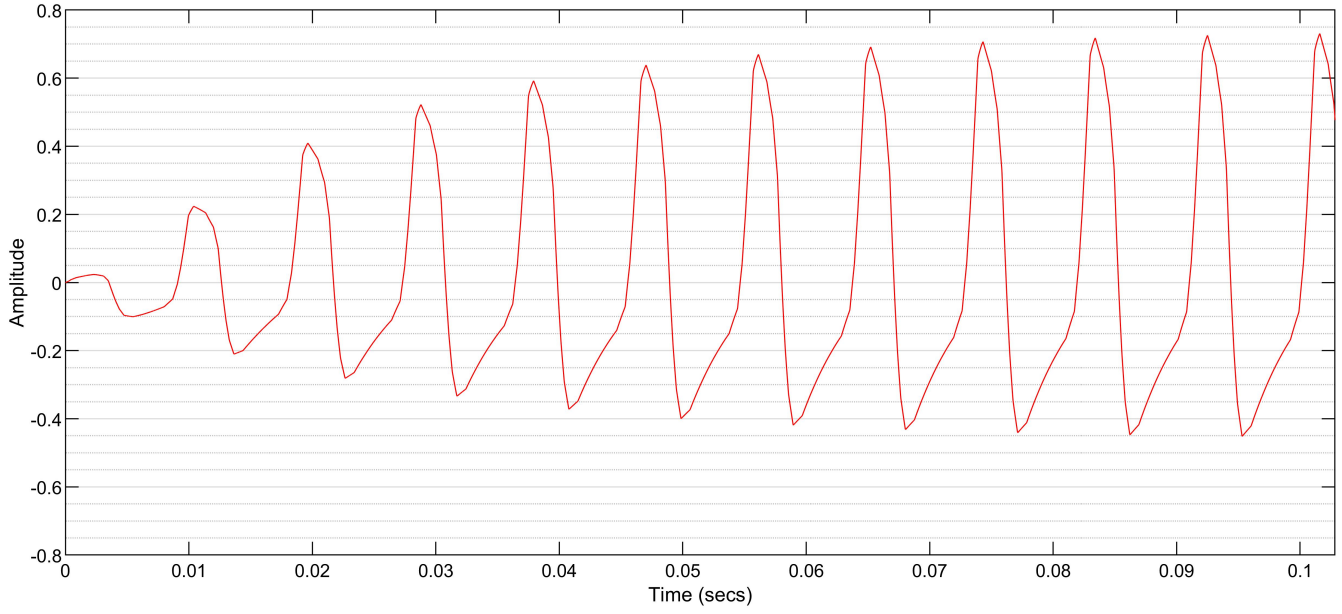

Figure D.14: Izotope Triode - Triangle Wave.

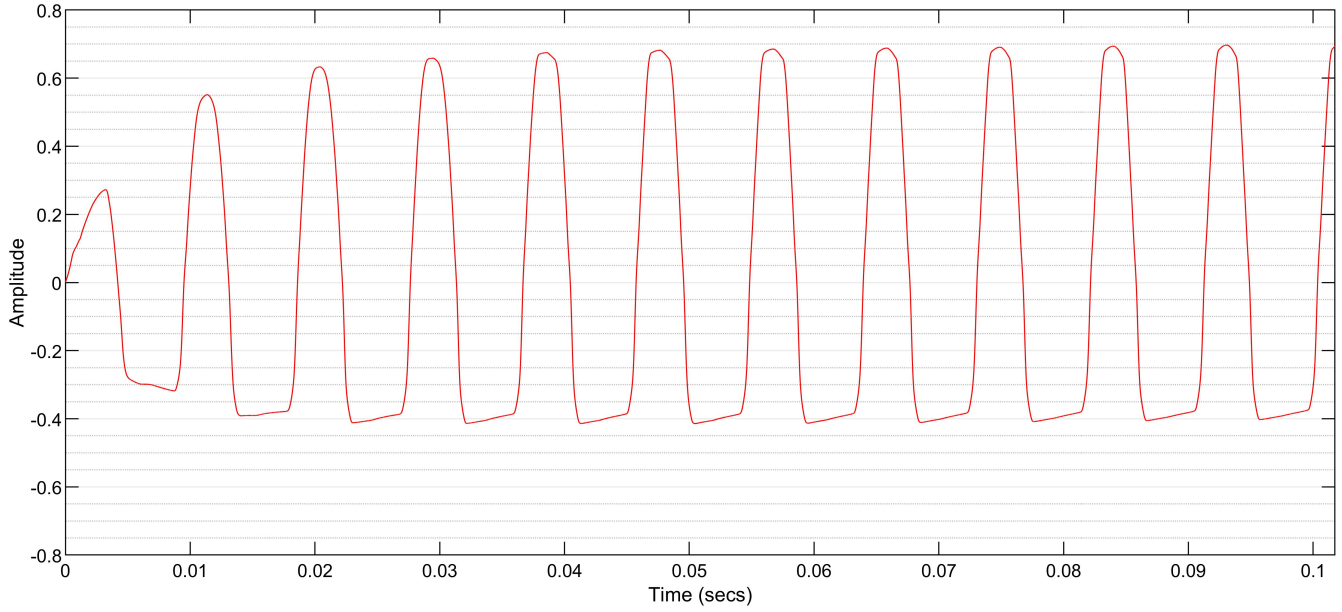

Figure D.15: Soundtoys Radiator - Triangle Wave.

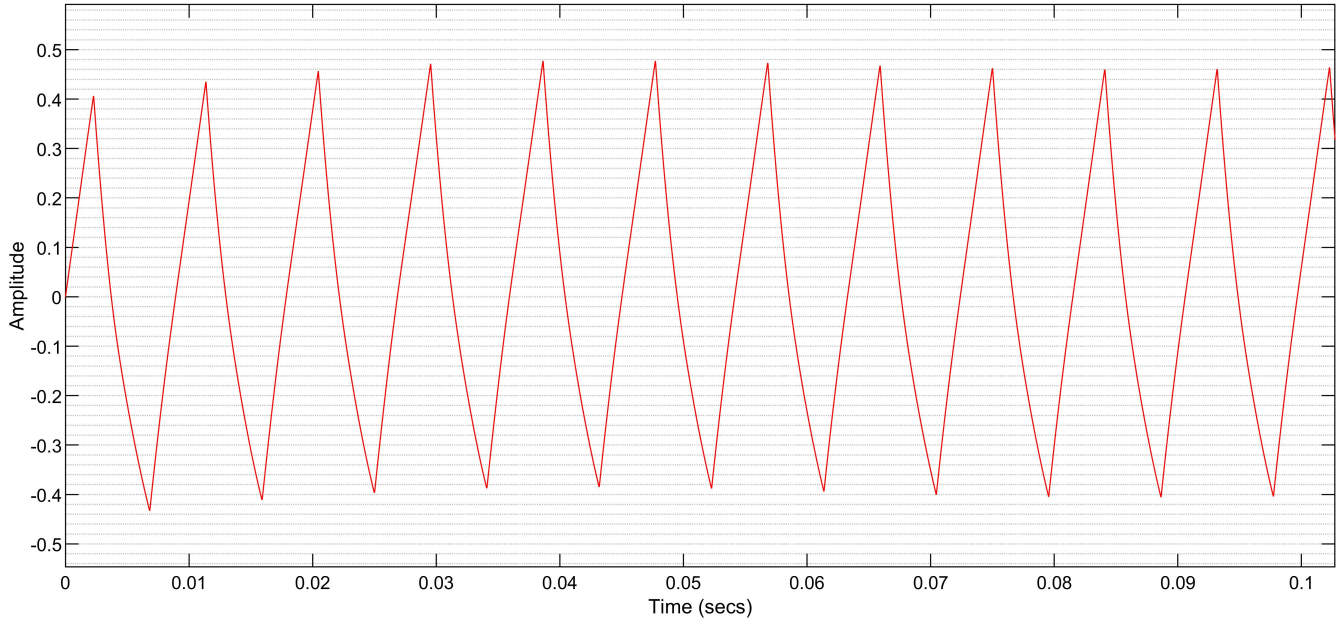

Figure D.16: 12AY7 - Triangle Wave.

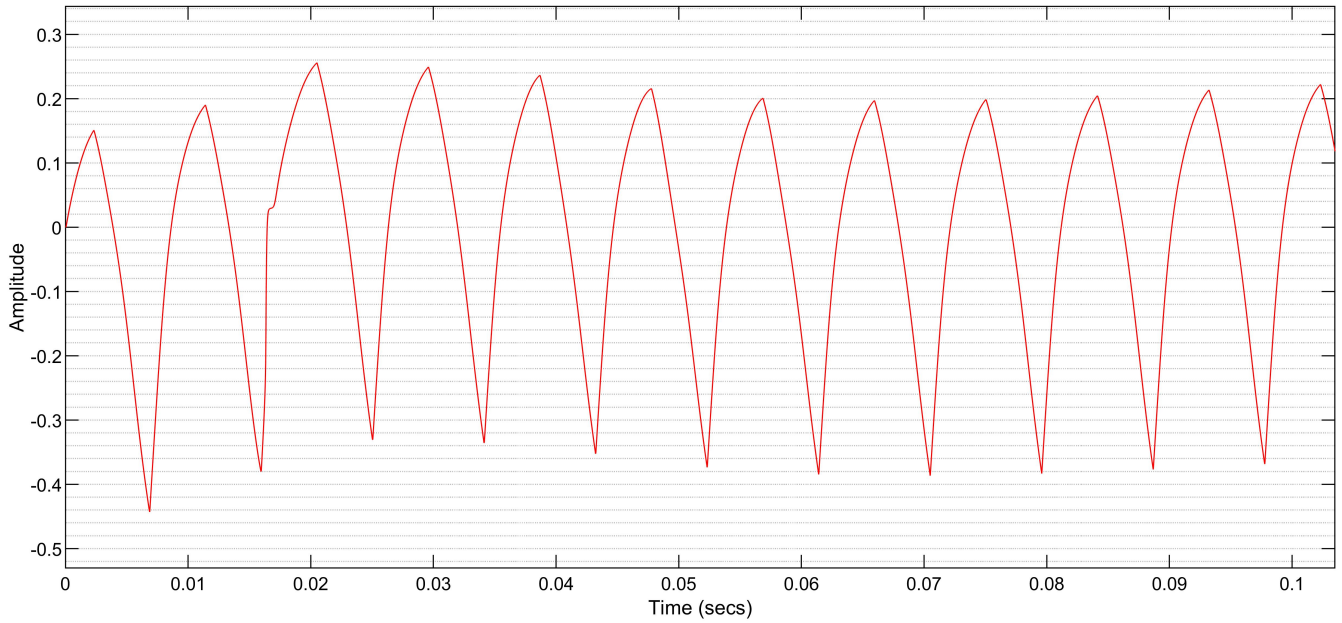

Figure D.17: 12AX7 - Triangle Wave.

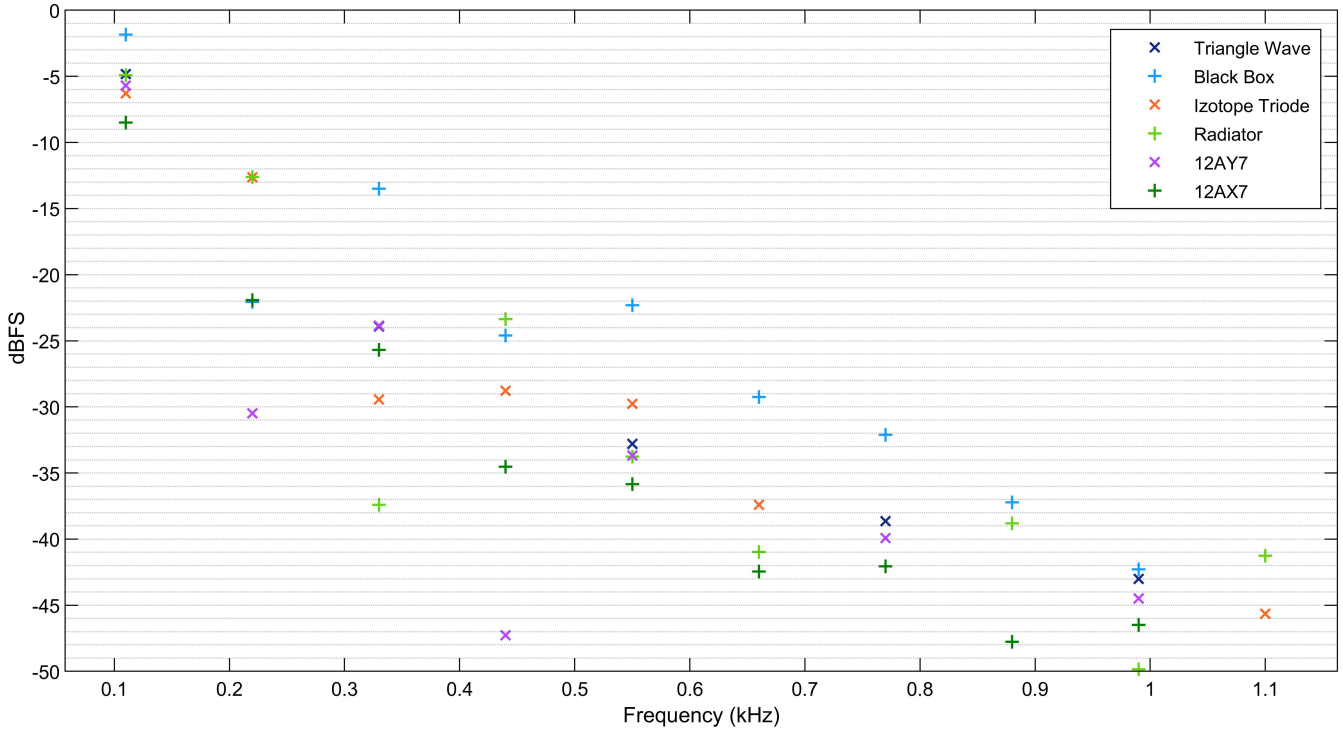

Figure D.18: Combined spectrum of each device's response to triangle waveforms.

D.4 Impulse Train

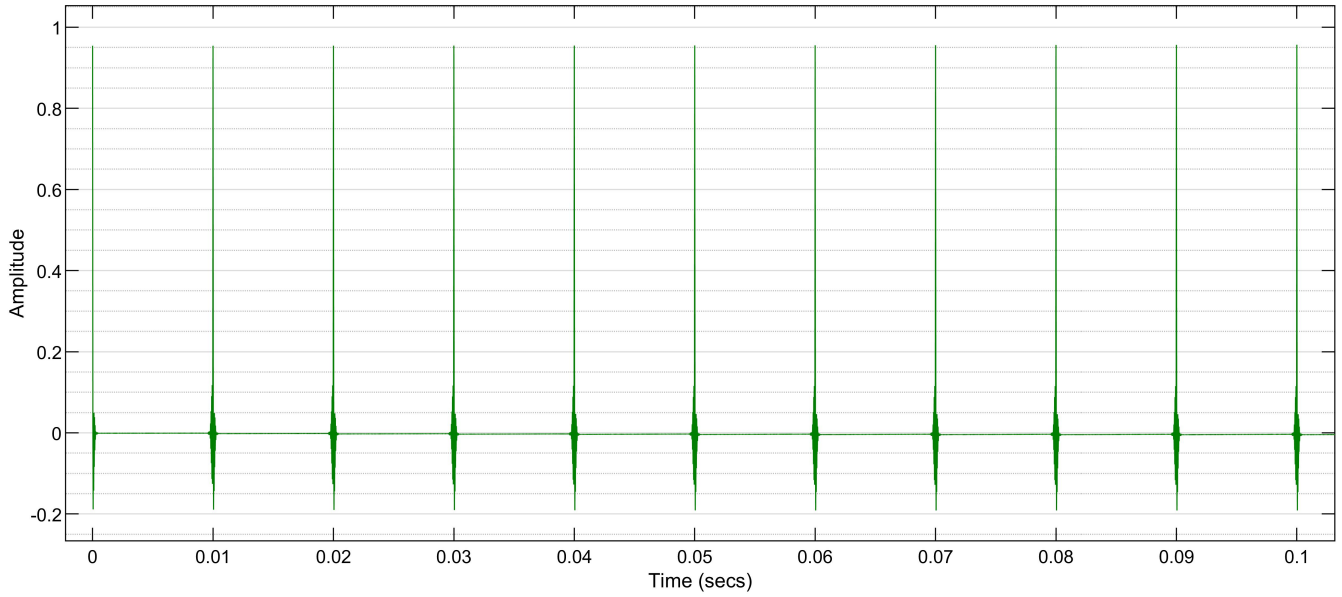

Figure D.19: Black Box - Impulse Train.

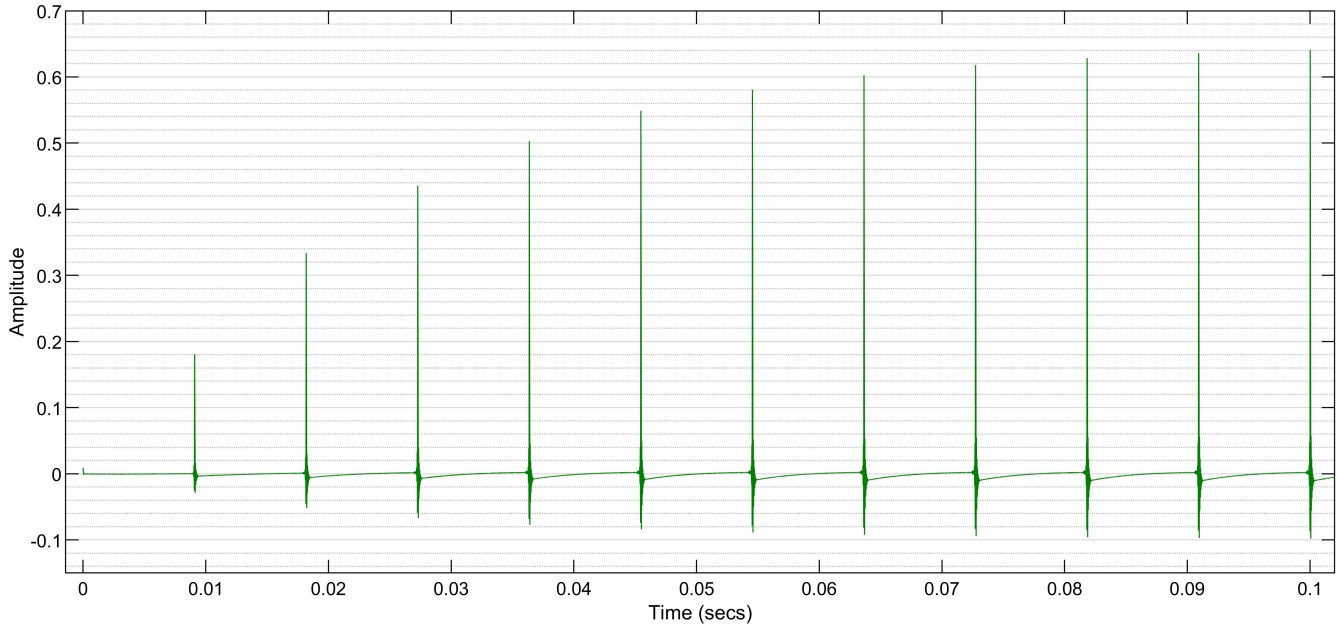

Figure D.20: Izotope Triode - Impulse Train.

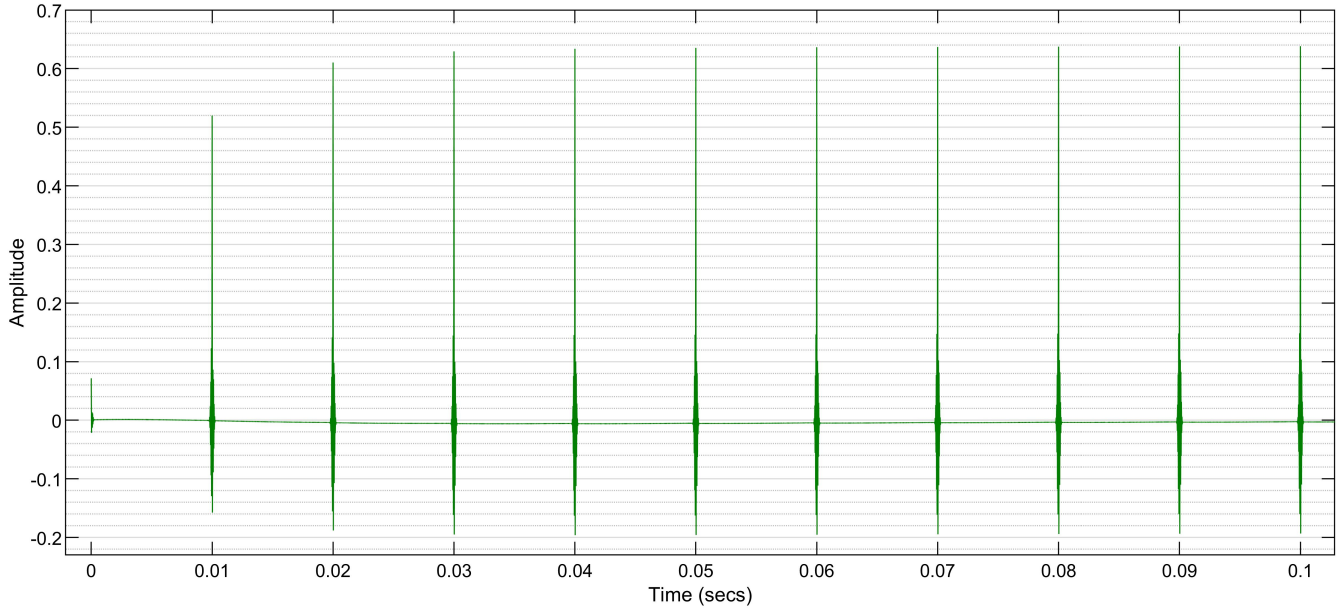

Figure D.21: Soundtoys Radiator - Impulse Train.

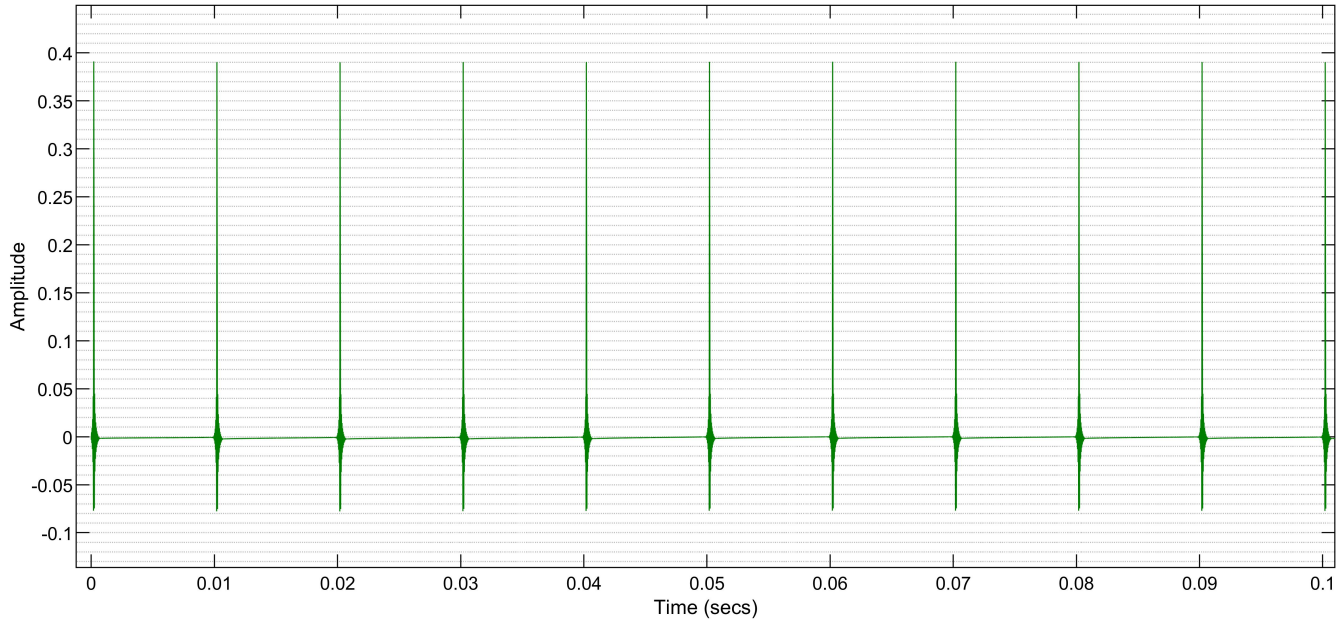

Figure D.22: 12AY7 - Impulse Train.

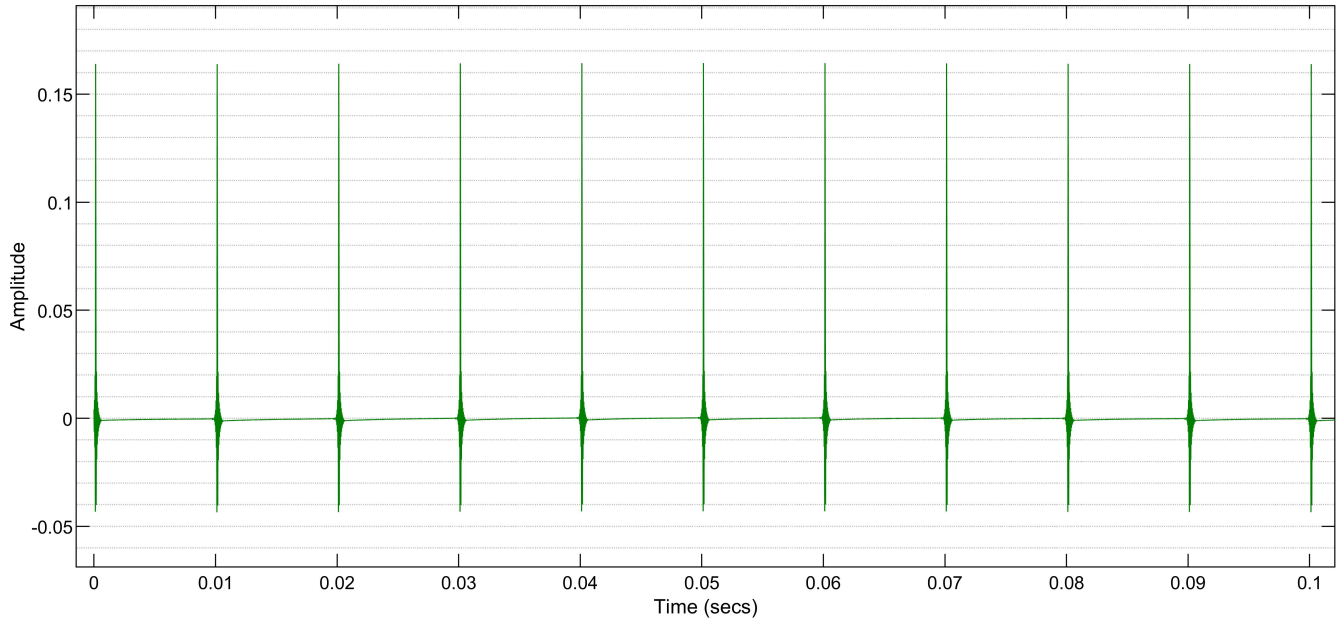

Figure D.23: 12AX7 - Impulse Train.

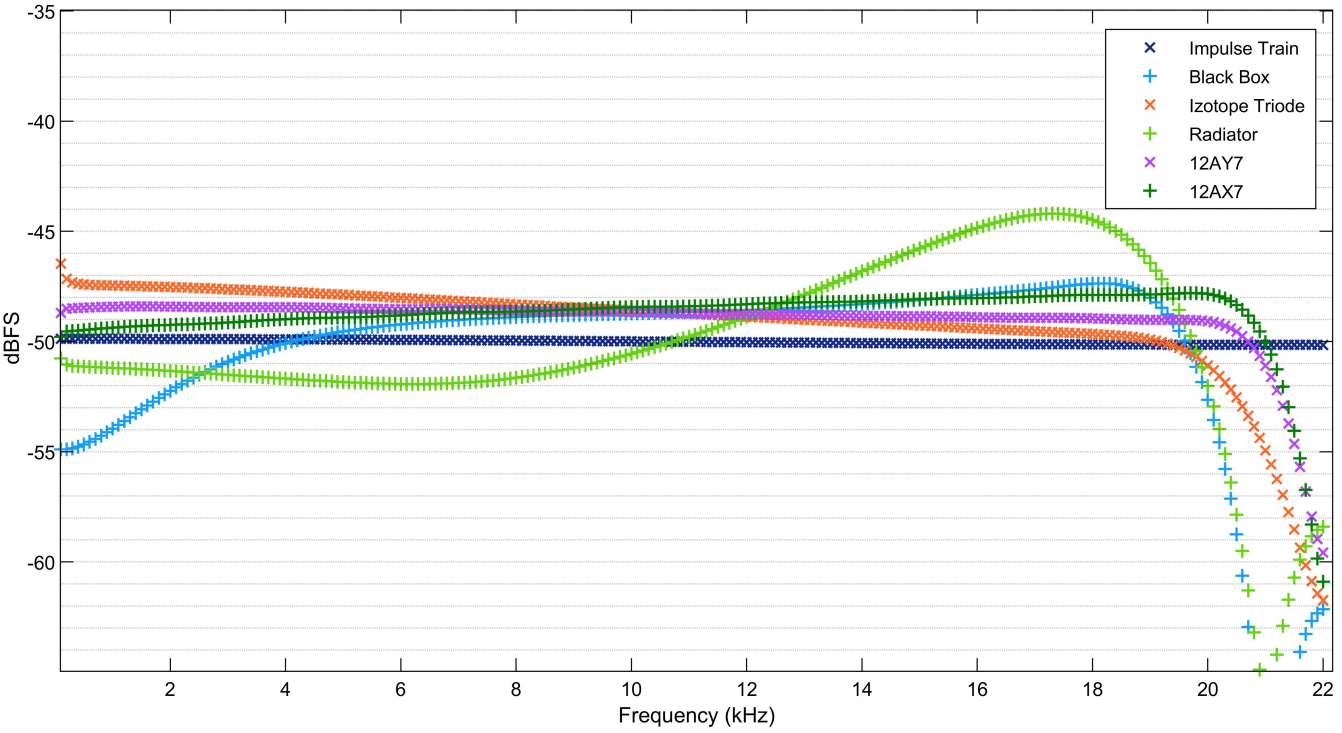

Figure D.24: Combined spectrum of each device's response to impulse trains.

Appendix E

Raw Data

E.1 Plugin Alliance - Black Box

- Harmonic Distortion Values
- Audio Test Files

E.2 Izotope Ozone Exciter - Triode

- Harmonic Distortion Values
- Audio Test Files

E.3 Soundtoys - Radiator

- Harmonic Distortion Values
- Audio Test Files

E.4 V1: 12AY7

- Harmonic Distortion Values
- Audio Test Files

E.5 V1: 12AX7

- Harmonic Distortion Values
- Audio Test Files

List of References

12AX7. 1954. General Electric receiving tube manual [Online]. Available: http://www.r-type.org/pdfs/12ax7.pdf [2020, May 12].

12AY7. 1954. General Electric five star and special purpose tube manual [Online]. Available: http://www.r-type.org/pdfs/12ay7.pdf [2020, May 12].

Alexander, C. & Sadiku, M. 2012. *Fundamentals of Electric Circuits*. 5th edition. New York: McGraw-Hill Education.

ANSI S1.1-1994. 2005. *American National Standard Acoustical Terminology*. Acoustical Society of America.

Barbour, E. 1998. The cool sound of tubes. *IEEE Spectrum*, 35(8):24–35.

Barlindhaug, G. 2007. Analogue sound in the age of digital tools: The story of the failure of digital technology. In R. Skare, N. Windfeld Lund & A. Varheim (eds.), *A Document (Re)turn - Contributions from a Research Field in Transition*, pages 73–93. Frankfurt: Lang.

Bennett, S. 2012. Situating vintage technologies in the contemporary recording workplace. *Journal on the Art of Record Production*, 7:1–18.

Blencowe, M. 2016. *Designing High-Fidelity Valve Preamps*. s.l: Merlin Blencowe.

Bohn, D. 2016. Pro audio reference [Electronic]. Available: http://www.aes.org/par/ [2019, April 21].

Butterfield, A. & Ngondi, G. 2016. *A Dictionary of Computer Science*. 7th edition. Oxford: Oxford University Press.

Cabot, R. 1997. Fundamentals of modern audio measurement. In *Advances in Engineering Software - AES*, volume 47, pages 3–29.

Case, A. 2011. *Mix Smart: Pro Audio Tips for Your Multitrack Mix*. Oxford: Focal Press.

Corey, J. & Benson, D. 2017. *Audio Production and Critical Listening: Technical Ear Training*. Audio Engineering Society Presents, 2nd edition. New York: Routledge.

Crowhurst, N. 1959. *Basic Audio Volume 2*. New York: John F. Rider.

Davis, M. 2007. Audio and electroacoustics. In T. Rossing (ed.), *Springer Handbook of Acoustics*, Springer Handbook of Acoustics. New York: Springer.

Donmoyer, R. 2008. Quantitative research. In L. Given (ed.), *The Sage Encyclopedia Of Qualitative Research Methods*. Los Angeles: Sage Publications.

Everest, F. *&* Pohlmann, K. 2014. *Master Handbook of Acoustics*. 6th edition. New York: McGraw-Hill Education.

Geddes, E. *&* Lee, L. 2003b. Auditory perception of nonlinear distortion. In *115th Audio Engineering Society Convention 2003*, pages 1–6. Audio Engineering Society.

Gilat, A. 2017. *Matlab: An Introduction with Applications*. 6th edition. Hoboken: Wiley.

Gottinger, B. 2007. Rethinking distortion: Towards a theory of 'sonic signatures'. Ph.D. thesis, New York University, New York.

Hamm, R. 1973. Tubes versus transistors - is there an audible difference? *Journal of the Audio Engineering Society*, 21:267–273.

Hampton, S. 2002. Build a tube mic pre: Build your own two channel vacuum tube mic preamp! *Tape Op*, 30:42–44.

Horowitz, P. *&* Hill, W. 2015. *The Art of Electronics*. 3rd edition. New York: Cambridge University Press.

Howard, D. *&* Angus, J. 2006. *Acoustics and Psychoacoustics*. Audio and music technology, 3rd edition. Oxford: Focal Press.

Hummersone, C. 2020. ISO 226:2003 Normal equal loudness level contours [Online]. Available: `https://github.com/IoSR-Surrey/MatlabToolbox` [2020, July 8].

Hurley, W. *&* Wölfle, W. 2013. *Transformers and Inductors for Power Electronics: Theory, Design and Applications*. Chichester: Wiley.

IEEE Std 315. 1975. IEEE Standard American National Standard Canadian Standard Graphic Symbols for Electrical and Electronics Diagrams (Including Reference Designation Letters). *IEEE Std 315-1975*.

Izotope. 2017. Ozone Exciter [Online]. Available: `https://s3.amazonaws.com/izotopedownloads/docs/ozone8/exciter/index.html` [2020, June 11].

Johnston, I. *&* Johnston, I. 2009. *Measured Tones: The Interplay of Physics and Music*. 3rd edition. Boca Raton: Taylor & Francis.

Jones, M. 2012. *Valve Amplifiers*. 4th edition. Oxford: Elsevier.

Jung, W., Stephens, M. *&* Todd, C. 1979. An overview of SID and TIM. *Audio*, 63:59–64.

Kadis, J. 2012. *The Science Of Sound Recording*. Waltham: Focal Press.

Krumhansl, C. 1989. Why is musical timbre so hard to understand. *Structure and Perception of Electroacoustic Sound and Music*, 846:43–53.

Langford-Smith, F. 1963. *Radiotron Designer's Handbook*. 6th edition. London: Iliffe Books Ltd.

Laplante. 2005. *Comprehensive Dictionary of Electrical Engineering*. 2nd edition. Boca Raton: CRC Press.

Laplante. 2018. *Technical Writing: A Practical Guide for Engineers, Scientists, and Nontechnical Professionals*. 2nd edition. Boca Raton: CRC Press.

Lerch, A. 2012. *An Introduction to Audio Content Analysis: Applications in Signal Processing and Music Informatics*. Piscataway: Wiley.

Linsey-Hood, J. 2009. Preamplifiers and input signals. In *Audio Engineering: Know It All*. Burlington: Elsevier Science.

Matlab. 2020a. DSP System Toolbox - Reference [Online]. Available: `https://www.mathworks.com/help/pdf_doc/dsp/dsp_ref.pdf` [2020, June 11].

Matlab. 2020b. DSP System Toolbox - Users Guide [Online]. Available: `https://www.mathworks.com/help/pdf_doc/dsp/dsp_ug.pdf` [2020, June 11].

Matlab. 2020c. Mathematics [Online]. Available: `https://www.mathworks.com/help/pdf_doc/matlab/matlab_math.pdf` [2020, June 11].

Mcmanus, S. 2008. Filters and equalizers. In G. Ballou (ed.), *Handbook for Sound Engineers*, 4th edition. Burlington: Focal Press.

Metzler, B. 2005. *Audio Measurement Handbook*. 2nd edition. Beaverton: Audio Precision.

Miller, P. 2008. Quantitative research. In L. Given (ed.), *The Sage Encyclopedia Of Qualitative Research Methods*. Los Angeles: Sage Publications.

Moore, A., Till, R. & Wakefield, J. 2016. An investigation into the sonic signature of three classic dynamic range compressors. In *140th Audio Engineering Society International Convention 2016*, pages 601–610. Audio Engineering Society.

Moore, B. 2012. *An Introduction to the Psychology of Hearing*. 6th edition. Cambridge: Emerald.

Newell, P. 2012. *Recording Studio Design*. 3rd edition. Burlington: Focal.

O'Connor, T. & Wong, H.Y. 2015. Emergent Properties. In E.N. Zalta (ed.), *The Stanford Encyclopedia of Philosophy*. Metaphysics Research Lab, Stanford University [Electronic]. Available: `https://plato.stanford.edu/archives/sum2015/entries/properties-emergent/` [2020, May 31].

Parncutt, R. 1989. *Harmony: A Psychoacoustical Approach*. Heidelberg: Springer-Verlag.

Patronis, Jr, E. 2008. Amplifier design. In G. Ballou (ed.), *Handbook for Sound Engineers*, 4th edition. Burlington: Focal Press.

Pedhazur, E. & Schmelkin, L. 1991. *Measurement, Design, And Analysis: An Integrated Approach*. Hillsdale: Lawrence Erlbaum Associates.

Pinch, T. & Reinecke, D. 2009. Technostalgia: How old gear lives on in new music. In K. Bijsterveld & J. van Dijck (eds.), *Sound Souvenirs: Audio Technologies, Memory and Cultural Practices*, Transformations in art and culture. Amsterdam: Amsterdam University Press.

Plugin Alliance. 2020. Black Box HG-2 plugin manual [Online]. Available: `https://files.plugin-alliance.com/products/black_box_analog_design_hg-2/black_box_analog_design_hg-2_manual_en.pdf` [2020, June 10].

Preis, D. 1976. Linear distortion. *J. Audio Eng. Soc*, 24(5):346–367.

Robjohns, H. 2010. Analogue warmth: The sound of tubes, tape & transformers. *Sound on Sound*, February.

Roederer, J. 2008. *The Physics and Psychophysics of Music: An Introduction*. 4th edition. New York: Springer.

Russ, M. 2012. *Sound Synthesis and Sampling*. 3rd edition. Burlington: Taylor & Francis.

Self, D. 2015. *Small Signal Audio Design*. 2nd edition. Burlington: Taylor & Francis.

Soundtoys. 2015. Radiator user's guide [Online]. Available: `https://www.soundtoys.com/wp-content/uploads/Radiator-Manual.pdf` [2020, June 10].

Sueur, J. 2018. *Sound Analysis and Synthesis with R*. s.l.: Springer International Publishing.

Tal, E. 2020. Measurement in Science. In E.N. Zalta (ed.), *The Stanford Encyclopedia of Philosophy*. Metaphysics Research Lab, Stanford University [Electronic]. Available: `https://plato.stanford.edu/archives/fall2020/entries/measurement-science/` [2020, May 31].

Tarr, E. 2018. *Hack Audio: An Introduction to Computer Programming and Digital Signal Processing in MATLAB*. Audio Engineering Society Presents. New York: Routledge.

Temme, S. 1992. *Application Note: Audio Distortion Measurement*. Nærum: Brüel & Kjær.

Truax, B. 1984. *Acoustic Communication*. Norwood: Ablex Publishing Corporation.

Tye, M. 2018. Qualia . In E.N. Zalta (ed.), *The Stanford Encyclopedia of Philosophy*. Metaphysics Research Lab, Stanford University [Electronic]. Available: `https://plato.stanford.edu/archives/sum2018/entries/qualia/` [2020, May 31].

Waters, C.K. 2007. The nature and context of exploratory experimentation: An introduction to three case studies of exploratory research. *History and Philosophy of the Life Sciences*, 29(3):275–284.

Weisstein, E. 2002. *CRC Concise Encyclopedia of Mathematics*. Boca Raton: CRC Press.

White, E. 1941. Improvements in or relating to thermionic valve amplifier circuit arrangements. U.K. Patent: 564,250.

White, G. & Louie, G. 2005. *The Audio Dictionary*. 3rd edition. Seattle: University of Washington Press.

Whitlock, B. 2008. Audio transformer basics. In G. Ballou (ed.), *Handbook for Sound Engineers*, 4th edition. Burlington: Focal Press.

Winer, E. 2017. *The Audio Expert: Everything You Need to Know About Audio*. 2nd edition. Burlington: Taylor & Francis Group.

Zagorski-Thomas, S. & Frith, S. 2012. Introduction. In S. Zagorski-Thomas & S. Frith (eds.), *The Art of Record Production: An Introductory Reader for a New Academic Field*, Ashgate Popular and Folk Music Series. Surrey: Ashgate Publishing Limited.

Zwicker, E. & Fastl, H. 2007. *Psychoacoustics: Facts And Models*. Berlin: Springer.

Zwicker, E. & Zwicker, T. 1991. Audio engineering and psychoacoustics: Matching signals to the final receiver, the human auditory system. *Journal of the Audio Engineering Society*, 39(3):115–126.